

**Development of Dynamic, Bioorthogonal Peptide Cross-Linking Methods**

by

Conor Michael Haney

B. S. Chemistry, University of Pittsburgh, 2009

Submitted to the Graduate Faculty of  
the Kenneth P. Dietrich School of Arts and Sciences in partial fulfillment  
of the requirements for the degree of  
Doctor of Philosophy

University of Pittsburgh

2014

UNIVERSITY OF PITTSBURGH  
KENNETH P. DIETRICH SCHOOL OF ARTS AND SCIENCES

This dissertation was presented

by

Conor M. Haney

It was defended on

August 14<sup>th</sup>, 2014

and approved by

Dr. Alexander Deiters, Professor, Department of Chemistry

Dr. Xinyu Liu, Assistant Professor, Department of Chemistry

Dr. Ronald Wetzel, Professor, Department of Structural Biology

Dissertation Advisor: Dr. W. Seth Horne, Assistant Professor, Department of Chemistry

Copyright © by Conor M. Haney

2014

# DEVELOPMENT OF DYNAMIC, BIOORTHOGONAL PEPTIDE CROSS-LINKING

## METHODS

Conor M. Haney, PhD

University of Pittsburgh, 2014

Short peptide sequences typically lack well-defined structure when removed from the context of a larger protein. In order to constrain peptides into well-defined structures, nature often relies on the formation of disulfides between cysteine residues. Chemists have leveraged alternative chemoselective reactions to constrain peptides into defined folded conformations. Chemoselective cyclization strategies typically require extensive synthetic manipulation or the use of conditions which are incompatible with biological systems.

This work encompasses the development of alternative peptide cyclization strategies that can be utilized under conditions compatible with biological systems. The strategies we have focused on offer the possibility of implementing cross-linking in a dynamic and reversible manner in aqueous solutions. We have chosen to take advantage of the bioorthogonal and reversible nature of oxime and hydrazone formation in the development of bioorthogonal and dynamic side chain cross-linking.

We have demonstrated that an oxime formed by a cyclization reaction between aminoxy- and aldehyde-functionalized side chains in peptide sequences proceeds rapidly and in high yield. These cross-links have been shown to affect peptide folding and are capable of dynamic covalent exchange. Oxime cross-links have been shown to stabilize a model protein-protein interaction, with a dependence upon the sequence context and structure of the cross-link formed. Analysis of a high-resolution structure of the cross-linked oligomer demonstrates that the oxime side chain cross-link is well accommodated into an  $\alpha$ -helical fold. We have also demonstrated that the product distribution of a cross-linking reaction in which

multiple cross-linked regioisomers can be generated is dependent upon the folded state of the peptide at the time of cross-link formation.

An alternative strategy which employs the use of an intermolecular cyclization between a bifunctionalized peptide and dialdehyde functionalized small molecules has also been explored. The intermolecular cyclization strategy has been shown to affect peptide folded structure and be capable of dynamic covalent exchange. Intermolecular cyclization offers a generally applicable and convergent manner to synthesize multiple cross-linked species in a combinatorial manner. This strategy has then been employed to template formation of different cross-linked structures based on the presence of an expressed protein receptor.

## TABLE OF CONTENTS

TABLE OF CONTENTS .....	VI
LIST OF TABLES.....	X
LIST OF FIGURES .....	XI
LIST OF SCHEMES .....	XV
LIST OF EQUATIONS.....	XVI
LIST OF ABBREVIATIONS .....	XVII
1.0 INTRODUCTION .....	1
1.1 DYNAMIC COVALENT CHEMISTRY .....	1
1.2 PEPTIDES AS THERAPEUTICS .....	5
1.3 FORMATION OF SECONDARY STRUCTURES IN PEPTIDES .....	8
1.3.1 Controlling $\alpha$ -Helical Folding Patterns.....	10
1.4 COVALENT CONSTRAINTS IN PEPTIDE FOLDING.....	11
1.4.1 On-Resin Peptide Cyclization Techniques.....	12
1.4.2 Solution Phase Peptide Cyclization Techniques.....	15
1.5 PROJECT GOALS.....	18
1.5.1 Intramolecular Oxime Cross-link Formation.....	19
1.5.2 Intermolecular Oxime and Hydrazone Cross-link Formation .....	20
1.5.3 Cross-Linking Peptide Ligands In The Presence Of A Protein Receptor.....	20
2.0 INTRAMOLECULAR OXIME CROSS-LINK FORMATION .....	22
2.1 PROMOTING $\alpha$ -HELIX FORMATION IN A SHORT PEPTIDE.....	23

2.1.1	Design Of The Peptide Model System .....	23
2.1.2	Oxime Cross-Link Formation And Exchange In A Simple $\alpha$ -Helix .....	26
2.1.3	Dynamic Covalent Exchange In A Helical Peptide .....	30
2.1.4	Oxime Cross-Link Effect On Folding In A Simple $\alpha$ -Helix .....	33
2.1.5	Conclusions .....	34
2.2	OXIME SIDE CHAIN CROSS-LINKS IN A MODEL QUATERNARY STRUCTURE	35
2.2.1	Examination Of The Sensitivity Of Methionine To Periodate Oxidation .....	37
2.2.2	Cross-Link Structure And Connectivity In An $\alpha$ -Helical Coiled-Coil .....	38
2.2.3	High-Resolution Structural Analysis Of The Optimal Oxime Cross-Link .....	47
2.2.4	Cross-Link Structure And Sequence Position In An $\alpha$ -Helical Coiled Coil .....	49
2.2.4.1	Regioisomers Of Previously Utilized Cross-Links .....	49
2.2.4.2	Sequence Positional Effects Of Residue Placement .....	53
2.2.5	Folding-Templated Synthesis Of A Multiply Cross-Linked Oligomer .....	58
2.2.6	Conclusions .....	62
2.3	SUMMARY OF INTRAMOLECULAR OXIME CROSS-LINKING .....	64
2.4	EXPERIMENTAL .....	66
2.4.1	General Information .....	66
2.4.2	Aminoxy-Functionalized Monomer Synthesis .....	67
2.4.3	Serine-Acylated Monomer Synthesis .....	73
2.4.4	Peptide Synthesis And Purification .....	76
2.4.5	Peptide Oxidation And HPLC Analysis .....	79
2.4.5.1	Helical Peptide Model System .....	79
2.4.5.2	Coiled-Coil Model System .....	79
2.4.6	NMR Assignment Of Oxime Isomers .....	80
2.4.7	Oxime Isomerization Experiments .....	80
2.4.8	Oxime Exchange Experiments .....	81

2.4.9	Circular Dichroism (CD) Spectroscopy .....	82
2.4.9.1	CD Of The Helical Peptide Model System .....	82
2.4.9.2	CD Of $\alpha$ -Helical Coiled Coils.....	83
2.4.10	Methionine Oxidation Stability Studies .....	86
2.4.11	Crystallization, Data Collection, And Structure Determination .....	86
3.0	INTERMOLECULAR OXIME AND HYDRAZONE CROSS-LINKS.....	88
3.1	MODEL SYSTEM FOR INTERMOLECULAR CROSS-LINK FORMATION .....	89
3.2	CROSS-LINK FORMATION .....	90
3.3	INTERMOLECULAR CROSS-LINKS AFFECT FOLDING.....	92
3.4	CROSS-LINK EXCHANGE WITH A SMALL MOLECULE.....	94
3.5	LINKER SELECTION IN A HELICAL MODEL SYSTEM.....	95
3.6	CROSS-LINK EXCHANGE FROM SEQUENTIAL ADDITION OF TWO LINKERS	96
3.7	INTERMOLECULAR CROSS-LINK FORMATION CONCLUSIONS.....	98
3.8	EXPERIMENTAL.....	100
3.8.1	General Information .....	100
3.8.2	Hydrazide-Functionalized Monomer Synthesis .....	101
3.8.3	Peptide Synthesis And Purification .....	104
3.8.4	Cross-Link Formation Reactions.....	105
3.8.5	Circular Dichroism Spectroscopy.....	106
3.8.6	Cross-Link Exchange With <i>O</i> -Methylhydroxylamine .....	106
3.8.7	Linker Mixing Experiments.....	107
3.8.7.1	Simultaneous Addition Of Two Linkers.....	107
3.8.7.2	Sequential Addition Of Two Linkers.....	107
4.0	CROSS-LINKING PEPTIDE LIGANDS BOUND TO A PROTEIN RECEPTOR.....	108
4.1	PROTEIN RECEPTOR SELECTION AND PEPTIDE DESIGN .....	108
4.2	CROSS-LINKING OF GP41-5 LIGANDS AFFECTS FOLDING AND AFFINITY....	114

<b>4.3</b>	<b>EFFECT OF RECEPTOR PRESENCE ON CROSS-LINKING REACTIONS.....</b>	<b>120</b>
4.3.1	Reactions Utilizing A Single Organic Linker .....	120
4.3.2	Reactions Utilizing Two Organic Linkers Simultaneously .....	123
<b>4.4</b>	<b>CONCLUSIONS AND PROSPECTIVE.....</b>	<b>129</b>
<b>4.5</b>	<b>EXPERIMENTAL.....</b>	<b>131</b>
4.5.1	Peptide Synthesis And Purification .....	131
4.5.2	Expression And Purification Of gp41-5 .....	133
4.5.3	Refolding Of gp41-5.....	134
4.5.4	Cross-Linking Reactions .....	134
4.5.5	Circular Dichroism Spectroscopy.....	135
4.5.6	Fluorescence Polarization Assays .....	136
<b>APPENDIX A.</b>	<b>INVESTIGATION OF THE THERMODYNAMICS OF CROSS-LINKING .</b>	<b>138</b>
A.1.	INTRODUCTION .....	138
A.2.	MODEL SYSTEM SELECTION AND DESIGN .....	139
A.3.	CROSS-LINK EFFECT ON FOLDING AND STABILITY.....	143
A.4.	THERMODYNAMICS OF UNFOLDING BY THERMAL-CHEMICAL DENATURATION.....	145
A.5.	CONCLUSIONS.....	151
A.6.	EXPERIMENTAL .....	152
<b>APPENDIX B.</b>	<b>HPLC CHROMATOGRAMS .....</b>	<b>159</b>
<b>APPENDIX C.</b>	<b>NMR SPECTRA .....</b>	<b>164</b>
<b>BIBLIOGRAPHY</b>	<b>.....</b>	<b>200</b>

## LIST OF TABLES

Table 1. Data from CD and thermodynamic analysis for peptides 18-26.....	44
Table 2. Data from CD and thermodynamic analysis for peptides 27-30.....	52
Table 3. Circular dichroism data for peptides 31-33.....	56
Table 4. MALDI-TOF data for peptides 1-6 and reaction products. ....	78
Table 5. MALDI-TOF data for peptides 17-34 and cyclized products.....	78
Table 6. Crystallographic data collection and refinement statistics for 22 and 22b. ....	87
Table 7. MALDI-TOF data for peptides 1, 35-37 and cyclized products.....	105
Table 8. Competition fluorescence polarization data for peptides 42 and 46-48.....	119
Table 9. MALDI-TOF Data for peptides 42-48, their cyclic products, protein gp41-5 and Flu-C38.....	132
Table A1. Thermodynamic parameters of unfolding for A1-A4, A2Cyc, A3Cyc, and A4Cyc. ....	146
Table A2. MALDI-TOF data for peptides A2-A4, A2Cyc, A3Cyc, and A4Cyc. ....	156

## LIST OF FIGURES

Figure 1. Schematic representation of templated DCC.....	2
Figure 2. DCL used to generate receptors for cationic polyamine guests.....	3
Figure 3. Strategy for DCL-based discovery of GAT1 inhibitors. ....	5
Figure 4. Crystal structure of the six helix bundle of gp41 from PDB: 1AIK. ....	7
Figure 5. Crystal structure of heparin analogue hirulog bound to thrombin from PDB: 2HGT .....	8
Figure 6. Common peptide secondary structures.....	9
Figure 7. Chemoselective peptide cyclization strategies and types of chemical bonds employed. ....	11
Figure 8. Common on-resin peptide cross-linking methods. ....	12
Figure 9. Examples of hydrogen bond surrogate helices. ....	14
Figure 10. Three examples of solution-phase cross-linking methods.....	16
Figure 11. Imine (Schiff base), hydrazone, and oxime structures, formation and hydrolysis. ....	18
Figure 12. Sequences of peptides 1-6 and schematic representation of cross-linking .....	24
Figure 13. Cross-link formation scheme and HPLCs. ....	27
Figure 14. Assignment of oxime stereoisomers of 2b.....	29
Figure 15. Mechanism and HPLC chromatograms of isomerization experiments. ....	31
Figure 16. Dynamic covalent exchange of cyclic oxime 2b and linear oxime 2c.....	32
Figure 17. Circular dichroism data for peptides 1-6. ....	34
Figure 18. Helical wheel, sequence, and crystal structure (PDB: 4DMD) of GCN4-p1. ....	36
Figure 19. Oxidation of methionine in the presence of serine-acylated U residue. ....	38

Figure 20. Sequences of peptides 18-26. ....	39
Figure 21. Example oxidation/cyclization reaction of peptide 22. ....	41
Figure 22. Helical signature by CD at 222 nm for peptides 19-26. ....	42
Figure 23. CD melts of peptides 18-26 and 19b-26b. ....	43
Figure 24. Percent recovery of helical minimum for peptides 19-26. ....	45
Figure 25. Thermodynamic impact of unnatural monomer insertion and cross-link formation. ....	46
Figure 26. Crystal structures of peptides 22 and 22b. ....	48
Figure 27. Sequences of peptides 27-30. ....	50
Figure 28. Helical signature by CD at 222 nm for peptides 27-30. ....	51
Figure 29. CD melts of peptides 18 and 27-30. ....	52
Figure 30. Thermodynamic data for peptides 27-30. ....	53
Figure 31. Sequences of peptides 18, 22, and 31-33. ....	54
Figure 32. Helical signature by CD at 222 nm for peptides 22 and 31-33. ....	55
Figure 33. CD melts of peptides 18, 22 and 31-33. ....	56
Figure 34. Thermodynamic data for peptides 22 and 31-33. ....	57
Figure 35. Sequence of peptide 34 and potential cross-linked products. ....	59
Figure 36. HPLC chromatograms of peptide 34 with and without added NaIO <sub>4</sub> . ....	60
Figure 37. CD Data for peptide 34. ....	61
Figure 38. HPLC chromatograms of oxidation reactions of peptide 34. ....	62
Figure 39. Sequences of peptides 1 and 35-37 and schematic representation of cross-linking. ....	90
Figure 40. Representative HPLC chromatograms of peptides 35-37 reacted with linker b. ....	92
Figure 41. Circular dichroism data for peptides 1 and 35-37. ....	93
Figure 42. Small molecule exchange reactions of peptides 35 and 37. ....	95
Figure 43. Chromatograms of simultaneous addition of linkers b and d to peptides 35-37. ....	96
Figure 44. Linker exchange reactions for peptides 35d and 37d treated with linker b. ....	98
Figure 45. Structure and sequence of gp41-5. ....	109

Figure 46. Sequences of designed CHR peptides. ....	110
Figure 47. CD and competition fluorescence polarization data for peptides 42-45.....	111
Figure 48. Sequence of Flu-C38 and scheme of competition fluorescence polarization. ....	113
Figure 49. Sequences of peptides 46-48 and schematic representation of cross-linking .....	115
Figure 50. HPLC chromatograms of cross-linking reactions with peptide 43 and linkers a-c. ....	116
Figure 51. CD Data for peptides 46-48.....	117
Figure 52. Competition fluorescence polarization data for peptides 46-48 and linkers a-c.....	118
Figure 53. Receptor-templated reactions of peptide 46 with linkers a-c. ....	122
Figure 54. Scheme and chromatograms for reactions involving addition of two linkers. ....	124
Figure 55. HPLC chromatograms of 46 with b and c treated simultaneously or independently. ....	126
Figure 56. Attempted exchange reactions of peptide 46 with linkers b and c. ....	127
Figure 57. Attempted protein-templated selection of a binary mixture of linkers with peptide 46. ....	128
Figure 58. Analytical HPLC chromatogram of purified gp41-5.....	133
Figure 59. Analytical GPC chromatogram of refolded gp41-5.....	134
Figure 60. Direct binding fluorescence polarization assay of gp41-5 and Flu-C38. ....	137
Figure A1. Sequence of VHP and peptide A1, wild-type structure, and CD spectrum of A1.....	140
Figure A2. CD thermal and thermal-chemical denaturation experiments of A1. ....	141
Figure A3. Sequences of peptides A1-A4, residue and cross-link chemical structures.....	142
Figure A4. CD scans of peptides A1-A4 and cyclic products A2Cyc, A3Cyc and A4Cyc.....	144
Figure A5. CD melts of peptides A1-A4 and cyclized products A2Cyc, A3Cyc, and A4Cyc.....	145
Figure A6. 3D melts of peptides A2-A4 and cyclic products A2Cyc, A3Cyc, and A4Cyc. ....	147
Figure A7. Enthalpy change of unfolding for peptides A2-A4 and cyclic products.....	148
Figure A8. Entropy change of unfolding for peptides A2-A4 and cyclic products. ....	149
Figure A9. Heat capacity and m for peptides A1-A4 and cyclic products. ....	150
Figure B1. Chromatograms of peptides 1, 6, and 6a. ....	159
Figure B2. Chromatograms of peptides 18-26 before (solid) and after (dashed) addition of NaIO <sub>4</sub> .....	159

Figure B3. Chromatograms of peptides 27-33 before (solid) and after (dashed) addition of NaIO <sub>4</sub> .....	160
Figure B4. Chromatograms of peptides 35-37 and cyclized products.....	161
Figure B5. Chromatograms of peptides 42-45. ....	162
Figure B6. Chromatograms of peptides 47-48 and cyclized products.....	162
Figure B7. Chromatograms of peptides A1-A4 and cyclic products A2Cyc, A3Cyc, and A4Cyc. ....	163

## LIST OF SCHEMES

Scheme 2.1. Synthesis of aminoxy-functionalized monomers 12a and 12b.....	24
Scheme 2.2. Synthesis of serine-acylated monomer 16a.....	25
Scheme 2.3. Synthesis of serine-acylated monomers 16a-16d.....	40
Scheme 3.1. Synthesis of hydrazide-functionalized monomer.....	101
Scheme A.1. Synthesis of Fmoc-L-azidolysine.....	143
Scheme A.2. Synthesis of Fmoc-L-azidolysine (A7).....	153

## LIST OF EQUATIONS

Equation 1 .....	83
Equation 2 .....	83
Equation 3 .....	84
Equation 4 .....	84
Equation 5 .....	85
Equation 6 .....	85
Equation 7 .....	85
Equation 8 .....	157
Equation 9 .....	157
Equation 10 .....	158
Equation 11 .....	158
Equation 12 .....	158

## LIST OF ABBREVIATIONS

Boc	<i>tert</i> -Butoxycarbonyl
DCC	Dynamic covalent chemistry
DCL	Dynamic covalent library
DCM	Dichloromethane
DIEA	<i>N,N'</i> -diisopropylethylamine
DMF	Dimethylformamide
Fmoc	9-fluorenylmethoxycarbonyl
Fmoc-OSu	9-fluorenylmethyl- <i>N</i> -succinimidyl carbonate
FPLC	Fast protein liquid chromatography
HCTU	2-(6-Chloro-1H-benzotriazole-1-yl)-1,1,3,3-tetramethylaminium hexafluorophosphate
HPLC	High performance liquid chromatography
HRMS	High resolution mass spectrometry
MALDI-TOF	Matrix-assisted laser desorption ionization-time of flight
MD	Molecular dynamics
MS	Mass spectrometry
NMR	Nuclear magnetic resonance
PPI	Protein-protein interaction
PyBOP	benzotriazol-1-yl-oxytripyrrolidinophosphonium hexafluorophosphate

RMSD	Root-mean-square deviation
TFA	Trifluoroacetic acid
THF	Tetrahydrofuran

## ACKNOWLEDGEMENTS

“If I have seen a little further it is by standing on the shoulders of Giants.” – Sir Isaac Newton, letter to Robert Hooke, 1676.

Earning an advanced degree like a PhD is never easy, nor is it a solitary undertaking. There are many people that have to be acknowledged – the giants on whose shoulders I have stood.

First, I have to thank my advisor Dr. W. Seth Horne, who is a great teacher and mentor. I originally met and talked to Seth in the fall of 2009 about joining his research group. At the time, there were several other students interested, and I’ll probably never know why he picked me. That decision probably ended up being the best thing that could have happened to me during graduate school. Seth’s guidance throughout the process of earning my PhD has been invaluable. From my earliest efforts in the lab – where I probably assumed that I knew too much – to the final project that has, unfortunately, failed to pan out precisely how I would have hoped, Seth’s understanding, patience, and dedication have been a model for the kind of scientist I hope to be one day.

The other members of the Horne lab have been a constant source of advice and camaraderie. I would particularly like to acknowledge Dr. George Lengyel and Zach Reinert, who no doubt remember some of the earliest, ridiculously inadequate attempts at presenting and writing about research, and who have become true friends. The other members of the Horne group – Kaylyn Oshaben, Nathan Tavenor, Halina Werner, Kelly George, and Hajira Hotiana – have helped me along the way, providing advice and assistance. There are several undergraduate students I’ve also had the pleasure of mentoring, and who have helped move along my research, even in unexpected ways – Matt Loch, Brian Sandridge, Joe Skowronski, and James McKay. Each of these individuals has been, in their own way, an inspiration and I wish them nothing but the best.

My family deserves more credit than can be expressed in words. My parents have been a constant source of support, and the love of learning they instilled in me growing up is what ultimately led to the

choice to go to graduate school. My grandmother and my aunts, who still live nearby, have also been a source of support and perspective, and I will miss them when I leave Pittsburgh.

To my girlfriend, Erin, who has been with me the entire time through graduate school and then some, I can only express the utmost gratitude. It isn't an exaggeration to say that I could not have done this without you, and I owe you more than I can ever hope to repay. This hasn't been easy, and I am forever grateful for your love and understanding through the stress, self-doubt, and sleepless nights. I love you.

## 1.0 INTRODUCTION

### 1.1 DYNAMIC COVALENT CHEMISTRY

Dynamic covalent chemistry (DCC) takes advantage of reversible covalent bond formation in order to obtain libraries of molecules at equilibrium under thermodynamic control.<sup>1,2,3</sup> The use of a small number of chemical building blocks can generate a relatively large number of library constituents. Due to the equilibrium achieved under the conditions of dynamic covalent exchange, DCC is a powerful tool to probe thermodynamic minima. Stabilization of library members can potentially result from favorable intramolecular interactions and has been utilized to investigate the design of folded structures based on natural and non-natural backbones.<sup>4</sup> Library members can also be stabilized by intermolecular interactions thereby providing a method to probe for structures which form stable assemblies or aggregates, or which participate in intermolecular binding interactions in a host-guest fashion or ligand-receptor fashion.<sup>4</sup>

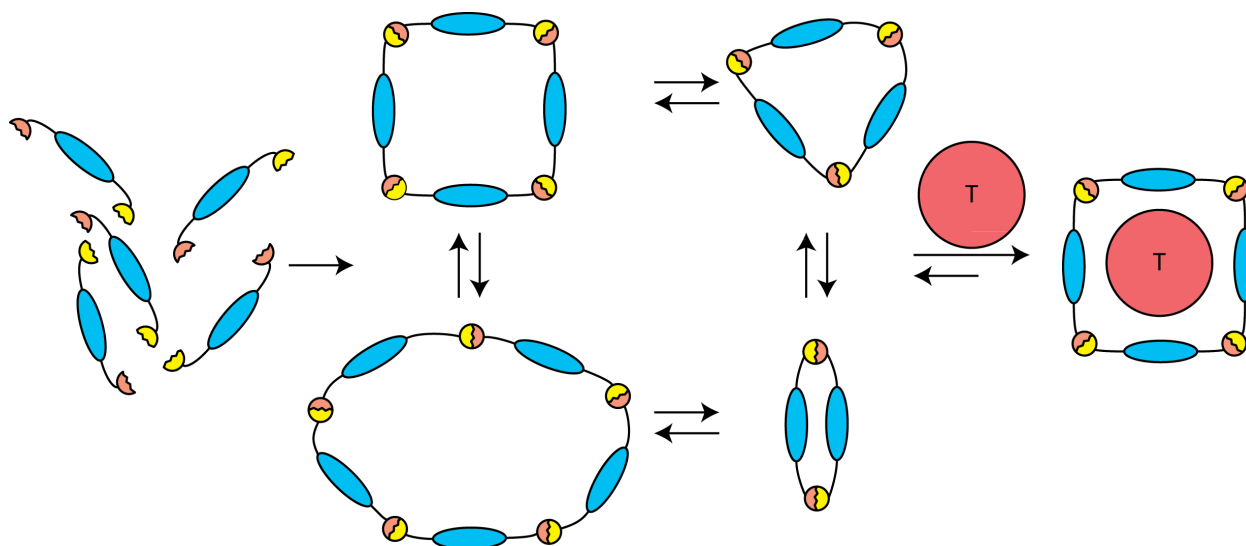


**Figure 1.** Schematic representation of templated DCC.

Due to the thermodynamic control of a dynamic covalent library (DCL), such systems have been shown to be responsive to stimuli. The use of pressure, temperature, or a molecular template can influence the product distribution in a DCL.<sup>1,2</sup> Molecular templating has been utilized for the selection of species that act as hosts or receptors, as well as for the discovery of new ligands.<sup>1,2,3,4</sup> Amplification is ideally selective for the compound with the most favorable binding to a given templating molecule, though there are exceptions due to the complex nature of DCLs (Figure 1). A report on the use of DCC to generate organic cages as receptors for positively charged polyamine guests made use of reversible disulfide bond formation to establish a DCL (Figure 2).<sup>5</sup> Addition of polyamine species, spermine and spermidine, was shown to change the product distribution of the disulfide-linked architectures in the DCL. This type of template-driven synthesis of multi-component organic cages can lead to the discovery of novel hosts for guest molecules. Similar principles have been applied to the generation of receptors for biologically relevant guests including but not limited to trimethyl lysine<sup>6</sup> and dimethyl arginine.<sup>7</sup>

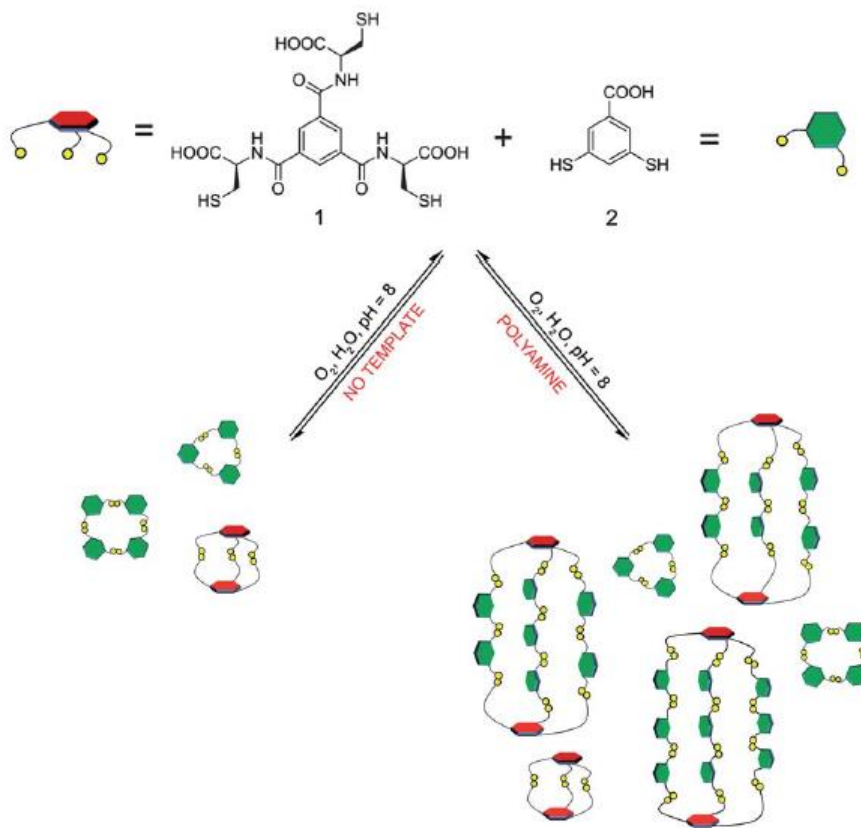


**Figure 2.** DCL used to generate receptors for cationic polyamine guests. Reproduced from Stefankiewicz, et al., *Chem. Sci.*, **2012**, 3, 2326. Permission for reproduction granted by The Royal Society of Chemistry, copyright 2012.

Peptide and protein folding offers a fertile ground for dynamic covalent chemistry given the subtle interplay among non-covalent interactions within and between ligands and proteins. The use of reversible chemistry to affect folded structures has included biologically-derived molecules wherein intermolecular and intramolecular interactions form the basis for amplification of folded structures. Prior applications of this strategy include the formation of a DCL based on disulfide formation and exchange in palindromic peptide sequences.<sup>8</sup> This library was capable of forming a number of possible products, including cyclic monomers, acyclic parallel and antiparallel species, cyclic trimers, and larger macrocyclic oligomers. The observed distribution of these products changed in response to concentration and solvent conditions. Further studies in biomolecule-inspired DLCs have been used to identify  $\beta$ -sheet

forming oligopeptide building blocks,<sup>9</sup> stable  $\alpha$ -helical bundles resulting from metal chelation,<sup>10</sup> and to estimate folded free energy in an equilibrating system based on bovine pancreatic polypeptide where an amide bond is replaced with an exchangeable thioester.<sup>11</sup>

Proteins and nucleic acids have also served as useful templates for the selection of small molecule ligands from DCLs.<sup>4, 12</sup> In these systems, a collection of small molecules capable of forming DCLs are equilibrated in the presence or absence of a protein target. The enhancement of particular library members in the presence of the protein receptor is inferred to be due to the enhanced interaction of those library members with the receptor. Subsequent analysis of the binding interaction can lead to the identification of small-molecule binders to protein receptors in a fashion that is complementary to high-throughput or fragment-based screening. A number of bioactive compounds have been identified for protein-based receptors through this methodology, where the receptors include carbonic anhydrase,<sup>13</sup> glutathione-S-transferases,<sup>14, 15</sup> and calmodulin.<sup>16</sup> The use of a hydrazone-based library targeting  $\gamma$ -aminobutyric acid transporter 1 (GAT1) was shown to lead to the discovery of novel compounds for GAT1 inhibition (Figure 3).<sup>17</sup> Mass spectrometry-based inhibition assays showed that the amplified library member had a  $pIC_{50}$  of 5.3, nearly identical to the natural substrate  $\gamma$ -aminobutyric acid. Further optimization of the lead compounds through synthesis of stable analogues showed maintenance of binding affinity.<sup>17</sup> Additionally, some small peptide-like substrates have been utilized in the generation of template-selected DCLs to target PPIs involved in HIV viral budding.<sup>18</sup> In these studies, templated selection of DCLs utilizing protein receptors is generally limited to relatively small library sizes, library members with high similarity to known binders to the target proteins, and to library members with limited size.

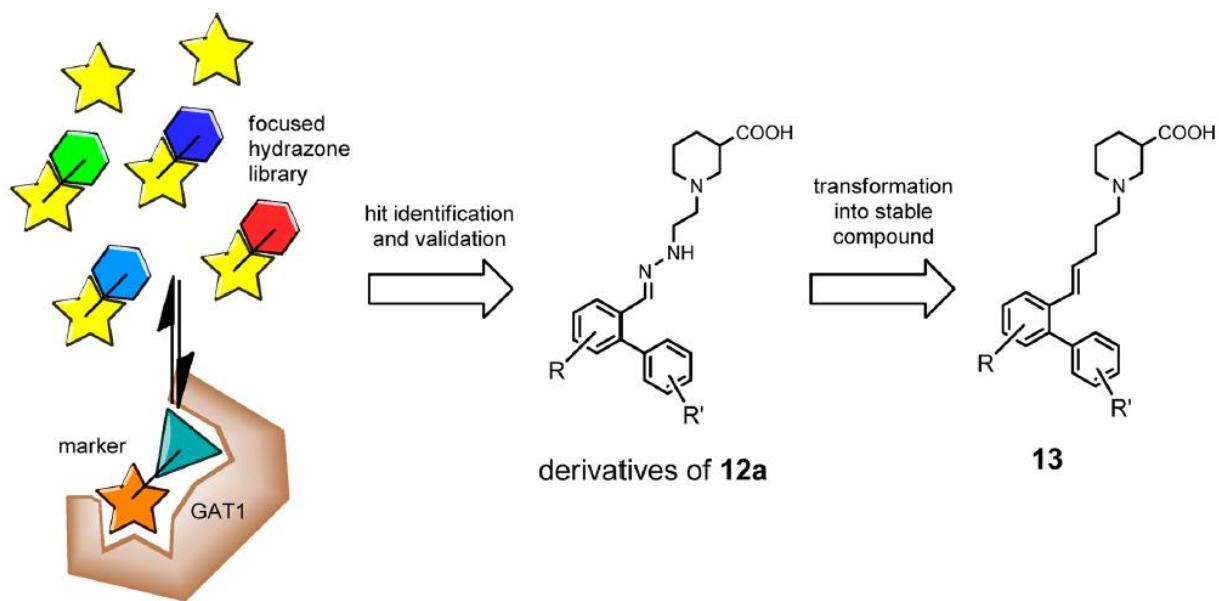


**Figure 3.** Strategy for DCL-based discovery of GAT1 inhibitors. Reproduced with permission from Sindelar, et al., *J. Med. Chem.*, **2013**, *56*, 1323. Copyright 2013 American Chemical Society.

Given the known applicability of biomolecules in DCC, we have sought to utilize the tools of dynamic selection to furnish a general strategy for the development of peptide based protein-protein interaction inhibitors. This requires the development of peptide cross-linking technology which is both bioorthogonal and potentially reversible under aqueous conditions. Development of this technology would allow for the use of peptide based DCLs to generate potent binders to protein-based targets.

## 1.2 PEPTIDES AS THERAPEUTICS

The ubiquitous nature of protein-protein interactions (PPIs) in biological systems and their importance in the genesis of disease makes specific binders to protein-protein interfaces paramount in biomedical research.<sup>19</sup> Scaffolds to inhibit protein-protein interactions include small molecules, peptides, and peptide mimetics.<sup>20</sup> Small molecules represent the largest class of PPI inhibitors, but are limited in applicability

due to relatively small binding surfaces.<sup>19</sup> Alternatively, due to their similarity to natural protein binders, peptides constitute an attractive class of therapeutics.<sup>21</sup> The ability of peptides to engage with extended binding interfaces, and their general non-immunogenicity, has led to increased interest in peptide-based PPI inhibitors in recent years. While naturally derived peptide based drugs, such as insulin, have been clinically relevant for decades, rationally designed peptide therapeutics have only been possible since the advent of solid phase peptide synthesis (SPPS) and biochemical tools for manipulation of protein sequences during or following *in vivo* expression.<sup>21</sup>

Rationally designed peptide therapeutics include enfuvirtide, which prevents HIV infection of host cells through interaction with the viral envelope glycoprotein gp41.<sup>22</sup> Upon recognition of lymphocyte receptors by viral proteins, gp41 undergoes a conformational change from an extended three-helix bundle to a more compact six-helix bundle. This conformational change brings the viral capsid and the cell membrane into proximity, triggering the formation of a fusion pore and release of the viral material into the host cell. By binding to gp41 in its extended conformation, enfuvirtide prevents the formation of the compact six helix bundle and thus fusion pore formation (Figure 4).

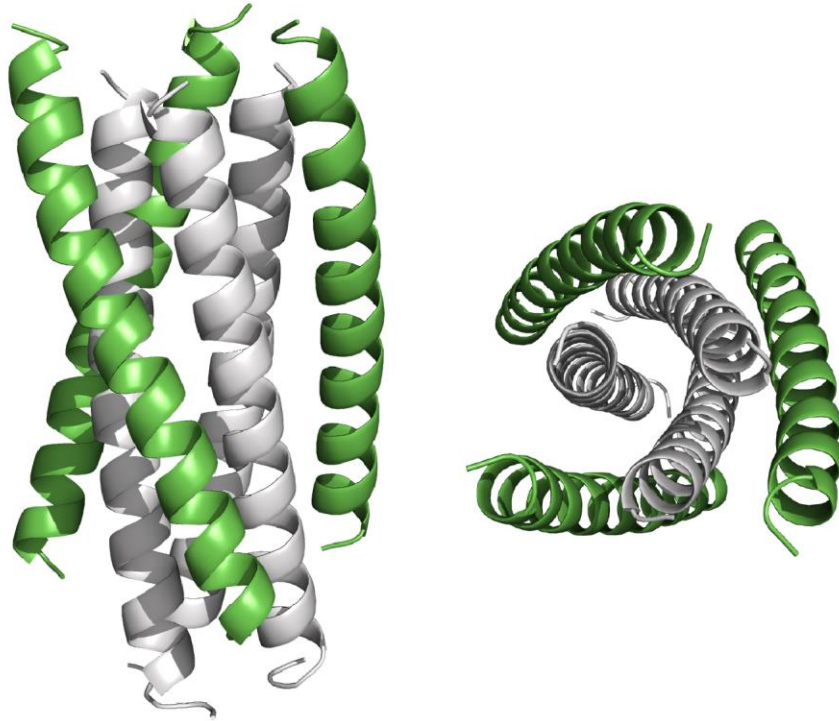


**Figure 4.** Crystal structure of the six helix bundle of gp41 from PDB: 1AIK. N-terminal and C-terminal helices are shown as grey and green, respectively.

Another known peptide drug is the 20-amino acid sequence bivalirudin which is an analogue of heparin that is clinically employed to slow blood clot formation as an alternative to heparin.<sup>23</sup> Bivalirudin binds to thrombin, a serine protease that is central to the clotting process, in an extended conformation occupying both the proteolytic active site and the anion-binding exosite similar to other heparin analogues (Figure 5).<sup>24</sup> Due to its high specificity and small size bivalirudin represents an ideal peptide therapeutic.

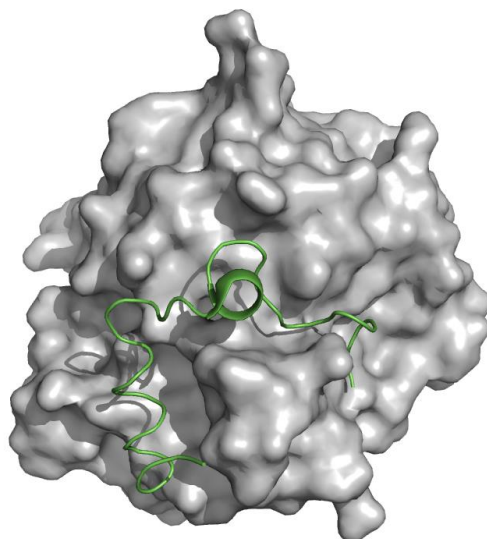


**Figure 5.** Crystal structure of heparin analogue hirulog bound to thrombin from PDB: 2HGT

Of note in both of these examples is that the peptide ligands are both principally unstructured in their unbound state. This represents one of the major limitations of peptide based therapeutics: due to their poorly structured nature, they can have lower inhibitory activity than well-structured proteins, and are easily degraded by proteases which typically recognize extended backbone conformations.<sup>25</sup> Additionally, peptide therapeutics are almost exclusively used to target extracellular proteins as poor cell permeability prevents application to intracellular targets.<sup>26</sup> Addressing these limitations constitutes an ongoing and active area of study towards improving peptide-based therapeutics for clinical applications.

### **1.3 FORMATION OF SECONDARY STRUCTURES IN PEPTIDES**

The emergence of secondary structural elements from primary amino acid sequences remains challenging to predict. However, efforts toward understanding polypeptide folding tendencies have

yielded information about how to predict – and in some cases control – folding patterns.<sup>27</sup> Each type of secondary structure is defined by a different intramolecular hydrogen bonding pattern (Figure 6).<sup>28</sup> Turn regions are characterized by close spatial relationships between amino acids spaced 1 to 5 residues apart, with corresponding hydrogen bonds between the residues in the turn motif.  $\beta$ -Sheets are defined by interstrand hydrogen bonds in a parallel or antiparallel fashion. Though several types of helices are found in nature,  $\alpha$ -helices are the most common and are delineated by a network of intramolecular hydrogen bonds between backbone amide protons and carbonyl oxygens arranged in an  $i \rightarrow i+4$  pattern. Secondary structural elements are often (though not exclusively) involved in protein-protein interaction interfaces.<sup>29</sup> Thus understanding of the folding in polypeptide sequences allows for identification of more potent inhibitors of protein-protein interactions. Such structures also contribute to fundamental understandings of physical interactions that drive folding.

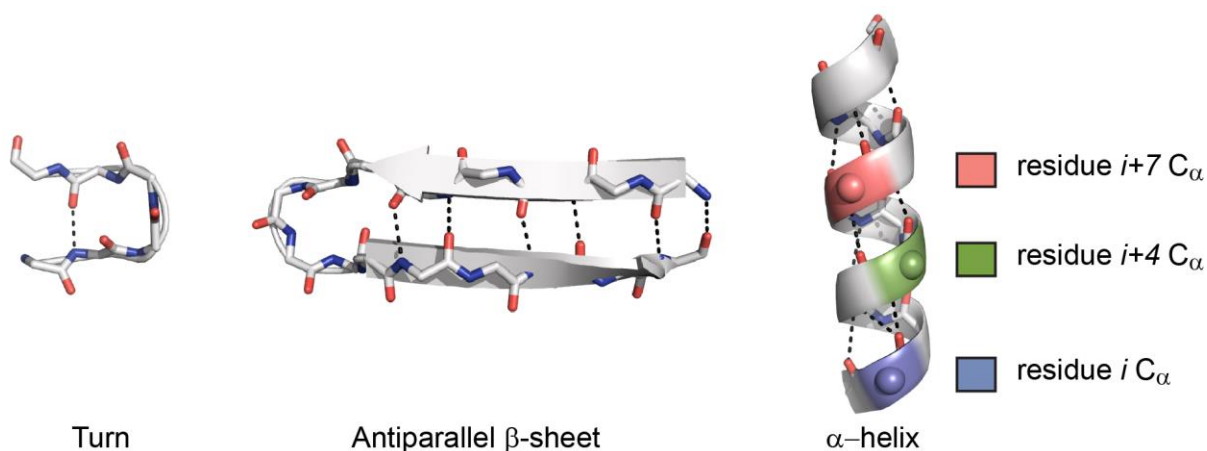


**Figure 6.** Common peptide secondary structures. Main-chain hydrogen bonds are shown as dashed lines.

### 1.3.1 Controlling $\alpha$ -Helical Folding Patterns

Amongst secondary structural elements in proteins, one of the most common is the  $\alpha$ -helix.<sup>28</sup> Helices are also the most common secondary structure found to participate in protein-protein binding interactions.<sup>30</sup> Accordingly, significant research has been invested in understanding and controlling helical folding patterns. The hydrogen bonding network of  $\alpha$ -helices results in a right-handed spiral conformation of the peptide backbone. The resulting 3.6 residues per helical turn leads to the display of amino acid side chains on the same face of the helix at an  $i \rightarrow i+7$  pattern (a heptad repeat). The side chains of residues at  $i \rightarrow i+4$  or  $i \rightarrow i+3$  are also spatially near each other (Figure 6).

Research into the primary sequences of naturally occurring and *de novo* designed  $\alpha$ -helices has revealed specific residue preferences for helical conformations.<sup>27, 31, 32</sup> The naturally occurring amino acids alanine, arginine, leucine, and lysine have high inherent helical propensity, while glycine and proline strongly disfavor  $\alpha$ -helical folds. Introduction of oppositely charged residues in close proximity in an  $\alpha$ -helix can stabilize the fold through electrostatic interactions called “salt bridges.”<sup>33</sup> Restricting the conformational preferences of the peptide backbone through  $C_\alpha$  disubstitution can also be used to influence helical folding.<sup>27</sup>

Due to the unidirectional arrangement of the backbone amides in an  $\alpha$ -helix, helices have a large net molecular dipole. The net dipole moment results in positive charge towards the N-terminus and negative charge towards the C-terminus of an  $\alpha$ -helix. Resulting unfavorable electrostatic interactions between the positively charged N-terminal amine or the negatively charged C-terminal carboxylate act to destabilize the helical fold.<sup>34</sup> Accordingly, strategies used to ameliorate this net molecular dipole, often termed “capping,” have been used to stabilize helical folds. This can be achieved through the introduction of negatively and positively charged residues at the N-terminus and C-terminus, respectively, or through N-terminal acylation and C-terminal amidation.<sup>27, 35</sup> Capping helps to ameliorate the helical dipole and thus stabilize the helical conformation.

## 1.4 COVALENT CONSTRAINTS IN PEPTIDE FOLDING

As discussed above, the development of well-folded peptide sequences is desirable for the generation of potential peptide-based therapeutics; however, short oligomers tend to be poorly structured under aqueous conditions. Nature often utilizes covalent bonds in the form of disulfides to constrain short sequences into defined folding patterns.<sup>36</sup> Disulfide cyclization is found in very short natural sequences with defined folds including conotoxins and defensins amongst other functional peptides.<sup>37, 38</sup> Taking inspiration from nature, chemists have sought to utilize disulfide formation and other chemoselective and/or biocompatible reactions to constrain short peptide sequences into defined folds. This strategy is generally referred to as “cross-linking” or “stapling.”<sup>39, 40</sup> Cross-linking strategies have commonly been employed to constrain peptides into helical conformations, though there are examples of covalent constraints being used to stabilize other structural elements.<sup>39, 41, 42</sup> A number of methods have been developed for both intramolecular side-chain to side-chain cross-linking as well as intermolecular cross-link formation by reaction of bifunctionalized peptides with bifunctionalized small molecules (Figure 7).

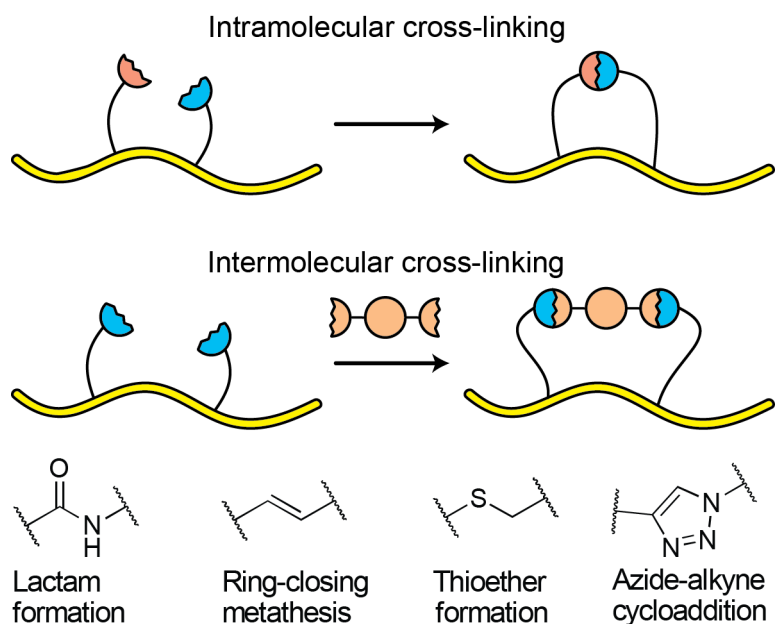


**Figure 7.** Chemoselective peptide cyclization strategies and types of chemical bonds employed.

### 1.4.1 On-Resin Peptide Cyclization Techniques

Peptide cyclization requires reactions that proceed cleanly even in the presence of other side chain functional groups. Though disulfide formation constitutes such a chemoselective reaction, disulfides are not fully bioorthogonal; chemoselective formation of disulfides can only be achieved using sequences which lack any other cysteine residues. Several alternative strategies have been developed for selective cross-linking of peptides during on-resin solid phase peptide synthesis (SPPS) (Figure 8).

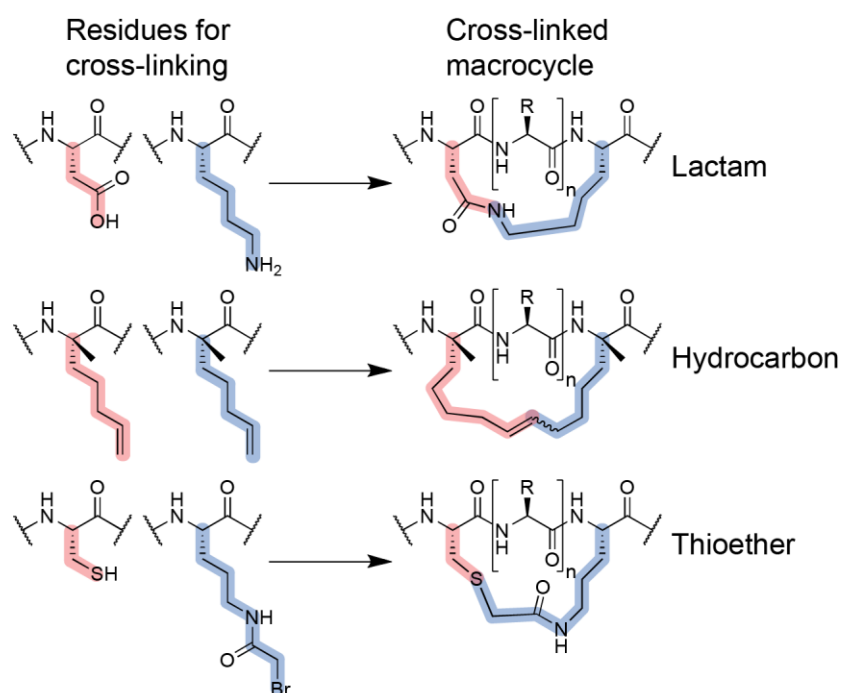


**Figure 8.** Common on-resin peptide cross-linking methods.

One of the earliest peptide cross-linking methods explored was amide bond formation, resulting in a cyclic lactam (Figure 8).<sup>43</sup> Lactam cyclization requires on-resin manipulation of side chains functionalized with carboxylic acids (e.g. aspartic acid, glutamic acid) and amines (e.g. lysine or lysine homologues). These groups must be protected orthogonally to the other functional side chains in the

peptide during SPPS. Both Boc- and Fmoc-based syntheses have been performed to install lactam side-chain cross links. Generally, orthogonally protected Asp, Glu, and Lys residues are utilized, where the orthogonal protecting groups are selectively cleaved under appropriate conditions, leaving the other side chain protecting groups intact. The peptide is then cyclized on-resin through the formation of an activated ester of the carboxylic acid and subsequent intramolecular reaction to form the lactam. Extensive work on lactam cyclization has been carried out to establish synthetic strategies, the structural features of lactam-cyclized peptides that best induce helical conformations, and how lactam cross-linked helices affect binding to biological receptors.<sup>44, 45, 46</sup>

An alternative to lactam formation is the reaction of unnatural olefin side chains to generate a hydrocarbon-based macrocycle through a ring closing metathesis reaction (Figure 8).<sup>47, 48</sup> This strategy has been widely examined to determine the structural and stereochemical factors that best induce helix formation,<sup>48, 49</sup> and to examine how such cross-linked helices behave in ligand-receptor interactions.<sup>50, 51, 52</sup> It has been postulated that side chain hydrocarbon cross-links can improve helicity and affinity for biomolecules.<sup>50, 51, 52, 53</sup> Additionally, some work suggests that hydrocarbon cross-links may improve cellular uptake<sup>50, 53</sup> but this remains a point of some controversy.<sup>54</sup>

Other chemoselective cross-linking methods include the formation of thioethers, which takes advantage of the general paucity of cysteine residues in naturally occurring sequences (Figure 8).<sup>55</sup> Although, in principle, thioether ligation can be performed on unprotected peptide substrates, most published examples of thioether cross-linking take advantage of on-resin manipulation of the peptide. This is necessary due to the difficulty in selectively installing an alkyl halide functionality on side chains of unprotected peptides and the inability of alkyl halides to persist through SPPS. Accordingly, one common strategy utilizes an orthogonally protected lysine, which can be deprotected and subsequently functionalized with an alkyl halide. A second orthogonal deprotection is then utilized to unmask a cysteine or other thiol-functionalized amino acid, which selectively reacts with the alkyl halide to form the thioether cross-link. Thioethers have been less well-studied than lactam or hydrocarbon cross-linking methods, possibly due to the synthetic difficulty in having two chemoselective deprotection/ligation steps;

however, there have been reports on the use of thioether-cyclized helices as ligands for protein receptors.<sup>55</sup>

Cyclization and helix induction can also be achieved through covalent constraint of backbone atoms (Figure 9). Early work towards this end utilized hydrazone formation between aldehyde-functionalized N-terminal amines on peptide substrates and a nearby hydrazide in the peptide backbone.<sup>56</sup> The resulting cyclic oligomer effectively replaces a backbone hydrogen bond with a covalent bond, generating a “hydrogen-bond surrogate,” (HBS) helix. More recent work employed other reactions for the creation of hydrogen bond surrogates, most notably ring-closing metathesis to generate hydrocarbon HBS helices.<sup>57</sup> The HBS strategy generally requires precise mimicry of the geometry of the hydrogen bond that is replaced. Hydrogen bond surrogacy has proven to be a useful technique to improve both helical folding and affinity for biomolecules.<sup>58, 59, 60, 61</sup>

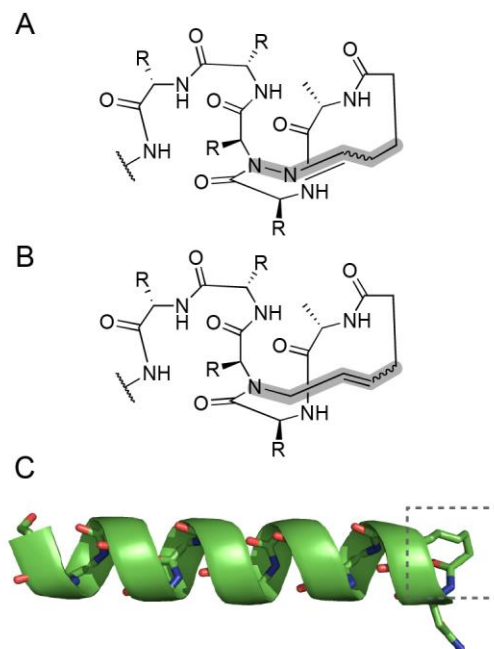


**Figure 9.** Examples of hydrogen bond surrogate helices.

(A) Structure of a HBS helix via hydrazone formation. (B) Structure of a HBS helix formed through olefin metathesis. (C) Hydrogen bond surrogate in an  $\alpha$ -helix from PDB: 4MZL. The surrogate bond is highlighted by a dashed box.

While on-resin cyclization techniques have proven to be useful for affecting helical folding patterns as well as improving affinity for biological targets, the complex manipulations necessary to introduce the cross-links limit accessibility to a large number of cyclic oligomers in a combinatorial manner.

#### **1.4.2 Solution Phase Peptide Cyclization Techniques**

Though there are many techniques to cyclize peptides on-resin, cyclizing fully unprotected peptides in solution is considerably more difficult. Cyclization of unprotected peptides requires orthogonal reactivity of the participating functional groups to the other functional groups found in polypeptide chains. Without orthogonal reactivity the primary sequence space amenable to these methods is severely limited. Accordingly, prior research has sought to develop peptide cyclization strategies which can take place on fully unprotected peptide substrates. Such work seeks to expand the scope of cross-linking of polypeptide sequences.

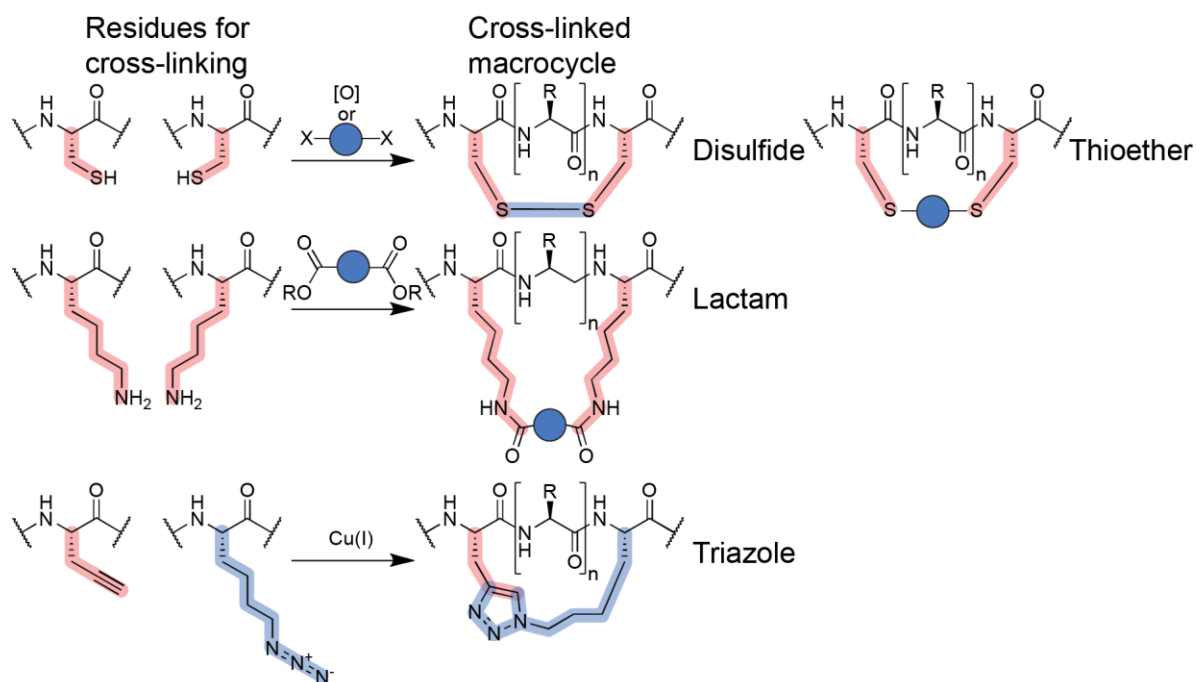


**Figure 10.** Three examples of solution-phase cross-linking methods.

Naturally occurring amino acid side chains have been employed for solution-phase cross-link formation, typically by utilizing cysteine<sup>62, 63</sup> or lysine<sup>64</sup> (Figure 10). Bis-lactam formation through reaction of peptidic amine side chains and activated diesters has been employed for selective cyclization in solution phase.<sup>64</sup> This strategy is amenable to use in developing peptides for biological applications, but is limited by the necessity of removing all other amine-functionalized side chains in order to obtain selective cross-link formation.<sup>65</sup> The unique reactivity of cysteine has been capitalized upon both in disulfide and thioether formation as a solution-phase cross-linking technique. Disulfide formation provides a ready access to cyclic peptides in aqueous solution, and has been applied to stabilize helices.<sup>66</sup> Peptides containing two cysteine residues have also been cyclized by thioether formation in solution phase, and applied to protein-protein interaction inhibitors.<sup>62, 63, 67</sup> A recently developed strategy for chemoselective cyclization in solution involves the exploitation of  $S_NAr$  coupling for perfluoroarylation of cysteine residues.<sup>68</sup> This cross-linking technique is amenable to combinatorial synthesis of a wide array of cyclic products,<sup>69</sup> and can affect folded structure and biomolecule affinity.<sup>68</sup> However, these techniques

are limited by the necessity of performing the cyclization reaction in the presence of organic solvent or co-solvent. Disulfide formation and related techniques for cysteine thioether cross-linking are also limited by the lack of orthogonality to cysteine residues in peptide substrates.

The use of unnatural residues offers greater selectivity in cross-link formation while limiting the necessity of primary sequence alteration. Azide-alkyne cycloaddition (“click chemistry”) has been widely employed for biomolecule labeling<sup>70</sup> as well as in the construction of hybrid backbones<sup>71, 72</sup> or cyclized biomolecules.<sup>42, 73, 74</sup> The orthogonality of click chemistry has enabled it to be employed for on-resin<sup>75</sup> and solution-phase cyclizations<sup>76</sup> of fully unprotected peptide substrates (Figure 10). It has been shown that triazole-cyclized peptides can have improved helical folding and increased biological activity.<sup>76</sup> However, the azide-alkyne cycloaddition reaction often requires the use of organic cosolvents and may not be compatible with redox-sensitive biomolecules.<sup>42, 76</sup>

The formation of Schiff bases and related molecules (oximes, hydrazones) offers an alternative strategy for solution-phase peptide cyclization, and has been employed previously for this purpose (Figure 11).<sup>77, 78</sup> The formation of oximes and hydrazones is generally recognized as bioorthogonal due to the relative scarcity of aldehyde or ketone functionalities in biological systems and the near complete lack of hydrazine or aminoxy functionalities. The enhanced nucleophilicity of hydrazine and aminoxy functionalities reportedly stems from the  $\alpha$ -effect due to the presence of an atom with unshared electron pairs adjacent to the nucleophilic center.<sup>79</sup> Owing to the poor hydrolytic stability of imines, they are rarely employed in the context of aqueous systems. Hydrazones and oximes, which are more hydrolytically stable than imines,<sup>80</sup> have been widely utilized in biomolecule related applications.<sup>81, 82</sup> Early work in the context of peptides employed oxime formation to form cyclic peptide backbones in solution on unprotected peptide substrates.<sup>77, 78</sup>

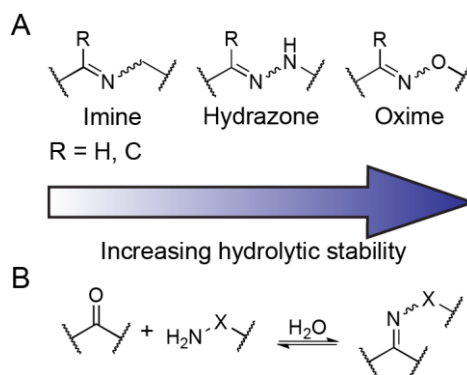


**Figure 11.** Imine (Schiff base), hydrazone, and oxime structures, formation and hydrolysis. (A) Imine, hydrazone, and oxime chemical structures and their hydrolytic stability. (B) Condensation and hydrolysis of generalized imine, hydrazone, oxime bonds.

While there are some solution-phase cyclization techniques available for use with peptides these methods have generally not been developed as fully as on-resin cyclization. Expanding the scope and applicability of solution-phase cyclization offers the possibility of performing cross-linking chemistry under conditions which are fully compatible with biological systems.

## 1.5 PROJECT GOALS

The use of chemoselective cyclization techniques to control peptide folding and affect biological activity remains an active area of research. However, previously developed techniques are limited in a number of ways. First, most techniques for peptide cyclization require extensive on-resin manipulation of the substrate, which introduces synthetic complexity as well as limits the scope of peptide sequences which can be efficiently synthesized. Second, though some solution-phase cyclization techniques have been developed, they are not fully bioorthogonal and cannot be employed without the use of organic solvents. Third, nearly all previous cross-linking types are irreversible; thus, evaluation of different target structures requires constant redevelopment and optimization of the cross-linked position and/or structure

within the peptide sequence. We have sought to create cross-linking chemistry that is employable in near-physiological conditions and which is dynamically reversible. Such technology offers distinct advantages over previously developed methods. First, the ability to form cross-links under benign buffered aqueous conditions allows for the possibility of utilizing receptor-based templating of the peptide structure during cross-link formation. Thus, one could employ a poorly structured peptide substrate which, when bound to an appropriate receptor, can be chemoselectively cyclized, effectively trapping the bioactive fold. Such chemistry could be used to discern the biologically active bound state of short sequences which bind to proteins. Second, employing dynamically reversible bonds offers the possibility of generating multiple different cross-linked structures, each of which has different folding tendencies, from a single peptide sequence. This allows the utilization of receptor templated selection of a particular cross-linked topology, as employed in DCC, to select for and isolate the structure which best binds to the receptor. We have pursued both of these goals through the use of oxime and hydrazone formation, which provides both a bioorthogonal and potentially reversible cross-link.

### **1.5.1 Intramolecular Oxime Cross-link Formation**

In early work in the generation of oxime cross-linked peptides, as discussed in detail in Chapter 2, we utilized an intramolecular strategy to generate the desired cross-link oxime. The oxime cyclization proceeds through a mild oxidative unmasking of a side chain glyoxyl aldehyde, which then undergoes a condensation reaction with an appropriately poised aminoxy-functionalized residue to furnish the cyclic oxime product as one of two (*E* or *Z*) stereoisomers. This type of cross-link formation was found to affect helical folding in a short (17-residue) polypeptide model system, and to undergo dynamic covalent exchange.

In a more complex quaternary structure, which provides the basis for investigating oxime side chain cross-links in a basic protein-protein interaction, we examined the importance of both the structure and sequence position of the oxime cross-links. In this system, the cross-links were found to be mildly

disruptive of the helical fold, though stabilizing to the protein-protein complex provided that no favorable intramolecular interactions are perturbed. Analysis of the structural factors important to quaternary structure stabilization allowed identification of an optimal residue pairing for future cross-linking studies. High-resolution structural data of the optimal cross-link demonstrates its compatibility with a helical fold. As a step towards receptor-templated cross-link formation in a bioactive fold, we utilized this model quaternary structure for the selective synthesis of one particular bicyclic species in a system where multiple possible cyclic products can result.

### **1.5.2 Intermolecular Oxime and Hydrazone Cross-link Formation**

Owing to the poor reversibility observed in the intramolecular formation of oxime cross-links, we sought to develop alternative methods based on intermolecular cross-linking between bifunctionalized peptides and bifunctionalized small molecules as discussed in Chapter 3. This strategy is capable of furnishing multiple cross-linked products depending on the small molecule utilized in cross-link formation, thus allowing for a general and divergent synthesis of different cross-linked structures from a small set of peptide sequences. Intermolecular cross-linking was found to be capable of affecting the folding in a short model peptide, albeit somewhat less predictably than was found in the case of intramolecular cross-links. However, the use of intermolecular oxime and hydrazone formation was found to furnish a system more readily capable of dynamic covalent exchange as demonstrated through the ability to remove the cross-link and regenerate the starting linear peptide and in the ability to exchange the cross-linking small molecule.

### **1.5.3 Cross-Linking Peptide Ligands In The Presence Of A Protein Receptor**

Having established a cross-linking method which is fully biocompatible through the use of intermolecular oxime formation, we demonstrated that the presence or absence of a protein receptor can influence the

product distribution amongst cross-linked species. In this work we utilized gp41-5, a protein consisting of five of the six helical segments of the HIV glycoprotein gp41, as the receptor. We generated peptides derived from the C-terminal heptad repeat of gp41 as ligands for the gp41-5 receptor. Through the combination of a small set of peptides with two nucleophilic aminoxy-functionalized residues and several commercially available dialdehydes, we demonstrate that the receptor can affect the outcome of cross-linking reactions. Attempts at screening cross-linking reactions which contain two dialdehydes in order to selectively amplify a single collection of cross-linked isomers are described. In these experiments, the outcome of the reaction does not demonstrate selectivity of a particular linker, suggesting that the kinetics and/or thermodynamics of the system are not suitably balanced to achieve linker selection. Nevertheless, further development of this cross-linking technology may achieve the desired goal of selective cross-linked product amplification.

## 2.0 INTRAMOLECULAR OXIME CROSS-LINK FORMATION

Work detailed in this chapter has been published as:

1. Haney, C. M.; Loch, M. T.; Horne, W. S.; “Promoting peptide  $\alpha$ -helix formation with dynamic covalent oxime side-chain cross-links.” *Chemical Communications*, **2011**, *47*, 10915-10917
2. Haney, C. M.; Horne, W. S.; “Oxime side-chain cross-links in an  $\alpha$ -helical coiled-coil protein: Structure, thermodynamics, and folding-templated synthesis of bicyclic species.” *Chemistry – A European Journal*, **2013**, *19*, 11342-11351

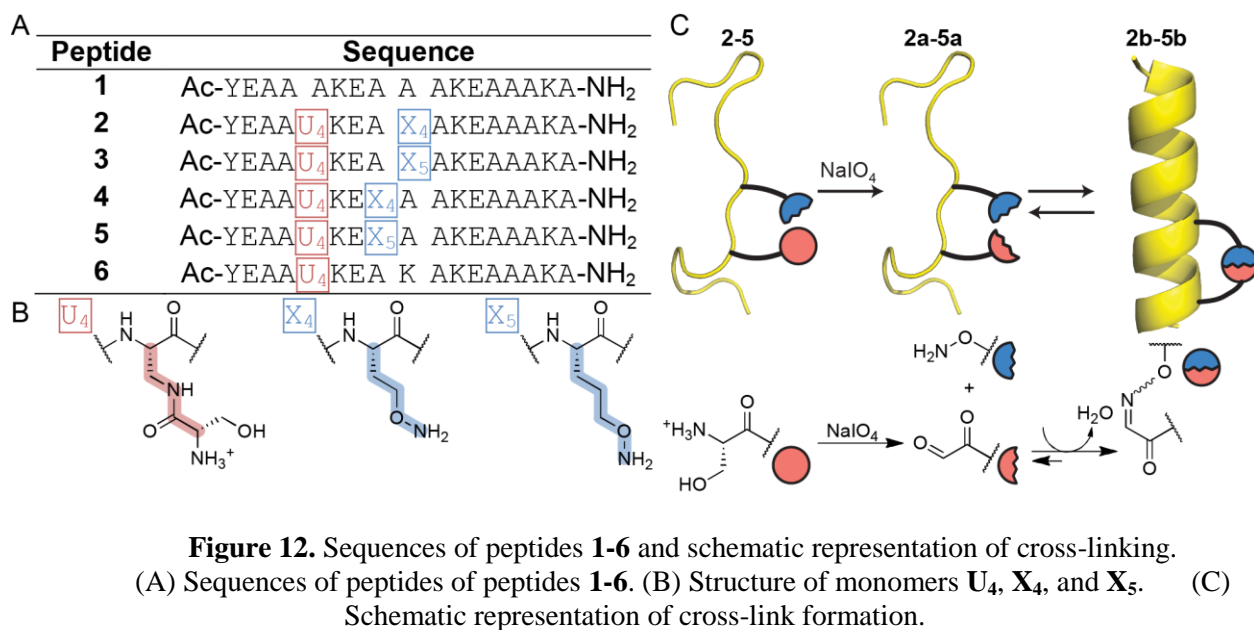
As detailed in Chapter 1, there is an unmet need for cross-linking methods that are bioorthogonal and dynamically reversible in aqueous conditions. Some cross-linking methods exist that are applicable to unprotected peptide substrates in solution but they are generally limited by the use of proteinogenic side chains (e.g. Cys, Lys) and the necessity of utilizing organic co-solvents. Owing to the bioorthogonality of oxime and hydrazone formation, and the ability of such linkages to undergo dynamic covalent exchange, we have sought to employ oximes as a side-chain to side-chain cross-linking method. We have utilized oxime cross-links in a model helical peptide and in an  $\alpha$ -helical coiled coil, which constitutes a basic protein-protein interaction. This work has demonstrated that oxime cross-links can influence helical folding, stabilize a protein quaternary structure, and undergo limited dynamic covalent exchange. We have also shown that the cross-linked products formed are sensitive to the folded state of the peptide when the reaction is performed.

## 2.1 PROMOTING $\alpha$ -HELIX FORMATION IN A SHORT PEPTIDE

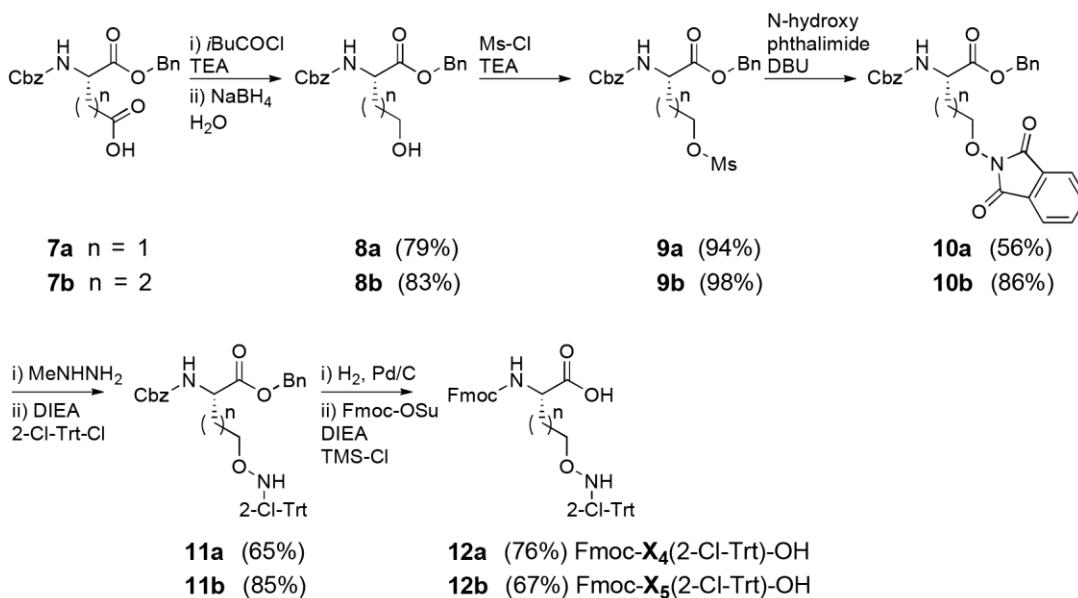
In a helical model system, we sought to investigate several factors necessary for the development of dynamic covalent peptide cross-linking methods. First, we established unnatural monomer inclusion able to chemoselectively form oxime side-chain cross-links. Second, we investigated how cross-links affect the helical folding pattern of the peptide and what structural factors of the cross-links are important to helix induction. Third, we assessed the capacity of the cross-links formed to undergo dynamic covalent exchange.

### 2.1.1 Design Of The Peptide Model System

As a  $\alpha$ -helix model system we utilized a 17-residue peptide, **1**, of *de novo* design which was originally developed to gauge the importance of salt bridge interactions on helix formation (Figure 12).<sup>33</sup> Peptide **1** is known to be partially helical in aqueous solution at pH 7.<sup>33</sup> We designed variants based on peptide **1** containing unnatural residues **U**<sub>4</sub>, **X**<sub>4</sub>, and **X**<sub>5</sub> to generate analogues **2-5** (Figure 12). Residues **X**<sub>4</sub> and **X**<sub>5</sub> are isosteres of ornithine and lysine, respectively, and bear aminoxy functionalities attached on the peptide side chain. Residue **U**<sub>4</sub> has a serine-acylated side chain, which can be unmasked by treatment with a mild oxidant under aqueous conditions to furnish a glyoxyl aldehyde yielding linear species **2a-5a**. These oxidized, linear species can then undergo oxime formation to furnish the corresponding cyclized peptides **2b-5b** (Figure 12C). Periodate oxidation of terminal serine residues has previously been used to generate protein aldehydes for bioconjugation<sup>82, 83</sup> and in the formation of oxime-cyclized peptide scaffolds.<sup>77, 78</sup> Peptide **6** is designed to isolate the effect of the inclusion of residue **U**<sub>4</sub>, which is bulky and cationic, and the subsequently unmasked glyoxyl aldehyde on the  $\alpha$ -helical structure.



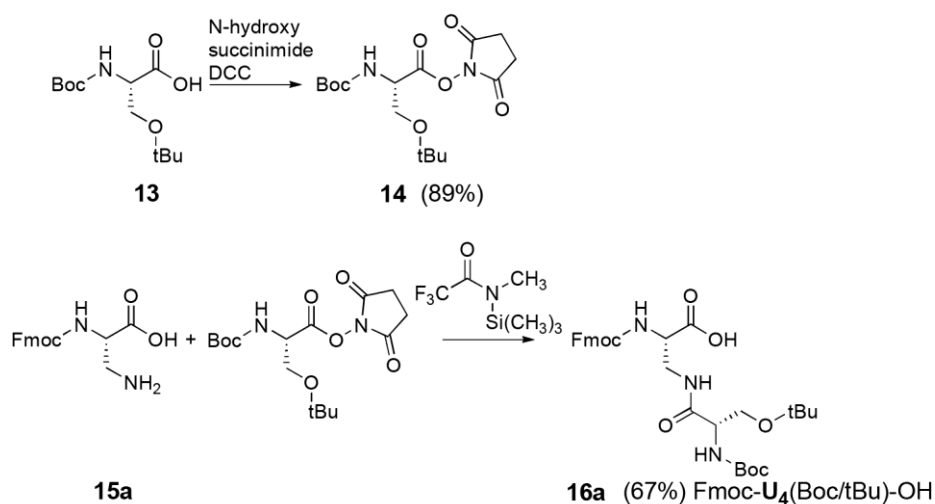
The required Fmoc-protected aminoxy-functionalized monomers, **12a**, **12b** were synthesized according to scheme 2.1.



**Scheme 2.1.** Synthesis of aminoxy-functionalized monomers **12a** and **12b**.

The monomers **12a** and **12b** were synthesized by adaptation of previously published methods.<sup>84</sup> The Cbz/Bn-protected derivative of aspartic acid (**7a**) was reduced to its corresponding alcohol by conversion to a mixed anhydride followed by treatment with aqueous sodium borohydride.<sup>85</sup> The alcohol in **8a** was transformed to a mesylate, and the aminoxy functionality installed by nucleophilic addition of N-hydroxyphthalimide to yield compound **10a**. The phthalimide protecting group was then cleaved by addition of methyl hydrazine; subsequent treatment with 2-chlorotriyl chloride yielded compound **11a**. Hydrogenolysis of the backbone protecting benzyl carbamate and benzyl ester followed by Fmoc protection of the free amine yielded protected monomer **12a**. An identical sequence of reactions was used to obtain protected aminoxy-functionalized molecule **12b** starting from the protected derivative of glutamic acid (**7b**).

Serine-acylated monomer **16a** was prepared according to previously reported procedures (Scheme 2.2).<sup>78</sup> The succinimidyl ester of Boc-Ser(tBu)-OH (**13**) was prepared by reaction with N-hydroxysuccinimide and DCC to yield compound **14**. Fmoc-protected diaminopropionic acid (**15a**) is then reacted with the succinimidyl ester of serine to yield the desired monomer **16a**.



**Scheme 2.2.** Synthesis of serine-acylated monomer **16a**.

With protected amino acids **12a**, **12b**, and **16a** in hand, peptides **1-6** were synthesized by standard Fmoc-based solid-phase peptide synthesis (SPPS) and purified by HPLC. A few observations regarding the synthesis of aminoxy-functionalized residues are notable. We found that cleavage of the peptides from resin using standard reagent cocktails (TFA/water/triisopropylsilane) yielded no isolatable product. The addition of ethanedithiol as a nucleophilic scavenger led to yields and crude purities of aminoxy-functionalized peptides **2-5** similar to sequence **1** prepared by the same method. The loss of material during peptide cleavage from resin in the absence of ethanedithiol can be attributed to the irreversible attachment of the peptide to resin by alkylation of the aminoxy functionality.<sup>86</sup> It was also observed that some C<sub>18</sub> reverse-phase HPLC stationary phases irreversibly bound aminoxy-functionalized peptides. Although the cause of this phenomenon was never clear, we were able to find stationary phases free of this problem.

### 2.1.2 Oxime Cross-Link Formation And Exchange In A Simple $\alpha$ -Helix

With the desired peptides **1-6** in hand, we tested the efficiency of oxidation and cross-link formation under conditions which are typical for biophysical characterization of peptide folding. We prepared a 100  $\mu$ M solution of each peptide in 100 mM phosphate buffer at pH 7 and added aqueous sodium periodate to cleave the 1,2-aminoalcohol in the **U**<sub>4</sub> residue and unmask the glyoxyl aldehyde. Cross-link formation then proceeds via a condensation reaction between the aminoxy functionalized side chain of **X**<sub>4</sub> or **X**<sub>5</sub> and the unmasked aldehyde on **U**<sub>4</sub>. Each cross-linking reaction was analyzed by HPLC and MALDI-TOF MS of the collected HPLC eluent (Figure 13). Peptide **6**, which contains the **U**<sub>4</sub> residue but lacks the aminoxy functionality, was used in an identical series of reactions. The oxidation of peptide **6** furnished a single linear product, **6a**, demonstrating the impact of **U**<sub>4</sub> residue insertion and that lysine is incapable of forming a cyclic imine product under the conditions of the experiment.

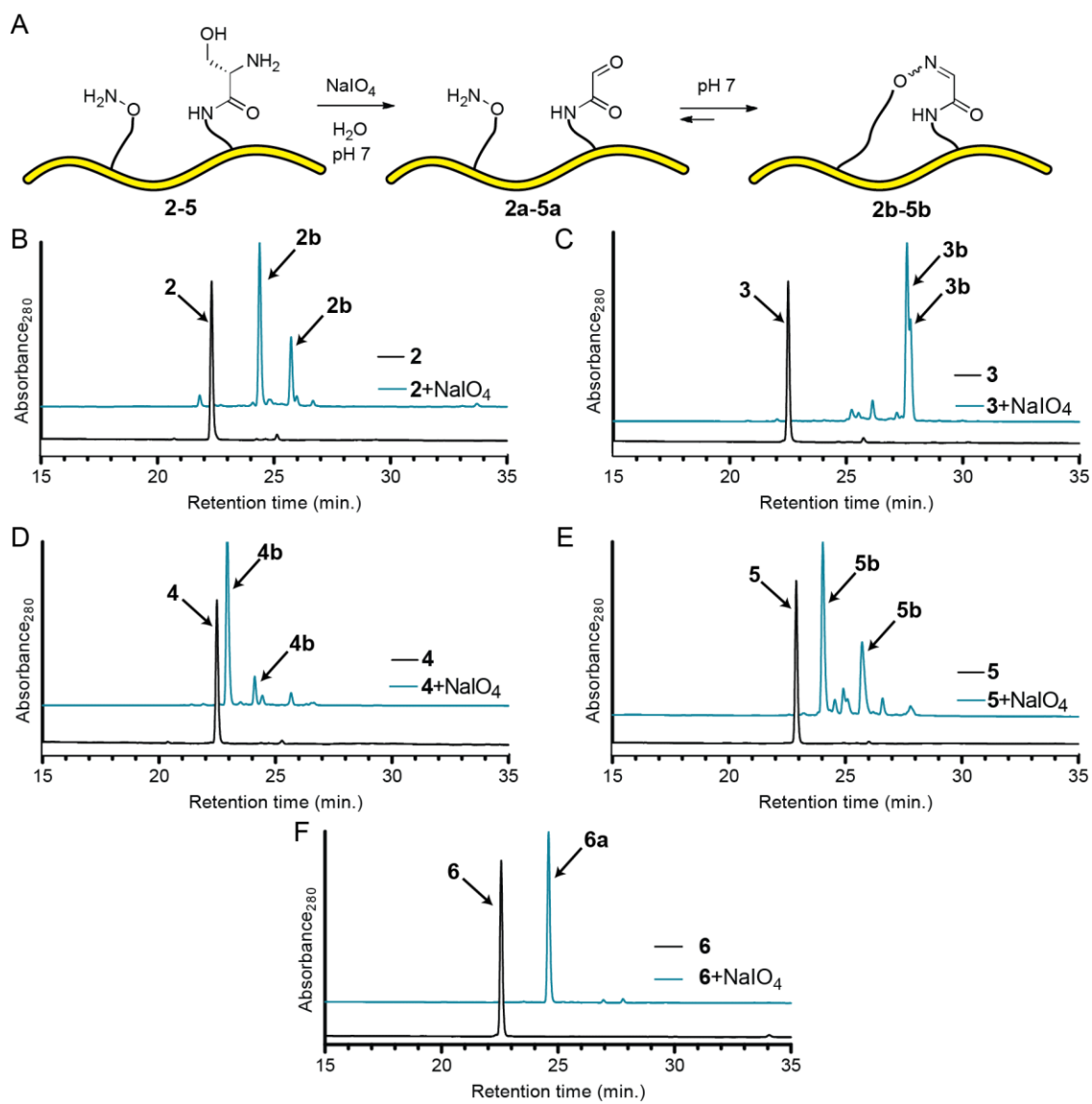


**Figure 13.** Cross-link formation scheme and HPLCs.

(A) Schematic representation of cross-link formation. (B-F) Chromatograms of peptide **2-6** with (blue) and without (black)  $200 \mu\text{M}$   $\text{NaIO}_4$  present.

In each case, we observed that the starting linear peptide was consumed in a matter of minutes to furnish two peaks in the HPLC chromatogram with masses that correspond to the cyclic oximes **2b-5b**. The cross-linking reactions were found to be high yielding (~85-90%) and to have few byproducts. We assigned the two major products observed as arising from *E*- and *Z*-oxime isomers, the ratio of which varied amongst **2b-5b** (Figure 13). Although the oxidized peptides are capable of establishing an equilibrium between linear species **2a-5a** and the oxime cyclized products **2b-5b**, the oxime products are thermodynamically favored. This accounts for the fact that linear species **2a-5a** were not observed by HPLC. The distribution of products observed after cross-link formation was unchanged even after 24 hours.

The observed product distribution from cross-link formation could result either from kinetic or thermodynamic control. In the case of kinetic control, the product distribution is dictated by the activation energy associated with the formation of each product; the oxime isomer distribution would depend on which isomer has a lower energy barrier associated with its formation. If the reaction is under thermodynamic control, the product distribution is determined by the relative stability of each product. In the case of thermodynamic control, the product distribution indicates which oxime isomer provides a more stable cyclized species. However, if the activation energy barrier for the interconversion of the two cyclized products is sufficiently high under the experimental conditions, the product distribution initially observed could be “trapped,” at a non-equilibrium position. The observation that the product distribution observed for the cross-linking reactions do not change argues either that the thermodynamic minimum of the system has been attained, or that the system is kinetically trapped. Determining which of these two circumstances is manifested by the reactions performed here is difficult. However, we hypothesize that the reaction mixtures observed constitute a thermodynamic minimum due to the lack of changes in product distribution over extended periods of time, and that the product distribution can change when changing the conditions of the experiment as described below.

In the case of peptide **2b**, the *E/Z* isomers were assigned by <sup>1</sup>H NMR spectroscopy after HPLC separation (Figure 14). While it is possible to completely separate the stereoisomers in this case, we found

that the two peaks interconvert rapidly in HPLC solvents, which contain trifluoroacetic acid, even during the short time between collection and freezing for lyophilization. Nevertheless, samples enriched in each observed stereoisomer could be obtained by rapid freezing of eluted material and subsequent lyophilization (Figure 14). The separation yielded two samples of **2b**, one composed of ~95% major isomer and the other composed of ~70% major isomer and ~30% minor isomer. Analysis of these samples by  $^1\text{H}$  NMR shows two singlets in the region expected for the oxime C-H bond. The oxime C-H resonance is dependent on the proximity of the proton to the nearby oxygen; the isomer with the proton closer to oxygen (*E*) is expected to be farther downfield, while the opposite (*Z*) configuration is expected to be farther upfield.<sup>87</sup> The two observed singlets are thus assigned as the respective stereoisomers of the oxime bond, where the *Z* isomer is the major product and the *E* isomer is the minor product.

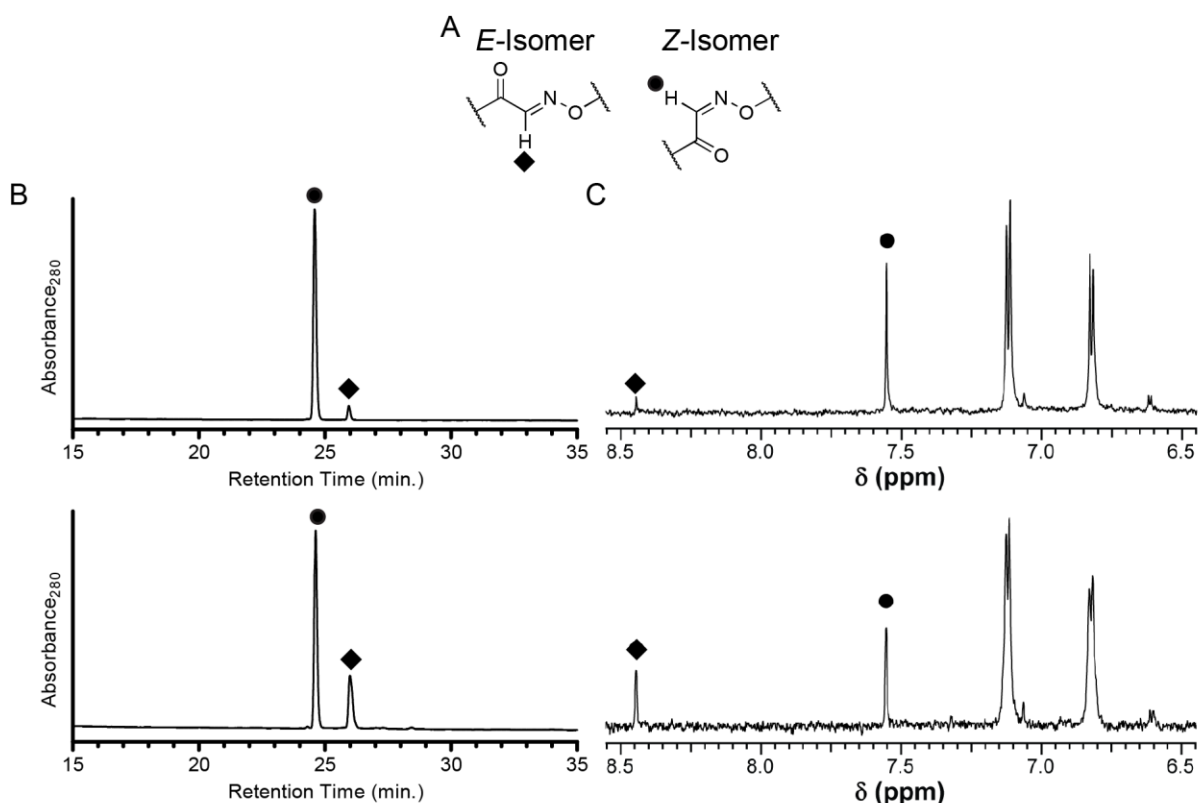


**Figure 14.** Assignment of oxime stereoisomers of **2b**.

(A) Structures of *E*- and *Z*-oxime isomers. (B) HPLC chromatograms of the isolated isomer samples. (C)  $^1\text{H}$  NMR spectra of isolated fractions of **2b** isomers used to assign as the *E* and *Z* oximes.

### 2.1.3 Dynamic Covalent Exchange In A Helical Peptide

As an initial test of whether oxime cross-linked peptides undergo dynamic exchange, we examined the interconversion of the *E* and *Z* isomers of **2b** (Figure 15). The proposed mechanism of isomerization involves the protonation of the oxime nitrogen, followed by attack by water on the carbonyl carbon involved in the oxime bond. This process leads to the formation of a tetrahedral intermediate ( $T_0$ ) which can undergo free rotation about the C-N bond. This intermediate can then proceed to complete hydrolysis, or re-form the oxime as either the *E*- or *Z*-stereoisomer. Though other mechanisms for isomerization have been proposed, kinetic experiments suggest that this pathway is the predominant mechanism of isomerization in aqueous solution.<sup>88</sup> Since isomerization by this mechanism shares a common pathway with the hydrolysis required for dynamic covalent exchange, observation of isomerization indicates that the hydrolytic pathway is available for the cyclic oxime products generated, even if the linear species is not observed.

Following HPLC separation, rapid freezing, and subsequent lyophilization, enriched samples of the *E* and *Z* isomers of **2b** were obtained. Each fraction was split into two aliquots: one in pH 7 phosphate buffered water and one in water containing 0.1% by volume trifluoroacetic acid. It was observed that the isomers are capable of interconverting at pH 7, albeit slowly; this isomerization was observed to be faster at acidic pH. This suggests that the system is in dynamic exchange at pH 7, but is kinetically trapped at a non-equilibrium state. The rate determining step of oxime exchange in mildly acidic or neutral pH solution is known to be the protonation of the nitrogen, which is also the first step in isomerization.<sup>89</sup> This suggests that dynamic covalent exchange of the oxime side chain cross-links may be possible under conditions known to favor oxime and hydrazone exchange (acidic pH, aniline catalyst).<sup>90</sup>

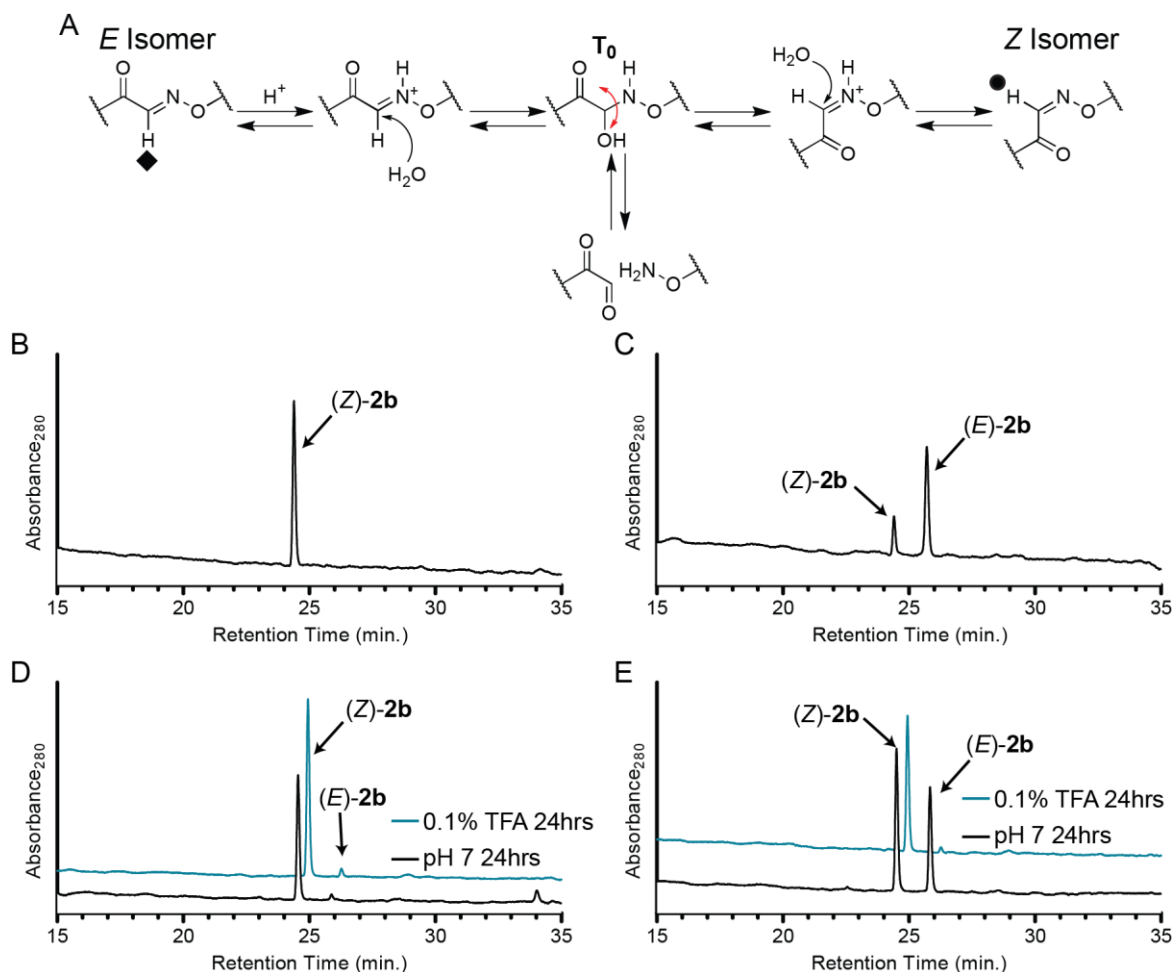


**Figure 15.** Mechanism and HPLC chromatograms of isomerization experiments.

(A) Mechanism of oxime isomerization in aqueous solution proceeds through tetrahedral intermediate  $T_0$ . (B, C) Major (B) and minor (C) oxime isomer peaks as isolated by analytical HPLC, following lyophilization and immediate injection after dissolving in water. (D,E) HPLC chromatograms of lyophilized samples dissolved in either 0.1 M pH 7 phosphate buffer or in 0.1% by volume TFA in water.

In order to further examine the ability of the oxime cross-links to undergo dynamic covalent exchange, we tested the ability of the cyclized product **2b** to undergo ring-opening to form product **2c** (Figure 16). We prepared an equilibrating mixture of peptide **2b** and added an exogenous aminoxy-functionalized small molecule, *O*-methylhydroxylamine, under conditions that are known to facilitate oxime exchange. Under these conditions, the *O*-methylhydroxylamine can compete with the peptide **X<sub>4</sub>** residue for reaction with the glyoxyl aldehyde. Thus, the above conditions set up a dynamic equilibrium

between species **2b** and **2c**. We found that treatment of cyclic product **2b** under the conditions described above at pH 7 led to limited exchange to form product **2c** to a final composition of **2c** after 48 hours of ~3% by HPLC analysis. At pH 4, the exchange was considerably faster and ~10% of the material was converted to product **2c** after 24 hours.

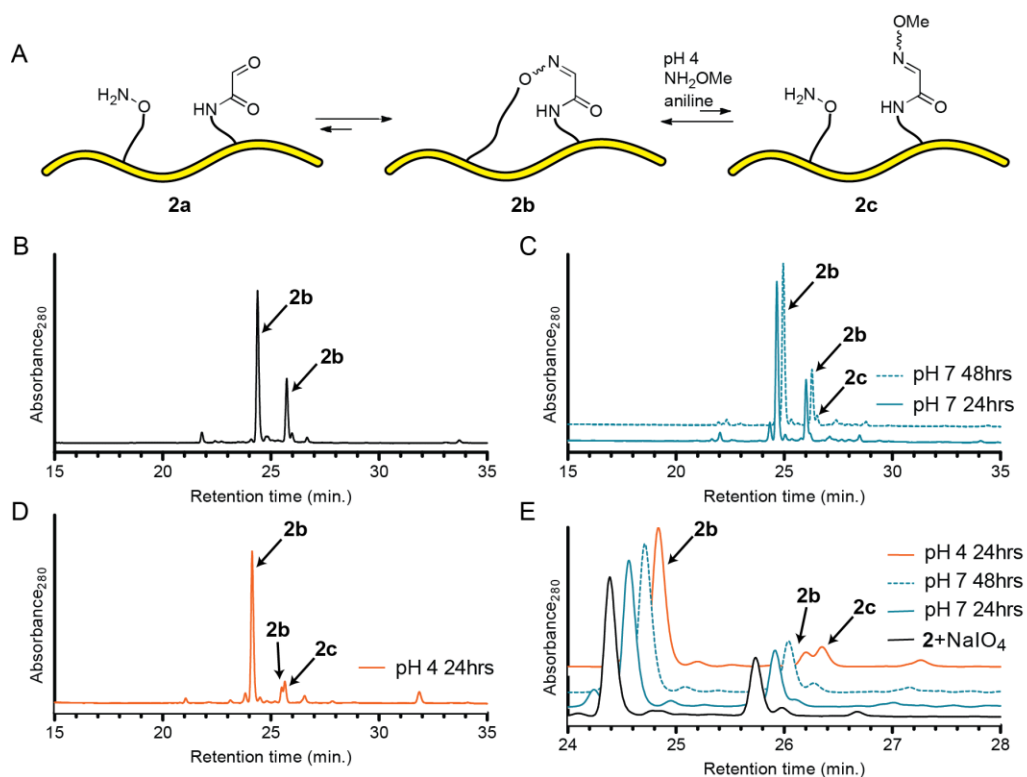


**Figure 16.** Dynamic covalent exchange of cyclic oxime **2b** and linear oxime **2c**.

(A) Schematic representation of cross-link exchange experiments, where cyclic product **2b** is in equilibrium with linear species **2a** and **2c**. (B) Representative chromatogram of peptide **2** 10 minutes after addition of NaIO<sub>4</sub>. (C) Chromatograms of exchange experiments performed at pH 7 24 hours (solid blue line) and 48 hours (dashed blue line) after addition of aniline catalyst and *O*-methylhydroxylamine. (D) Chromatogram of exchange experiment performed at pH 4 24 hours after addition of aniline catalyst and *O*-methylhydroxylamine. (E) Overlay of the chromatograms in B-D illustrating the change over time of product **2c**.

### 2.1.4 Oxime Cross-Link Effect On Folding In A Simple $\alpha$ -Helix

In order to examine the ability of the oxime cross-links to influence helix formation in peptides **2-5**, we utilized circular dichroism (CD) spectroscopy. CD spectroscopy is commonly used to gauge the folding of peptides and proteins, wherein an  $\alpha$ -helix is indicated by minima at 208 and 222 nm.<sup>91</sup> We prepared samples of peptides **1-6** at 100  $\mu$ M concentration in 100 mM phosphate buffer at pH 7. Separate samples prepared with aqueous sodium periodate furnished linear product **6a** and cross-linked products **2b-5b**, allowing for direct comparison of the linear and cyclized peptides (Figure 17).

Parent peptide **1** is approximately 40% helical under the conditions of the experiment as indicated by minima at 208 and 222 nm. Prior to oxidation and cyclization, peptides **2-5** exhibit almost no helical secondary structure (Figure 17A). We attribute this to the inclusion of the bulky, cationic **U<sub>4</sub>** residue in place of alanine in parent sequence **1**. In order to test this hypothesis directly, we examined a peptide (**6**) which lacks the aminoxy-functionalized **X** residue but which still contains the serine-acylated **U<sub>4</sub>** residue. Peptide **6** also lacks strong helical minima, supporting the hypothesis that the **U<sub>4</sub>** residue is responsible for abolishing the helical fold (Figure 17C). Upon oxidation and unmasking of the glyoxyl aldehyde – removing some of the steric bulk and charge of the **U<sub>4</sub>** residue – peptide **6a** was found to recover moderate helical folding.

Following oxidation and cyclization, peptides **2b-5b** were found by CD to increase in helical structure relative to their linear counterparts (Figure 17B). The  $\alpha$ -helical population among **2b-5b** varied as a function of the structure of the oxime cross-links, where an  $i \rightarrow i+4$  spacing of residues leads to more helical population than the corresponding  $i \rightarrow i+3$  spacing of the same monomer pair. Additionally, it was found that the thermal stability of the partially helical fold varies as a function of the cross-link structure. While very similar by CD scans, peptides **2b** and **3b** exhibit different thermal stability of their fold as judged by monitoring the helical minimum at 222 nm as a function of temperature (Figure 17D). Overall, these data demonstrate that oxime cross-links can be utilized to stabilize a helical fold with a strong dependence on the structure of the cross-link formed.

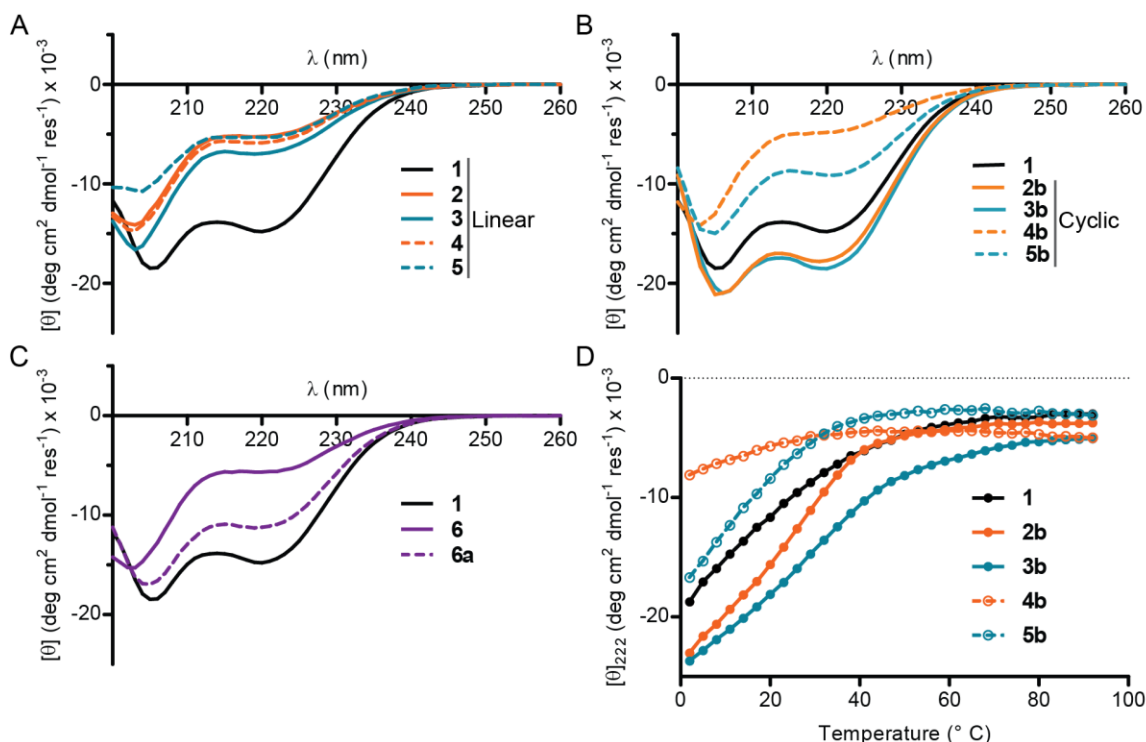


**Figure 17.** Circular dichroism data for peptides **1-6**.

(A) CD scans of peptides **1-5** without added periodate at 100  $\mu\text{M}$  concentration in 0.1 M phosphate buffer, pH 7. (B) CD scans of peptides **2b-5b** with added periodate at 100  $\mu\text{M}$  concentration in 0.1 M phosphate buffer, pH 7. (C) CD scans of peptides **1**, **6**, and **6a** at 100  $\mu\text{M}$  concentration in 0.1 M phosphate buffer, pH 7. (D) CD melts of peptides **1** and **2b-5b** where molar ellipticity at 222 nm is monitored as a function of temperature.

## 2.1.5 Conclusions

Work utilizing a 17-residue peptide demonstrates that oxime side chain cross-links provide a potential bioorthogonal cross-linking strategy that is readily implemented in buffered aqueous solution. The cross-links are formed rapidly (in a matter of minutes) and cleanly in aqueous buffered solution to furnish the cyclic peptides as *E*- and *Z*- oxime isomers. In the case of peptide **2b**, the *Z*-oxime isomer is determined to be the major product.

One of the motivations for developing oxime side-chain cross-links is to provide a dynamic covalent cross-linking method. We found that the isomer distribution can change upon isolation of the *E*-

and Z-oxime isomers and redissolving in aqueous solution at either neutral or acidic pH; however, the observation that isomerization occurs only slowly at pH 7 suggests that the system is kinetically trapped at neutral pH. Additionally, attempts to implement dynamic covalent exchange to form a linear oxime species demonstrate that although the cyclic oxime is capable of dynamic exchange the extent of exchange is limited, presumably by the thermodynamic favorability of the cyclic species.

We found that the oxime cross-links are capable of affecting the helical structure of the peptide, with a strong dependence on the connectivity and ring size of the cross-linked macrocycle. Additionally, it appears that the serine acylated U<sub>4</sub> residue is detrimental to helical folding prior to cleavage of the 1,2-aminoalcohol to furnish the corresponding glyoxyl aldehyde. Overall, the observed differences in helicity by CD suggest that an  $i \rightarrow i+4$  spacing of the two residues is necessary for accommodation into a helical fold.

## 2.2 OXIME SIDE CHAIN CROSS-LINKS IN A MODEL QUATERNARY STRUCTURE

Having established a foundation for the use of oxime side chain cross-links in an  $\alpha$ -helical peptide, we sought to increase the complexity of the system to include a model protein-protein interaction or quaternary structure. Towards that end, we chose to use the GCN4-p1 sequence **17**, which is the dimerization domain from the yeast transcriptional activator GCN4 (Figure 18).<sup>92</sup> This 33-residue sequence is known to form a dimeric  $\alpha$ -helical coiled coil in aqueous solution based on the formation of a hydrophobic interface along one face of the helix.<sup>92</sup> In a helical wheel, each amino acid is assigned a letter code ( $a-g$ ) based on its position in the sequence. In GCN4-p1, hydrophobic amino acids (Leu or Val) predominate at heptad repeat positions  $a$  and  $d$  (Figure 18).<sup>92</sup> Packing of the hydrophobic surfaces formed by two such helices leads to dimerization. GCN4-p1 has offered a fertile ground for the study of the kinetics and thermodynamics of peptide folding with both natural and unnatural  $\alpha$ -residue replacements.<sup>93,</sup>

<sup>94, 95</sup> The GCN4-p1 model system has since been employed in detailed analyses of the thermodynamic

contributions of primary sequence changes in the stability of the coiled-coil fold,<sup>96, 97</sup> and thus offers a platform for investigating the contribution of cross-linking for the thermodynamic folded stability of the coiled coil.

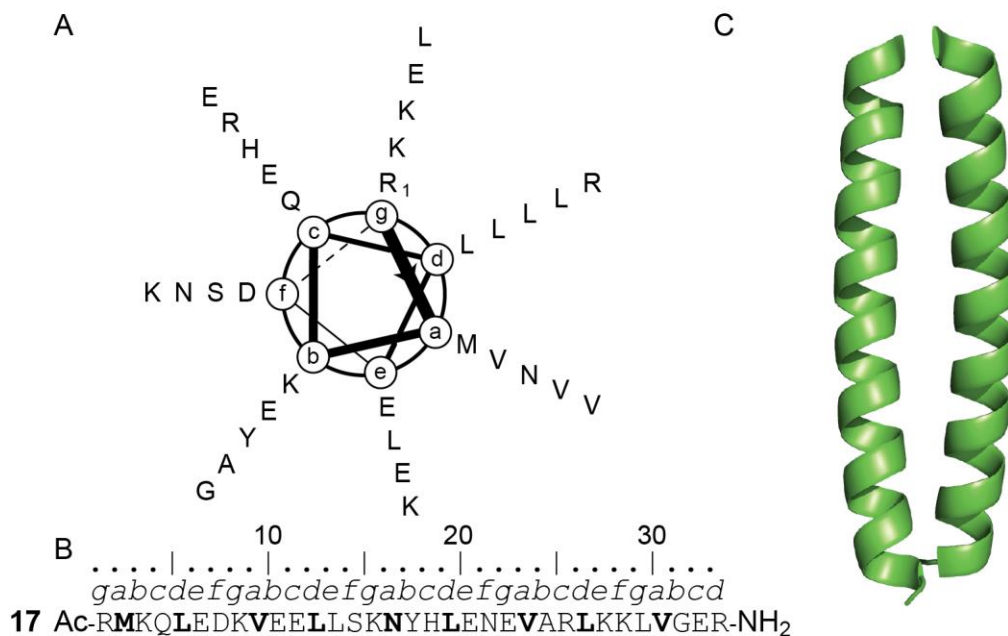


**Figure 18.** Helical wheel, sequence, and crystal structure (PDB: 4DMD) of GCN4-p1. (A) Helical wheel representation of the GCN4-p1 sequence. Hydrophobic residues are found at positions *a* and *d*. (B) Sequence of GCN4-p1, **17**; hydrophobic interface residues are in bold font. (C) Crystal structure of GCN4-p1 from PDB ID: 4DMD.

We utilized this model system to further investigate the influence of the structure and placement of oxime side chain cross-links within a helical sequence by examining a wide range of cross-linked macrocycle sizes, connectivities, and sequence positions. Having identified an optimal cross-link structure, we then prepared a bicyclic peptide based on the best residue pairing and demonstrated that the distribution of the products formed is dependent upon the folded structure of the peptide at the time of cross-link formation.

### 2.2.1 Examination Of The Sensitivity Of Methionine To Periodate Oxidation

The GCN4-p1 sequence (**17**) includes methionine at position 2. Converting the serine 1,2-aminoalcohol in **U** residues to an aldehyde requires the use of a mild oxidant, which could potentially oxidize methionine to the corresponding sulfoxide or sulfone. However, methionine has been reported to be stable to treatment with dilute sodium periodate.<sup>98</sup> A more complete understanding of the competitive oxidation of methionine is of interest not just in the study of oxime side chain cross-links, but also broader applications of serine oxidation as a protein labeling tool. In order to address these general questions, and the specific suitability of peptide **17** as a host sequence for cross-linking **U** and **X** residues, we examined whether or not periodate would selectively oxidize a **U** residue in the presence of methionine.

In order to quantify the oxidation sensitivity of methionine, we used a solution containing 100  $\mu\text{M}$  of **17** 0.1 M phosphate buffer at pH 7 to which was added one equivalent of aqueous periodate. An identical analysis of the oxidation of the **U**<sub>4</sub> residue in peptide **6** was also performed. Time dependent analysis of the mixture by HPLC and MALDI-TOF MS demonstrated that the **U** residue in peptide **6** is cleanly oxidized with a half-life of less than 0.3 minutes. The methionine residue in peptide **17** was found to be oxidized to the methionine sulfoxide with a half-life of 51 minutes.<sup>99</sup> The relative rates apparently favor selective oxidation of the **U** residue. To test this hypothesis directly, we subjected a single sample containing 100  $\mu\text{M}$  of both peptides **17** and **6** to a limiting single equivalent of sodium periodate in 0.1 M phosphate buffer at pH 7. Under these conditions, it was found that the **U** residue in **6** is cleanly converted to the corresponding glyoxyl aldehyde, with no appreciable formation of the methionine sulfoxide in **17** observed (Figure 19).

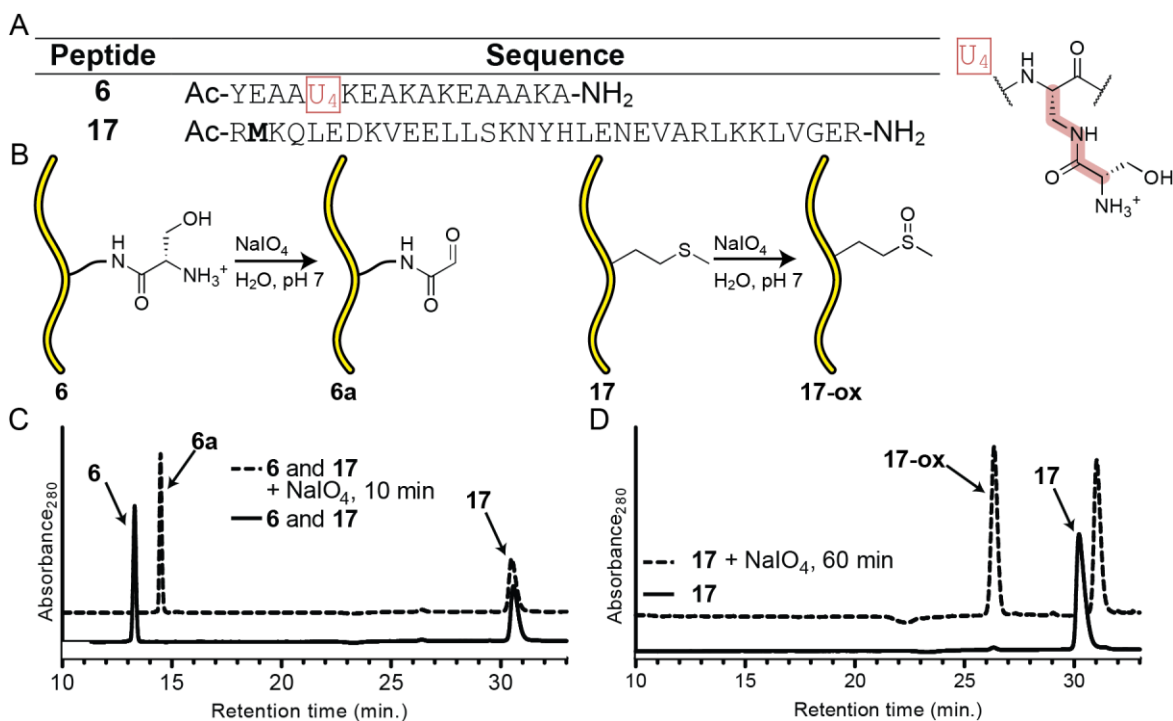


**Figure 19.** Oxidation of methionine in the presence of serine-acylated U residue.

(A) Sequences of peptides **6** and **17**. (B) Schematic representation of the oxidation reaction of each peptide. (C) HPLC chromatogram of a 100  $\mu$ M sample of each peptide in pH 7 phosphate buffer before and 10 minutes after NaIO<sub>4</sub> addition. (D) HPLC chromatograms of peptide **17** in pH 7 phosphate buffer before (solid) and 60 minutes after (dashed) NaIO<sub>4</sub> addition.

### 2.2.2 Cross-Link Structure And Connectivity In An $\alpha$ -Helical Coiled-Coil

GCN4-p1 provides a useful system to examine open questions relating to the use of oxime side chain cross-links for the stabilization of protein helices. GCN4-p1 has a well-folded quaternary structure and exhibits a two-state thermal unfolding transition. In order to rigorously exclude the possibility of methionine oxidation during cross-link formation, we replaced methionine at position 2 with its hydrocarbon isostere, norleucine, to generate sequence **18** (Figure 20). We then utilized residues **X<sub>4</sub>** and **X<sub>5</sub>**, and **U<sub>4</sub>** along with three additional serine acylated residues (**U<sub>5</sub>**-**U<sub>7</sub>**) as a means to construct differing macrocycle sizes and connectivities at a single sequence position in GCN4-p1. Sequences **19-26** were used to probe different oxime cross-link structures, as a function of side chain length, and compare their

effect on the stabilization of a quaternary fold. Comparison of the linear sequences **19-26** to the corresponding cyclized species **19b-26b** allow for quantification of the stabilization due to the introduction of oxime cross-links of varying structure and macrocycle size. Of the monomer pairs utilized, only two ( $U_4$  and  $X_4$  or  $X_5$ ; peptides **19** and **20**) were examined previously in the 17-residue helical peptide (see section 2.1).

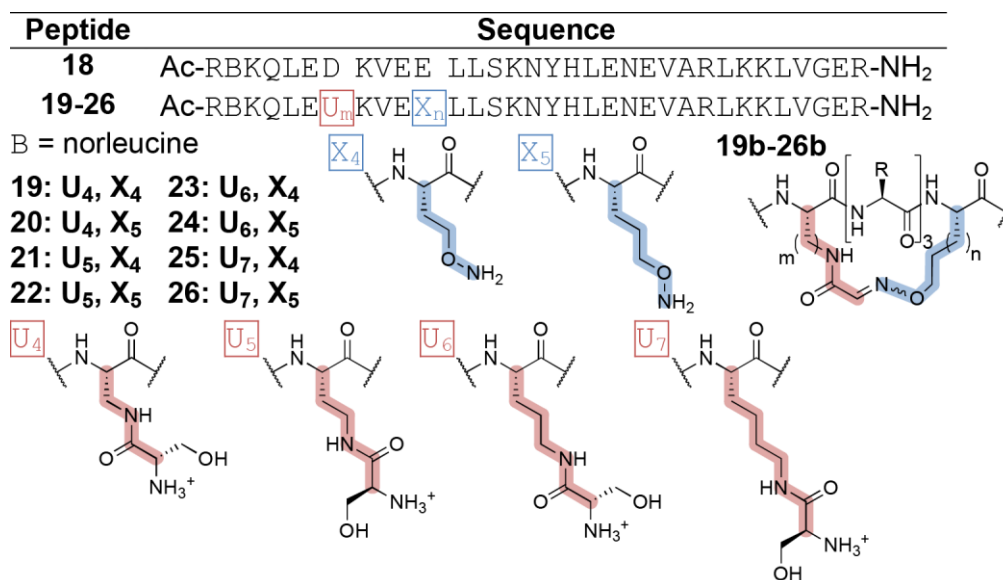
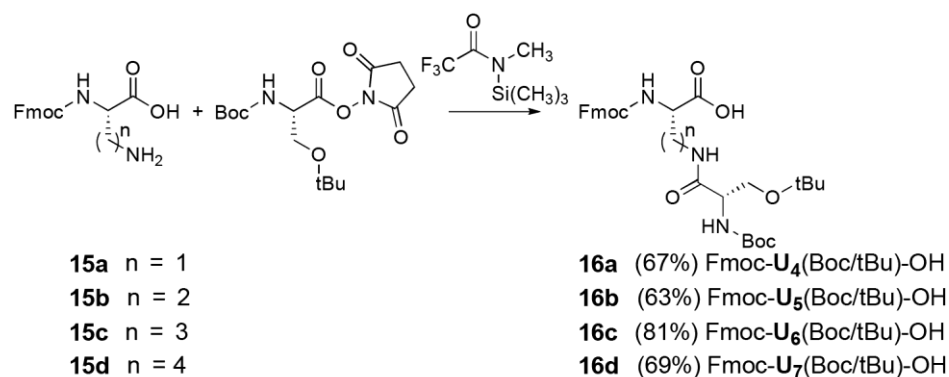


**Figure 20.** Sequences of peptides **18-26**.

Fmoc-protected aminoxy monomers **12a** and **12b** and the serine-acylated monomer **16a** were prepared as described in section 2.1.1. Additional serine-acylated monomers, **16b-16d** were prepared by adaptation of the methods used for synthesis of monomer **16a** (Scheme 2.3).



**Scheme 2.3.** Synthesis of serine-acylated monomers **16a-16d**.

With the desired monomers in hand, peptides **19-26** were prepared by solid-phase peptide synthesis, then cleaved from resin and purified by HPLC. We first examined the conversion of linear peptides **19-26** to the corresponding cross-linked counterparts, **19b-26b** by treatment of 100  $\mu$ M solutions of each peptide in 0.1 M phosphate buffer at pH 7 with 1 equivalent of aqueous sodium periodate. As previously observed in the simpler 17-residue model system, the starting linear peptide was consumed in 10 minutes or less, and the majority of the material (~85-90%) observed by HPLC was identified as the cyclic oxime species by MALDI-TOF MS (Figure 21). We did not observe any evidence of cross-links occurring between two independent peptide chains, which we attributed to the favorable kinetics of intramolecular cyclization versus intermolecular ligation.

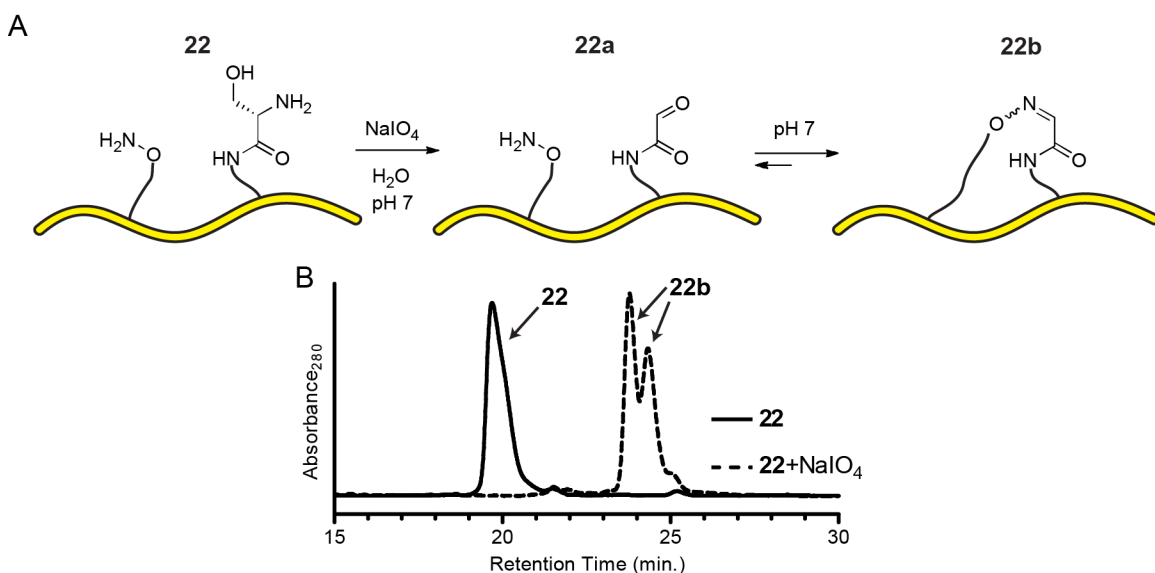


**Figure 21.** Example oxidation/cyclization reaction of peptide **22**. (A) Schematic representation of oxidation and cross-link formation. (B) HPLC chromatogram of peptide **22** before and 10 minutes after addition of 1 equivalent of aqueous periodate.

We employed CD spectroscopy to compare the quaternary folded structure of each cross-linked coiled-coil, **19b-26b**, to its linear counterpart **19-26**. In all cases, the CD samples contained 100  $\mu$ M peptide in 0.1 M phosphate buffer at pH 7, with or without an added single equivalent of sodium periodate. In CD scans, the magnitude of the minimum observed at 222 nm informs about the helicity of the peptide; thus, changes in this helical signature revealed any perturbation of the helical fold either by inclusion of the unnatural residues (e.g. **19-26** vs. **18**) or from cross-link formation (e.g. **19b-26b** vs. **19-26**). We observed that the CD signature at 222 nm changes upon introduction of the unnatural residues in peptides **19-26**, with a dependence on the unnatural residue substitutions (Figure 22, Table 1). The observed decrease in the amplitude of the helical minimum was most pronounced for the monomer pairs with the shortest (e.g. **U<sub>4</sub>**, **X<sub>4</sub>**) and longest (e.g., **U<sub>7</sub>**, **X<sub>5</sub>**) side chains. We attributed this decrease in helical content to fraying of the N-terminus near the site of the unnatural residue placement; however, without detailed solution-phase structural data, we cannot rule out other possible causes.

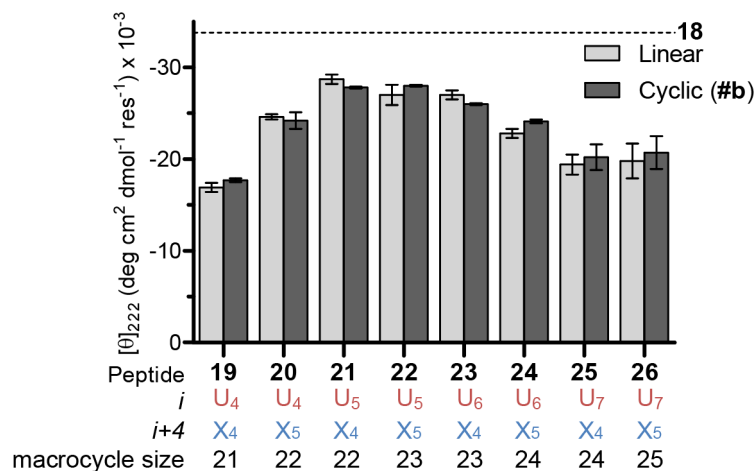


**Figure 22.** Helical signature by CD at 222 nm for peptides **19-26**.

All peptides are measured at 100  $\mu$ M peptide in 0.1 M phosphate buffer at pH 7, with (dark grey) or without (light grey) 100  $\mu$ M sodium periodate. Error bars represent the standard deviation from two independent experiments.

The use of temperature-dependent CD spectroscopy can inform about the thermal stability of the coiled-coil fold. Monitoring the helical minimum at 222 nm as a function of temperature and fitting the resulting cooperative unfolding transition to a two-state thermal denaturation model allows for a quantitative measurement of the thermal melting temperature ( $T_m$ ) of each peptide in its linear and cross-linked form. Thermal melt data of peptides **19-26** shows that the inclusion of the unnatural residues is generally destabilizing, though mildly so, as evidenced by a decrease in  $T_m$  (Figure 23, Table 1). There is a general correlation between the length of the monomers and the resulting destabilization of the coiled coil, where shorter **U** and **X** residues are particularly unfavorable. Some monomer pairs, as in linear peptide **22** (**U**<sub>5</sub> and **X**<sub>5</sub>) increase the stability of the coiled coil above that of the parent sequence, **18**. Cyclization by treatment with periodate universally increases the melting temperature of the coiled coil, demonstrating that the oxime side chain cross-links can stabilize the quaternary fold. The size of the macrocycle has a definite impact on the stability of the coiled coil, where the smallest increase in  $T_m$  is observed for smallest macrocycle sizes, and the 23-membered macrocycle generated in peptide **22b** is particularly favorable (Table 1).

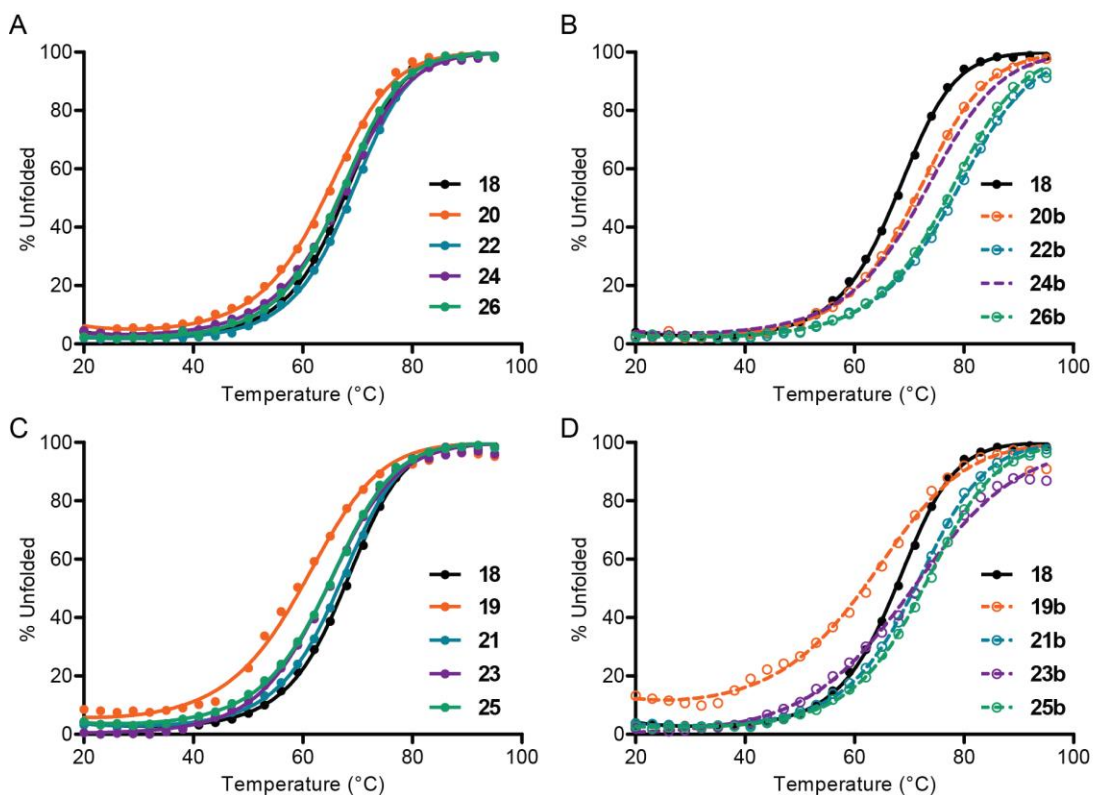


**Figure 23.** CD melts of peptides **18-26** and **19b-26b**.

(A) CD melts of peptides **18, 20, 22, 24,** and **26** prior to addition of  $\text{NaIO}_4$ . (B) CD melts of peptides **18, 20b, 22b, 24b,** and **26b** after addition of  $\text{NaIO}_4$ . (C) CD melts of peptides **18, 19, 21, 23,** and **25** prior to addition of  $\text{NaIO}_4$ . (D) CD melts of peptides **18, 19b, 21b, 23b,** and **25b** after addition of  $\text{NaIO}_4$ .

**Table 1.** Data from CD and thermodynamic analysis for peptides **18-26**.

Peptide	$[\theta]_{222}$ (deg cm <sup>2</sup> dmol <sup>-1</sup> res <sup>-1</sup> )	T <sub>m</sub> (°C)	$\Delta\Delta G_{\text{fold}}$ # vs. <b>18</b> (kcal mol <sup>-1</sup> )	Peptide	$[\theta]_{222}$ (deg cm <sup>2</sup> dmol <sup>-1</sup> res <sup>-1</sup> )	T <sub>m</sub> (°C)	$\Delta\Delta G_{\text{fold}}$ # <b>b</b> vs. # (kcal mol <sup>-1</sup> )
<b>18</b>	-33.8 ± 0.4	67.0 ± 0.6					
<b>19</b>	-16.9 ± 0.5	57.8 ± 0.7	1.23 ± 0.14	<b>19b</b>	-17.7 ± 0.2	61 ± 1	0.3 ± 0.2
<b>20</b>	-24.6 ± 0.3	65.3 ± 0.2	0.28 ± 0.04	<b>20b</b>	-24.2 ± 0.9	71.0 ± 0.2	0.68 ± 0.04
<b>21</b>	-28.7 ± 0.6	66.5 ± 0.1	0.13 ± 0.05	<b>21b</b>	-27.8 ± 0.1	71.1 ± 0.1	0.56 ± 0.02
<b>22</b>	-27.0 ± 0.9	69.0 ± 0.6	-0.13 ± 0.03	<b>22b</b>	-28.0 ± 0.1	77.6 ± 0.6	1.0 ± 0.1
<b>23</b>	-27.0 ± 0.5	63.8 ± 0.6	0.39 ± 0.05	<b>23b</b>	-26.0 ± 0.1	69.8 ± 0.7	0.7 ± 0.1
<b>24</b>	-22.7 ± 0.5	66.9 ± 0.2	0.1 ± 0.05	<b>24b</b>	-24.1 ± 0.2	72.2 ± 0.1	0.63 ± 0.03
<b>25</b>	-19 ± 1	64.0 ± 0.4	0.38 ± 0.05	<b>25b</b>	-20 ± 1	74 ± 2	1.2 ± 0.2
<b>26</b>	-20 ± 2	66.6 ± 0.1	0.11 ± 0.04	<b>26b</b>	-21 ± 2	78 ± 1	1.4 ± 0.2

An additional important measurement of the system is the ability of the peptide to adopt its original folded structure following thermal denaturation. Recovery of molar ellipticity at 222 nm can be used as a measure of the ability of the peptide to re-fold. Following thermal denaturation experiments by CD, the peptides were allowed to equilibrate at 20 °C for five minutes prior to measurement of ellipticity at 222 nm. Analysis of the restoration of ellipticity values suggests that all of the linear peptides (**19-26**) recover their initial helicity and thus original folded structure (Figure 24). Following oxidation and cyclization, peptides **19b-26b** do not fully recapitulate the observed ellipticity prior to thermal denaturation (Figure 24). Peptide **19b** only regains ~65% of its initial helical signature, which suggests that the small, highly constrained macrocycle does not allow the peptide to re-fold. The remaining peptides, **20b-26b** exhibit small differences but all recover ~85-90% of their initial helicity. These data illustrate that the highly constrained macrocycle in **19b** prevents the denatured peptide backbone from full recovery of helical secondary structure. Larger macrocycles, as in **20b-26b**, do not greatly constrain the denatured backbone and allow for return of helical structure.

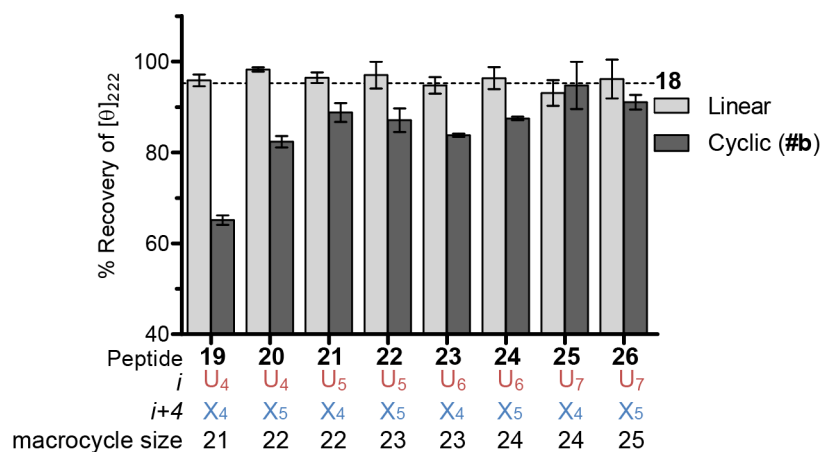


**Figure 24.** Percent recovery of helical minimum for peptides **19-26**.

Thermal melt data can additionally be used to quantify the impact of the inclusion of the unnatural residues **X** and **U** on the stability of the coiled-coil fold. This can be done by estimation of the difference in free energy of folding between two peptides ( $\Delta\Delta G_{\text{fold}}$ ). This estimate is calculated as detailed in section 2.4.9.2; the calculations assume that the heat capacity change associated with unfolding is the same for all peptides. The calculation of  $\Delta\Delta G_{\text{fold}}$  provides an estimation of the overall stabilization of the coiled-coil. However, the origin of the difference in the free energy change may arise from the stabilization of the folded state or from changes in the chain entropy or enthalpy in the unfolded state. Thus, while  $\Delta\Delta G_{\text{fold}}$  used here provides a quantitative estimate of stabilization of the coiled-coil due to cross-link formation, the physical basis for the stabilization of the fold may not be clear.

Comparison of the linear peptides **19-26** versus the starting sequence **18** demonstrates the thermodynamic consequence of the insertion of unnatural monomers (Figure 25A, Table 1). Replacement of natural  $\alpha$ -residues independent of cyclization is generally destabilizing, though this effect is most pronounced in the shortest **X** and **U** monomer pairing in peptide **19**. The analogous peptide with a single extra methylene unit in the **X** side chain (**20**, U<sub>4</sub>, X<sub>5</sub>) is significantly less destabilized in comparison to peptide **19**. In general, the pairing of any **U** residue with the shorter aminoxy functionalized X<sub>4</sub> residue is more destabilizing than the same length **U** residue paired with the longer aminoxy functionalized X<sub>5</sub>

residue (e.g. peptide **21** versus **22**). This suggests that the bulky, cationic **U** residue is not solely responsible for destabilization of the linear peptide sequence in **19-26**. Interestingly, the monomer pairing in peptide **22** is slightly stabilizing to the coiled-coil fold, suggesting that this pairing may reduce or eliminate unfavorable interactions and/or participate in favorable interactions with local regions of the folded protein.

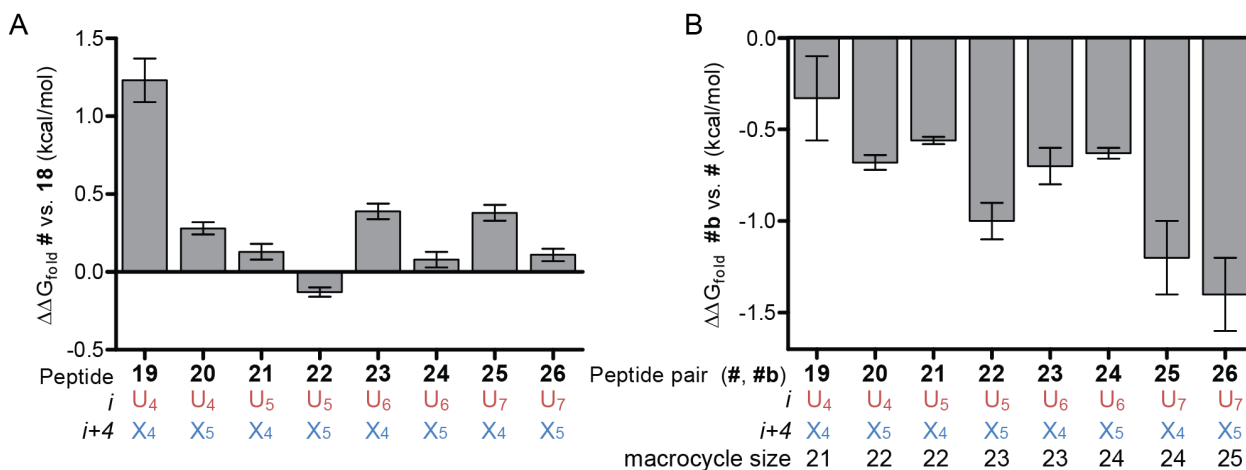


**Figure 25.** Thermodynamic impact of unnatural monomer insertion and cross-link formation. (A) Change in folding free energy ( $\Delta\Delta G_{\text{fold}}$ ) for linear peptides **19-26** versus model sequence **18**. (B) Change in folding free energy ( $\Delta\Delta G_{\text{fold}}$ ) for linear peptides **19b-26b** versus the corresponding linear peptide, **19-26**. Error bars represent uncertainty from two independent experiments.

The comparison of the oxidized, cyclized sequences **19b-26b** to their linear counterparts, **19-26**, allows for quantitative analysis of the thermodynamic impact of cross-link formation on the coiled-coil fold. Because a wide range of macrocycle sizes and connectivities are examined, this analysis can help to establish basic structural requirements for an oxime side chain cross-link to effectively stabilize the coiled-coil. This comparison suggests that macrocycle size is a key parameter in determining the extent of stabilization of the coiled-coil fold (Figure 25B, Table 1). Additionally, differing connectivity within a single macrocycle size (e.g. peptide **23** versus peptide **22**) leads to different degrees of stabilization. Of

note is the stability imparted by the 23-membered macrocycle in **22b**, when compared to the closely analogous macrocycle in **23b**. Peptide **26b** is also found to form a particularly stable coiled-coil fold. Overall, this data set suggests that certain macrocycles may participate in particularly favorable interactions, and/or have particularly favorable ring torsional angles, that contribute to stabilization of the coiled-coil.

Overall, the CD and thermodynamic analysis suggests that certain macrocycles are particularly favorable to the stability of the GCN4-p1 coiled-coil. This is supported by the minimal decrease in helicity observed in CD scans and the considerable degree of increased resistance to thermal denaturation observed after cross-link formation.

### 2.2.3 High-Resolution Structural Analysis Of The Optimal Oxime Cross-Link

Among the eight macrocycle sizes and connectivities examined in peptides **19-26**, the oxime side chain cross-link resulting from an  $i \rightarrow i+4$  spacing of **U<sub>5</sub>** and **X<sub>5</sub>** monomers was optimal for stabilizing the coiled-coil quaternary fold. We applied X-ray crystallography to determine the high-resolution structure of both linear and cyclized peptides containing this monomer pairing. These experiments allowed for determination of what, if any, impact on the coiled-coil fold results from unnatural residue substitution in the linear precursor and cross-link formation in the cyclic product.

We obtained crystals of linear species **22** by hanging drop vapor diffusion and the structure was solved to 2.3 Å resolution (Figure 26A). The dimeric coiled coil is virtually identical to that of the native GCN4-p1 sequence from a previously published crystal structure ( $C_{\alpha}$  RMSD = 0.30 Å compared to PDB: 2ZTA).<sup>92</sup> The **U<sub>5</sub>** and **X<sub>5</sub>** residues are accommodated into the helical fold without any local disruption. Fraying of the N-terminus past the unnatural residues is not observed in the crystal structure; however, this does not necessarily bear on the dynamics of the coiled-coil in solution, where N-terminal fraying may be responsible for the observed decrease in helical CD signature at 222 nm. Similar to other conformationally flexible side chains in solvent-exposed positions in the crystal structure, the unnatural

side chains were not well resolved in electron density. This observation likely indicates that the  $U_5$  and  $X_5$  residues lack defined polar contacts that constrain their conformational flexibility.

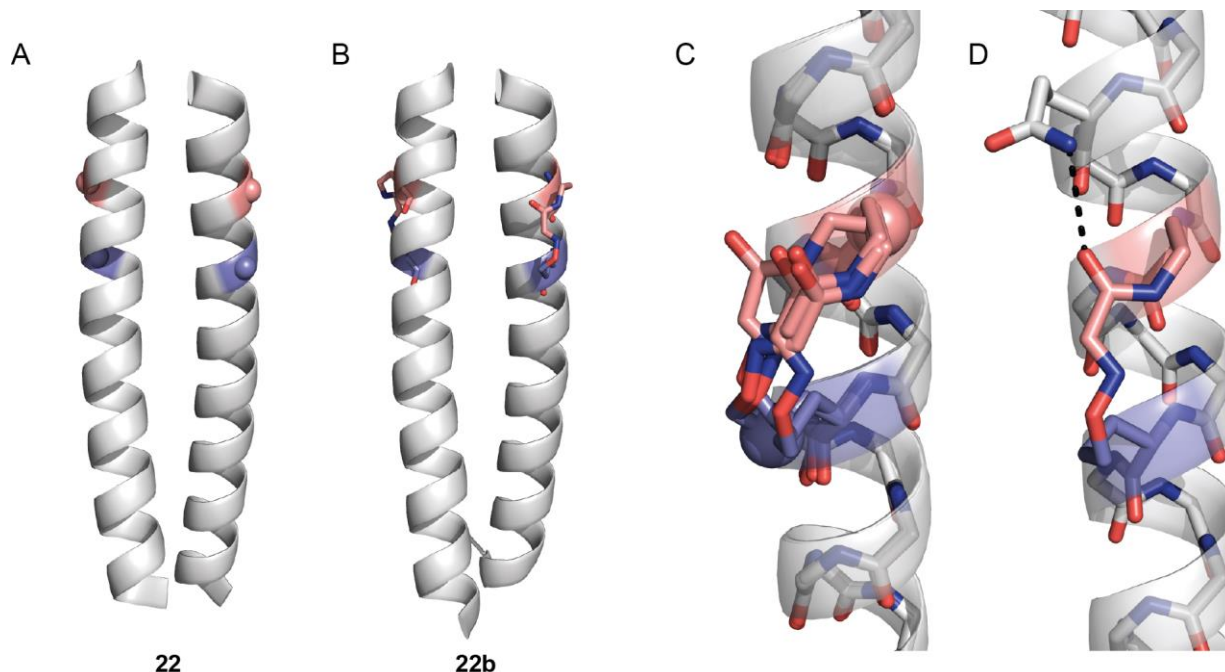


**Figure 26.** Crystal structures of peptides **22** and **22b**.

(A) Crystal structure of linear peptide **22**. (B) Crystal structure of cyclized peptide **22b**. (C) Overlay of the four independent chains of **22b** in the crystallographic asymmetric unit. Both *E* and *Z* stereoisomers are observed. (D) A polar contact between Gln<sub>4</sub> and the glyoxyl oxime carbonyl oxygen observed in one of the four chains of **22b**.

Given the solvent-accessible nature of the unnatural residues as well as their proximity to solvent channels in the crystal lattice, we hypothesized that the  $U_5$  and  $X_5$  side chains could be chemoselectively cyclized in the crystal. Soaking crystals of linear peptide **22** with buffer supplemented with periodate led to the formation of cyclized peptide **22b** without disruption of the fold or crystal packing. The ability to generate the oxime cross-link in the fragile crystal lattice underscores the mild and chemoselective nature of the cross-linking chemistry. The resulting crystal structure of oligomer **22b** was refined to 2.3 Å resolution and shows a coiled-coil fold almost identical to its linear counterpart ( $C_\alpha$  RMSD = 0.25 Å) (Figure 26B). The crystallographic asymmetric unit, unlike that of **22**, contains four independent peptide chains in two dimeric coiled-coils due to the loss of a crystallographic 2-fold symmetry axis. This

serendipitous outcome allowed for examination of the oxime cross-links in different chemical environments. Although the electron density of the cross-linked residues is not as well-defined as side-chains involved in direct packing interactions, sufficient electron density is visible in the refined structure to allow for structural analysis of the cross-links themselves. Overlay of the oxime cross-links found in each of the independent chains shows several side-chain conformations, including both *E* and *Z* oxime stereoisomers, are accommodated into the helical fold (Figure 26C). The presence of multiple conformations and stereoisomers likely accounts for the modest electron density observed for the cross-linked side chains. In one of the four chains containing the oxime cross-links, a potentially stabilizing polar interaction was observed between the carbonyl oxygen of the glyoxyl oxime and the side chain of Gln<sub>4</sub> (Figure 25D). This finding suggests that the oxime cross-link itself can participate in stabilizing polar interactions with nearby side-chains.

#### **2.2.4 Cross-Link Structure And Sequence Position In An A-Helical Coiled Coil**

In order to more fully investigate the structural factors of importance in the use of oxime side-chain cross links, we investigated additional sequences based on GCN4-p1. One subset of these sequences is regioisomers of previously described cross-links, and a second subset consists of a single cross-link moved to different sequence positions along the backbone. Each of these sets of peptides provides valuable information regarding the ability to stabilize a coiled-coil fold and how the stabilization depends on the sequence environment into which the unnatural **X** and **U** residues are substituted for natural  $\alpha$ -residues.

##### **2.2.4.1 Regioisomers Of Previously Utilized Cross-Links**

Peptides **27-30** are regioisomers of sequences **20**, **22**, **24** and **26**, where the **X** and **U** residues are swapped. Each of these peptides has an **X**<sub>5</sub> residue at position 7 (rather than position 11), and a serine-acylated

residue ( $U_4$ - $U_7$ ) at position 11 (Figure 27). Biophysical characterization of these regioisomer linear sequences and their cross-linked counterparts, as in peptides **19-26**, provides valuable information about the importance of sequence position which can be applied in the design of oxime cross-links.

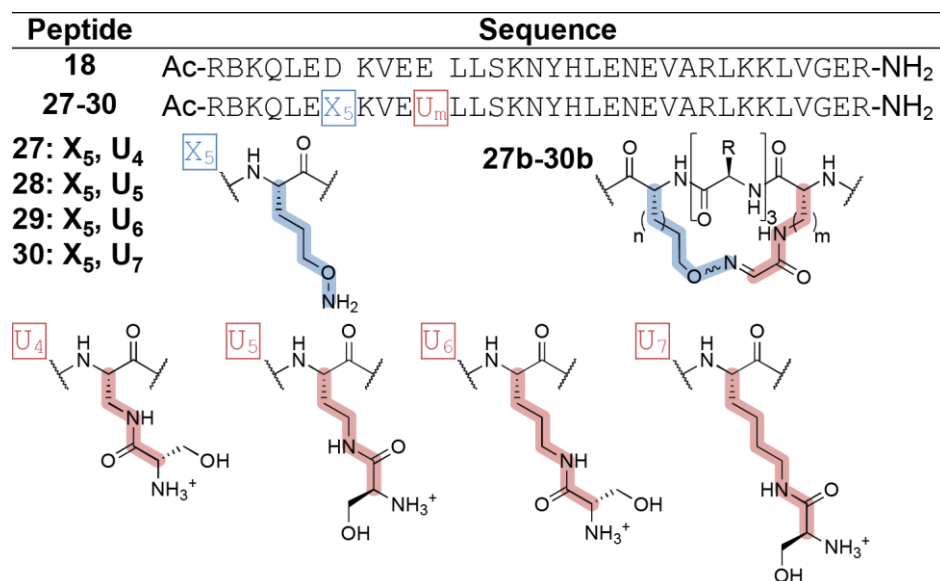


**Figure 27.** Sequences of peptides **27-30**.

Analysis of CD scans of peptides **27-30** shows that switching positions of the unnatural residues does not eliminate the mild disruption of the helical folding pattern observed previously (Figure 28). The detrimental impact on helicity is again most pronounced for the shortest side chains utilized (e.g.  $U_4$  in **27**,  $U_5$  in **28**). Interestingly, the decrease of the helical signature is diminished considerably in peptides **29** and **30** compared to **27** and **28** or their regioisomer counterparts, **24** and **26**. We hypothesized that the trend observed in peptides **27-30** may be due to the introduction of an unfavorable electrostatic interaction between the cationic  $U$  residue at position 11 and Lys<sub>15</sub>. This electrostatic interaction may be ameliorated in longer side chain lengths (e.g. **29** and **30**) where increased flexibility and solvation of the  $U$  residue allows it to avoid the unfavorable repulsion between adjacent positive charges.

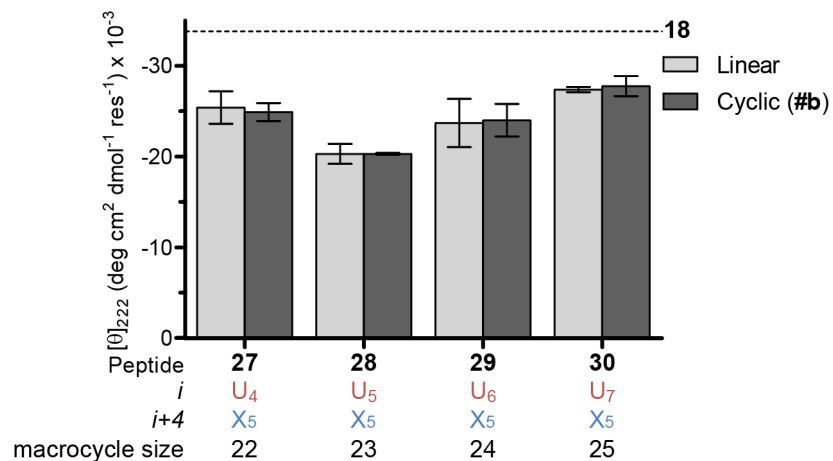


**Figure 28.** Helical signature by CD at 222 nm for peptides **27-30**.

All peptides are measured at 100  $\mu$ M peptide in 0.1 M phosphate buffer at pH 7, with (dark grey) or without (light grey) 100  $\mu$ M sodium periodate. Error bars represent the standard deviation of two independent experiments.

Thermal melts of peptides **27-30** show that swapping the **X** and **U** residue positions decreases the thermal stability of the resulting coiled-coil (Figure 29). Generally, the shorter **U** residues at position 11 are less well tolerated than the longer **U** residues, as illustrated by higher thermal melting temperatures for peptides **29** and **30** versus **27** and **28** (Figure 29, Table 2). This trend further supports the hypothesis that the introduction of the **U** residue at position 11 may create an unfavorable ionic interaction that is reduced in longer side chains. Formation of the cross-linked macrocycle is found to stabilize the coiled-coil fold, with a dependence on the structure of the oxime cross-link formed.

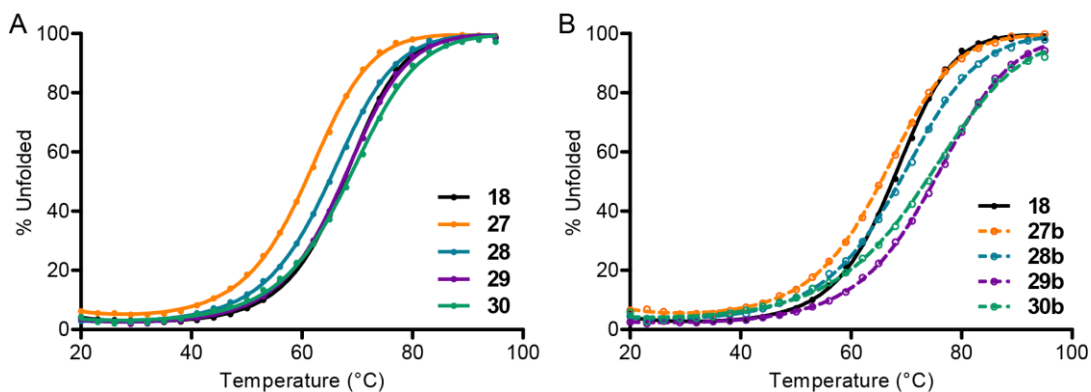


**Figure 29.** CD melts of peptides **18** and **27-30**.  
 (A) CD melts of peptides **18** and **27-30** prior to addition of  $\text{NaIO}_4$ . (B) CD melts of peptides **18** and **27b-30b** after addition of  $\text{NaIO}_4$

**Table 2.** Data from CD and thermodynamic analysis for peptides **27-30**.

Peptide	$[\theta]_{222}$ (deg $\text{cm}^2 \text{dmol}^{-1} \text{res}^{-1}$ )	$T_m$ ( $^\circ\text{C}$ )	$\Delta\Delta G_{\text{fold}} \#$ vs. <b>18</b> (kcal $\text{mol}^{-1}$ )	Peptide	$[\theta]_{222}$ (deg $\text{cm}^2 \text{dmol}^{-1} \text{res}^{-1}$ )	$T_m$ ( $^\circ\text{C}$ )	$\Delta\Delta G_{\text{fold}} \#b$ vs. # (kcal $\text{mol}^{-1}$ )
<b>18</b>	$-33.8 \pm 0.4$	$67.0 \pm 0.6$		<b>27b</b>	$-24.9 \pm 0.9$	$65.6 \pm 0.3$	$-0.59 \pm 0.04$
<b>27</b>	$-25 \pm 2$	$60.7 \pm 0.1$	$0.83 \pm 0.04$	<b>28b</b>	$-20.3 \pm 0.1$	$68.6 \pm 0.3$	$-0.45 \pm 0.04$
<b>28</b>	$-20 \pm 1$	$64.8 \pm 0.1$	$0.32 \pm 0.02$	<b>29b</b>	$-24 \pm 2$	$74 \pm 2$	$-0.9 \pm 0.3$
<b>29</b>	$-24 \pm 2$	$66 \pm 1$	$0.02 \pm 0.01$	<b>30b</b>	$-28 \pm 1$	$73.6 \pm 0.0$	$-0.7 \pm 0.1$
<b>30</b>	$-27.4 \pm 0.3$	$67.9 \pm 0.9$	$-0.09 \pm 0.05$				

Quantitative analysis of the thermodynamic impact of unnatural residue replacement in peptides **27-30** illustrates that insertion of the unnatural residues at position 7 for **X** and 11 for **U** is generally destabilizing to the coiled-coil fold. This is not observed when the longest **U** residue is utilized as in peptide **30** (Figure 30A). However, amongst this smaller data set there is a clear trend which suggests that the shorter monomer combinations are destabilizing to the coiled-coil fold. This effect is reduced as the monomer length increases. Formation of the macrocycle is stabilizing to the coiled-coil fold to a similar degree in all cases with the exception of peptide **29** (Figure 30B). The 24-membered macrocycle generated in peptide **29** is found to be most favorable. The macrocycle formed in peptide **29b** is one methylene unit larger than the optimal size formed in peptides **19-26**, where the positions of **X** and **U** residues are swapped.

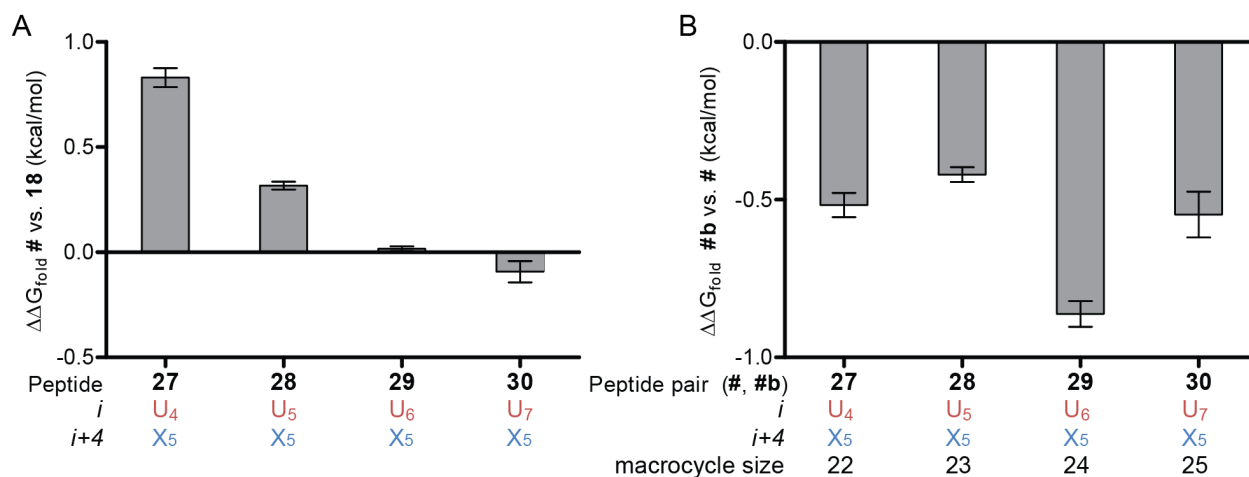


**Figure 30.** Thermodynamic data for peptides **27-30**.

- (A) Change in folding free energy ( $\Delta\Delta G_{\text{fold}}$ ) for linear peptides **27-30** versus model sequence **18**.  
 (B) Change in folding free energy ( $\Delta\Delta G_{\text{fold}}$ ) for linear peptides **27b-30b** versus the corresponding linear peptide, **27-30**. Error bars represent the standard deviation of two independent experiments.

In total, the CD and thermodynamic data for sequences **27-30** suggest that the particular substitution pattern of **X** and **U** residues affect both the folding and stability of the coiled-coil. This is somewhat surprising, given the previous examination of multiple macrocycle sizes and connectivities in peptides **19-26**. Switching of the **X** and **U** residues was not expected to have a significant impact on the stabilization of the coiled-coil fold. However, it is possible that the differences in **27-30** versus **19-26** result primarily from the introduction of unfavorable ionic interactions between **U** residues at position 11 and Lys<sub>15</sub>. This underlines the necessity for judicious choice of monomer substitution pattern in order to maintain the native folded state and thermodynamic stability.

#### 2.2.4.2 Sequence Positional Effects Of Residue Placement

As an additional gauge of the structural factors that are important in the introduction of oxime side chain cross-links, we generated sequences (**31-33**) which change the position of residue insertion along the

backbone of GCN4-p1 (Figure 31). Each sequence thus represents the movement of the same pairing of unnatural residues,  $U_5$  and  $X_5$ , along one heptad repeat of the sequence from the N-terminus towards the C-terminus.

Peptide	Sequence
<b>18</b>	Ac-RBKQLED KVEE LLS KNYH LEN EVAR LKK LVGE R-NH <sub>2</sub>
<b>22</b>	Ac-RBKQLE $U_5$ KVE $X_5$ LLS KNYH LEN EVAR LKK LVGE R-NH <sub>2</sub>
<b>31</b>	Ac-RBKQLED KVEE LL $U_5$ KNY $X_5$ LEN EVAR LKK LVGE R-NH <sub>2</sub>
<b>32</b>	Ac-RBKQLED KVEE LLS KNYH LE $U_5$ EVA $X_5$ LKK LVGE R-NH <sub>2</sub>
<b>33</b>	Ac-RBKQLED KVEE LLS KNYH LEN EVAR LK $U_5$ LVG $X_5$ R-NH <sub>2</sub>

**Figure 31.** Sequences of peptides **18**, **22**, and **31-33**.

Peptides **22** and **31-33** show similar helical signatures by CD, which indicates that the inclusion of the  $U_5$  and  $X_5$  residues at varying backbone positions does not significantly distort the helical structure (Figure 32). Of particular note is that the substitution of residues  $U_5$  and  $X_5$  at positions 14 and 18, respectively, in peptide **31** does not significantly alter the secondary structure versus control sequence **18**. This suggests that oxime side chain cross-links can be used in a number of sequence positions. In addition, the inclusion of the unnatural residues far from the termini decreases the negative impact on helicity attributed to fraying towards the termini.

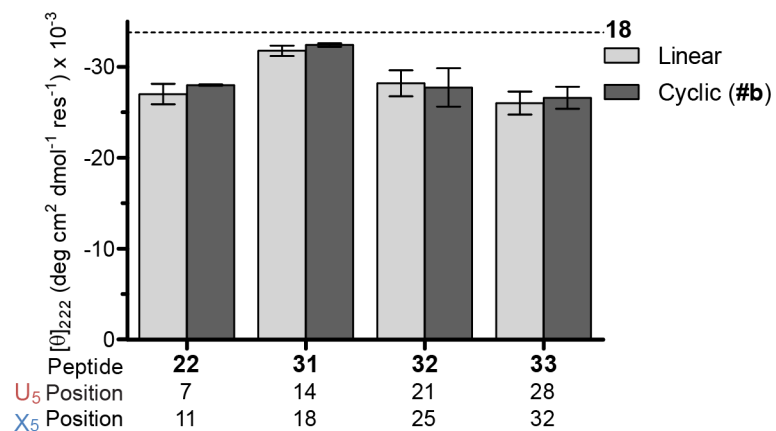


**Figure 32.** Helical signature by CD at 222 nm for peptides **22** and **31-33**.

All peptides are measured at 100  $\mu$ M peptide in 0.1 M phosphate buffer at pH 7, with (dark grey) or without (light grey) 100  $\mu$ M sodium periodate. Error bars represent the standard deviation of two independent experiments.

Thermal melts of peptide **22** and **31-33** reveal modest differences in the thermal stability of the linear sequences as the position of the unnatural residues changes along the backbone (Figure 33). Upon cross-link formation, peptides **22b**, **31b**, and **33b** are found to increase in thermal stability. Peptide **32b**, in contrast to all other sequences studied, decreases in thermal stability slightly upon formation of the cross-link ( $\Delta T_m = -3.6$  °C). Overall, the CD results show that cross-links at different positions along the backbone are well-accommodated into the helical fold with minimal disruption of the coiled-coil.

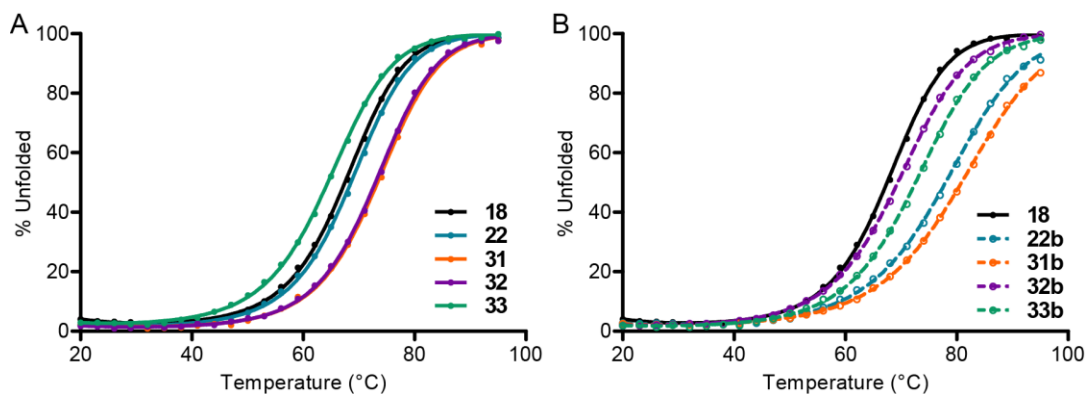


**Figure 33.** CD melts of peptides **18**, **22** and **31-33**.  
 (A) CD melts of peptides **18**, **22** and **31-33** prior to addition of NaIO<sub>4</sub>. (B) CD melts of peptides **18**, **22b** and **31b-33b** after addition of NaIO<sub>4</sub>

**Table 3.** Circular dichroism data for peptides **31-33**.

Peptide	$[\theta]_{222}$ (deg cm <sup>2</sup> dmol <sup>-1</sup> res <sup>-1</sup> )	T <sub>m</sub> (°C)	$\Delta\Delta G_{\text{fold}}$ vs. <b>18</b> (kcal mol <sup>-1</sup> )	#b	Peptide	$[\theta]_{222}$ (deg cm <sup>2</sup> dmol <sup>-1</sup> res <sup>-1</sup> )	T <sub>m</sub> (°C)	$\Delta\Delta G_{\text{fold}}$ vs. # (kcal mol <sup>-1</sup> )	#b
<b>18</b>	-33.8 ± 0.4	67.0 ± 0.6			<b>31b</b>	-32.4 ± 0.4	80.9 ± 0.6	-0.90 ± 0.04	
<b>31</b>	-31.7 ± 0.6	73.3 ± 0.9	-0.71 ± 0.04		<b>32b</b>	-28 ± 2	69.4 ± 0.8	0.43 ± 0.03	
<b>32</b>	-28 ± 1	72 ± 1	-0.66 ± 0.04		<b>33b</b>	-26 ± 1	72.6 ± 0.8	-0.77 ± 0.07	
<b>33</b>	-26 ± 1	64.4 ± 0.9	0.65 ± 0.05						

Comparison of the linear peptides **22** and **31-33** to peptide **18** shows that the insertion of unnatural residues **U**<sub>5</sub> and **X**<sub>5</sub> is mildly stabilizing to the coiled-coil fold in most sequence positions (Figure 33, Table 3). This trend does not hold for substitution very close to the C-terminus, as in peptide **33**. However, this region of the coiled-coil is known to be relatively unstructured from crystallographic analysis.<sup>92</sup> Insertion of the unnatural residues near the C-terminus may increase the unstructured nature of the C-terminal region, leading to an unfavorable change in the folded structure. Analyses of peptide **22b** along with peptides **31b-33b** compared to their linear counterparts, **22** and **31-33** show that the cross-links stabilize the coiled coil when placed at most positions in the primary sequence. The destabilization observed for peptide **32b** may be attributable to the loss of a favorable polar interaction. In the wild-type

GCN4-p1 crystal structure, Arg<sub>25</sub> is observed to have a polar contact with Glu<sub>21</sub>. Replacement of Arg<sub>25</sub> with the unnatural X<sub>5</sub> residue can maintain this polar contact, as the X<sub>5</sub> residue can act as a hydrogen bond donor although it is not charged at pH 7. Upon formation of the cross-link, the hydrogen bond donor capability of the X<sub>5</sub> side chain is lost, and the side chain is sequestered in the cross-linked macrocycle, leading to the loss of the favorable polar contact.

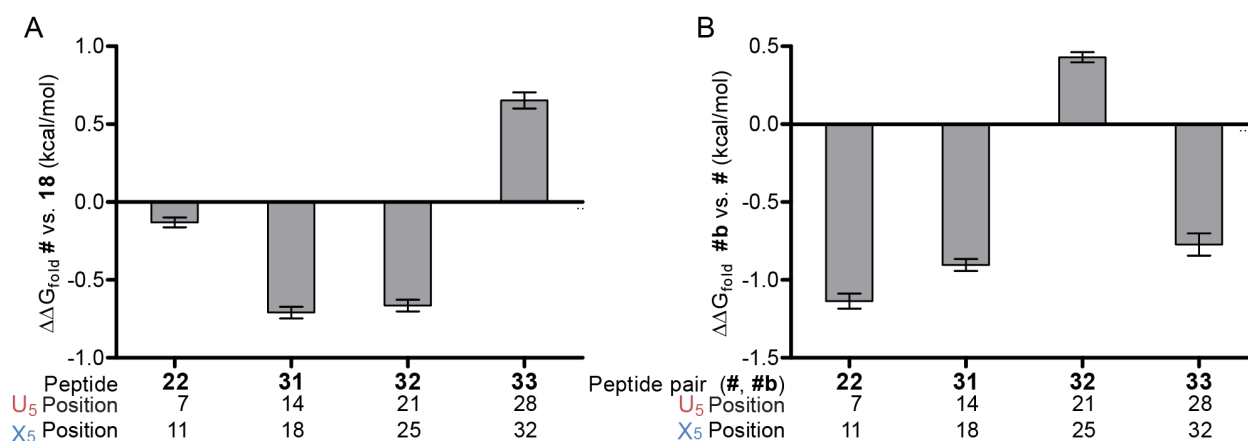


**Figure 34.** Thermodynamic data for peptides **22** and **31-33**.

(A) Change in folding free energy ( $\Delta\Delta G_{\text{fold}}$ ) for linear peptides **22** and **31-33** versus model sequence **18**. (B) Change in folding free energy ( $\Delta\Delta G_{\text{fold}}$ ) for linear peptides **22b** and **31b-33b** versus the corresponding linear peptide, **22** or **31-33**. Error bars are the uncertainty from two independent experiments.

As discussed for peptides **27-30**, the overall data obtained for peptides **22** and **31-33** argues for judicious replacement of natural residues with the unnatural residues used to form oxime side chain cross-links. The series of peptides **19-33** suggests a few general rules for the introduction of oxime side chain cross-links into helical sequences. First, sequence positions should be chosen where the unnatural residues will not introduce unfavorable electrostatic interactions (e.g., the proposed interaction between U at residue 11 and Lys<sub>15</sub>). Second, cross-link formation may actually remove a favorable polar contact if the residues are placed in positions where side-chain to side-chain hydrogen bonds are likely. Third, the

unnatural residue replacement may introduce fraying at the termini of helices, and thus optimal positioning may be in the middle of a helical region in order to minimize disruption of the fold.

### 2.2.5 Folding-Templated Synthesis Of A Multiply Cross-Linked Oligomer

Based on the results described above, we hypothesized that chemoselective oxime cross-links could prove useful for the folding-templated synthesis of a more complex polycyclic species under benign buffered conditions. X-ray structural analysis of **22** and **22b** showed that the coiled-coil fold is relatively unchanged upon cross-link formation. Thus, it is possible that the folded state at the time of cross-link formation will dictate the product distribution for a sequence where many cross-linked products are possible. In order to test this hypothesis, we generated peptide **34** which combines the unnatural residue insertions from sequences **22** and **30**. Sequence **34** contains two  $U_5$  residues and two  $X_5$  residues in an  $i, i+4, i+7, i+11$  arrangement (Figure 35A).

After addition of periodate and unmasking of two aldehydes from the  $U_5$  residues in **34**, the resulting linear species can establish an equilibrium between a range of cross-linked products (Figure 35B). These cross-linked products can potentially include a single cross-link (**34b**), of which there are four possible regioisomers and eight total possible products accounting for *E* and *Z* isomers of the oxime. Two possible regioisomeric products may result with two cross-links (**34c**), each of which has four possible stereoisomers, resulting in eight total possible doubly cross-linked species. Overall, this single oligomer can potentially have sixteen products, accounting for stereochemistry.

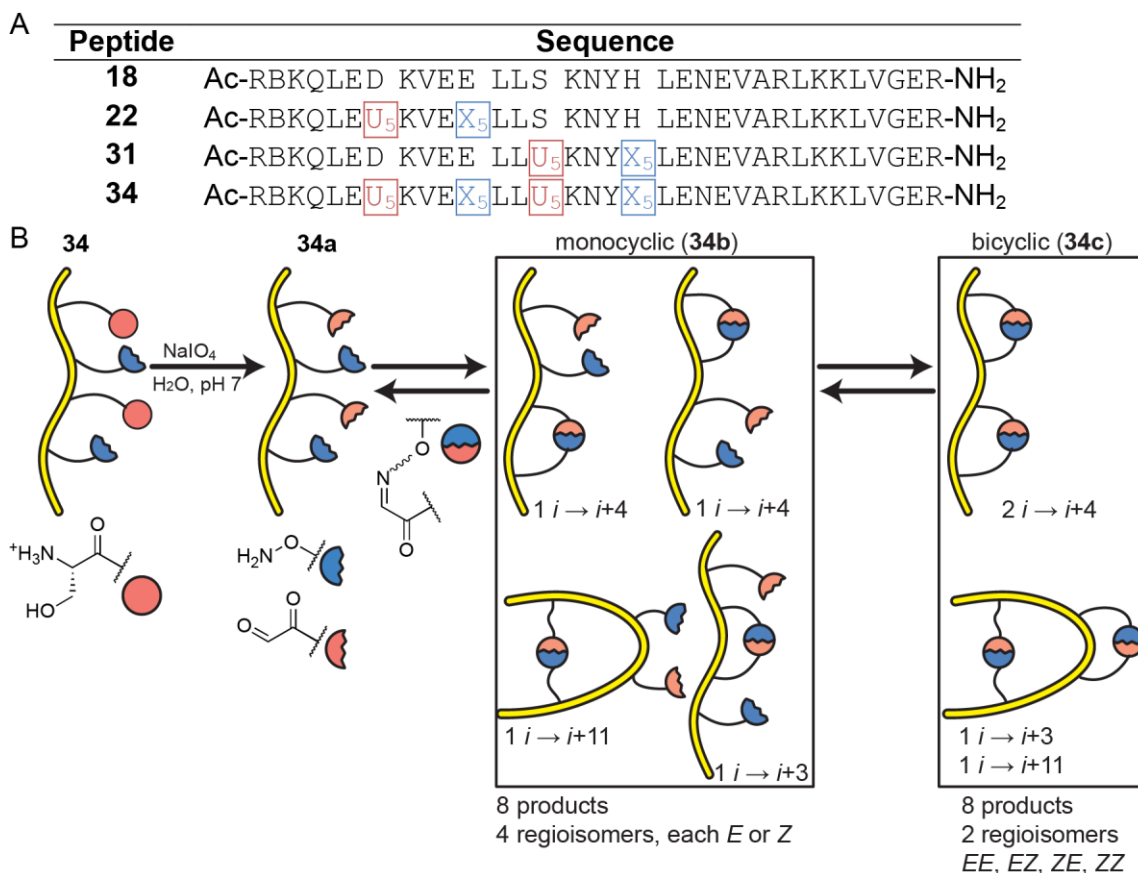


**Figure 35.** Sequence of peptide **34** and potential cross-linked products. (A) Sequences of peptides **18**, **22**, **31**, and **34**. (B) Schematic representation of cross-link formation and the possible products that result as monocyclic or bicyclic species.

Treatment of peptide **34** with a slight excess of sodium periodate in pH 7 phosphate buffer leads to complete consumption of the starting material in a matter of minutes, as was observed for the other coiled-coil peptides. The distribution of products obtained is considerably simpler than one would expect from a statistical mixture of all of the possible products. The majority of the material (~80-85%) observed by HPLC was found in two peaks and had a mass corresponding to a doubly cross-linked product by MALDI-TOF MS (isomers of **34c**, Figure 36). The remaining material is distributed over several peaks with masses corresponding to singly cross-linked species (**34b**) or doubly cross-linked species (**34c**). No evidence was observed by MS of the mixture for products resulting from the intermolecular cross-linking of two or more peptide chains.

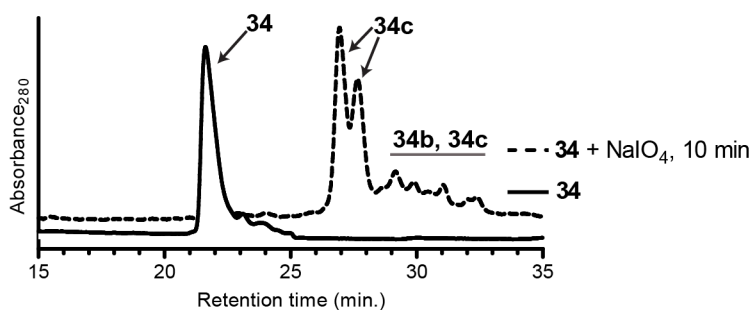


**Figure 36.** HPLC chromatograms of peptide **34** with and without added  $\text{NaIO}_4$ .

CD measurements of peptide **34** both prior to addition of periodate and after cyclization shows a similar helical signature to peptide **22** on which its design is based (Figure 37, Table 1). After periodate addition, the collective mixture of cross-linked products shows an overall CD signature nearly identical to the linear precursor (Figure 37A). This observation argues against the formation of significant amounts of oxime cross-linked products incompatible with a helical fold. The potential products containing an  $i \rightarrow i+1$  or  $i \rightarrow i+3$  cross-links would lead to destabilization of the helix. Biophysical characterization suggests that the major products observed by HPLC correspond to partially resolvable stereoisomers of the bicyclic oligomer containing two  $i \rightarrow i+4$  cross-links which are compatible with the coiled-coil.

In temperature-dependent CD analysis, the linear precursor **34** showed slightly greater thermal stability than either **22** or **31** ( $T_m = 78.0 \pm 0.1$  °C), upon which it is based; the origin of this stabilization is not clear (Figure 37B). Upon formation of the cross-links, the resulting mixture (primarily composed of **34c**) does not show a complete unfolding transition up to 95 °C, the highest temperature tested in the experiment. The apparent  $T_m$  is greater than 90 °C, and the thermal transition is no longer cooperative, instead showing almost linear temperature dependence.

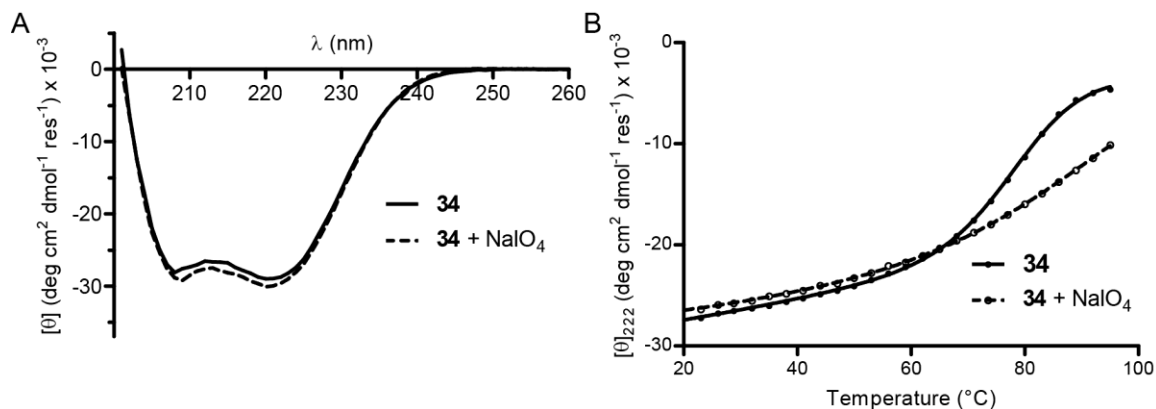


**Figure 37.** CD Data for peptide **34**.

All peptides are measured at 100  $\mu$ M peptide in 0.1 M phosphate buffer at pH 7, with (dashed) or without (solid) 210  $\mu$ M sodium periodate.

The above data suggest that the product distribution of cross-linked oligomers can be influenced by the folded state of the peptide at the time of cross-link formation. In order to test this hypothesis directly, an oxidation/cyclization reaction was carried out at a temperature (80 °C) where peptide **34** is approximately 50% unfolded by CD analysis. Upon addition of periodate and equilibration for an additional 10 minutes at 80 °C, the distribution of products observed by HPLC is considerably different than observed during identical oxidation reactions performed at room temperature (Figure 38). The two major peaks previously assigned as species **34c** change in ratio and several new peaks are observed with masses corresponding to other isomers of **34c**. The sensitivity of the product distribution obtained from **34** to its folded state prior to oxidation and cross-linking demonstrates the potential application of triggered oxime formation to identify cross-linked topologies best able to stabilize a particular fold. Though here the fold desired was known *a priori*, in principle this technique could be applied to a case in which the folded state is not known (e.g. a peptide ligand bound to its receptor).

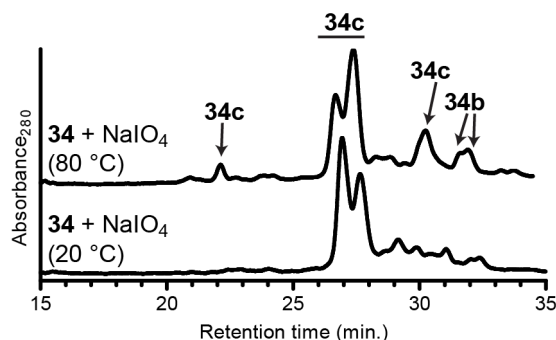


**Figure 38.** HPLC chromatograms of oxidation reactions of peptide **34**. Each sample contained 100  $\mu\text{M}$  peptide **34** in 0.1 M phosphate buffer with 210  $\mu\text{M}$   $\text{NaIO}_4$  added at either 20  $^\circ\text{C}$  (bottom) or 80  $^\circ\text{C}$  (top).

## 2.2.6 Conclusions

In summary, oxime side chain cross-linking through chemoselective reaction between aminoxy- and aldehyde-functionalized amino acids can be utilized to enhance quaternary structure stability of a coiled-coil protein. Triggered unmasking of glyoxyl aldehydes *in situ* and subsequent oxime cross-linking proceeds rapidly and cleanly in pH 7 buffered aqueous solution with a folded protein substrate. A series of sequence variants of the GCN4-p1 dimeric coiled coil with different oxime structures (both macrocycle size and connectivity) placed towards the N-terminus were examined. Additional sequence positions were tested where the cross-linked residues are placed along the solvent-exposed face of the coiled-coil.

Quantitative comparison of folding thermodynamics show that oxime cross-links are consistently stabilizing to the quaternary structure with the caveat that residues involved in polar contacts should not be replaced. The extent of stabilization is sensitive to the size, structure, and sequence position of the resulting cross-links. Examination of eight different cross links of varying macrocycle size and connectivity led to the identification of an ideal 23-membered macrocycle resulting from pairing a  $\text{U}_5$  and  $\text{X}_5$  residue at an  $i \rightarrow i+4$  residue spacing. X-ray crystallographic analysis of this linear precursor (**22**) and its corresponding cross-linked product (**22b**) show how the cross-links are accommodated into the helix.

The ability to form the cross-link in a protein crystal lattice underscores the mild and chemoselective nature of the cross-linking chemistry.

A series of regioisomers in which the sequence positions of **X** and **U** residues are flipped and in which the residues are moved along the sequence were also analyzed. These peptides (**27-33**) demonstrate the importance of maintaining native side chain functionality where polar contacts are involved. Unfavorable electrostatic interactions may be introduced by substitution of the bulky, cationic **U** residue, and care must be taken in substitution choice to avoid this. Introduction of unnatural residues at sequence positions involved in favorable polar contacts was found to be destabilizing to the coiled-coil fold. Amongst the sequences bearing oxime cross-links, cyclization is almost universally stabilizing to the coiled-coil fold, with the exception of sequence **32**. In this case, the decrease in stability may be attributed to loss of a favorable polar contact upon cyclization. The disruption of the helical fold by introduction of unnatural **U** and **X** residues near the N-terminus or C-terminus is minimized by insertion of the unnatural residues in the middle of the peptide sequence.

Interpretation of the biophysical data is complicated somewhat by the fact that helix formation is coupled to self-assembly to form the coiled coil in GCN4-p1. Incorporation of the unnatural residues **U** and **X** near the termini slightly decreases helicity of linear precursor sequences, yet these peptides still show clear fully folded baselines in CD thermal denaturation experiments. This behavior has been reported previously upon mutations to the GCN4-p1 N-terminus,<sup>100</sup> and may be attributed to the fraying of the helix in the folded coiled coil. The fact that moving the unnatural residues toward the middle of the sequence, as in peptide **31**, ameliorates the decrease in helicity supports this hypothesis. The formation of oxime cross-links in GCN4-p1 is stabilizing to the coiled-coil but does not alter the helicity of the folded state. While surprising, this result does not inherently negate the use of oxime cross-links for the stabilization of bioactive helical folds. In prior applications of cross-linking towards stabilizing bioactive conformations, the motivation for cross-linking is not necessarily to generate maximally helical peptides but rather to stabilize the bound peptide-receptor complex. In many cases, these goals are aligned and the more helical peptide is also the most potent inhibitor; however, this is not always the case. In the GCN4-

p1 system, the stability of the coiled-coil can be viewed as the best measure of the ability of oxime cross-links to stabilize a helical fold in a protein-protein complex.

Triggered oxime formation can be used to selectively form cross-links that stabilize a particular folded conformation in a quaternary structure context. This was demonstrated by use of an oligomer capable of forming bicyclic products (peptide **34**). This oligomer contained unnatural residues at four sequence positions; triggered unmasking of glyoxyl aldehydes and subsequent oxime cyclization proceeds cleanly under buffered aqueous conditions. A single cross-linked topology was favored out of many possible, and this resulting bicyclic oligomer was highly resistant to thermal denaturation. The distribution of products obtained is altered by formation of the cross-links under conditions where the coiled-coil fold is partially disrupted. Collectively, these data suggest that triggered oxime formation can be utilized to trap and stabilize a particular peptide fold in its bound state.

### 2.3 SUMMARY OF INTRAMOLECULAR OXIME CROSS-LINK FORMATION

The use of oxidative unmasking of aldehydes from unnatural 1,2-aminoalcohol functionalized side chains and subsequent chemoselective reaction with aminoxy-functionalized residues to form oxime side chain cross-links in an intramolecular fashion has been investigated in two systems.

The first system is a short  $\alpha$ -helix of limited sequence diversity. In this context, oxime side chain cross-links are formed rapidly and in high yield under benign buffered aqueous conditions. The resulting cross-links are formed as a mixture of *E*- and *Z*-oxime isomers, which are capable of interconverting at neutral pH and isomerize more rapidly under acidic conditions. The resulting cyclic oxime can undergo dynamic covalent exchange to form a linear oxime species, which suggests the applicability of oxime cross-links in peptide-based dynamic covalent chemistry. Oxime cross-links are found to be capable of enhancing helical folding with a strong dependence on the structure of the cross-links generated. Smaller

macrocycle sizes formed by oxime cyclization appear to be poorly accommodated into the helical fold, suggesting that an  $i \rightarrow i+4$  spacing of **U** and **X** residues is required to stabilize a helix.

Data from the second model system, based on the  $\alpha$ -helical coiled coil GCN4-p1, demonstrates the utility of oxime side chain cross-links in stabilizing a protein-protein complex. Amongst a range of structural variants containing a single cross-link, an optimal side chain pairing was identified and a high-resolution structure of the oligomer in both linear and cyclized forms obtained. This structure demonstrates the compatibility of oxime cross-links with an  $\alpha$ -helical fold. A further survey of regioisomers suggests some basic rules for the introduction of oxime cross-links into helical sequences. Positions for substitution with unnatural residues should be chosen which do not introduce potentially unfavorable ionic interactions and/or remove stabilizing polar interactions present in the natural sequence. Amongst the large number of oxime cross-links examined (a total of 15 different monocyclic oligomers), the cross-links are generally well-accomodated and stabilizing to the coiled-coil fold. The synthesis of a bicyclic oligomer demonstrates the potential applicability of oxime cross-links to trap a bioactive fold under conditions where a peptide is bound to a protein receptor.

In summary, intramolecular peptide cross-linking via oxime formation is a viable and attractive method to control peptide folding in aqueous buffered solution. Intramolecular oxime cross-links can stabilize helical folds and protein quaternary structures. The observation that dynamic covalent exchange is severely limited in cases where intramolecular oxime cross-links are employed suggests that applications of this technology in the context of dynamic covalent chemistry are limited. The future implementation of this type of cross-linking strategy for applications in DCC may be possible by utilizing hydrazone formation rather than oxime formation, as hydrazones are more hydrolytically labile than oximes.

## 2.4 EXPERIMENTAL

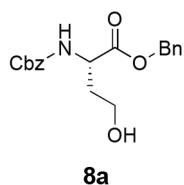
### 2.4.1 General Information

Solvents and all other reagents were purchased from Sigma Aldrich, Baker, EMD, Fisher, Acros Organics, or TCI and used as received unless otherwise specified. Cbz-Asp-OBn, Cbz-Glu-OBn, 2-chlorotrityl chloride, Boc-Ser(tBu)-OH, Fmoc-Dap-OH, Fmoc-Dab-OH, Fmoc-Orn-OH hydrochloride, and Fmoc-Lys-OH were purchased from Chem-Impex. 2-(6-chloro-1H-benzotriazole-1-yl)-1,1,3,3-tetramethylamminium hexafluorophosphate (HCTU), (benzotriazol-1-yloxy)tripyrrolidinophosphonium hexafluorophosphate (PyBOP), NovaPEG Rink Amide Resin, 9-fluorenylmethoxycarbonyl-N-hydroxysuccinimide (Fmoc-OSu), and Fmoc-protected  $\alpha$ -amino acids were purchased from NovaBiochem and used as received. Flash column chromatography was performed using Silicycle SiliaFlash P60 (230-400 mesh) or SorbTech (60 Å, 40-63  $\mu$ m) silica gel. Optical rotations were measured on a Perkin-Elmer 241 digital polarimeter with a sodium lamp at ambient temperature. NMR spectra were recorded on Bruker Avance-400 or Bruker Avance-300 spectrometers. MALDI-TOF mass spectrometry was carried out on a Voyager DE Pro instrument. Circular dichroism spectra were recorded on an Olis DSM17 Circular Dichroism Spectrometer using quartz cuvettes of 0.2 cm or 0.1 cm path length. Preparative and analytical HPLC were performed with Phenomenex Luna C<sub>18</sub> columns.

## 2.4.2 Aminoxy-Functionalized Monomer Synthesis

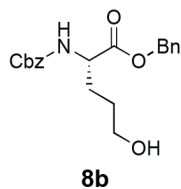
Fmoc-protected aminoxy monomers **12a** and **12b** were synthesized by adaptation of a previously reported procedure shown in Scheme 2.1 and as described below.<sup>84</sup>

**Standard Procedure A. Reduction of Carboxylic Acids:**<sup>85</sup> The carboxylic acid (Cbz-Asp-OBn, **7a** or Cbz-Glu-OBn, **7b**, 1.0 equiv) was dissolved in anhydrous tetrahydrofuran and cooled to  $-15\text{ }^{\circ}\text{C}$  under nitrogen. Triethylamine (1.1 equiv) was added, followed by isobutylchloroformate (1.1 equiv). The reaction was stirred 10-15 minutes, then sodium borohydride (3.0 equiv) dissolved in water was added slowly. The reaction was stirred 20-30 minutes until vigorous bubbling ceased and the reaction vessel poured into water. The solution was then extracted three times with ethyl acetate. The organic layers were combined, washed with brine, dried over anhydrous magnesium sulfate, and concentrated. Silica gel chromatography (25%→50% ethyl acetate in hexanes) afforded the corresponding alcohols **8a** and **8b**.



**benzyl ((benzyloxy)carbonyl)-L-homoserinate (8a):** Standard procedure A was employed using Cbz-Asp-OBn (1.99 g, 5.59 mmol) (**7a**) in 15 mL THF with triethylamine (858  $\mu\text{L}$ , 6.16 mmol) and isobutyl chloroformate (798  $\mu\text{L}$ , 6.16 mmol).

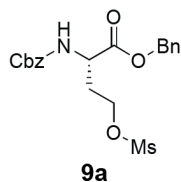
Sodium borohydride (634 mg, 16.8 mmol) was used in 5.0 mL of water. Product **8a** was isolated as a white solid (1.51 g, 4.42 mmol, 79.1% yield).  $[\alpha]_{\text{D}} = +0.6$  ( $c = 1$ ,  $\text{CHCl}_3$ ).  $^1\text{H NMR}$  (400 MHz,  $\text{CDCl}_3$ )  $\delta = 7.36$  (10H, m) 5.67 (1H, d,  $J = 7.4$  Hz), 5.16 (4H, m), 4.60 (1H, m), 3.68 (2H, m), 2.76 (1H, br s), 2.19 (1H, m), 1.71 (1H, m);  $^{13}\text{C NMR}$  (100 MHz,  $\text{CDCl}_3$ )  $\delta = 172.47$ , 156.88, 136.12, 135.23, 128.74, 128.67, 128.38, 128.25, 67.48, 67.38, 58.43, 51.45, 35.65; HRMS  $m/z$  calculated for  $\text{C}_{19}\text{H}_{21}\text{NO}_5\text{Na}$   $[\text{M}+\text{Na}]^+$ : 366.1317; found: 366.1322



**benzyl (S)-2-(((benzyloxy)carbonyl)amino)-5-hydroxypentanoate (8b):** Standard procedure A was employed using Cbz-Glu-OBn (1.99g, 5.53 mmol) (**7a**) in 15 mL THF with triethylamine (847  $\mu$ L, 6.08 mmol) and isobutyl chloroformate (788  $\mu$ L, 6.08 mmol). Sodium borohydride (628 mg, 16.6 mmol) was used in 5 mL of water. Product

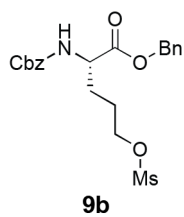
**8b** was isolated as a white solid (1.61 g, 4.49 mmol, 81.2%).  $[\alpha]_D = -1.9$  ( $c = 1.0$ ,  $\text{CHCl}_3$ ).  $^1\text{H NMR}$  (400 MHz,  $\text{CDCl}_3$ )  $\delta = 7.35$  (10H, m), 5.48 (1H, d,  $J = 8.0$  Hz), 5.17 (2H, m), 5.10 (2H, s), 4.47 (1H, m), 3.62 (2H, t,  $J = 5.7$  Hz), 1.95 (1H, m), 1.78 (1H, m), 1.56 (3H, m);  $^{13}\text{C NMR}$  (100 MHz,  $\text{CDCl}_3$ )  $\delta = 172.40$ , 156.17, 136.30, 135.36, 128.71, 128.61, 128.51, 128.40, 128.26, 128.18, 67.27, 67.10, 61.99, 53.77, 29.29, 28.18; HRMS  $m/z$  calculated for  $\text{C}_{20}\text{H}_{23}\text{NO}_5\text{Na}$   $[\text{M}+\text{Na}]^+$ : 380.1474; found: 380.1477.

**Standard Procedure B. Mesylation:**<sup>84</sup> The primary alcohol (**8a** or **8b**, 1.0 equiv) was dissolved in anhydrous dichloromethane and cooled to 0  $^\circ\text{C}$  under nitrogen. Triethylamine (1.5 equiv) was added and the solution stirred 15 minutes. Methanesulfonyl chloride (1.2 equiv) was added and the reaction stirred for 1-1.5 hours at 0  $^\circ\text{C}$ . The reaction was then diluted with additional dichloromethane and washed twice with brine. The organic layer was dried over magnesium sulfate and concentrated. The resulting mesylate (isolated as a yellow oil) was used directly in the next step without further purification.



**benzyl N-((benzyloxy)carbonyl)-O-(methylsulfonyl)-L-homoserinate (9a):** Standard procedure B was employed using compound **8a** (1.41 g, 4.11 mmol) in 10 mL dichloromethane, triethylamine (858  $\mu$ L, 6.16 mmol) and methanesulfonyl chloride (383

$\mu$ L, 4.93 mmol). Product **9a** was isolated as a yellow oil (1.62 g, 3.85 mmol, 93.7%).  $[\alpha]_D = +3.8$  ( $c = 1.0$ ,  $\text{CHCl}_3$ ).  $^1\text{H NMR}$  (400 MHz,  $\text{CDCl}_3$ )  $\delta = 7.38$  (10H, m), 5.61 (1H, d,  $J = 7.5$  Hz), 5.20 (2H, s), 5.13 (2H, s), 4.57 (1H, m), 4.29 (2H, m), 2.92 (3H, s), 2.38 (1H, m), 2.19 (1H, m);  $^{13}\text{C NMR}$  (100 MHz,  $\text{CDCl}_3$ )  $\delta = 171.34$ , 155.99, 136.11, 135.01, 128.76, 128.64, 128.50, 128.35, 128.19, 67.74, 67.25, 65.75, 50.97, 45.85, 37.13, 31.79.

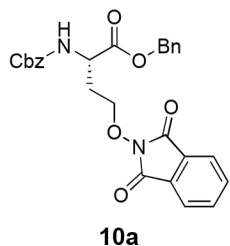


**9b**

**benzyl (S)-2-(((benzyloxy)carbonyl)amino)-5-((methylsulfonyl)oxy)pentanoate (9b):**

Standard procedure B was employed using compound **8b** (1.55 g, 4.33 mmol) in 10 mL dichloromethane, triethylamine (905  $\mu$ L, 6.49 mmol) and methanesulfonyl chloride (404  $\mu$ L, 5.19 mmol). Product **9b** was isolated as a yellow oil with a small amount of residual dichloromethane and triethylamine (1.85 g, 4.24 mmol, 97.9%).  $[\alpha]_D = +0.6$  ( $c = 1$ ,  $\text{CHCl}_3$ ).  $^1\text{H NMR}$  (300MHz,  $\text{CDCl}_3$ )  $\delta = 7.36$  (10H, m), 5.40 (1H, d,  $J = 7.7$  Hz), 5.19 (2H, br s), 5.11 (2H, s), 4.46 (1H, m), 4.20 (2H, t,  $J = 5.5$  Hz), 2.00 (1H, m), 1.79 (3H, m).

**Standard Procedure C. Installation of Pthalimide:**<sup>84</sup> *N*-hydroxyphthalimide (2.0 equiv) was dissolved in anhydrous dimethylformamide and cooled to 0 °C on an ice bath under nitrogen. 1,8-Diazabicyclo[5.4.0]undec-7-ene (DBU) (2.0 equiv) was added and the solution stirred for 20 minutes at 0 °C. The mesylate **9a** or **9b** (1.0 equiv) was dissolved in anhydrous DMF and added to the reaction via syringe. The reaction was allowed to warm to room temperature and stirred for two days. Following this time, the reaction was diluted with ethyl acetate, washed twice with water, twice with saturated sodium carbonate, and twice with brine. The organic layer was dried over magnesium sulfate and concentrated. When necessary, the resulting oil was purified by silica gel chromatography (20%→25% ethyl acetate in hexanes).

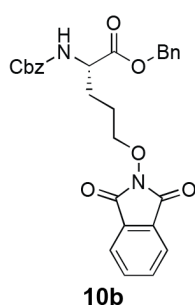


**10a**

**benzyl N-(((benzyloxy)carbonyl)-O-(1,3-dioxoisindolin-2-yl)-L-homoserinate**

**(10a):** Standard procedure C was employed with *N*-hydroxyphthalimide (1.26 g, 7.72 mmol) in 7 mL anhydrous DMF with DBU (1.15 mL, 7.72 mmol) The mesylate **9a** (1.62 g, 3.85 mmol) was added in 10 mL anhydrous DMF. Product **10a** was isolated

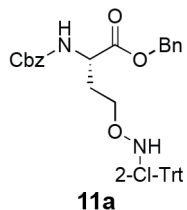
as a white solid (1.05 g, 2.16 mmol, 56.1% yield).  $[\alpha]_D = +1.0$  ( $c = 1.0$ ,  $\text{CHCl}_3$ ).  $^1\text{H NMR}$  (400 MHz,  $\text{CDCl}_3$ )  $\delta = 7.79$  (4H, m), 7.29 (10H, m), 6.22 (1H, d,  $J = 8.3$  Hz), 5.19 (4H, m), 4.68 (1H, m), 4.28 (2H, m), 2.35 (2H, q,  $J = 5.6$  Hz);  $^{13}\text{C NMR}$  (100 MHz,  $\text{CDCl}_3$ )  $\delta = 171.49$ , 163.55, 156.31, 135.41, 134.72, 128.93, 128.63, 128.58, 128.55, 128.44, 128.14, 128.09, 74.94, 67.43, 67.03, 51.68, 30.30; HRMS  $m/z$  calculated for  $\text{C}_{27}\text{H}_{24}\text{N}_2\text{O}_7\text{Na}$   $[\text{M}+\text{Na}]^+$ : 511.1481; found 511.1484.



**benzyl (S)-2-(((benzyloxy)carbonyl)amino)-5-((1,3-dioxoisindolin-2-yl)oxy)pentanoate (10b):** Standard procedure C was employed with *N*-hydroxyphthalimide (1.38 g, 8.48 mmol) in 10 mL anhydrous DMF with DBU (1.27 mL, 8.48 mmol) The mesylate **9b** (1.85 g, 4.24 mmol) was added in 10 mL anhydrous DMF. Product **10b** was isolated as a white solid (1.83 g, 3.65 mmol, 86.1%).  $[\alpha]_D = -6.8$  ( $c =$

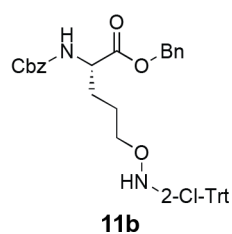
1.0, CHCl<sub>3</sub>). <sup>1</sup>H NMR (400 MHz, CDCl<sub>3</sub>)  $\delta = 7.78$  (4H, m), 7.34 (10H, m), 5.51 (1H, d,  $J = 8.2$  Hz), 5.20 (2H, s), 5.10 (2H, s), 4.49 (1H, m), 4.18 (2H, m), 2.16 (1H, m), 2.01 (1H, m), 1.80 (2H, m); <sup>13</sup>C NMR (100 MHz, CDCl<sub>3</sub>)  $\delta = 172.13, 163.76, 156.12, 136.39, 135.40, 134.64, 129.02, 128.74, 128.62, 128.56, 128.40, 128.24, 128.16, 123.68, 77.58, 67.38, 67.08, 53.81, 28.96, 24.44$ ; HRMS  $m/z$  calculated for C<sub>27</sub>H<sub>24</sub>N<sub>2</sub>O<sub>7</sub>Na [M+Na]<sup>+</sup>: 525.1638; found 525.1613.

**Standard Procedure D. Phthalimide Deprotection and Trityl Protection.**<sup>84</sup> The phthalimide compound **10a** or **10b** (1.0 equiv) was dissolved in anhydrous DCM and cooled to 0 °C under nitrogen. Methyl hydrazine (1.5 equiv) was added and the reaction stirred for 1.5 hours at 0 °C. The reaction was then filtered through celite, washed with dichloromethane, and concentrated. The resulting oil was used directly in the next step without additional purification. The intermediate (1.0 equiv) was dissolved in anhydrous dichloromethane under nitrogen. DIEA (2.0 equiv) was added, followed by 2-chlorotrityl chloride (1.5 equiv). The reaction was stirred at room temperature for 2 hours. After this time, the reaction was diluted with ethyl acetate, washed with water and brine, then dried over magnesium sulfate and concentrated. Silica gel chromatography (15%→25% ethyl acetate in hexanes) yielded the product **11a** or **11b**.



**benzyl N-((benzyloxy)carbonyl)-O-(((2-chlorophenyl)diphenylmethyl)amino)-L-homoserinate (11a):** Standard procedure D was employed using **10a** (871 mg, 1.78 mmol) in 8 mL anhydrous methylene chloride with methyl hydrazine (141  $\mu$ L, 2.67 mmol). The resulting aminoxy compound (1.78 mmol) was dissolved in 8 mL anhydrous methylene chloride with diisopropylethylamine (620  $\mu$ L, 3.56 mmol) and 2-chlorotrityl

chloride (836 mg, 2.67 mmol). The product was isolated as a viscous, light yellow oil (733 mg, 1.15 mmol, 64.6% yield).  $[\alpha]_D = -10$  ( $c = 1.0$ ,  $\text{CHCl}_3$ ).  $^1\text{H NMR}$  (400 MHz,  $\text{CDCl}_3$ )  $\delta = 7.19$  (24H, m), 5.28 (1H, d,  $J = 7.7$  Hz), 5.09 (2H, s), 5.03 (2H, s), 4.70 (1H, s), 4.37 (1H, m), 3.81 (2H, m), 1.98 (2H, q,  $J = 5.4$  Hz);  $^{13}\text{C NMR}$  (100 MHz,  $\text{CDCl}_3$ )  $\delta = 171.72$ , 156.04, 143.11, 142.94, 140.37, 136.46, 135.56, 133.86, 132.76, 131.64, 128.81, 128.75, 128.70, 128.59, 128.49, 128.37, 128.32, 128.24, 128.00, 127.97, 127.18, 127.15, 126.49, 74.90, 70.46, 67.13, 66.98, 52.68, 30.51; HRMS  $m/z$  calculated for  $\text{C}_{38}\text{H}_{35}\text{ClN}_2\text{O}_5\text{Na}$   $[\text{M}+\text{Na}]^+$ : 657.2132; found: 657.2145.



**benzyl**

**(S)-2-(((benzyloxy)carbonyl)amino)-5-(((2-**

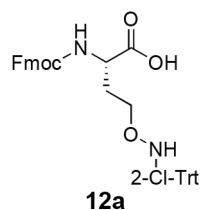
**chlorophenyl)diphenylmethyl)amino)oxy)pentanoate (11b):** Standard procedure

D was employed using **10b** (647 mg, 1.28 mmol) in 7 mL anhydrous methylene chloride with methyl hydrazine (101  $\mu\text{L}$ , 1.92 mmol). The resulting aminoxy

compound (1.28 mmol) was dissolved in 7 mL anhydrous methylene chloride with diisopropylethylamine (446  $\mu\text{L}$ , 2.56 mmol) and 2-chlorotritylchloride (601 mg, 1.92 mmol). Product **11b** was isolated as pale yellow oil (709 mg, 1.09 mmol, 85.2%).  $[\alpha]_D = +1.4$  ( $c = 1.0$ ,  $\text{CHCl}_3$ ).  $^1\text{H NMR}$  (400 MHz,  $\text{CDCl}_3$ )  $\delta = 7.29$  (24H, m), 5.19 (1H, d,  $J = 6.2$  Hz), 5.12 (2H, s), 5.09 (2H, s), 4.30 (1H, m), 3.20 (2H, t,  $J = 5.4$  Hz), 1.69 (1H, m), 1.48 (3H, m);  $^{13}\text{C NMR}$  (100 MHz,  $\text{DMSO}-d_6$ )  $\delta = 172.18$ , 156.12, 142.09, 141.05, 138.86, 135.92, 133.36, 131.75, 131.04, 128.81, 128.38, 128.32, 128.00, 127.81, 127.73, 127.39, 126.65, 126.49, 73.89, 71.87, 65.84, 65.47, 59.73, 53.76, 27.25, 24.50, 20.73, 14.06; HRMS  $m/z$  calculated for  $\text{C}_{39}\text{H}_{37}\text{ClN}_2\text{O}_5\text{Na}$   $[\text{M}+\text{Na}]^+$ : 671.2288; found: 671.2299.

**Standard Procedure E. Hydrogenolysis and Fmoc Protection:**<sup>84</sup> The fully protected compound **11a** or **11b** (1.0 equiv) was dissolved in anhydrous methanol. The vessel was thoroughly flushed with nitrogen, and Pd/C (20 wt%) was added. The headspace of the reaction vessel was purged, and the vessel was fitted with a hydrogen filled balloon and stirred overnight. After this time, the reaction was filtered through celite, washed with methanol, and concentrated. The resulting white solid was dissolved in anhydrous DCM and placed under nitrogen atmosphere. DIEA (4.0 equiv) was added, followed by addition of

trimethylsilyl chloride (2.0 equiv). The reaction was stirred at room temperature for 15 minutes, then Fmoc-OSu (1.1 equiv) was added and the reaction stirred overnight under nitrogen. Following this time, the reaction was diluted with ethyl acetate and washed twice with brine. The resulting organic layer was dried over magnesium sulfate and concentrated. Silica gel chromatography (33%→100% ethyl acetate in hexanes) yielded product **12a** or **12b**.



***N*-(((9*H*-fluoren-9-yl)methoxy)carbonyl)-*O*-(((2-**

**chlorophenyl)diphenylmethyl)amino)-*L*-homoserine (**12a**):** Standard procedure E

was used starting from compound **11a** (643 mg, 1.01 mmol) in 8 mL anhydrous

methanol with Pd/C, 20 wt% (50 mg, 8% w/w). The resulting white solid was dissolved

in 8 mL anhydrous DCM with DIEA (703  $\mu$ L, 4.04 mmol), trimethylsilyl chloride (256  $\mu$ L, 2.02 mmol)

and Fmoc-OSu (408 mg, 1.21 mmol). Product **12a** was isolated as a white solid (489 mg 0.773 mmol,

76.5%).  $[\alpha]_D = -2.7^\circ$  ( $c = 1.0$ ,  $\text{CHCl}_3$ ).  $^1\text{H NMR}$  (400 MHz,  $\text{DMSO-}d_6$ )  $\delta = 12.31$  (1H, s), 7.90 (1H, d,  $J =$

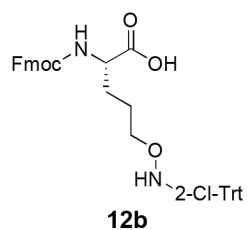
7.5 Hz), 7.73 (1H, m), 7.58 (1H, s), 7.52 (2H, m), 7.42 (2H, m), 7.29 (17H, m), 5.03 (1H, s), 4.25 (2H,

m), 3.90 (1H, m), 3.61 (2H, m), 1.84 (1H, m), 1.70 (1H, m);  $^{13}\text{C NMR}$  (100 MHz,  $\text{DMSO-}d_6$ )  $\delta = 173.76$ ,

156.01, 143.83, 142.07, 140.97, 140.72, 136.97, 133.36, 131.79, 131.09, 128.86, 128.33, 127.77, 127.47,

127.45, 127.07, 126.74, 126.59, 125.30, 120.11, 79.18, 73.94, 69.47, 65.61, 65.40, 51.02, 46.63, 29.69;

HRMS  $m/z$  calculated for  $\text{C}_{38}\text{H}_{33}\text{ClN}_2\text{O}_5\text{Na}$   $[\text{M}+\text{Na}]^+$ : 655.1976; found: 655.1963.



**(*S*)-2-(((9*H*-fluoren-9-yl)methoxy)carbonyl)amino)-5-(((2-**

**chlorophenyl)diphenylmethyl)amino)oxy)pentanoic acid (**12b**):** Standard

procedure E was used starting from compound **11b** (640 mg, 0.990 mmol) in 8 mL

anhydrous methanol with Pd/C, 20 wt% (50 mg, 8% w/w). The resulting white solid

was dissolved in 8 mL anhydrous DCM with DIEA (696  $\mu$ L, 3.99 mmol), trimethylsilyl chloride (251  $\mu$ L,

1.98 mmol) and Fmoc-OSu (367 mg, 1.09 mmol). Product **12b** was isolated as a white solid (428 mg,

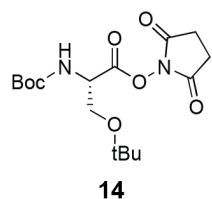
0.663 mmol, 67.0%).  $[\alpha]_D = +9.5^\circ$  ( $c = 1.0$ ,  $\text{CHCl}_3$ ).  $^1\text{H NMR}$  (400 MHz,  $\text{DMSO-}d_6$ )  $\delta = 12.16$  (1H, s),

7.90 (1H, d,  $J = 7.5$  Hz), 7.72 (1H, d,  $J = 7.5$  Hz), 7.54 (3H, m), 7.42 (2H, t,  $J = 7.4$  Hz), 7.30 (17H, m),

5.03 (1H, s), 4.27 (2H, m), 3.85 (1H, m), 3.53 (2H, m), 1.53 (1H, m), 1.42 (3H, m);  $^{13}\text{C}$  NMR (100 MHz, DMSO- $d_6$ )  $\delta$  = 173.84, 156.07, 143.84, 143.77, 142.16, 141.09, 140.69, 137.00, 133.39, 131.08, 128.84, 128.31, 127.62, 127.43, 126.04, 126.69, 126.54, 125.27, 120.08, 114.15, 79.18, 73.92, 72.13, 65.56, 65.35, 53.64, 46.65, 27.41, 24.72; HRMS  $m/z$  calculated for  $\text{C}_{39}\text{H}_{35}\text{ClN}_2\text{O}_5\text{Na}$   $[\text{M}+\text{Na}]^+$ : 669.2132; found: 669.2129.

### 2.4.3 Serine-Acylated Monomer Synthesis.

Serine-acylated monomers **16a-16d** were synthesized by adaptation of previously published methods as shown in Schemes 2.2 and 2.3 and described below.<sup>78</sup>

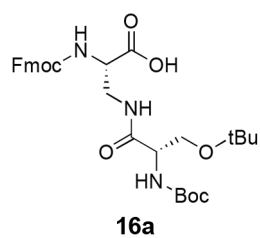


**(S)-tert-butyl (1-(tert-butoxy)-4-(2,5-dioxopyrrolidin-1-yl)-3-oxobutan-2-yl)carbamate (14):**<sup>78</sup> Boc-Ser(*t*Bu)-OH (500 mg, 1.91 mmol, 1.0 equiv) was dissolved in 7.5 mL water and 7.5 mL dioxane under nitrogen. *N*-hydroxysuccinimide (242 mg,

2.10 mmol, 1.1 equiv) was added and the reaction was cooled to 0 °C. *N,N'*-dicyclohexylcarbodiimide (433 mg, 2.10 mmol, 1.1 equiv) was added to the reaction vessel. The reaction was allowed to warm to room temperature and stirred for 3 hours. Following this time, the mixture was filtered through celite, washed with ethyl acetate and concentrated. The resulting oil was dissolved in 75 mL ethyl acetate and washed twice each with 30 mL saturated aqueous  $\text{NaHCO}_3$ , water, and brine. The organic layer was dried over anhydrous sodium sulfate and concentrated to afford compound **14** isolated as a white solid (606 mg, 1.69 mmol, 88.5%).  $^1\text{H}$  NMR (400 MHz,  $\text{CDCl}_3$ )  $\delta$  = 5.40 (1H, d,  $J$  = 9.0 Hz), 4.75 (1H, m), 3.89 (1H, m), 3.64 (1H, m), 2.80 (4H, s), 1.43 (9H, s), 1.18 (9H, s);  $^{13}\text{C}$  NMR (100 MHz,  $\text{CDCl}_3$ )  $\delta$  = 168.59, 166.96, 155.13, 80.43, 73.94, 61.81, 53.07, 28.34, 27.22, 25.64; HRMS  $m/z$  calculated for  $\text{C}_{16}\text{H}_{26}\text{N}_2\text{O}_7\text{Na}$   $[\text{M}+\text{Na}]^+$ : 381.1638; found: 381.1645.

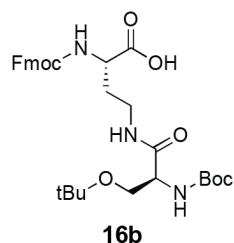
**Standard Procedure G. Coupling of Serine to Amine Side-Chain Compounds:**<sup>78</sup> The Fmoc-protected amino acid **15a-d** (1.0 equiv) was suspended in anhydrous dimethylformamide under nitrogen. *N*-methyl-

*N*-(trimethylsilyl) trifluoroacetamide (MSTFA) (2.1 equiv) was added and the reaction stirred 4 hours at room temperature. Following this time, Boc-Ser(*t*Bu)-NHS (**14**) (1.2 equiv) was added and the reaction was stirred for 2-3 days. The reaction was then diluted with ethyl acetate and washed twice with brine. Silica gel chromatography (33% → 100% ethyl acetate in hexanes) afforded products **16a-d**.



**(S)-2-((((9H-fluoren-9-yl)methoxy)carbonyl)amino)-3-((S)-3-(tert-butoxy)-2-((tert-butoxycarbonyl)amino)propanamido)propanoic acid (16a):** Standard procedure G was employed starting with Fmoc-diaminopropionic acid (Fmoc-Dap-OH, **15a**) (1.06 g, 3.05 mmol) in 20 mL anhydrous dimethyl formamide with

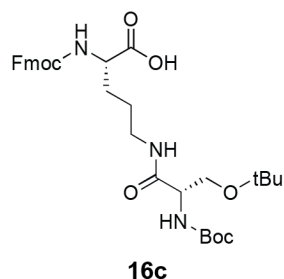
*N*-methyl-*N*-(trimethylsilyl) trifluoroacetamide (1.19 mL, 6.42 mmol) and Boc-Ser(*t*Bu)-NHS (1.31 g, 3.67 mmol). Product **16a** was isolated as a white solid (1.17 g, 2.05 mmol, 67%).  $[\alpha]_D = +11$  ( $c = 1.0$ , CHCl<sub>3</sub>). <sup>1</sup>H NMR (400 MHz, DMSO-*d*<sub>6</sub>)  $\delta = 12.84$  (1H, s), 7.95 (1H, m), 7.90 (2H, d,  $J = 7.53$ ), 7.70 (2H, d,  $J = 7.53$ ), 7.49 (1H, d,  $J = 8.0$ ), 7.43 (2H, t,  $J = 7.28$ ), 7.35 (2H, m), 6.57 (1H, d,  $J = 8.3$ ), 4.32 (1H, m), 4.24 (2H, m), 4.09 (1H, m), 4.03 (1H, m), 3.62 (1H, m), 3.46 (1H, m), 3.40 (1H, m), 3.26 (1H, m), 1.38 (9H, s), 1.09 (9H, s); <sup>13</sup>C NMR (100 MHz, DMSO-*d*<sub>6</sub>)  $\delta = 171.98$ , 156.01, 155.16, 143.80, 143.75, 140.74, 127.66, 127.12, 125.24, 120.15, 79.20, 78.18, 72.78, 65.78, 61.95, 55.05, 53.99, 46.61, 28.17, 26.17, 25.25; HRMS  $m/z$  calculated for C<sub>30</sub>H<sub>39</sub>N<sub>3</sub>O<sub>8</sub>Na [M+Na]<sup>+</sup>: 592.2635; found: 592.2648.



**(S)-2-((((9H-fluoren-9-yl)methoxy)carbonyl)amino)-4-((S)-3-(tert-butoxy)-2-((tert-butoxycarbonyl)amino)propanamido)butanoic acid (16b):** Standard procedure G was employed starting from Fmoc-diaminobutyric acid (Fmoc-Dab-OH, **15b**) (499 mg, 1.46 mmol) in 10 mL anhydrous DMF with *N*-methyl-*N*-

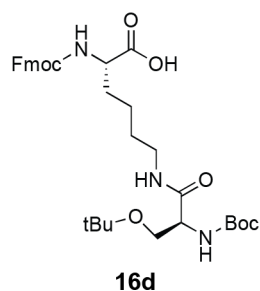
(trimethylsilyl)trifluoroacetamide (568  $\mu$ L, 3.07 mmol) and Boc-Ser(*t*Bu)-NHS (624 mg, 1.75 mmol). Product **16b** was isolated as a white solid with residual DMF present (540 mg, 0.93 mmol, 63%).  $[\alpha]_D = +4.7$  ( $c = 1.0$ , CHCl<sub>3</sub>). <sup>1</sup>H NMR (400 MHz, DMSO-*d*<sub>6</sub>)  $\delta = 12.63$  (1H, s), 7.90 (2H, m), 7.74 (2H, d,  $J = 7.40$ ), 7.69 (1H, d,  $J = 8.03$  Hz), 7.42 (2H, t,  $J = 7.40$  Hz), 7.34 (2H, t,  $J = 7.40$  Hz), 6.51 (1H, d,  $J = 8.53$  Hz), 4.27 (2H, m), 3.99 (2H, m), 3.42 (2H, m), 3.18 (1H, m), 3.07 (1H, m), 1.92 (1H, m), 1.71 (1H, m),

1.37 (9H, s), 1.09 (9H, s);  $^{13}\text{C}$  NMR (100 MHz, DMSO- $d_6$ )  $\delta$  = 173.71, 173.04, 170.08, 162.30, 156.12, 155.06, 143.81, 140.71, 127.64, 127.09, 125.29, 120.12, 78.15, 72.68, 65.65, 62.03, 55.01, 51.63, 46.64, 35.78, 30.76, 28.15, 27.19; HRMS  $m/z$  calculated for  $\text{C}_{31}\text{H}_{41}\text{N}_3\text{O}_8$   $[\text{M}+\text{H}]^+$ : 584.2972; found: 584.2983.



**(S)-2-(((9H-fluoren-9-yl)methoxy)carbonyl)amino)-5-((S)-3-(tert-butoxy)-2-((tert-butoxycarbonyl)amino)propanamido)pentanoic acid (14c):** Standard procedure G was employed with a slight modification. Fmoc-ornithine hydrochloride **15c** (494 mg, 1.26 mmol) was suspended in 5 mL anhydrous dimethyl formamide under nitrogen with DIEA (225  $\mu\text{L}$ , 1.26 mmol) and stirred

for 5 min. Following this time, *N*-methyl-*N*-(trimethylsilyl) trifluoroacetamide (492  $\mu\text{L}$ , 2.65 mmol) and Boc-Ser(tBu)-NHS (541 mg, 1.52 mmol) were added. Product **16c** was isolated as a white solid with residual DMF present (614 mg, 1.02 mmol, 80.9%).  $[\alpha]_{\text{D}} = +20$  ( $c = 1.0$ ,  $\text{CHCl}_3$ ).  $^1\text{H}$  NMR (400 MHz, DMSO- $d_6$ )  $\delta$  = 12.56 (1H, s), 7.89 (2H, d,  $J = 7.40$  Hz), 7.82 (1H, t,  $J = 5.02$  Hz), 7.72 (2H, d,  $J = 7.40$  Hz), 7.64 (1H, d,  $J = 8.03$  Hz), 7.42 (2H, t,  $J = 7.34$  Hz), 7.32 (2H, m), 6.48 (1H, d,  $J = 8.41$  Hz), 4.26 (3H, m), 3.94 (2H, m), 3.41 (2H, m), 3.06 (2H, m), 1.72 (1H, m), 1.55 (1H, m), 1.48 (3H, m), 1.37 (9H, s), 1.08 (9H, s);  $^{13}\text{C}$  NMR (100 MHz, DMSO- $d_6$ )  $\delta$  = 173.86, 169.95, 156.15, 155.06, 143.85, 143.80, 140.73, 127.65, 127.09, 125.31, 120.12, 78.15, 72.66, 65.63, 62.05, 55.03, 53.67, 46.66, 38.18, 28.16, 27.21, 25.89; HRMS  $m/z$  calculated for  $\text{C}_{32}\text{H}_{43}\text{N}_3\text{O}_8$   $[\text{M}+\text{H}]^+$ : 598.3128; found: 598.3154.



**(S)-2-(((9H-fluoren-9-yl)methoxy)carbonyl)amino)-6-((S)-3-(tert-butoxy)-2-((tert-butoxycarbonyl)amino)propanamido)hexanoic acid (16d):** Standard procedure G was employed starting from Fmoc-Lys-OH **15d** (502 mg, 1.36 mmol) in 10 mL anhydrous DMF with *N*-methyl-*N*-(trimethylsilyl) trifluoroacetamide (528  $\mu\text{L}$ , 2.85 mmol) and Boc-Ser(tBu)-NHS (581 mg, 1.63 mmol). Product **16d**

was isolated as a viscous colorless oil with a small amount of residual DMF present (576 mg, 0.942 mmol, 69%).  $[\alpha]_{\text{D}} = -6.5$  ( $c = 1.0$ ,  $\text{CHCl}_3$ ).  $^1\text{H}$  NMR (400 MHz, DMSO- $d_6$ )  $\delta$  = 12.55 (1H, s), 7.88 (2H, d,  $J = 7.53$  Hz), 7.81 (1H, t,  $J = 5.02$  Hz), 7.74 (2H, d,  $J = 7.40$  Hz), 7.62 (1H, d,  $J = 7.91$  Hz), 7.42 (2H, t,  $J$

= 7.28 Hz), 7.34 (2H, t,  $J = 7.40$  Hz), 6.48 (1H, d,  $J = 8.41$  Hz), 4.27 (3H, m), 3.97 (1H, m), 3.91 (1H, m), 3.42 (2H, m), 3.10 (1H, m), 3.01 (1H, m), 1.69 (1H, m), 1.61 (1H, m), 1.37 (12H, m), 1.08 (9H, s);  $^{13}\text{C}$  NMR (100 MHz,  $\text{DMSO-}d_6$ )  $\delta = 174.03, 169.86, 156.16, 155.05, 143.80, 140.73, 127.64, 127.07, 125.30, 120.12, 78.13, 72.63, 65.60, 62.03, 54.97, 53.77, 46.66, 30.38, 28.59, 28.14, 27.20, 25.23, 22.94$ ; HRMS  $m/z$  calculated for  $\text{C}_{33}\text{H}_{44}\text{N}_3\text{O}_8$   $[\text{M}+\text{H}]^+$ : 612.3285; found: 612.3271.

#### 2.4.4 Peptide Synthesis And Purification

Peptides **1-34** were synthesized on NovaPEG Rink Amide Resin either manually with microwave heating (MARS microwave reactor, CEM) or in an automated fashion on a Tribute synthesizer (Protein Technologies, Inc.)

In a typical microwave procedure, the desired amino acid (4.0 equiv to resin) was preactivated with HCTU (4.0 equiv to resin) and DIEA (6.0 equiv to resin) in NMP for 2-3 minutes. The preactivated amino acid was then added to the resin in a reaction vessel fit with a stir bar. The solution was subjected to a microwave coupling program run consisting of a 2 minute ramp to 70 °C and a 4 minute hold at 70 °C. After the coupling program completed, the resin was washed three times with DMF. Following washing, the resin was treated with 20% 4-methylpiperidine in DMF with a microwave deprotection program consisting of a 2 minute ramp to 80 °C and a 2 minute hold at 80 °C. Following completion of the deprotection program, the resin was washed three times with DMF, and the previous steps repeated until the peptide chain was completed on resin.

In a typical automated synthesis, Fmoc-protected amino acids (5.0 equiv to resin) were coupled with HCTU (5.0 equiv to resin) and DIEA (7.5 equiv to resin) for 45 minutes at room temperature. The N-terminus was deprotected by treatment with 20% 4-methylpiperidine in DMF, twice for 4 minutes at room temperature. Following each coupling or deprotection step, the resin was washed with DMF three times. The previous steps were repeated until the peptide chain was completed on resin.

Unnatural aminoxy-functionalized monomers **12a** and **12b** were coupled identically to the procedure described above for natural Fmoc-amino acids except that PyBOP was used in place of HCTU. This was required by the observation of guanidinium-capped peptide impurities when HCTU was utilized with monomers **12a** and **12b**.

Following completion of the peptide chain on resin and removal of the N-terminal Fmoc group, the N-terminus was acetylated by treatment with 8:2:1 v:v:v DMF:DIEA:Ac<sub>2</sub>O for 10-15 minutes at room temperature. Following acetylation, the resin was washed three times each with DMF, DCM, and methanol, then dried in a vacuum dessicator. Cleavage of the peptide from resin was accomplished by treatment with 92.5% trifluoroacetic acid, 3% water, 3% ethanedithiol, and 1.5% triisopropylsilane for 2-5 hours. The crude peptide was then precipitated in cold diethyl ether and centrifuged, the ether decanted, and the crude material dissolved in 0.1% TFA in water and 0.1% TFA in methanol for purification.

Peptides were purified by HPLC on a Luna C<sub>18</sub> preparative column using gradients between 0.1% TFA in water and 0.1% TFA in acetonitrile. Identities of the purified peptides were confirmed by MALDI-TOF MS. All peptides used for biophysical characterization were  $\geq 95\%$  pure by analytical HPLC.

A few observations regarding peptide synthesis and purification are of note. We found that cleavage of the peptides containing aminoxy functionalized **X** residues necessitated the use of ethanedithiol or other strong nucleophilic scavengers to avoid alkylation of the aminoxy functionality by the resin, leading to little or no isolatable product.<sup>86</sup> Additionally, peptides containing aminoxy-functionalized **X** residues were allowed to sit in acetonitrile for extended periods (>2 hours), significant amounts of unidentified byproduct were formed.<sup>101</sup> We attribute this formation to the reaction of the nucleophilic aminoxy residue with contaminants in acetonitrile. Finally, it was observed that some reverse-phase C<sub>18</sub> HPLC stationary phases irreversibly bind aminoxy-functionalized peptides. Although the cause of this phenomena was never clear, we were able to find stationary phases free of this problem (Phenomenex Luna C<sub>18</sub>).

**Table 4.** MALDI-TOF data for peptides **1-6** and reaction products.

Peptide	[M+H] <sup>+</sup> ( <i>m/z</i> )	
	Calculated	Observed
<b>1</b>	1704.9	1704.6
<b>2</b>	1851.9	1851.5
<b>3</b>	1865.9	1865.8
<b>4</b>	1851.9	1851.8
<b>5</b>	1865.9	1866.1
<b>6</b>	1863.9	1864.0
<b>2b</b>	1802.9	1802.5
<b>2c</b>	1849.9	1850.1
<b>3b</b>	1816.9	1816.8
<b>4b</b>	1802.9	1802.3
<b>5b</b>	1816.9	1817.1
<b>6a</b>	1854.9*	1854.6*

\*Calculated and observed for [M+Na]<sup>+</sup>**Table 5.** MALDI-TOF data for peptides **17-34** and cyclized products.

Peptide	[M+H] <sup>+</sup> ( <i>m/z</i> )		Peptide	[M+H] <sup>+</sup> ( <i>m/z</i> )	
	Calculated	Observed		Calculated	Observed
<b>17</b>	4036.2	4036.5	<b>17-ox</b>	4052.2	4052.4
<b>18</b>	4018.3	4018.2			
<b>19</b>	4063.3	4063.1	<b>19b</b>	4014.3	4014.0
<b>20</b>	4077.3	4077.3	<b>20b</b>	4028.3	4028.3
<b>21</b>	4077.3	4077.6	<b>21b</b>	4028.3	4028.6
<b>22</b>	4091.4	4091.6	<b>22b</b>	4042.3	4042.5
<b>23</b>	4091.4	4091.4	<b>23b</b>	4042.3	4042.3
<b>24</b>	4105.4	4104.4	<b>24b</b>	4056.3	4055.9
<b>25</b>	4105.4	4105.1	<b>25b</b>	4056.3	4056.6
<b>26</b>	4119.4	4119.0	<b>26b</b>	4070.3	4070.1
<b>27</b>	4077.3	4077.4	<b>27b</b>	4028.3	4028.6
<b>28</b>	4091.4	4091.4	<b>28b</b>	4042.3	4041.9
<b>29</b>	4105.4	4105.8	<b>29b</b>	4056.3	4056.5
<b>30</b>	4119.4	4119.1	<b>30b</b>	4070.3	4070.4
<b>31</b>	4111.3	4111.7	<b>31b</b>	4062.2	4062.5
<b>32</b>	4065.3	4065.1	<b>32b</b>	4016.2	4016.1
<b>33</b>	4078.3	4078.5	<b>33b</b>	4029.2	4028.9
<b>34</b>	4184.4	4184.6	<b>34b</b>	4104.4	4104.0
			<b>34c</b>	4086.2	4086.8

## 2.4.5 Peptide Oxidation And HPLC Analysis

### 2.4.5.1 Helical Peptide Model System

Stock solutions of peptides **1-6** were prepared in 100 mM phosphate buffered aqueous solution at pH 7 and the concentration of each peptide determined by UV-Vis spectroscopy based on tyrosine absorbance at 276 nm ( $\epsilon_{276} = 1450 \text{ M}^{-1} \text{ cm}^{-1}$ ).<sup>102</sup> Oxidation and cross-linking reactions were performed by dilution of the peptide stock with 100 mM phosphate buffer to a final peptide concentration of 100  $\mu\text{M}$  and subsequent addition of 2 equivalents of aqueous sodium periodate, which oxidizes the serine-acylated U residue to the corresponding glyoxyl aldehyde.<sup>77, 78, 98</sup> Following addition of periodate, aliquots were removed from the oxidized solutions and diluted by 10% with 0.1% TFA in water for analysis by HPLC. Complete consumption of the starting peptide was observed within 10 minutes in all cases. The identity of the observed chromatographic peaks was determined by collection of the eluent from analytical HPLC and analysis by MALDI-TOF MS.

### 2.4.5.2 Coiled-Coil Model System

Stock solutions of peptides **17-34** were prepared in water and the concentration of each peptide determined by UV-Vis spectroscopy based on tyrosine absorbance and 276 nm ( $\epsilon_{276} = 1450 \text{ M}^{-1} \text{ cm}^{-1}$ ).<sup>102</sup> A stock of sodium periodate in water was made and the concentration of periodate determined by UV-Vis spectroscopy ( $\epsilon_{280} = 317 \text{ M}^{-1} \text{ cm}^{-1}$ ).<sup>103</sup> Oxidation and cross-linking reactions were performed by dilution of the peptide stock with phosphate buffer, water, and aqueous sodium periodate to yield samples comprised of 100  $\mu\text{M}$  peptide and 100  $\mu\text{M}$   $\text{NaIO}_4$  in 0.1 M phosphate buffer at pH 7.

The cyclization of peptide **34**, to form a bicyclic oligomer, was carried out identically except that 2.1 equiv of periodate relative to peptide were used to a final concentration of 210  $\mu\text{M}$   $\text{NaIO}_4$ . For experiments performed at 80 °C, peptide **34** at 100  $\mu\text{M}$  concentration in 0.1 M phosphate buffer at pH 7

was heated to 80 °C in a water bath. After 5-10 minutes, sodium periodate was added as described above. The sample was maintained at 80 °C for an additional 10 minutes, and then analyzed.

Following addition of periodate, aliquots were removed from the peptide solutions and analyzed by HPLC. Complete consumption of the starting material was observed in 10 minutes or less in all cases. The identity of observed chromatographic peaks was determined by collection of analytical HPLC eluent and MALDI-TOF MS.

#### 2.4.6 NMR Assignment Of Oxime Isomers

An oxidation reaction of peptide **2** was performed as described in section 2.4.5.1 with a total volume of 2 mL. After 15 minutes, the oxidized peptide was diluted by 10% with 0.1% TFA solution and injected on to preparative-scale HPLC. Two fractions, corresponding to the two observed oxime isomers of species **2b** were collected, frozen immediately, and lyophilized. Though the isomers were fully separated by HPLC, it was observed that the minor observed isomer of **2b** partially equilibrates to the major isomer of **2b** in the short period of time required to freeze the collected fraction for lyophilization. Two fractions were thus obtained, one composed of primarily (~95%) the major isomer of **2b** and one composed of a mixture (~70% major, ~30% minor) of the two isomers of **2b**. The lyophilized powder from each fraction was taken up in D<sub>2</sub>O containing 100 mM phosphate buffer at pH 7 uncorrected for the presence of D<sub>2</sub>O and 20 μM DSS as an internal standard. The sample was allowed to stand for 1 hour to fully exchange amide protons with deuterium, then analyzed by <sup>1</sup>H NMR at 700 MHz using excitation sculpting to suppress the residual H<sub>2</sub>O signal.

#### 2.4.7 Oxime Isomerization Experiments

For the isomerization experiments described in **Section 2.1.2**, an oxidation reaction of peptide **2** was carried out as described in section 2.1.2 with a total volume of 200 μL. Peaks corresponding to the two

isomers were collected from analytical HPLC eluent. Approximately one-third of the eluent was frozen until completion of the previous HPLC run from which the eluent was collected, then thawed and injected immediately to ascertain the composition of the isolated material. Partial conversion of the *E*- and *Z*-oxime isomers of **2b** was observed even in the short time between isolation and freezing. The remaining frozen eluent of each fraction was lyophilized and the lyophilized powder used directly in the experiments detailed below.

Following lyophilization, samples of each isomer were dissolved in either (1) 200  $\mu$ L of 0.1 M phosphate buffer at pH 7.0 or (2) 200  $\mu$ L of 0.1% TFA in water. Aliquots were then removed from each sample and analyzed by HPLC after 24 and 48 hours. It was observed that the sample in 0.1% TFA in water rapidly converts to a product ratio composed primarily of the *Z*-oxime isomer of **2b**, while at neutral pH the system does not reach equilibrium up to 48 hours after redissolving.

#### 2.4.8 Oxime Exchange Experiments

Stock solutions of *O*-methylhydroxylamine hydrochloride were prepared at 1 M concentration in either 0.1 M phosphate buffer at pH 7 or pH 1. An aniline stock solution was prepared at 0.1 M in 0.1 M pH 7 phosphate buffer. An oxidation and cross-linking reaction of peptide **2** was carried out by addition of sodium periodate to yield a sample comprised of 125  $\mu$ M peptide, 250  $\mu$ M sodium periodate in 0.1 M phosphate buffer at pH 7. The oxidized sample was then split into two aliquots and diluted with a combination of *O*-methylhydroxylamine stock, aniline stock, and phosphate buffer to yield two samples of the following compositions: (1) 100  $\mu$ M peptide, 100 mM *O*-methylhydroxylamine (from pH 7 stock), 10 mM aniline in 0.1 M phosphate at pH 7 or (2) : (1) 100  $\mu$ M peptide, 100 mM *O*-methylhydroxylamine (from pH 7 stock), 10 mM aniline in 0.1 M phosphate at pH 4. The reactions were monitored by analytical HPLC, collection of the eluent, and MALDI-TOF MS to monitor the formation of linear oxime **2c**.

## 2.4.9 Circular Dichroism (CD) Spectroscopy

### 2.4.9.1 CD Of The Helical Peptide Model System

Circular dichroism samples were prepared by dilution of stock solutions of peptides **1-6** in water with phosphate buffer and water to a final concentration of 100  $\mu\text{M}$  peptide in 0.1 M phosphate buffer at pH 7. For cyclized peptides **2b-5b** and oxidized peptide **6a**, identical samples were prepared except with the addition of aqueous sodium periodate to a final concentration of 200  $\mu\text{M}$  periodate. CD scans were carried out from 200 to 260 nm with 1 nm step size, 2 nm bandwidth, and 5 second integration times at each wavelength. Spectra were corrected for buffer blanks of identical composition lacking peptide and for baseline molar ellipticity from 255-260 nm. Variable temperature CD data were obtained by monitoring ellipticity at 222 nm from 2-95  $^{\circ}\text{C}$  in 3  $^{\circ}\text{C}$  intervals with a dead band of 0.5  $^{\circ}\text{C}$  and a 2 minute equilibration at each temperature. Circular dichroism scan data was smoothed by the Savitsky-Golay method as implemented in GraphPad Prism. The fraction helical content for each peptide was calculated as previously described in the literature using equation 1 below.<sup>91</sup>

### Equation 1

$$f_{helix} = \frac{[\theta]_{222} - [\theta]_{coil}}{[\theta]_{helix} - [\theta]_{coil}}$$

In the above equation,  $[\theta]_{222}$  is the observed molar ellipticity at 222 nm,  $[\theta]_{helix}$  is the molar ellipticity at 222 nm for a fully folded  $\alpha$ -helix, and  $[\theta]_{coil}$  is the molar ellipticity at 222 nm for a random coil. Values of  $[\theta]_{coil}$  for each peptide were determined from the high-temperature baseline from thermal unfolding experiments. The value of  $[\theta]_{helix}$  was calculated as  $-29,800 \text{ deg cm}^2 \text{ dmol}^{-1} \text{ res}^{-1}$  according to equation 2 below.

### Equation 2

$$[\theta]_{helix} = (-44000 + 250T)(1 - \frac{k}{n})$$

In the above equation,  $T$  is temperature in  $^{\circ}\text{C}$ ,  $n$  is the number of residues in the peptide, and  $k$  is a constant (4.0) taken from literature precedent.<sup>91</sup>

#### 2.4.9.2 CD Of $\alpha$ -Helical Coiled Coils

Measurements were performed at 100  $\mu\text{M}$  peptide concentration in 100 mM phosphate buffer at pH 7, with and without 1 equivalent (peptides **19-33**) or 2.1 equivalents (peptide **34**) of aqueous sodium periodate. Samples for circular dichroism were prepared by an identical method as that described for analysis by HPLC. CD scans were carried out from 260 to 200 nm with 5 second averaging times, 1 nm step size, and 2 nm bandwidth at 20  $^{\circ}\text{C}$ . Spectra were corrected for a buffer blank and baseline molar ellipticity at 260 nm. Variable temperature CD data was obtained by monitoring molar ellipticity at 222 nm from 2-95  $^{\circ}\text{C}$  at 3  $^{\circ}\text{C}$  intervals with a dead band of 0.5  $^{\circ}\text{C}$ , 2 minute equilibration time between

measurements, and 5 second averaging times. Acquisition of molar ellipticity at 222 nm following thermal melts was obtained by cooling of the sample and equilibration for 5 minutes at 20 °C.

Melt data was processed utilizing GraphPad Prism, and fit to a two-state thermal denaturation model to obtain melting temperatures ( $T_m$ ).<sup>104</sup> The percentage of unfolded peptide at each temperature was calculated as in equation 3. Additional parameters used in the calculation of  $\Delta\Delta G$  were obtained as described below.

### Equation 3

$$\%unfolded = \left[ 1 - \frac{[\theta]_T - [\theta]_{unfold}}{([\theta]_{fold} + T \times M_{fold}) - [\theta]_{unfold}} \right] \times 100$$

In the above equation,  $[\theta]_T$  is the molar ellipticity at 222 nm at the temperature of the measurement,  $[\theta]_{unfold}$  is the molar ellipticity at 222 nm of the fully unfolded peptide obtained from the two-state denaturation fit,  $[\theta]_{fold}$  is the molar ellipticity at 222 nm of the fully folded peptide obtained from the two-state denaturation fit, T is the temperature in degrees Celsius, and  $M_{fold}$  is the slope of the fully folded measurements at low temperature from the two-state denaturation fit.<sup>104</sup> The analysis of the percentage of unfolded peptide at a given temperature is utilized to more easily visualize the change in the shape of the two-state denaturation sigmoidal curve. Analysis of the percentage of unfolded peptide from thermal melt data does not change the measured  $T_m$  value.

Estimation of the change in folded stability upon cyclization was obtained by calculating  $\Delta\Delta G_{fold}$  as detailed below from equation 4.<sup>105</sup>

### Equation 4

$$\Delta\Delta G_{fold} = \Delta H_{T_m} \frac{\Delta T_m}{T_{m,w.t.}}$$

In the above equation,  $\Delta H_{TM}$  is the enthalpy obtained for the wild-type peptide (**18**) from thermal melt analysis,  $T_{m,w.t.}$  is the melting temperature of peptide **18** from thermal melt analysis in Kelvin (K), and  $\Delta T_m$  is calculated as in equation 5.

**Equation 5**

$$\Delta T_m = T_{m,w.t.} - T_{m,mut.}$$

Error propagation in the calculation of  $\Delta\Delta G_{fold}$  is obtained from equation 6 below, where  $\delta\{\Delta H_{TM}\}$ , and  $\delta\{T_{m,w.t.}\}$  are values obtained as standard error of the two-state thermal denaturation curve fit.<sup>104</sup>

**Equation 6**

$$\delta\{\Delta\Delta G_{fold}\} = \Delta\Delta G_{fold} \sqrt{\left(\frac{\delta\{\Delta H_{T_m}\}}{\Delta H_{T_m}}\right)^2 + \left(\frac{\delta\{T_{m,w.t.}\}}{T_{m,w.t.}}\right)^2 + \left(\frac{\delta\{\Delta T_m\}}{\Delta T_m}\right)^2}$$

The value of  $\delta\{\Delta T_m\}$  is obtained from equation 7 below, where values of  $\delta\{T_{m,mut.}\}$  and  $\delta\{T_{m,w.t.}\}$  are obtained from the two-state thermal denaturation curve fit.

**Equation 7**

$$\delta\{\Delta T_m\} = \sqrt{(\delta\{T_{m,w.t.}\})^2 + (\delta\{T_{m,mut.}\})^2}$$

This analysis allows us to calculate  $\Delta\Delta G_{fold}$  values for comparison of peptides with unnatural residues inserted in comparison to the wild type peptide. A comparison can also be made between the cross-linked peptide and the linear peptide of the same type prior to oxidation and cross-linking by changing parameters in the above equations to be  $T_{m,lin.}$  and  $\delta\{T_{m,lin.}\}$  in place of  $T_{m,w.t.}$  and  $\delta\{T_{m,w.t.}\}$ , respectively. Accordingly, in comparison of the linear peptide to its oxidized, cross-linked counterpart,  $\Delta H_{TM}$  is taken to be the change in enthalpy for the linear peptide rather than the wild type peptide.

#### 2.4.10 Methionine Oxidation Stability Studies

A stock solution of sodium periodate in water was prepared and the concentration of periodate quantified by UV-Vis spectroscopy ( $\epsilon_{280} = 317 \text{ M}^{-1} \text{ cm}^{-1}$ ).<sup>103</sup> Peptide stocks of **6** and **17** were prepared in water and the concentration of peptide determined by UV-Vis spectroscopy as discussed previously (Section 2.3.5). Three parallel reactions were prepared in 0.1 M phosphate buffer at pH 7. First, a 100  $\mu\text{M}$  solution of peptide **6** and 100  $\mu\text{M}$  periodate; second, a 100  $\mu\text{M}$  solution of peptide **17** and 100  $\mu\text{M}$  periodate; third, solution containing 100  $\mu\text{M}$  peptide **6**, 100  $\mu\text{M}$  peptide **17**, and 100  $\mu\text{M}$  periodate. After addition of periodate, each sample was analyzed by HPLC at varying time points between 2 minutes (the fastest possible time between periodate addition and automated injection by HPLC) and 60 minutes on a  $\text{C}_{18}$  column. MALDI-TOF MS was utilized to identify the products following collection of the HPLC eluent.

#### 2.4.11 Crystallization, Data Collection, And Structure Determination

Crystals of peptide **22** were grown by hanging drop vapor diffusion in 24-well plates (Hampton). 1  $\mu\text{L}$  of peptide stock with a peptide concentration of 10-15 mg/mL in water was mixed with 1  $\mu\text{L}$  of crystallization buffer comprised of 0.1 M sodium acetate pH 4.6, 1.6 M NaCl, and 5% v/v PEG-1500 and equilibrated against 1 mL of crystallization buffer at room temperature. Crystals of **22b** were obtained by formation of the oxime cross-links in the crystal lattice of crystals of **22**. Crystals of **22** were grown as described above, and a solution of sodium periodate in crystallization buffer (1.5 equivalents to peptide) was added to the drop and allowed to equilibrate over crystallization buffer. Confirmation of the formation of **22b** was obtained by diluting crystal-containing drops 1:100 with water and analysis by MALDI-TOF MS. Time-dependent analysis of replicate drops treated with periodate showed complete cyclization within 48 hours after addition of periodate. The optimized conditions were used to generate crystals of **22b** for diffraction analysis. Crystals of **22** and **22b** were flash frozen in liquid nitrogen after cryoprotection in well buffer supplemented with 25% v/v glycerol. Diffraction data were collected using

CuK $\alpha$  radiation on a Rigaku/MSD diffractometer (FR-E generator, VariMax optics, AFC-Kappa goniometer, Saturn 944 CCD detector) equipped with an X-stream 2000 low temperature system operated at 100 K. The linear peptide **22** crystallized in a C2 lattice with one dimeric coiled coil in the asymmetric unit. In the oxime cross-linked structure of **22b**, the crystallographic 2-fold symmetry axis was lost resulting in a lower-symmetry P1 cell with two coiled coils in the asymmetric unit (four independent peptide chains) related by non-crystallographic symmetry. Coordinates and structure factors for **22** and **22b** are deposited in the Protein Data Bank under accession codes 4HU5 and 4HU6, respectively.

**Table 6.** Crystallographic data collection and refinement statistics for **22** and **22b**.

	Peptide <b>22</b>	Peptide <b>22b</b>
<b>Data Collection</b>		
Unit cell dimensions (Å, °)	$a = 76.7, b = 30.9, c = 33.3$ $\beta = 97.7$	$a = 30.9, b = 33.1, c = 41.1$ $\alpha = 93.9, \beta = 112.0, \gamma = 98.7$
Space group	C2	P1
Resolution (Å)	50.00-2.30 (2.38-2.30)	28.52-2.30 (2.38-2.30)
Total observations	16,894	11,907
Unique observations	3,576	6,255
Redundancy	4.7 (4.7)	1.90 (1.91)
Completeness (%)	99.7 (100)	95.2 (91.7)
$I/\sigma$	20.2 (6.5)	9.2 (2.1)
$R_{merge}$ (%)	10.6 (30.7)	5.0 (22.3)
<b>Refinement</b>		
Resolution (Å)	25.00-2.30	28.52-2.30
$R$ (%)	20.6	26.0
$R_{free}$ (%)	26.8	29.2
Avg. B factor (Å <sup>2</sup> )	30.2	38.8
RMSD		
Bonds (Å)	0.012	0.009
Angles (°)	1.26	1.48

### 3.0 INTERMOLECULAR OXIME AND HYDRAZONE CROSS-LINKS

Work detailed in this chapter has been published as:

1. Haney, C. M.; Horne, W. S.; “Dynamic covalent side-chain cross links via intermolecular oxime or hydrazone formation from bifunctional peptides and simple organic linkers.” *Journal of Peptide Science*, **2014**, *20*, 108-114

In addition to the intramolecular cross-link strategy outlined in Chapter 2, intermolecular cross-links formed by reaction of a linear peptide chain bearing two identical side chains and a bifunctionalized small molecule have also been examined. After such a reaction sequence, the small molecule becomes an integral part of the macrocycle, offering variability of the cross-link connectivity and size in a divergent manner from a single peptide sequence. Previous applications of intermolecular cross-linking include reactions between peptide thiols and alkyl or aryl dihalides to form thioethers,<sup>62, 63, 67, 68, 69, 106</sup> peptide amines and dicarboxylic acids to form lactams,<sup>64, 65</sup> and peptide azides and dialkynyl linkers to form ditriazole-cyclized products.<sup>107</sup> As with intramolecular cross-linking methods, intermolecular cross-link formation has been utilized to modulate peptide folding, affinity for biomolecules, and cellular uptake.<sup>107</sup>

We sought to adapt the strategy for oxime cross-linking described in the previous chapter to an intermolecular system in which peptides bearing two nucleophilic side chains react with dialdehyde-functionalized small molecules. This approach offers an alternate methodology to the intramolecular cross-link formation outlined in Chapter 2 without the need for oxidative conditions. Though the previously utilized strategy was capable of eliciting helical folding and stabilizing a protein quaternary assembly, the cross-links generated showed only limited dynamic covalent exchange. We hypothesized

that the intermolecular formation of oxime and hydrazone cross-links could allow for more facile exchange of the cross-linking moiety.

### 3.1 MODEL SYSTEM FOR INTERMOLECULAR CROSS-LINK FORMATION

In order to establish methods for intermolecular cross-link formation, we utilized sequence **1**, described in Chapter 2. We replaced selected residues with either aminoxy-functionalized residue **X<sub>5</sub>** or a new, hydrazide-functionalized residue **Z<sub>5</sub>** to generate derivatives **35-37** (Figure 39). The hydrazide-functionalized **Z<sub>5</sub>** residue leads to a hydrazone cross-link. We hypothesized that the hydrazone cross-links would offer more facile exchange given the known difference in hydrolytic lability of hydrazones versus oximes.<sup>81</sup> Sequences **35** and **36** were designed to test the effect of residue spacing ( $i \rightarrow i+4$ , **35** or  $i \rightarrow i+11$ , **36**) or the stability of the bis-oxime cross-link formed, as in peptide **37**, an analogue of **35** but containing hydrazides at an  $i \rightarrow i+4$  spacing to generate a bis-hydrazone cross-link.

We reacted peptides **35-37** with four different commercially available dialdehyde small molecules (**a-d**) to form cyclic products (**35a-35d**, **36a**, **36d**, and **37a-37d**), wherein the peptide number and letter combination indicate the cross-linked product formed (e.g. peptide **35** with linker **a** becomes **35a**) (Figure 39). We examined the formation of the cross-linked species, the effect of cross-link formation upon helical folding, and the ability of the cross-links to undergo dynamic covalent exchange.

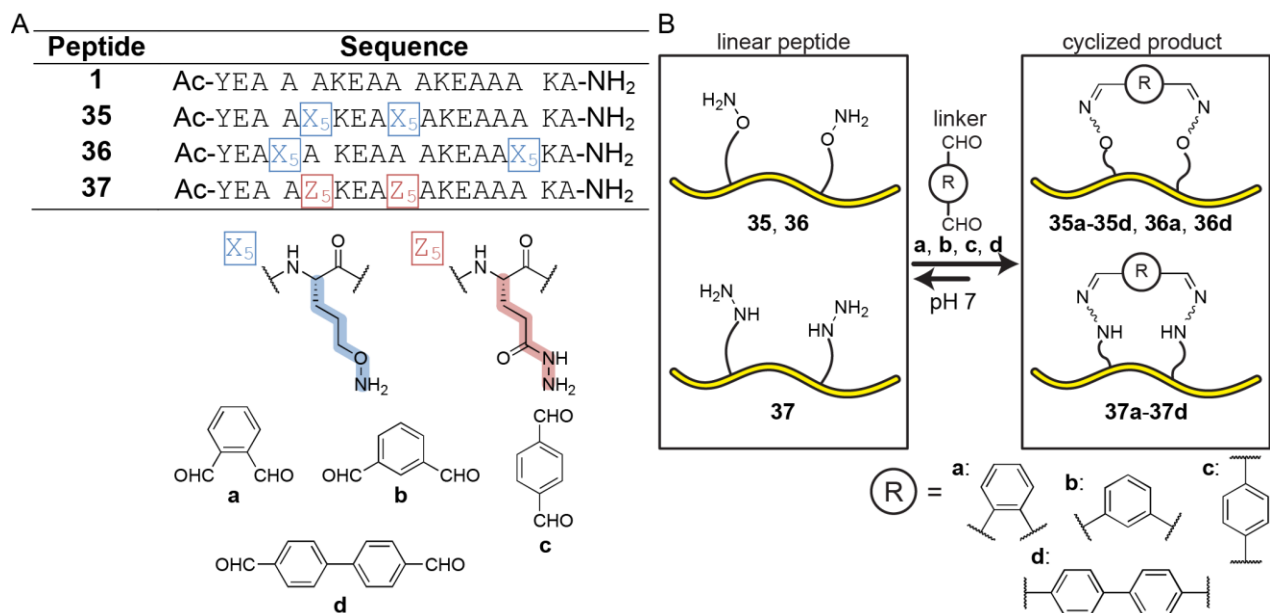


**Figure 39.** Sequences of peptides **1** and **35-37** and schematic representation of cross-linking. (A) Sequences of peptides **1** and **35-37**, structures of residues **X**<sub>5</sub> and **Z**<sub>5</sub> and linkers **a-d**. (B) Peptides **35-37** were used in combination with linkers **a-d** to generate a family of cyclized products (**35a-35d**, **36a**, **36d** and **37a-37d**).

### 3.2 CROSS-LINK FORMATION

We examined ten different combinations of peptides **35-37** and linkers **a-d** to prepare cyclic species **35a-35d**, **36a**, **36d** and **37a-37d** (representative examples, Figure 40). Each reaction consisted of peptide in pH 7 phosphate buffer with excess linker (4 equiv), and was monitored by HPLC and mass spectrometry. It was observed that the intermolecular cross-link formation is considerably slower than observed for the intramolecular case, though the reaction goes to completion in 1-2 hours. In most cases, more than one peak was observed in the chromatogram with a mass corresponding to the cyclized product. Each new oxime bond can form as an *E* or *Z* isomer, resulting in cyclic products with four possible stereochemical configurations (*EE*, *EZ*, *ZE*, *ZZ*). As shown in work described in Chapter 2, oxime stereoisomers can be separable by HPLC and typically interconvert slowly under neutral buffered aqueous conditions.

Peptide **35**, which contains two  $X_5$  residues at an  $i \rightarrow i+4$  spacing was efficiently cyclized in 2 hours or less with each linker, **a-d**. Not all cyclic products showed separable stereoisomers by HPLC; however, it is unclear if this is a result of the thermodynamic stability of particular isomers favoring their formation, or a lack of chromatographic resolution. Peptide **36**, which contains the same  $X_5$  residues but at an  $i \rightarrow i+11$  spacing, was efficiently cyclized by both a small benzene-based core (linker **b**) and by a larger biphenyl linker (**d**). Changing the identity of the nucleophilic side chain but maintaining the residue spacing, as in peptide **37** versus peptide **35**, had a minimal effect on peptide cyclization efficiency, except in the reaction with biphenyl-based linker **d** which generated a mixture of linear starting material and cyclic products. The observation that the ratio of linear peptide **37** to cyclized product **37d** did not change considerably over time suggests that an equilibrium was established between the two species. In none of the reactions detailed above was a product observed arising from the reaction of two independent peptide chains. We attributed this finding to the favorable kinetics of intramolecular ring-closing and cyclization following the first side-chain to linker condensation reaction versus the potential competing reaction that would cross-link independent peptide chains.

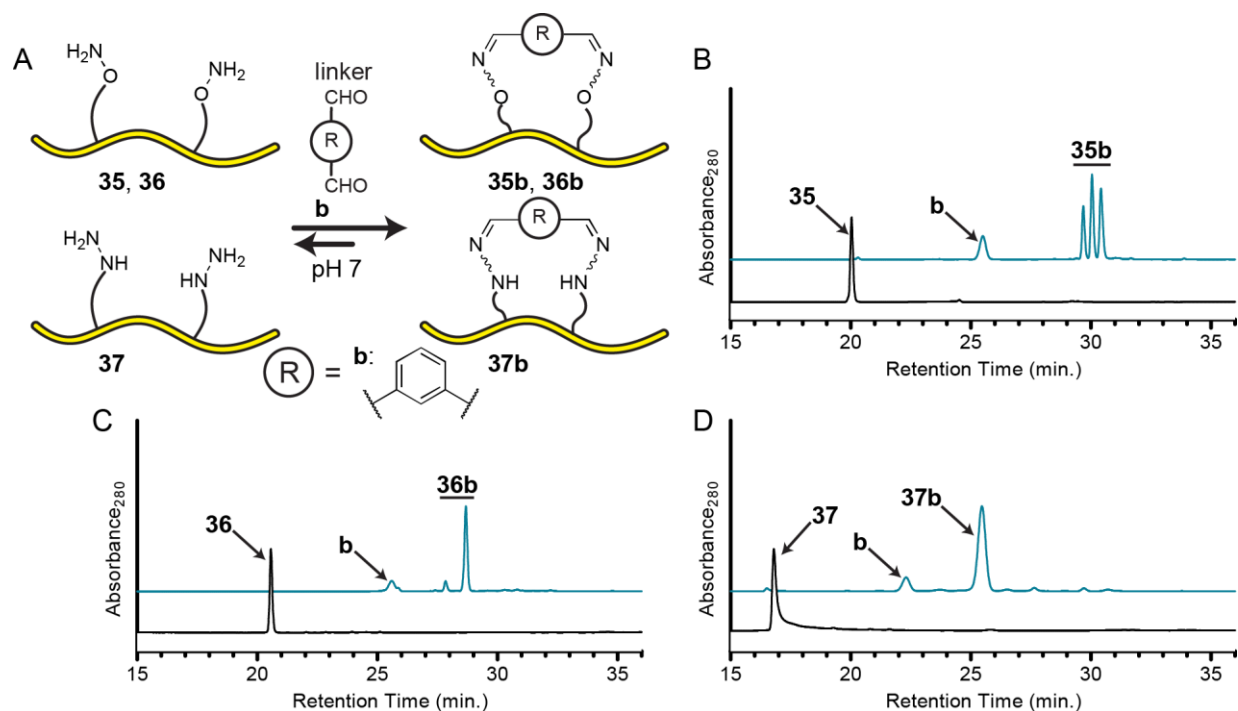


**Figure 40.** Representative HPLC chromatograms of peptides **35-37** reacted with linker **b**. (A) Schematic representation of the cross-linking reactions in HPLC chromatograms. (B) Chromatograms of peptide **35** (black) and peptide **35** with 4 equiv linker **b** two hours after linker addition (blue). (C) Chromatograms of peptide **36** (black) and peptide **36** with 4 equiv linker **b** two hours after linker addition (blue). (D) Chromatograms of peptide **37** (black) and peptide **37** with 4 equiv linker **b** two hours after linker addition (blue).

### 3.3 INTERMOLECULAR CROSS-LINKS AFFECT FOLDING

In order to assess the ability of intermolecular cross-links to influence the folded state of the peptide, we examined the folding behavior of peptides **35-37** and their cyclized products by CD spectroscopy. Peptide **1**, on which the other sequences are based, is partially helical in neutral aqueous solution. Linear peptides **35-37** also exhibit helical folding patterns, with a dependence on the side-chain identity. The hydrazide side chains in peptide **37** are slightly disruptive to helical folding, while aminoxy-functionalities in peptides **35** and **36** had little to no effect on helical folding (Figure 41).

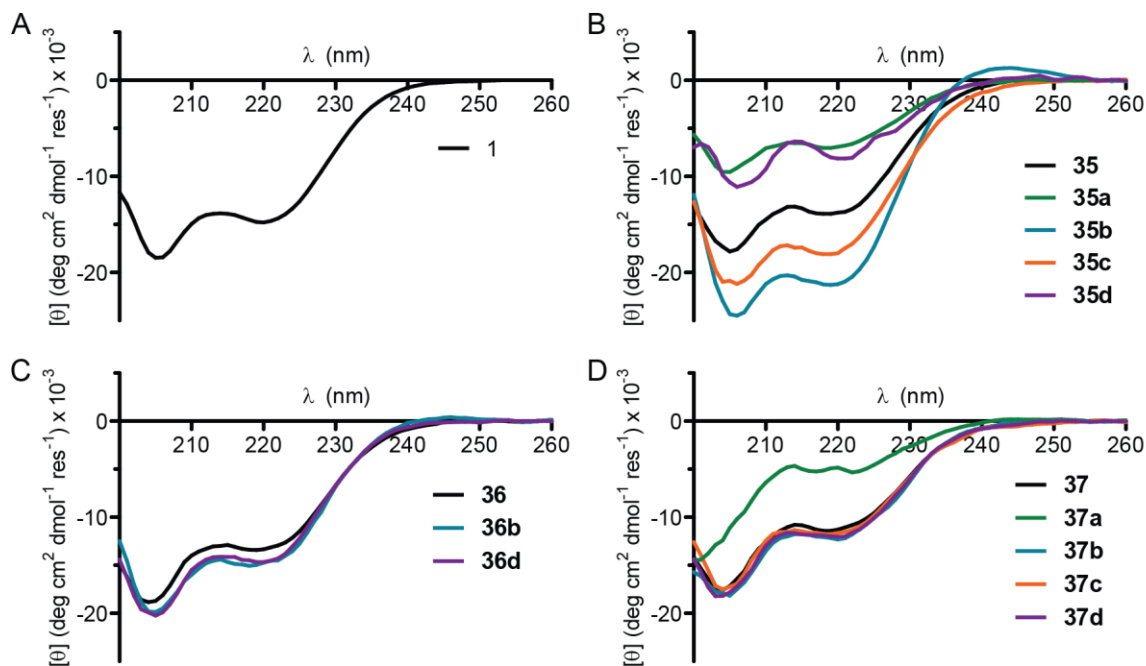


**Figure 41.** Circular dichroism data for peptides **1** and **35-37**.

(A) CD scan of peptide **1**. (B) CD scans of peptide **35** and cyclized products **35a-35d**. (C) CD scans of peptide **36** and cyclized products **36b** and **36d**. (D) CD scans of peptide **37** and cyclized products **37a-37d**. All CD scans contain 50  $\mu$ M peptide in 0.1 M phosphate buffer; cyclized samples analyzed 2 hours after addition of 4 equiv of linker.

Cyclic products based on peptide **35** (peptides **35a-35d**) showed differences in helical content depending on the identity of the organic linker (Figure 41B). Cyclic peptide **35b**, based on the *meta*-substituted dialdehyde linker exhibited greatest helicity among the series, while peptides **35a** and **35d** showed diminished helicity compared to the linear parent sequence **35**. In contrast, cyclization of **36**, which has an  $i \rightarrow i+11$  spacing of  $\mathbf{X}_5$  residues, showed no significant difference by CD of helical content upon cross-link formation with linkers **b** or **d** (Figure 41C). The origin of this effect is unclear, although we hypothesized that the large, flexible macrocycle formed was incapable of constraining the peptide backbone into a helical conformation. However, the observed maintenance of helical folding suggests that the cross-links are accommodated into the partially helical fold without disruption. Replacement of the aminoxy-functionalized residues (**35**) with hydrazides (**37**) led to less apparent influence of linker

identity on helical folding, although cyclized product **37a** was less helical than the starting linear peptide (Figure 41D). Overall, these results show that intermolecular oxime and hydrazone cross-links can influence helical folding, though less predictably than observed in intramolecular cross-link formation. In particular, both placement of the reactive residues and the dialdehyde linker are important. Some residue spacing and linker combinations elicit helical folding, while others do not.

### 3.4 CROSS-LINK EXCHANGE WITH A SMALL MOLECULE

Several experiments were performed to gauge the capacity of the cyclic peptides formed through intermolecular cross-links to participate in dynamic covalent equilibria. In previous work, we observed that intramolecular cyclization through oxime formation provided only limited dynamic covalent exchange (Chapter 2). In order to assess the ability of bis-oxime and bis-hydrazone cross-links to exchange, we carried out analogous reactions in which cyclic peptides **35b** and **37b** were treated with a large excess of *O*-methylhydroxylamine under conditions known to favor exchange (aniline as a catalyst, mildly acidic pH).<sup>90</sup> Product **35b** which contains two oxime bonds remains cyclic after several hours though the ratio of isomers changes (Figure 42). This finding suggests that the oxime is capable of isomer exchange, but is sufficiently thermodynamically stable to remain cyclized. Treatment of cyclic peptide **37b** under the same conditions showed nearly quantitative conversion to the linear precursor, **37**, in one hour (Figure 42). This result is reasonable given that hydrazones are known to be less hydrolytically stable than oximes,<sup>81</sup> it also provides a potential handle for the generation of peptide-based DCLs. The ease of hydrazone exchange may facilitate protein template-mediated selection of cross-linked structures.

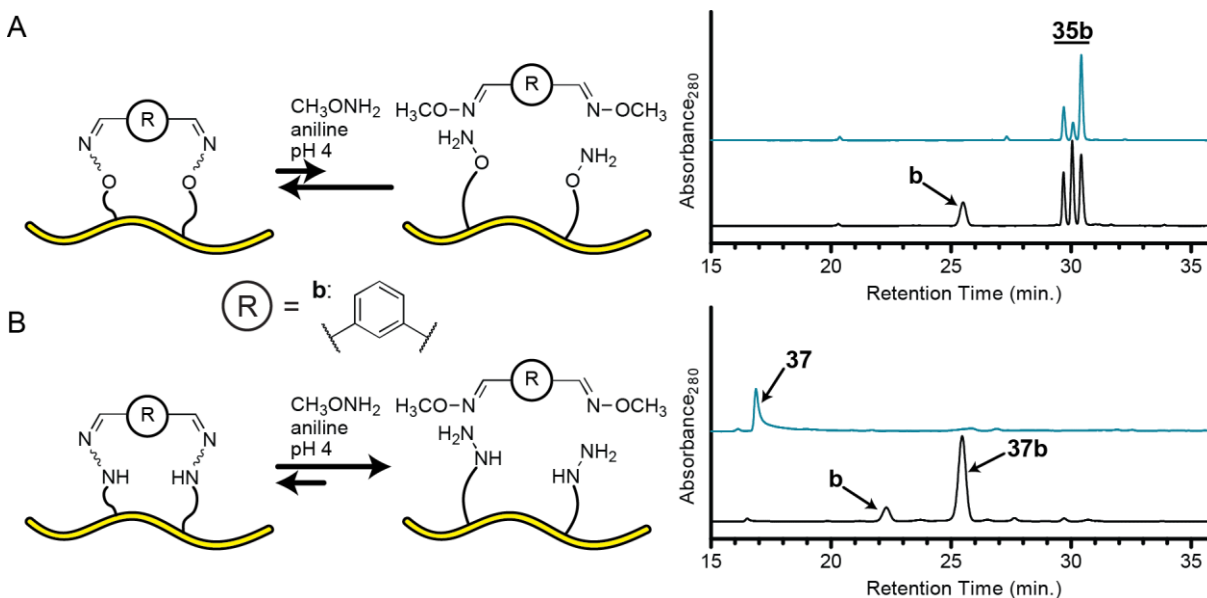


**Figure 42.** Small molecule exchange reactions of peptides **35** and **37**.

(A) Schematic representation of the reaction of cyclized product **35b** with *O*-methylhydroxylamine and aniline at pH 4. The chromatograms show the starting point of the reaction (black) and the reaction 5 hours after acidification and addition of *O*-methylhydroxylamine and aniline (blue). (A) Schematic representation of the reaction of cyclized product **37b** with *O*-methylhydroxylamine and aniline at pH 4. The chromatograms show the starting point of the reaction (black) and the reaction 1 hour after acidification and addition of *O*-methylhydroxylamine and aniline (blue).

### 3.5 LINKER SELECTION IN A HELICAL MODEL SYSTEM

While the ability to ring open cyclic peptides as described in the previous section is interesting as a proof of concept of dynamic covalent exchange, direct selection of linkers in a dynamic covalent equilibrium would provide more compelling evidence for the promise of intermolecular bis-oxime or bis-hydrazone formation to facilitate discovery of peptide-based inhibitors of protein-protein interactions. In order to investigate this issue, we carried out competition experiments in which two different linkers (**b** and **d**) were added simultaneously in excess to a single linear peptide (**35-37**). In these experiments, we found that peptide **35** strongly favors the formation of product **35b** over **35d** (Figure 43). Peptide **36**, upon simultaneous addition of linkers **b** and **d** formed a mixture of **36b** and **36d**, where **36b** was favored

(Figure 43). Similarly, linear peptide **37** showed favored formation of cyclic product **37b** with both **37d** and **37** (the linear precursor) still present (Figure 43). In the prior two cases, the distribution of products remained unchanged after up to 5 hours after linker addition. In the case of simultaneous addition of linkers to peptide **35**, it was observed that the small amount of product **35d** formed after two hours was no longer present four hours following linker addition; this serendipitous finding suggested the possibility of dynamic covalent exchange being responsible for the selection of a single cross-linked product.

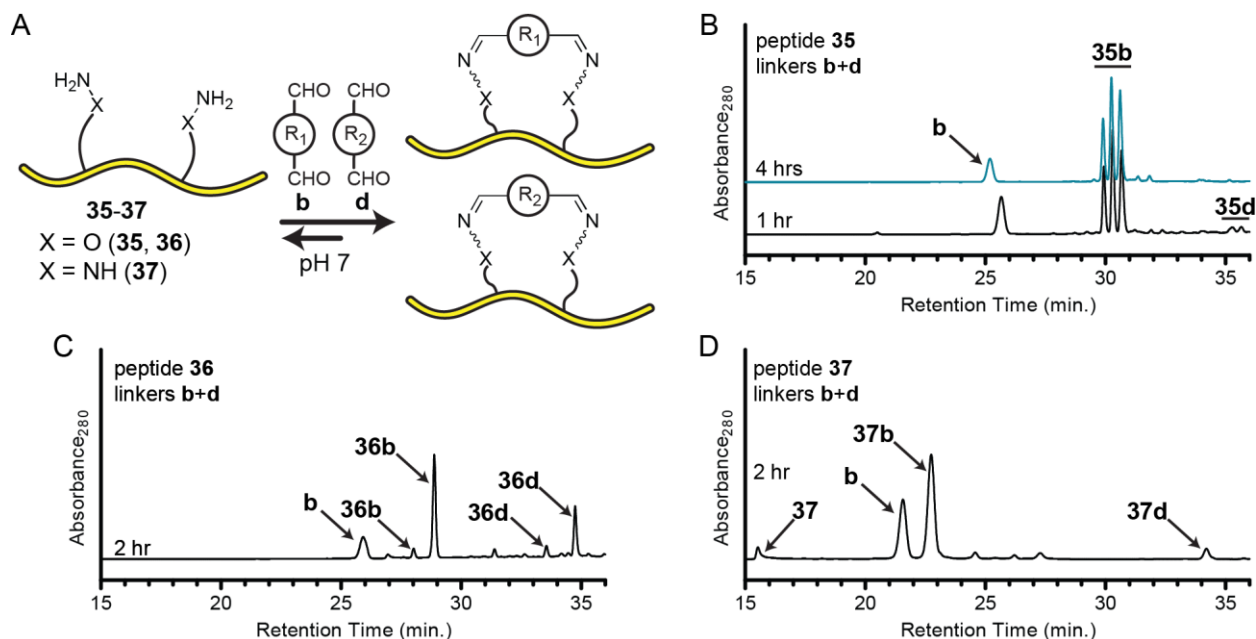


**Figure 43.** Chromatograms of simultaneous addition of linkers **b** and **d** to peptides **35-37**. (A) Schematic representation of the simultaneous addition of two linkers to form cyclic products. (B) HPLC chromatogram of peptide **35** at indicated time points after addition of linkers **b** and **d** simultaneously. (C) HPLC chromatogram of peptide **36** 2 hours after simultaneous addition of linkers **b** and **d**. (D) HPLC chromatogram of peptide **37** 2 hours after simultaneous addition of linkers **b** and **d**.

### 3.6 CROSS-LINK EXCHANGE FROM SEQUENTIAL ADDITION OF TWO LINKERS

The observation that product **35d** may exchange linkers to form product **35b** was somewhat surprising, given the known tendency for oxime exchange to require acidic pH or nucleophilic catalysis to achieve

reasonable rates.<sup>108</sup> In order to test the hypothesis that peptide **35d** exchanges to form cyclic product **35b** directly, we prepared samples of **35d** and then added linker **b** (Figure 44). In these experiments, a sample of peptide **35** was treated with linker **d** and allowed to proceed until complete cyclization occurred. Following this time, linker **b** was added (4 equiv) and the mixture monitored over time by analytical HPLC. Over the course of five hours, the initial product distribution of **35d** was found to exchange almost quantitatively to form product **35b** (Figure 44). This result provided strong support for the possibility that the organic linker component can be exchanged in a dynamic covalent manner. The oxime exchange reaction between cyclic products **35d** and **35b** was found to proceed more quickly with aniline as an added nucleophilic catalyst (completion in ~2 hours vs. 5 hours). However, the reaction in neutral buffered aqueous solution even in the absence of catalyst proceeds on a time scale that may be appropriate for dynamic combinatorial selection in systems involving peptide folding and/or binding.

An additional experiment in which a sample of peptide **37d** was treated with an excess of linker **b** was found to lead to a mixture of products **37b** and **37d**. Unlike the behavior in the oxime-based system, the hydrazone-based system (**37b** and **37d**) shows a different distribution of products when the linkers are added simultaneously (Figure 43) versus when they are added sequentially (Figure 44). This may be due to the small differences in peptide and linker concentrations when the linkers are added simultaneously versus sequentially. Nevertheless, this result demonstrates that the hydrazone cross-links may be able to undergo dynamic covalent exchange of the linker component, though the equilibrium established is more complex and does not exclusively favor a single product.

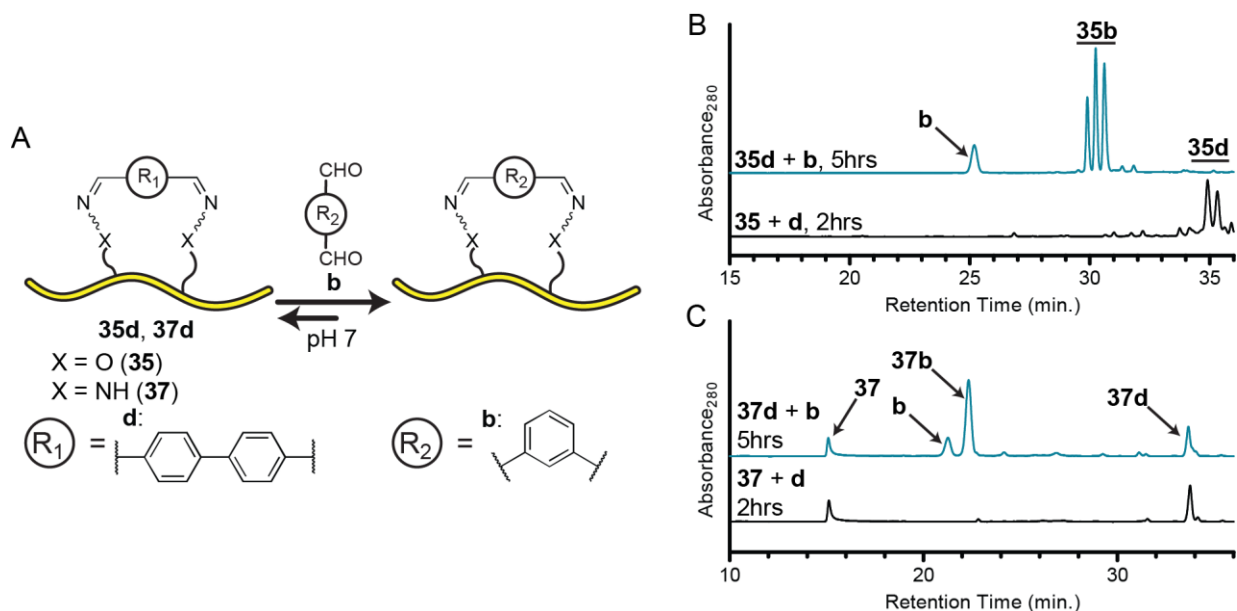


**Figure 44.** Linker exchange reactions for peptides **35d** and **37d** treated with linker **b**. (A) Schematic representation of linker exchange at pH 7. (B) HPLC chromatogram of a mixture of peptide **35** and linker **d** after complete conversion to **35d** (black) and the same mixture 5 hours after addition of linker **b** (blue). (C) HPLC chromatogram of a mixture of peptide **37** and linker **d** after establishing an equilibrium of **37** and **37d** (black) and the same mixture 5 hours after addition of linker **b** (blue).

### 3.7 INTERMOLECULAR CROSS-LINK FORMATION CONCLUSIONS

An alternative strategy employing the intermolecular formation of cross-links through the reaction of a bifunctionalized peptide with a dialdehyde-functionalized small molecule has been explored. Intermolecular cross-link formation was found to proceed rapidly (~1-2 hours) to furnish up to four chromatographically resolvable isomers. The cross-links formed under these conditions require no reagents other than peptide and linker, and the reactions proceed cleanly under neutral buffered aqueous conditions. The divergent and modular nature of this synthetic method can potentially be used for the rapid generation of a library of cross-linked compounds for screening against biological targets.

Intermolecular cyclization reactions proceed with reasonable rates under neutral buffered aqueous conditions to yield cyclic products through either oxime or hydrazone formation. The resulting cyclic

oligomers present differences in helical content depending on the identity of the organic linker group, the spacing of the nucleophilic residues involved in cross-link formation, and the identity of the cross-link bonds (e.g. oxime vs. hydrazone). While in many cases the origins of the differences in helicity are not obvious, this cross-linking strategy can furnish more helical oligomers (e.g. **35b** vs. **35**) provided judicious choice of cross-linking residues, their spacing, and the organic linker involved. Residues cross-linked via oxime formation at an  $i \rightarrow i+4$  spacing elicit very different helical folding patterns based on the linker utilized. However, the same oxime formation at an  $i \rightarrow i+11$  spacing show little difference in helical folding by CD. The same residue spacing ( $i \rightarrow i+4$ ) used to form hydrazones show little difference in helical folding except in the case of linker **a**, which diminishes helical folding.

Examination of the ability of bis-oxime or bis-hydrazone cross-links to undergo exchange via reaction with an exogenous aminoxy-functionalized small molecule demonstrated that oxime cross-links do not exchange, though hydrazone-based cross-links do. This is not surprising given the known chemistry of hydrazones and oximes, but does provide valuable information about the use of hydrazone cross-links in the context of dynamic covalent chemistry.

The ability to select a particular organic linker group from a complex mixture provides information about the relative stability of different cyclic products, e.g. **35b** vs. **35d**. Of note is the fact that despite different cross-linking residue spacings (e.g. **35** vs. **36**) or cross-link types (e.g. **35** vs. **36**) products cyclized by linker **b** were consistently favored. However, the extent differed depending on peptide; peptide **35** favored linker **b** almost exclusively, while peptide **36** led to a mixture of products. Bis-hydrazone formation by reaction of peptide **37** with linkers **b** and **d** was found to lead to a mixture of products, including linear peptide **37**, though product **37b** was still favored.

The most direct test of the applicability of intermolecular oxime and hydrazone formation for dynamic covalent chemistry applications involves the ability to exchange one organic linker for another. Several experiments were performed toward this end, which demonstrated that the oxime cross-linked peptide **35d** can exchange to form cyclic species **35b** in a reasonable time frame for peptide folding and/or binding. Interestingly, analogous experiments with peptide **37d** and exchange to form peptide **37b**

did not show an equal preference of organic linker. This may be due to the increased exchange possible with hydrazone cross-links.

In summary, the above data suggest the possibility of using intermolecular oxime and hydrazone formation as a strategy to establish dynamic covalent libraries (DCLs) amongst a single peptide sequence and multiple dialdehyde functionalized linkers. Consideration must be taken as to the substitution pattern of unnatural side chains (e.g. **35** vs **36**) to elicit a particular fold, and of the side chain identity; however, this strategy is divergent and modular for establishing a library of cyclic peptides based on a single linear sequence. In addition, the observation that such cross-linked peptides may be capable of dynamic covalent exchange suggests their use as a direct application for protein-templated construction of a DCL.

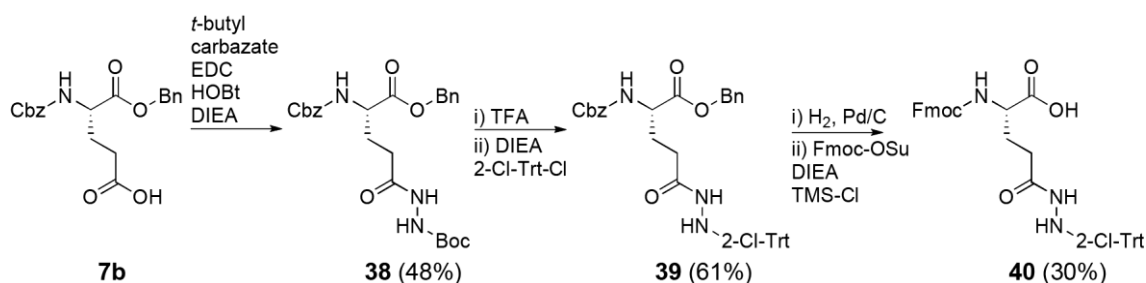
## 3.8 EXPERIMENTAL

### 3.8.1 General Information

Solvents and all other reagents were purchased from Sigma Aldrich, Baker, EMD, Fisher, Acros Organics, or TCI and used as received unless otherwise specified. Cbz-Glu-OBn and 2-chlorotriptyl chloride were purchased from Chem-Impex. 2-(6-chloro-1H-benzotriazole-1-yl)-1,1,3,3-tetramethylammonium hexafluorophosphate (HCTU), (benzotriazol-1-yloxy)tripyrrolidinophosphonium hexafluorophosphate (PyBOP), NovaPEG Rink Amide Resin, 9-fluorenylmethoxycarbonyl-N-hydroxysuccinimide (Fmoc-OSu), and Fmoc-protected  $\alpha$ -amino acids were purchased from NovaBiochem and used as received. Fmoc-protected aminoxy-functionalized monomer **12b** was synthesized as described in Chapter 2, Section 2.4.1. Flash column chromatography was performed using SorbTech (60 Å, 40-63  $\mu$ m) silica gel. Optical rotations were measured on a Perkin-Elmer 241 digital polarimeter with a sodium lamp at ambient temperature. NMR spectra were recorded on Bruker Avance-400 or Bruker Avance-300 spectrometers. MALDI-TOF mass spectrometry was carried out on a Voyager

DE Pro instrument. Circular dichroism spectra were recorded on an Olis DSM17 Circular Dichroism Spectrometer using quartz cuvettes 0.1 cm path length. Preparative and analytical HPLC were performed with Phenomenex Luna C<sub>18</sub> columns.

### 3.8.2 Hydrazide-Functionalized Monomer Synthesis

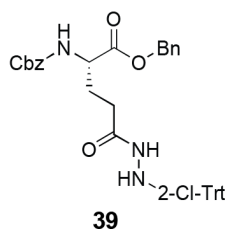


**Scheme 3.1.** Synthesis of hydrazide-protected monomer.

Fmoc-protected hydrazide functionalized monomer **40** was prepared by adaptation of previously reported procedures as described below.<sup>109</sup>

**tert-Butyl (S)-2-(5-(benzyloxy)-4-(((benzyloxy)carbonyl)amino)-5-oxopentanoyl)hydrazine-1-carboxylate (38):** Cbz-L-Glu-OBn (**7b**, 3.71 g, 10.0 mmol) was dissolved in 50 mL anhydrous DCM under nitrogen. DIEA (5.22 mL, 30.0 mmol) was added, followed by *tert*-butylcarbazate (1.45 g, 11.0 mmol), 1-hydroxybenzotriazole (HOBt) hydrate (1.68 g, 11.0 mmol), and *N*-(3-dimethylaminopropyl)-*N'*-ethylcarbodiimide hydrochloride (EDC • HCl) (2.11 g, 11.0 mmol). The reaction was stirred under nitrogen at room temperature overnight. The solution was then diluted with 150 mL ethyl acetate and washed once each with 50 mL of the following: 1 M HCl, water, saturated sodium carbonate, and brine. The organic layer was dried over anhydrous magnesium sulfate and concentrated. Silica gel chromatography (33%→66% ethyl acetate in hexanes) afforded product **38** as a white solid (2.34 g, 4.83

mmol, 48%).  $[\alpha]_D = +1.8$  ( $c = 1.0$ ,  $\text{CHCl}_3$ ).  $^1\text{H NMR}$  (400 MHz,  $\text{CDCl}_3$ )  $\delta = 8.10$  (1H, s), 7.34 (10H, m), 6.67 (1H, s), 5.88 (1H, d,  $J = 6.9$  Hz), 5.16 (2H, s), 5.09 (2H, s), 4.45 (1H, m), 2.26 (3H, m), 1.99 (1H, m), 1.44 (9H, s);  $^{13}\text{C NMR}$  (100 MHz,  $\text{CDCl}_3$ )  $\delta = 171.69$ , 156.42, 155.48, 136.06, 135.10, 128.57, 128.47, 128.26, 128.15, 128.07, 81.67, 67.30, 67.07, 53.37, 29.88, 28.25, 28.05; HRMZ  $m/z$  calculated for  $\text{C}_{25}\text{H}_{32}\text{N}_3\text{O}_7$   $[\text{M}+\text{H}]^+$ : 486.2240; found: 486.2245.



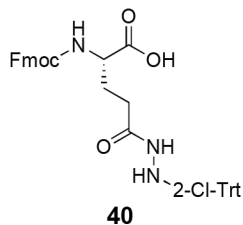
**(S)-Benzyl-2-(((benzyloxy)carbonyl)amino)-5-(2-((2-**

**chlorophenyl)diphenylmethyl)hydrazinyl)-5-oxopentanoate (39):** Compound **38**

(2.19 g, 4.52 mmol) was dissolved in 20 mL DCM. TFA (5 mL) was added and the reaction stirred at room temperature for 2.5 hours. The reaction was then diluted with

50 mL DCM and washed with 30 mL 5% w/v  $\text{NaHCO}_3$  and 30 mL brine, then dried over anhydrous magnesium sulfate and concentrated. The resulting residue was dissolved in 20 mL anhydrous DCM under nitrogen and DIEA (1.18 mL, 6.79 mmol) was added. 2-Chlorotrityl chloride (1.41 g, 4.52 mmol) was dissolved in 10 mL anhydrous DCM and added to the reaction over 15 minutes. The reaction was stirred at room temperature under nitrogen overnight, then diluted with 100 mL ethyl acetate and washed with 30 mL 10% w/v citric acid, then twice with 30 mL brine. The organic layer was dried over anhydrous magnesium sulfate and concentrated. Silica gel chromatography (33%→50% ethyl acetate in hexanes) afforded product **39** as a yellow solid with a small amount of residual ethyl acetate (1.83 g, 2.76 mmol, 61%). NMR spectra recorded in deuterated chloroform showed two conformers in slow exchange on the NMR timescale;  $^1\text{H NMR}$  is reported in  $\text{DMSO}-d_6$  where only a single set of peaks was observed, and  $^{13}\text{C NMR}$  is reported in  $\text{CDCl}_3$  with all signals reported.  $[\alpha]_D = -1.2$  ( $c = 1.0$ ,  $\text{CHCl}_3$ ).  $^1\text{H NMR}$  (400 MHz,  $\text{DMSO}-d_6$ ):  $\delta = 9.01$  (1H, d,  $J = 8.3$  Hz), 7.79 (1H, d,  $J = 7.4$  Hz), 7.65 (1H, d,  $J = 7.7$  Hz), 7.42 (4H, m), 7.35 (1H, m), 7.28 (8H, m), 7.19 (2H, m), 6.10 (1H, d,  $J = 8.3$  Hz), 5.11 (2H, m), 5.02 (2H, m), 3.88 (1H, m), 1.88 (2H, t,  $J = 7.4$  Hz), 1.56 (1H, m), 1.44 (1H, m);  $^{13}\text{C NMR}$  (100 MHz,  $\text{CDCl}_3$ ):  $\delta = 177.24$ , 171.54, 169.03, 156.19, 155.98, 141.83, 139.60, 138.04, 136.06, 135.03, 134.50, 133.41, 132.44, 132.04, 131.32, 129.68, 128.90, 128.68, 128.59, 128.52, 128.48, 128.43, 128.35, 128.30, 128.18, 128.14,

128.10, 128.04, 127.93, 127.70, 126.90, 126.27, 74.20, 73.68, 67.29, 67.05, 66.83, 53.84, 53.24, 30.42, 28.70, 26.41; HRMS  $m/z$  calculated for  $C_{39}H_{37}ClN_3O_5$   $[M+H]^+$ : 662.2422; found: 662.2396.



**(S)-2-(((9H-Fluoren-9-yl)methoxy)carbonyl)amino)-5-(2-((2-chlorophenyl)diphenylmethyl)hydrazinyl)-5-oxopentanoic acid (40):** Compound

**39** (1.71 g, 2.58 mmol) was dissolved in 20 mL anhydrous methanol under nitrogen.

Palladium on carbon (0.171 g, 10 wt%) was added, the atmosphere was purged, and

the reaction vessel fit with a hydrogen-filled balloon. The resulting mixture was stirred overnight, then filtered through celite, washed with methanol, and concentrated. The resulting white solid was dissolved in anhydrous DCM under nitrogen. DIEA (1.79 mL, 10.32 mmol) was added, followed by trimethylsilyl chloride (TMS-Cl) (0.655 mL, 5.16 mmol) and stirred for 15 minutes at room temperature. Fmoc-OSu (1.04 g, 3.09 mmol) was then added and the reaction stirred at room temperature overnight. The reaction was then diluted with 150 mL ethyl acetate and washed twice with 50 mL brine. The organics were then dried over anhydrous magnesium sulfate and concentrated. Silica gel chromatography (50%→100% ethyl acetate in hexanes) afforded product **40** as a white solid (518.8 mg, 0.79 mmol, 30%).  $[\alpha]_D = +1.9$  ( $c = 1.0$ ,  $CHCl_3$ ).  $^1H$  NMR (400MHz,  $DMSO-d_6$ ):  $\delta = 12.58$  (1H, s), 9.04 (1H, d,  $J = 8.2$  Hz), 7.89 (2H, d,  $J = 7.5$  Hz), 7.80 (1H, d,  $J = 7.8$  Hz), 7.70 (2H, d,  $J = 7.4$  Hz), 7.49 (1H, d,  $J = 7.8$  Hz), 7.41 (4H, m), 7.31 (10H, m), 7.19 (2H, m), 6.11 (1H, m), 5.00 (1H, s), 4.24 (2H, m), 4.20 (1H, m), 3.72 (1H, m), 1.85 (2H, t,  $J = 7.8$  Hz), 1.54 (1H, m), 1.42 (1H, m);  $^{13}C$  NMR (100 MHz,  $CDCl_3$ ):  $\delta = 170.40$ , 156.26, 143.77, 143.56, 141.59, 141.23, 139.39, 134.46, 132.11, 131.25, 129.02, 128.71, 128.32, 128.00, 127.71, 127.03, 126.38, 125.04, 119.95, 73.70, 66.99, 60.42, 53.54, 53.06, 47.05, 30.47, 28.80, 28.29; HRMS calculated for  $C_{39}H_{33}ClN_3O_5$   $[M-H]^-$ : 658.2109; found: 658.2137.

### 3.8.3 Peptide Synthesis And Purification

Peptides **35-37** were prepared by manual Fmoc-solid phase peptide synthesis on NovaPEG Rink Amide Resin with microwave heating. Coupling reactions were performed in *N*-methyl-2-pyrrolidinone (NMP) using 4 equiv of amino acid, 4 equiv of activating agent (HCTU for natural Fmoc-protected amino acids; PyBOP for unnatural residues **12b** and **40**) and 6 equiv of DIEA. The microwave coupling program consisted of a 2-minute ramp to 70 °C, followed by a 4-minute hold at 70 °C. Removal of the N-terminal Fmoc protecting group was achieved by treatment with 20% 4-methylpiperidine in DMF. The microwave deprotection program consisted of a 2-minute ramp to 80 °C and a 2 minute hold at 80 °C. The resin was washed three times with DMF after each coupling and deprotection reaction. Once the peptide sequence was completed on resin, the N-terminus was acetylated by treatment with 8:2:1 v:v:v DMF:DIEA:Ac<sub>2</sub>O for 10-15 minutes at room temperature. The resin was then washed and dried, and the peptide cleaved from resin with concomitant side chain deprotection by treatment with 92.5:3:3:1.5 TFA:H<sub>2</sub>O:EDT:TIS. The cleaved peptide was precipitated into cold diethyl ether, centrifuged, and the ether decanted. The pelleted crude peptide was dissolved in 0.1% TFA in water for purification by preparative HPLC. Peptides were purified by HPLC on a Luna C18 preparative column using gradients between 0.1% TFA in water and 0.1% TFA in acetonitrile. Fractions containing the desired peptide were frozen immediately and lyophilized. Identities of the purified peptides were confirmed by MALDI-TOF MS, and all peptides used in biophysical characterization and cross-linking experiments were  $\geq 95\%$  pure by analytical HPLC.

**Table 7.** MALDI-TOF data for peptides **1**, **35-37** and cyclized products.

Peptide	[M+H] <sup>+</sup> ( <i>m/z</i> )		Peptide	[M+H] <sup>+</sup> ( <i>m/z</i> )	
	Calculated	Observed		Calculated	Observed
<b>1</b>	1704.9	1704.8	<b>37</b>	1848.9	1849.0
<b>35</b>	1822.9	1822.7	<b>37a</b>	1951.0	1950.7
<b>35a</b>	1925.0	1924.7	<b>37b</b>	1951.0	1951.3
<b>35b</b>	1925.0	1924.8	<b>37c</b>	1951.0	1951.1
<b>35c</b>	1925.0	1925.1	<b>37d</b>	2027.5	2027.2
<b>35d</b>	2001.0	2001.2			
<b>36</b>	1822.9	1822.8			
<b>36b</b>	1925.0	1924.8			
<b>36d</b>	2001.0	2000.7			

### 3.8.4 Cross-Link Formation Reactions

Stock solutions of peptides **35-37** were prepared in water and their concentration determined by UV-Vis spectroscopy (Tyr absorbance at 276 nm,  $\epsilon = 1450 \text{ M}^{-1} \text{ cm}^{-1}$ ).<sup>102</sup> Stock solutions of organic linkers **a-d** were prepared in water. For solutions of linkers **a-c**, concentration was determined by UV-Vis spectroscopy (**a**,  $\epsilon_{300} = 255 \text{ M}^{-1} \text{ cm}^{-1}$  for the corresponding cyclic hydrate; **b**,  $\epsilon_{292} = 1120 \text{ M}^{-1} \text{ cm}^{-1}$ ; **c**,  $\epsilon_{296} = 1950 \text{ M}^{-1} \text{ cm}^{-1}$ ).<sup>110</sup> *ortho*-Pthaldialdehyde (**a**) was allowed to equilibrate in water for at least 30 minutes prior to concentration determination to ensure complete conversion to the cyclic hydrate.<sup>110</sup> The concentration of linker **d** in aqueous stock solution was determined by mass to volume. Cross-linking reactions were performed in 0.1 M phosphate buffer, pH 7, with 50  $\mu\text{M}$  peptide and 4 equiv (200  $\mu\text{M}$ ) linker. The benzene-based dialdehydes (**a-c**) were well soluble in water and were delivered to reactions from aqueous stock solutions of 500-700  $\mu\text{M}$  concentration. Biphenyl-based linker **d** was less soluble in water and consequently was added from a stock solution just below its solubility limit in water (~300  $\mu\text{M}$ ). Following addition of the linker, aliquots were removed from cross-linking reactions and analyzed by HPLC and MALDI-TOF MS of collected eluent. Cyclization reactions were performed utilizing peptides **35-37** and various combinations of linkers as detailed above to prepare cyclic species **35a-35d**, **36b**, **36d**, and **37a-d**. In all cases, complete consumption of the starting linear peptide was observed in 1-2

hours (~2 hour reaction times were required with linker **d**) with the appearance of one to four separable HPLC peaks with masses corresponding to the cyclized product(s). Cross-link formation with peptide **37** yielded complete cyclization with linkers **a-c** and a mixture of cyclized product and linear peptide with linker **d**.

### 3.8.5 Circular Dichroism Spectroscopy

Samples of linear peptides **1** and **35-37** were prepared in 0.1 M phosphate buffer, pH 7 at a concentration of 50  $\mu$ M peptide. Samples of cyclized peptides **35a-35d**, **36b**, **36d**, and **37a-37d** at 50  $\mu$ M concentration were prepared in 0.1 M phosphate buffer at pH 7 by addition of 4 equiv (200  $\mu$ M) linker and analyzed directly after completion of the reaction as determined by HPLC. CD scans were performed from 200-260 nm with 5 second integration times, 2 nm bandwidth, and 1 nm step size at 20 °C, Raw CD data were smoothed by the Savitsky-Golay method as implemented in GraphPad Prism.

### 3.8.6 Cross-Link Exchange With *O*-Methylhydroxylamine

A sample of cyclic peptide **35b** was prepared in 0.1 M phosphate buffer from peptide **35** (50  $\mu$ M) and linker **b** (200  $\mu$ M). Following complete conversion to form cyclic product **35b**, the solution was acidified to pH 4 with 1 M HCl, then *O*-methylhydroxylamine (10  $\mu$ L from a 1 M stock in water) and aniline (10  $\mu$ L from a 0.1 M stock in water) were added to yield a sample composed of ~42  $\mu$ M peptide **35b**, residual linker **b** (~160  $\mu$ M), 1000 equiv of *O*-methylhydroxylamine and 100 equiv of aniline. The reaction was monitored by HPLC at time points from 1 to 5 hours. An identical experiment was carried out by preparation of cyclic product **37b** and treatment as described above.

### 3.8.7 Linker Mixing Experiments

#### 3.8.7.1 Simultaneous Addition Of Two Linkers

A sample of peptide **35**, **36**, or **37** was prepared and linkers **b** and **d** added together to create a solution consisting of 50  $\mu\text{M}$  peptide, 150  $\mu\text{M}$  linker **b** and 150  $\mu\text{M}$  linker **d** in 0.1 M phosphate buffer at pH 7. The reactions were monitored by HPLC and MALDI-TOF MS of collected eluent.

#### 3.8.7.2 Sequential Addition Of Two Linkers

A sample of cyclic peptide **35d** or **37d** was prepared in 0.1 M phosphate buffer at pH 7 from peptide **35** or **37** (50  $\mu\text{M}$ ) and linker **d** (200  $\mu\text{M}$ ). After complete conversion to **35d** or the establishment of equilibrium between **37** and **37d** was confirmed by HPLC, linker **b** (4 equiv) was added from an aqueous stock solution. The sequential addition of linker **b** diluted the concentration of peptide and linkers slightly versus conditions where the linkers were added simultaneously. The reactions were monitored by HPLC and MALDI-TOF MS of collected eluent.

## 4.0 CROSS-LINKING PEPTIDE LIGANDS BOUND TO A PROTEIN RECEPTOR

As noted in Chapter 1, peptide cyclization has proven to be a useful strategy for generating peptide-based inhibitors of PPIs. The use of aminoxy-bifunctionalized peptides with dialdehyde linkers, as described in Chapter 3, furnishes a possible cross-linking technology amenable to use under conditions involving peptide binding to biological receptors. We investigated the use of designed peptide ligands for a protein receptor and the effect of cross-link formation on folding and affinity for a protein target. Additionally, we tested the ability of the presence of the protein receptor to affect the outcome of the cross-linking reactions. We utilized reactions involving a single linker, in which the oxime isomer distribution may be affected by the presence of the receptor. Alternatively, we examined reactions involving the use of two linkers in which the proportion of each cross-linked product may depend on the presence of the receptor.

### 4.1 PROTEIN RECEPTOR SELECTION AND PEPTIDE DESIGN

We chose to utilize gp41-5, a soluble, single-chain construct derived from the HIV membrane protein gp41 as a model protein receptor.<sup>111</sup> The protein consists of three N-terminal heptad repeat sequences and two C-terminal heptad repeat sequences from gp41-5 that are joined by short linker segments (Figure 45). The molecule contains five of the six helices found in the gp41 six-helix bundle formed during viral-cell fusion (see Section 1.2), and provides an exposed groove for binding molecules with affinity for gp41. This construct has previously been used in high-throughput screens to identify small molecule inhibitors of HIV fusion<sup>111</sup> as well as in the development of mixed  $\alpha/\beta$ -peptide backbones with antiviral activity.<sup>112</sup>

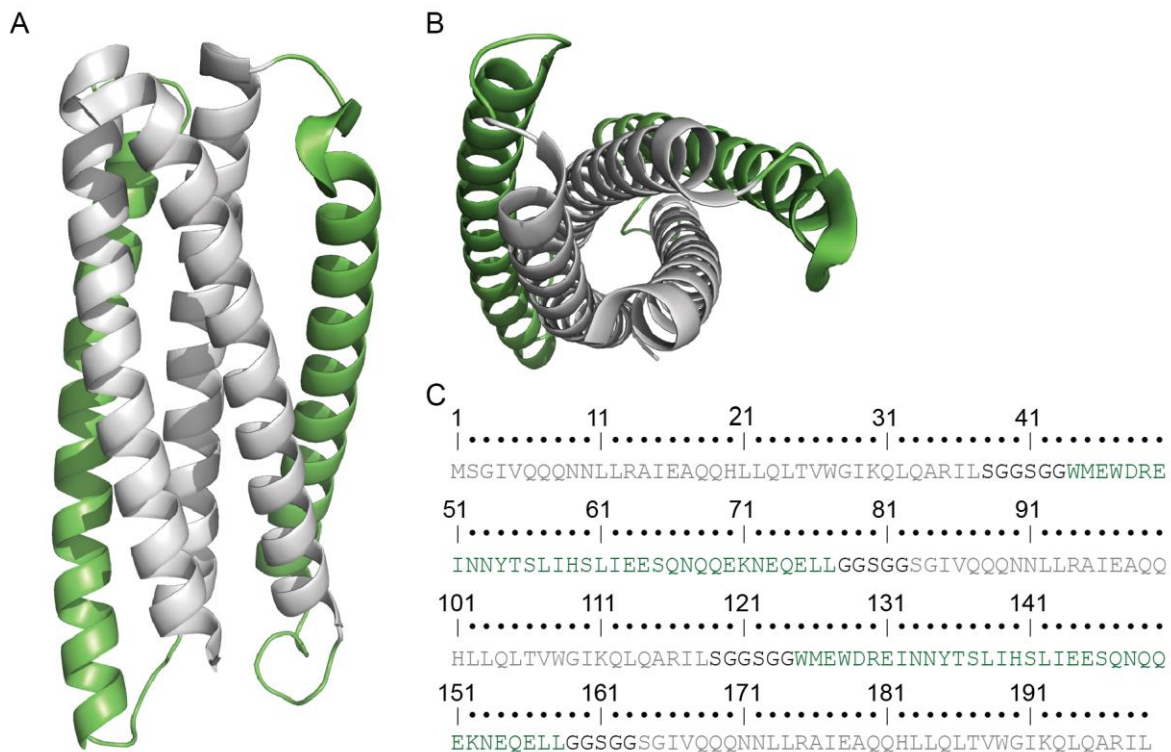


**Figure 45.** Structure and sequence of gp41-5.

(A) Side view of the gp41-5 helix bundle. (B) Top view of the gp41-5 helix bundle. Structures from PDB: 3O3X. (C) Sequence of gp41-5. N-terminal and C-terminal heptad repeat helices are colored grey and green, respectively.

Based on the C-terminal heptad repeat (CHR) sequence of gp41, we designed potential ligands for the gp41-5 helix bundle to have several important characteristics. We sought to decrease any residual secondary structure in the unbound ligand, as we reasoned that this may provide additional driving force for receptor-mediated selectivity in cross-linking reactions. In this case, stabilizing the helical, bound state is uncoupled from stabilizing the helical conformation of the unbound peptide ligand. Peptides based on the CHR sequence of gp41 have also been shown to undergo spontaneous oligomerization with changes to the sequence;<sup>113</sup> this oligomerization could potentially interfere with ligand-receptor interactions. Therefore, we attempted to minimize any potential oligomerization in our designs. In order to achieve these goals, the 36-residue CHR sequence was truncated to 21 residues. We then generated several

mutants starting from the wild type CHR sequence based on literature precedent for residue changes affecting helicity and/or oligomerization of CHR sequences (Figure 46).<sup>113</sup>

Peptide	Sequence
gp41 CHR	WMEWDREINNYTSLIHSLIEE
<b>41</b>	Ac-WBEWDREINNYTSLIHSLIEE-NH <sub>2</sub>
<b>42</b>	Ac-WEEWDKEINKYTKLIHKLIRE-NH <sub>2</sub>
<b>43</b>	Ac-WEEWDRAINEYASRIE SLIRE-NH <sub>2</sub>
<b>44</b>	Ac-WEAWDKAIAKYAKRIEKLIRA-NH <sub>2</sub>
<b>45</b>	Ac-WEAWDRAIAEYAARIEALIRA-NH <sub>2</sub>
T-2635	WEAWDRAIAEYAARIEALIRA

B = norleucine

**Figure 46.** Sequences of designed CHR peptides.

Peptide **41** is the native 21 residue sequence from the wild-type CHR domain with a single amino acid substitution of Met<sub>2</sub> to its hydrocarbon isostere, norleucine (made to avoid any potential oxidation). This sequence proved to be insoluble following synthesis and cleavage from the resin. Peptides **42-45** were then generated with increasing degrees of mutation away from the natural CHR sequence and towards the homologous residues of a previously reported helical CHR mimic, T-2635.<sup>113</sup> Peptide **42** contains six mutations from the wild-type sequence. Two substitutions (Met<sub>2</sub>→Glu and Glu<sub>20</sub>→Arg) were made to promote helical structure and solubility. Four lysines were inserted to act as isosteres of the aminoxy-functionalized residues to be subsequently included for cross-link formation. These residues were placed in solvent-exposed sequence positions based on analysis of crystal structures of the gp41 six-helix bundle and of a CHR-based peptide bound to gp41-5.<sup>112</sup> Peptide **43** maintains the Met<sub>2</sub>→Glu and Glu<sub>20</sub>→Arg mutations of **42**, but lacks the lysine mutations and contains additional substitutions from T-2635: Glu<sub>7</sub>→Ala, Thr<sub>12</sub>→Ala, and His<sub>16</sub>→Ala. Peptide **43** combines the mutations from peptide **42** and **43** and contains three additional alanine residues found in T-2635; Glu<sub>3</sub>→Ala, Asn<sub>9</sub>→Ala, and Glu<sub>21</sub>→Ala. Peptide **45** is simply the 21 residue truncation of T-2635. All peptides include an N-terminal acetyl cap to aid in stabilization of the helical fold. With these peptides in hand, we assessed their folding

behavior by CD spectroscopy and affinity for gp41-5 through a previously developed competition fluorescence polarization assay (Figure 47).<sup>111</sup>

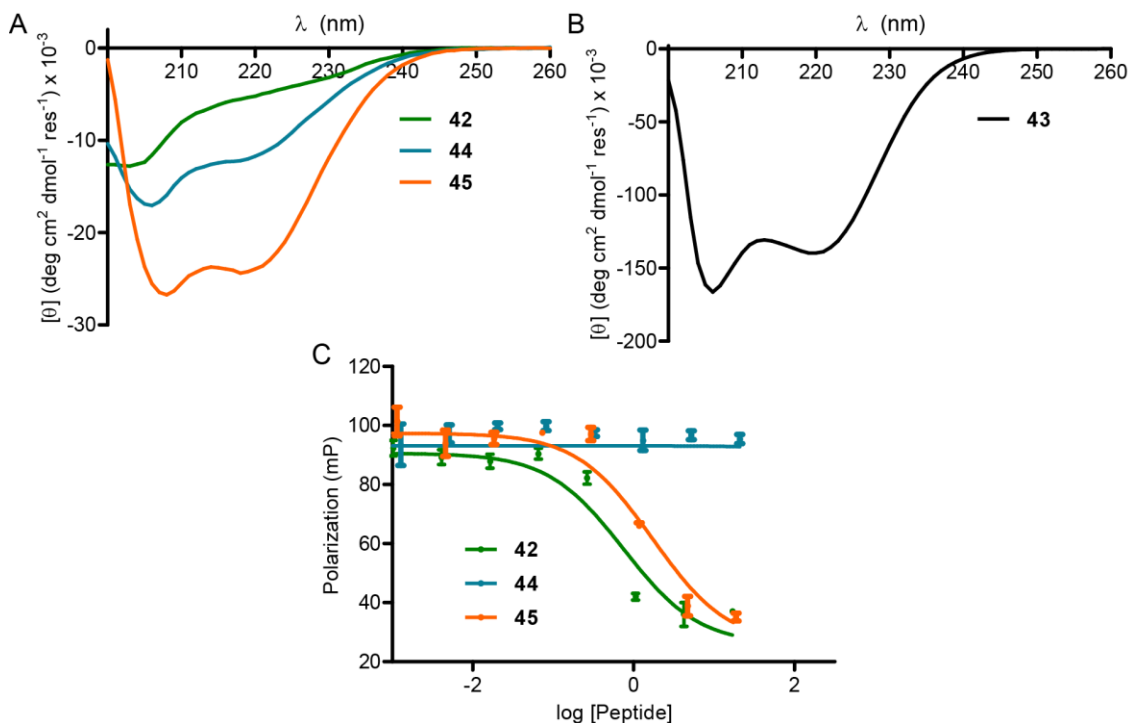


**Figure 47.** CD and competition fluorescence polarization data for peptides **42-45**. (A) CD spectra of peptides **42**, **44**, and **45** at 50 μM concentration in 0.1 M phosphate buffer, pH 7. (B) CD spectra of peptide **43** at 50 μM concentration in 0.1 M phosphate buffer, pH 7. (C) Competition fluorescence polarization data for peptides **42**, **44**, and **45**. Peptides were titrated into FP solution containing 2 nM gp41-5 and 1 nM Flu-C38. Data points average and standard deviation from triplicate measurements.

Circular dichroism spectroscopy of peptides **42-45** indicated differing helical content (Figure 46A, B). Peptide **42** has a CD signature consistent with random coil, as desired in our ligand design. Peptide **43** proved to be slightly helical, while peptide **45** showed much stronger helical folding characteristics by CD. Interestingly, peptide **43** proved to have a strongly helical CD signature, above that expected even for a fully folded monomeric helix of 21 residues (calculated  $[\theta]_{222} = -31.6 \text{ (deg cm}^2 \text{ dmol}^{-1} \text{ res}^{-1}) \times 10^{-3}$ ). This uncharacteristically large CD intensity was found to be independent of concentration.

Because of its unusual CD behavior this peptide was not investigated further as a potential ligand for gp41-5.

Peptides **42**, **44** and **45** were tested in competition fluorescence polarization assays to determine their affinity for gp41-5 (Figure 47C). Fluorescence polarization measures the change in fluorescence anisotropy associated with the binding of a fluorescently labeled “tracer” ligand to a protein receptor. In the unbound state, the rate of rotation of the ligand is rapid, and causing polarized light to be fluorescently emitted as depolarized light (Figure 48). In the bound state, the ligand-protein complex tumbles more slowly, leading to retention of polarization in the fluorescence emission (Figure 48). Competitive inhibition of the interaction between the fluorescent ligand and the protein receptor by an unlabeled competitor leads to emission of depolarized light from the liberated tracer. In the assay used here, the fluorescent ligand is the 38-residue CHR domain of gp41 with an N-terminal fluorescein tag, termed Flu-C38. Serial dilutions of peptides **42**, **44**, and **45** against protein and fluorescent tracer thus provide a measure of fluorescence anisotropy as a function of peptide concentration. This data provides competitive inhibition equilibrium constants ( $K_i$ ).

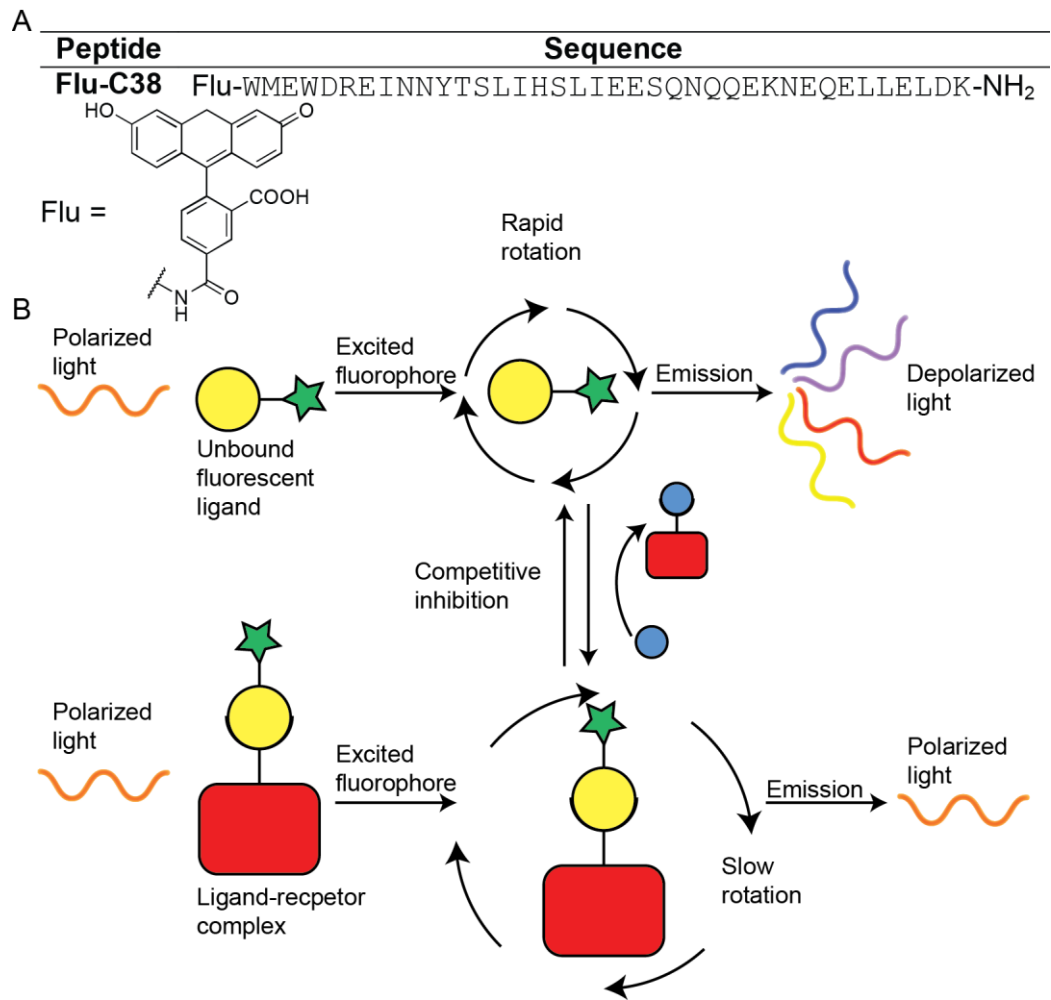


**Figure 48.** Sequence of Flu-C38 and scheme of competition fluorescence polarization. (A) Sequence of Flu-C38 and structure of the fluorescein label. (B) Schematic representation of competition fluorescence polarization. Competitive inhibition of the complex formed between the fluorescently-labeled ligand and the receptor leads to emission of depolarized light.

Peptide **44** showed no competitive inhibition of the Flu-C38–gp41-5 interaction (Figure 47C). Peptide **42** was determined to have a  $K_i$  of  $132 \pm 24$  nM, and peptide **45** was found to have a  $K_i$  of  $302 \pm 45$  nM (Figure 47C). Taken together with the CD characterization of the peptides, sequence **42** was chosen as the starting point for the generation of oligomers containing two aminoxy-functionalized residues for cross-link formation. This sequence was selected due to its unstructured nature by CD and moderately high affinity for gp41-5. These characteristics allow for either positive or negative changes in affinity due to cross-linking to be observed under the conditions of the competition fluorescence polarization assay.

## 4.2 CROSS-LINKING OF GP41-5 LIGANDS AFFECTS FOLDING AND AFFINITY

Having chosen peptide **42** as a starting point for the design of oligomers capable of cross-link formation, three new sequences (**46-48**) were generated, each containing two aminoxy residues (Figure 49). Peptide **46** has two aminoxy-functionalized isosteres of lysine ( $X_5$ ) at positions 13 and 17. The analogous sequence, **47**, substitutes two aminoxy-functionalized isosteres of ornithine ( $X_4$ ) at the same sequence positions in order to gauge the effect of macrocycle size and flexibility on cross-linking and affinity for gp41-5. Sequence **48** contains two  $X_5$  residues closer to the N-terminus of the sequence, at positions 6 and 10. Each peptide was reacted with three commercially available dialdehydes (**a-c**) to furnish cyclic products, where the cyclized product is the combination of the peptide and the linker used (e.g. peptide **46** cyclized with linker **a** furnishes product **46a**) (Figure 49B).

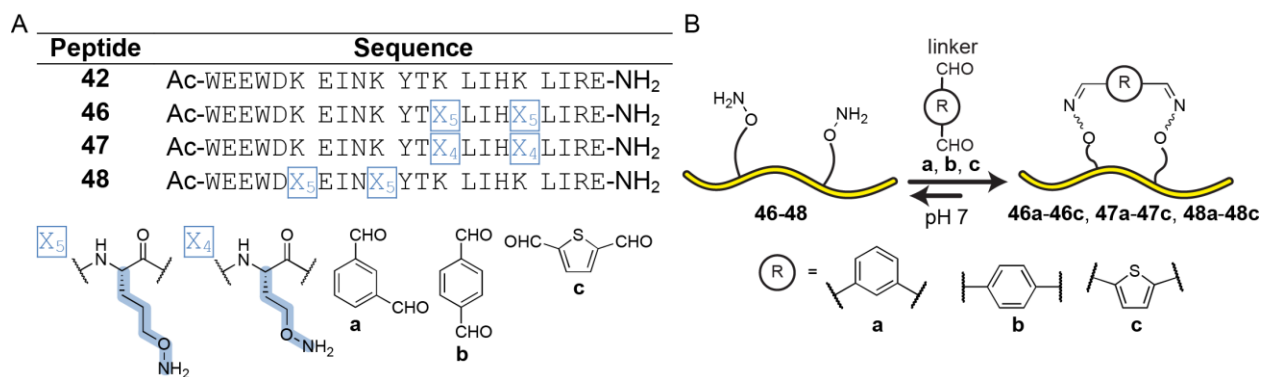


**Figure 49.** Sequences of peptides **46-48** and schematic representation of cross-linking. (A) Sequences of peptides **42** and **46-48**, with monomers and linkers utilized below. (B) Schematic representation of cross-linking reactions performed.

We first examined the efficiency of the cross-linking reaction for peptides **46-48** with linkers **a-c**. We performed reactions of each peptide at 10  $\mu\text{M}$  concentration with 40  $\mu\text{M}$  linker in 0.1 M phosphate buffer at pH 7. Each peptide was found to react cleanly with linkers **a-c**; however, the formation of cyclic products was considerably slower ( $\sim 4$  hours for the reaction to reach equilibrium) than in the peptides of limited sequence diversity utilized in Chapter 3 (Figure 50). Interestingly, this effect was concentration independent; when samples of 50  $\mu\text{M}$  peptide **46** were treated with 200  $\mu\text{M}$  of linker, the reaction was not found to reach equilibrium at an earlier time point. This result was surprising given that higher concentration should lead to a faster intermolecular reaction. However, as found previously in Chapter 3 and in accordance with literature precedent,<sup>108</sup> nucleophilic catalysis of the reaction through the use of aniline yielded cyclized product more rapidly. In each case, multiple chromatographic peaks were observed with masses corresponding to the cyclized species, and were assigned as stereoisomers of the desired oxime-cyclized products (Figure 50). Of note is the fact that linker **b**, in all cases, failed to quantitatively yield cyclic product; though the starting peptide is completely consumed after 4 hours, in each case a chromatographic peak was observed with a mass corresponding to the formation of a single oxime and an acyclic product (termed product **#b'**, e.g. **46b'**). It is unclear why this reaction failed to fully cyclize, though the product distribution observed 4 hours following linker addition did not change up to

12 hours following linker addition. In no case were products observed resulting from the reaction of two independent peptide chains reacting with a single linker.

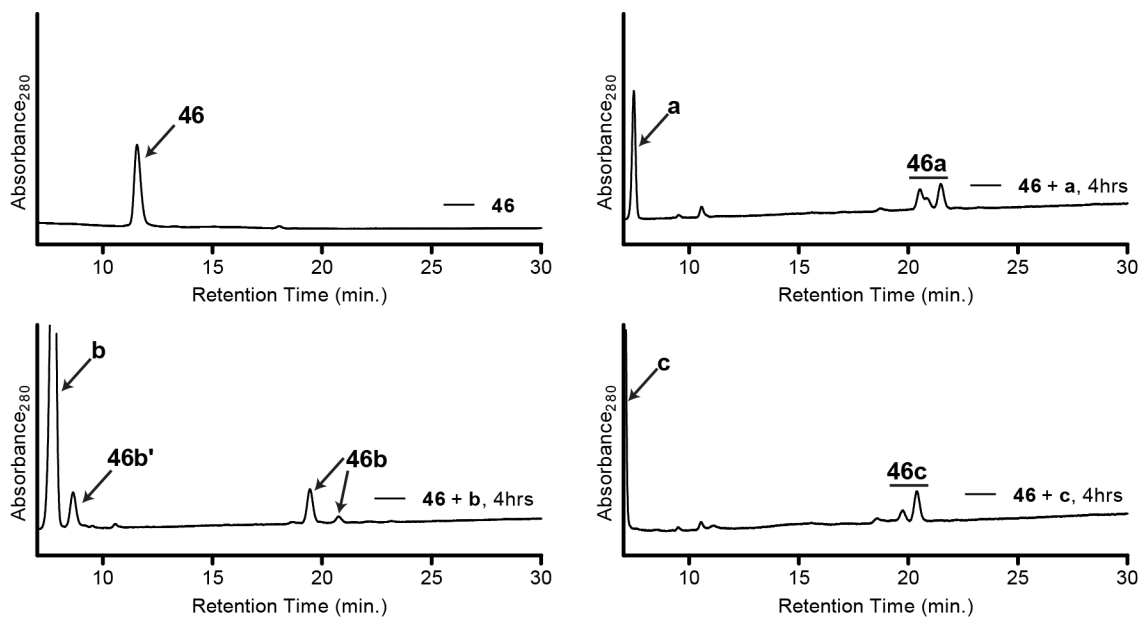


**Figure 50.** HPLC chromatograms of cross-linking reactions with peptide **43** and linkers **a-c**. All reactions were performed with 10  $\mu\text{M}$  peptide, 40  $\mu\text{M}$  linker in 0.1 M phosphate buffer, pH 7 and analyzed by HPLC and MALDI-TOF MS of collected eluent 4 hours following linker addition.

We next examined the folding behavior of each peptide and its corresponding cross-linked products by CD spectroscopy. For peptides **46** and **47**, it was found that neither the linear starting peptide nor its cyclic products show considerable helical structure (Figure 51). Interestingly, peptide **48**, where the aminoxy residues are located closer to the N-terminus of the sequence exhibited a CD signature indicative of  $\beta$ -sheet folding. Cross-linking this oligomer to generate products **48a-48c** affected the intensity of the  $\beta$ -sheet minimum at 216 nm, but did not lead to spectra strongly indicative of either helical or random coil conformations. Overall, the CD results suggest that the folding behavior of the peptides can be perturbed following cross-link formation; in the case of peptides **46** and **47**, it is possible that multiple conformations are present and equilibrating between random coil, sheet, and helical

conformations; in the case of peptide **45**, the  $\beta$ -sheet signature observed for the linear peptide can be diminished, but not abolished, by cross-link formation.

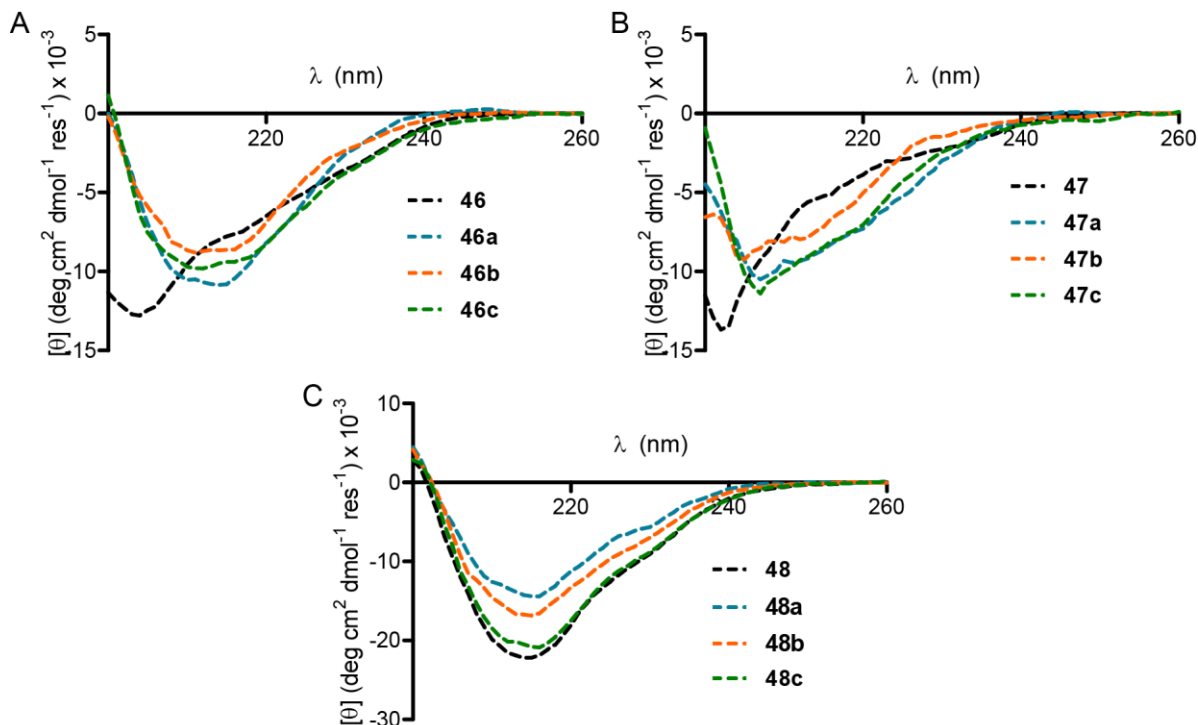


**Figure 51.** CD Data for peptides **46-48**.

(A) CD scans of peptide **46** and cross-linked products **46a-46c**. (B) CD scans of peptide **47** and cross-linked products **47a-47c**. (C) CD scans of peptide **48** and cross-linked products **48a-48c**. All CD scans were performed at 50  $\mu$ M concentration of peptide in 0.1 M phosphate buffer; cross-linking reactions contained 200  $\mu$ M linker and were analyzed four hours after linker addition.

We utilized the competition fluorescence polarization assay discussed previously to investigate the affinity for the linear peptides bearing unnatural residues, **46-48**, and their cyclic products for gp41-5. The linear peptides **46-48** were found to have somewhat higher affinity than the sequence upon which they are based (**42**) (Figure 52, Table 8). We hypothesized that this gain in affinity is due to the removal of two positively charged lysine residues; in the helical, bound state of the peptide, the lysine side chains are displayed on the same face of the helix, potentially leading to destabilizing charge-charge interactions.

Removal of this potential destabilizing interaction may correlate to the observed increase in inhibition equilibrium constant,  $K_i$ , in the competition assay.

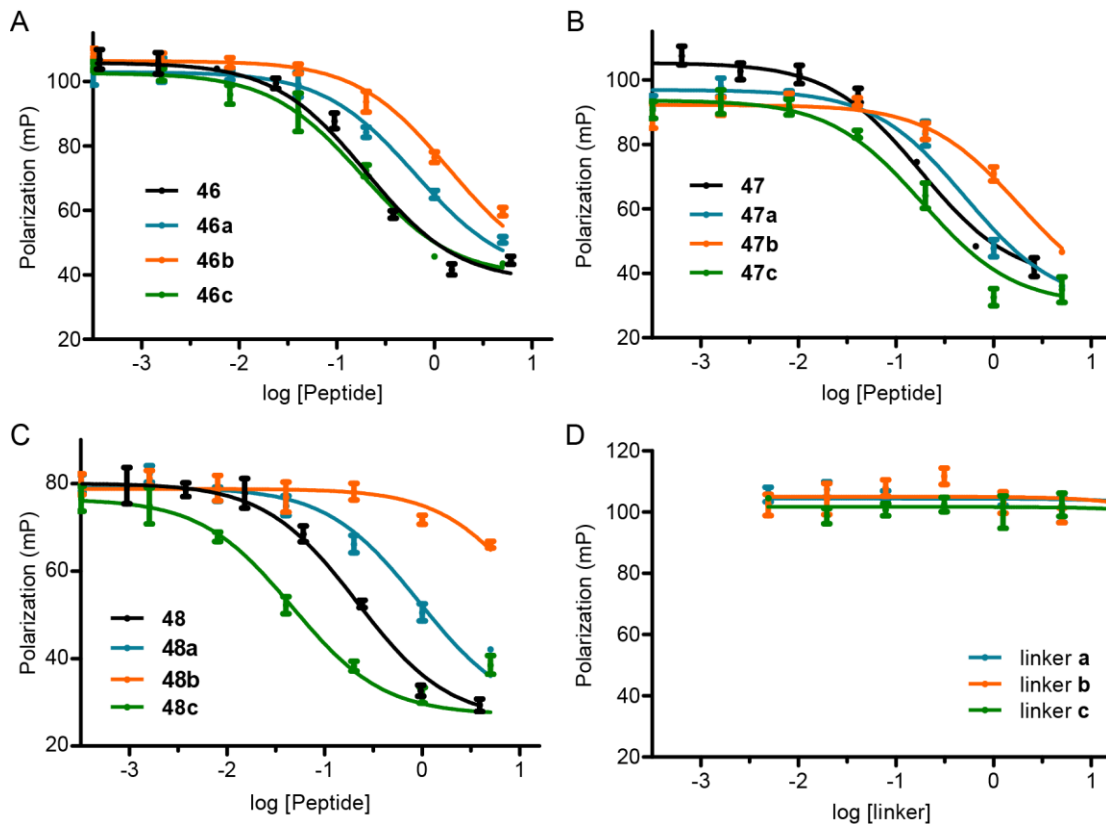


**Figure 52.** Competition fluorescence polarization data for peptides **46-48** and linkers **a-c**. (A) Competition fluorescence polarization data for peptide **46** and cyclic products **46a-46c**. (B) Competition fluorescence polarization data for peptide **47** and cyclic products **47a-47c**. (C) Competition fluorescence polarization data for peptide **48** and cyclic products **48a-48c**. (D) Competition fluorescence polarization data for linkers **a-c**, where no competitive binding is observed.

**Table 8.** Competition fluorescence polarization data for peptides **42** and **46-48**.

Peptide	FP Competition $K_i$ (nM)	Peptide	FP Competition $K_i$ (nM)
<b>42</b>	132 ± 24	<b>47</b>	31 ± 3
<b>46</b>	35 ± 3	<b>47a</b>	90 ± 13
<b>46a</b>	111 ± 11	<b>47b</b>	320 ± 31
<b>46b</b>	246 ± 23	<b>47c</b>	32 ± 5
<b>46c</b>	32 ± 4	<b>48</b>	37 ± 5
		<b>48a</b>	162 ± 22
		<b>48b</b>	2580 ± 430
		<b>48c</b>	8 ± 2

To assess the ability of cross-link formation to affect binding affinity, we prepared samples of cross-linked peptide wherein the linker was added 4-5 hours prior to the preparation of the fluorescence polarization assay wells to prepare the corresponding cyclized products **46a-46c**, **47a-47c**, and **48a-48c**. In order to ensure that the cross-link was maintained during serial dilutions of the cyclized samples, a constant concentration (40  $\mu$ M) of the appropriate linker was maintained (e.g., **46a** was serially diluted into buffer containing 40  $\mu$ M linker **a**). Using this sample treatment, we found that cross-link formation affects binding affinity, with linkers **a** and **b** making the binding affinity somewhat worse, while linker **c** maintains, but does not necessarily improve, the binding affinity compared to the linear starting peptide (Figure 52, Table 8). In only one case was a cross-linked oligomer obtained with a higher affinity for gp41-5 than its linear starting point, cross-linked product **48c**. This is interesting given that peptide **48**, even when cyclized with linker **c**, exhibits  $\beta$ -sheet like character by CD in the absence of the receptor. This indicates either that the cross-linked product is capable of undergoing a conformational change to a helical folding pattern in order to bind to gp41-5, or that it is capable of binding to gp41-5 as a  $\beta$ -sheet. In no case were the linkers alone responsible for competitive binding to gp41-5, as determined by competition assays of linker samples lacking peptide (Figure 52D).

### 4.3 EFFECT OF RECEPTOR PRESENCE ON CROSS-LINKING REACTIONS

Two types of experiments were designed to determine if the presence of gp41-5 affects the outcome of the cross-linking reaction. In the first, a peptide is treated with one or more linkers while bound to the receptor; in this case, the presence of the receptor can affect either the kinetic or thermodynamic outcome of the reaction (e.g. change the kinetics of the peptide-linker reaction and/or the equilibrium position of the reaction). In the second, a peptide is treated with one or more linkers, followed by the addition of the protein receptor to this mixture; in this case, any changes to the equilibrium position of the reaction would result in observed changes in the distribution of products of the reaction over time, as determined by HPLC. In the latter case, the observation of no change in the equilibrium position of the reaction may indicate either that the receptor is not changing the energetic landscape of the reaction mixture, that the changes to the energetic landscape are too small to lead to distinguishable changes by the analytical method employed, or that the reaction is kinetically trapped at a non-equilibrium position. In the case of kinetic control, prior studies have demonstrated that nucleophilic catalysis and/or mildly acidic pH can surmount the kinetic trapping effect.<sup>90</sup>

#### 4.3.1 Reactions Utilizing A Single Organic Linker

The simplest possible test of the effect of the presence of protein receptor on the cross-linking reactions used here is the use of a single peptide and a single linker in the presence or absence of the receptor. In order to test this directly, we utilized peptide **46** with each linker, **a-c**, in the absence or in the presence of 1 equivalent of gp41-5 relative to peptide (Figure 53). It is important to note that in this case any observed changes in the reaction outcome due to the presence of the receptor do not necessarily result from exchange between the possible products, but could also result from kinetic differences in the reaction outcome due to the presence of the receptor. In preparing reactions of peptide **46** with linkers **a-c**, it was observed that the presence of the receptor can affect the outcome of the cross-linking reactions to

differing extents based on the linker utilized. In the case of linker **c**, almost no differences are observed in HPLC chromatograms whether or not the receptor is present. In the case of peptide **46** reacted with linker **a**, only small changes are observed in the HPLC chromatogram, where the proportion of the cross-linked isomer eluting last in the chromatogram is slightly smaller than in the untemplated reaction. In the case of the reaction of peptide **46** with linker **b**, significant qualitative changes are observed by HPLC in the template reaction versus the untemplated reaction wherein gp41-5 is not present. Of note is that the product resulting from single oxime formation (product **46b'**) is no longer present when the reaction is performed in the presence of the receptor, and the distribution of isomers of product **46b** observed in the untemplated reaction is markedly different.

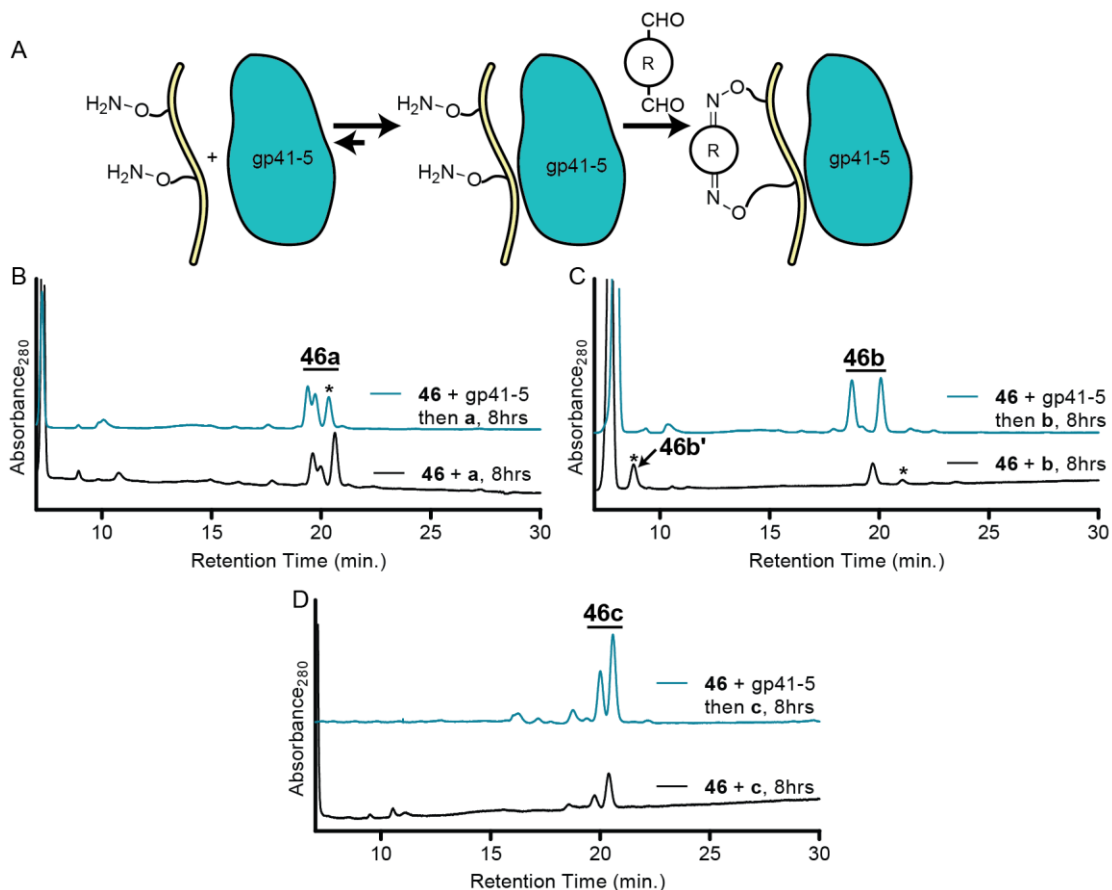


**Figure 53.** Receptor-templated reactions of peptide **46** with linkers **a-c**.

(A) Schematic representation of the experimental set-up. (B) HPLC chromatograms of cross-linking reactions with peptide **46** and linker **a** in the absence (black) and presence (blue) of 1 equiv gp41-5 relative to peptide. (C) HPLC chromatograms of cross-linking reactions with peptide **46** and linker **b** in the absence (black) and presence (blue) of 1 equiv gp41-5 relative to peptide. (D) HPLC chromatograms of cross-linking reactions with peptide **46** and linker **c** in the absence (black) and presence (blue) of 1 equiv gp41-5 relative to peptide. All chromatograms shown are 8 hours following linker addition. Peaks which qualitatively change in proportion in the chromatogram are denoted with an asterisk.

These experiments show that the presence of the receptor does not affect the efficiency of the cross-linking reaction, as the timescale of the reaction remained unchanged. The presence of the receptor was found to be capable of influencing the outcome of the reaction in some cases, but not all. Taken together with the fluorescence polarization data, these experiments suggest that in some cases the product mixture formed (as in the case of **46b**) may contain products which have poor affinity for gp41-5. The differences observed in reactions where the protein “template,” is present may indicate discrimination

between cross-linked products. The bound state of the peptide leads to differences in product distribution in some cases, particularly peptide **46** reacted with linker **b**. From these experiments it is unclear if the resulting differences in cross-linking reaction outcome arise from kinetic effects due to the presence of the template or from differences in the equilibrium position of the reaction (e.g., changes in the thermodynamics). However, these results encouraged further exploration of the ability of the protein receptor to affect cross-linking reaction outcomes, as discussed below.

#### 4.3.2 Reactions Utilizing Two Organic Linkers Simultaneously

Encouraged by the observed changes in isomer distribution based on the presence of the receptor for peptide **46** in a linker-dependent fashion, we undertook a series of experiments involving the simultaneous addition of two linkers (e.g., **a** and **b**) to peptide **46** in the presence or absence of gp41-5. In these experiments, any observed changes in the composition of the reaction mixture based on the presence of the receptor could indicate receptor-templated selection of a particular cross-linked product at the expense of other cross-linked products. Given this outcome, the possibility would exist of using this cross-linking method to directly screen for the most effective cross-linked oligomers for protein binding out of a complex mixture of possible products.

Experimental tests of this hypothesis utilized two parallel reactions: one in which peptide **46** was cross-linked by the simultaneous addition of two linkers in the absence of protein receptor and a second in which peptide **46** is cross-linked by the addition of two linkers in the presence of gp41-5. In these experiments, the analysis of the HPLC chromatograms is complicated by the considerable overlap amongst the various isomers of each cross-linked product. Nevertheless, some chromatographic peaks could be unambiguously assigned based on their retention time and/or observed mass by MALDI-TOF MS following collection of the HPLC eluent. In the case of the mixture of linkers **a** and **b**, the cross-linked products are mass degenerate, further complicating analysis of the reaction mixture.

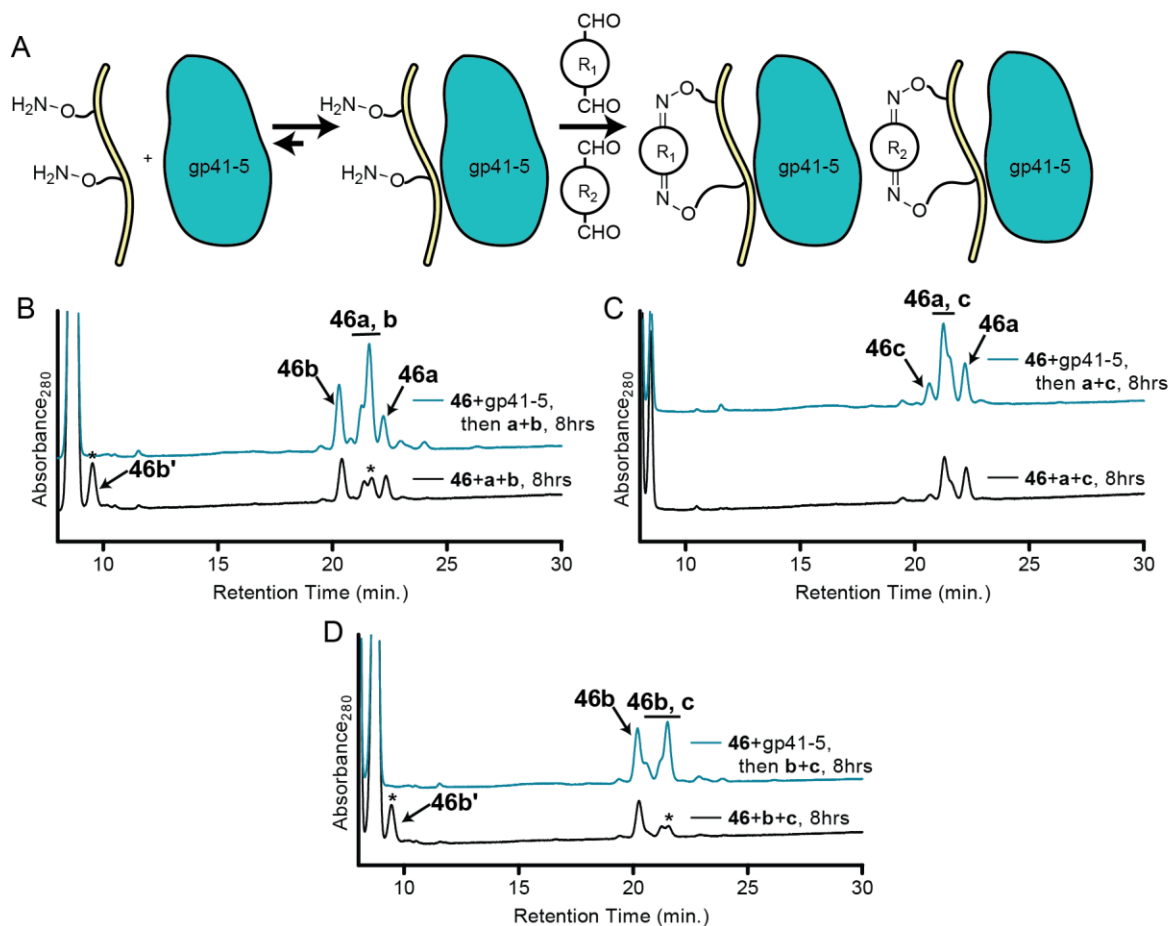


**Figure 54.** Scheme and chromatograms for reactions involving addition of two linkers.

(A) Schematic representation of the cross-linking reactions utilized; peptide bound to gp41-5 is treated simultaneously with two linkers (R<sub>1</sub> and R<sub>2</sub>). (B) HPLC chromatograms of the reactions between peptide **46** and linkers **a** and **b** either with (blue) or without (black) gp41-5 present. (C) HPLC chromatograms of the reactions between peptide **46** and linkers **a** and **c** either with (blue) or without (black) gp41-5 present. (D) HPLC chromatograms of the reactions between peptide **46** and linkers **b** and **c** either with (blue) or without (black) gp41-5 present. Peaks which show considerable change in the template versus untemplated reaction are highlighted with an asterisk.

It was found that the qualitative outcome of a reaction involving linker mixtures can depend on the presence of the receptor, particularly for reactions involving the use of linker **b** (Figure 54). However, in the binary combination of linkers **a** and **c**, there is little difference observed between template and untemplated reactions. We hypothesized that this may be due to the larger differences in binding affinity observed by fluorescence polarization for cross-linked products **a** or **c** versus **b** (e.g. in the case of linker **b** and **c**, an order of magnitude difference in observed  $K_i$ ). In the case of linkers **a** and **c**, the magnitude of

the difference in  $K_i$  is more modest, which may be responsible for the lack of protein-templated selection of a particular cross-linked product. However, an alternative hypothesis also exists: that the resulting differences in the templated versus untemplated reactions result not from the selection of a particular cross-linked product but from the observed effect of the protein template on individual cross-linking reactions. Prior observations suggested that there were considerable differences in the cross-linking reaction outcome for peptide **46** treated with linker **b** in the presence of the receptor versus in its absence; no differences were observed for peptide **46** treated with linker **c**, and considerably more modest differences were observed with linker **a**. The qualitative observation above that the binary mixture of two linkers only show differences by analytical HPLC when linker **b** is involved suggested the possibility that the protein template is not discriminating between different cross-linked macrocycles. Rather, the cross-linking reactions result in mixtures which are comprised of the sum of two individual cross-linking reactions in the presence of the protein receptor.

In order to test the hypothesis that the protein receptor is not discriminating between different cross-linked products we set up an experiment where two parallel reactions were prepared. In the first reaction, peptide **46** was treated with linker **b** in the presence of gp41-5; in the second, peptide **46** was treated with linker **c** in the presence of gp41-5. The two reactions were allowed to go to completion, then mixed in a 1:1 v:v ratio. The outcome of this experiment suggested that the observed differences in the protein-templated reaction involving linkers **b** and **c** above was due to the sum of the individual cross-linking reactions, as determined by qualitative comparison of the two samples (Figure 55). The observation that there is little or no difference between the two reactions (one where linkers are added simultaneously vs. one where independent reactions are mixed) shows that the protein template is not selecting for a given cross-linked product (e.g. **46c** versus **46b**), but that the outcome of the individual reactions of peptide **46** with either linker leads to the observed distribution of products.

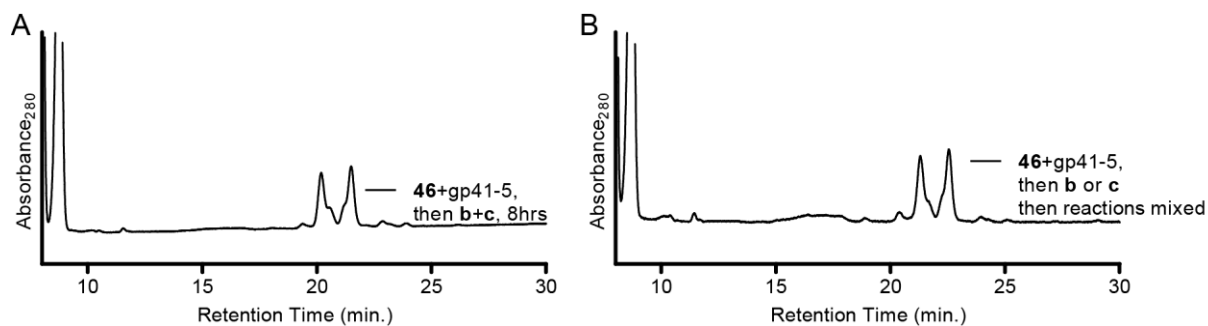


**Figure 55.** HPLC chromatograms of **46** with **b** and **c** treated simultaneously or independently. (A) Chromatogram of peptide **46** in the presence of gp41-5 treated with linkers **b** and **c** simultaneously. (B) Chromatogram of peptide **46** in the presence of gp41-5 treated with linker **b** or **c** in independent reactions, then mixed.

Despite the observation that gp41-5 is unable to selectively template the formation of a particular cross-linked product in the reactions with mixtures of linkers, the possibility remained that the lack of observed templating was due to the reaction mixture being kinetically trapped at a non-equilibrium position. In this case, the kinetic outcome of the reaction (a roughly statistical mixture of the two possible cross-linked products) would remain unchanged due to the inability of the system to undergo dynamic covalent exchange. An alternative hypothesis is that the reaction mixture observed represents the true equilibrium position of the reaction outcome, and that the system is at its thermodynamic minimum. It was observed that the product distribution of the reactions remained unchanged up to 24 hours following linker addition under the conditions utilized (pH 7 phosphate buffer, no nucleophilic catalyst).

We next undertook a series of experiments designed to test the possibility of the system to undergo dynamic covalent exchange. In these experiments, the objective is to first trap the system at a non-equilibrium position, then perturb the equilibrium by addition of a second linker or by addition of gp41-5.

In the first set of reactions, we utilized peptide **46** treated with linker **b** in the presence of aniline at pH 7 to form the product distribution of **46b** and **46b'** observed previously. A second linker, **c**, was then added and the reaction mixture monitored by HPLC for up to 24 hours (Figure 56). Nucleophilic catalysis of oxime or hydrazone ligation and/or exchange has previously been used in the context of

peptide or protein conjugation<sup>81, 108</sup> and in the construction of protein-templated DCLs.<sup>14</sup> In this case, there was found to be no change in the product distribution even after 24 hours, suggesting that the system is kinetically trapped at a non-equilibrium position. This is demonstrated by the difference in equilibrium position of the reaction for the simultaneous addition of linkers **b** and **c** than that observed for this sequential addition experiment. An additional experiment carried out under the same reaction conditions, except that the pH was decreased from 7 to 5, as mildly acidic pH has been found to facilitate exchange.<sup>90</sup> Even under these conditions, which should provide the most favorable possible conditions to facilitate exchange, the product distribution of the reaction was found to remain unchanged for up to 24 hours (Figure 56).

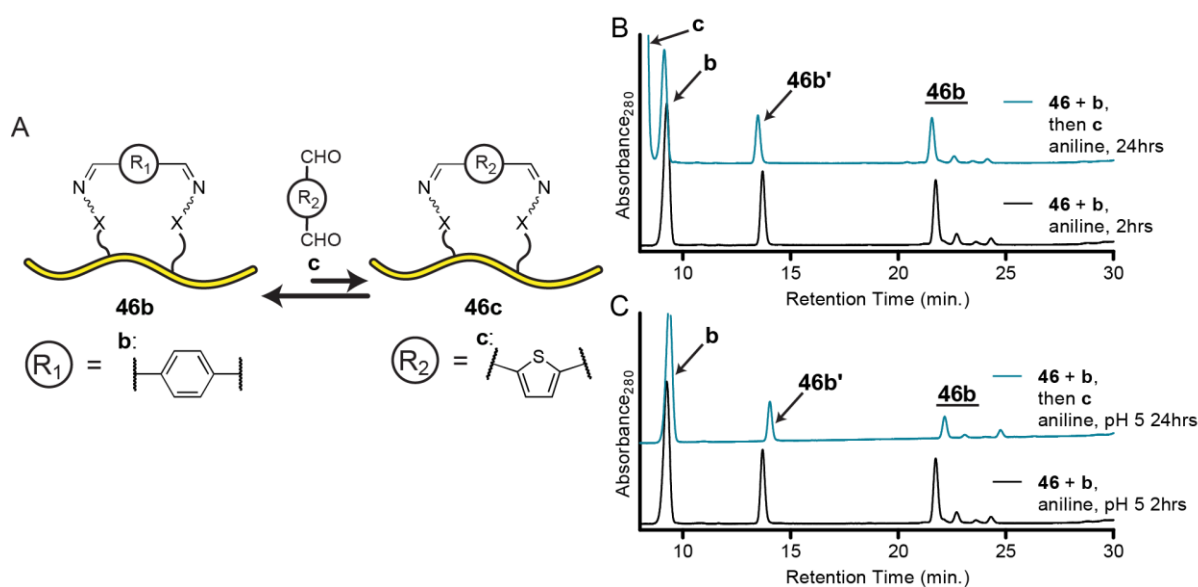


**Figure 56.** Attempted exchange reactions of peptide **46** with linkers **b** and **c**.

(A) Schematic representation of the possible exchange reaction of cross-linked product **46b** to form product **46c**. (B) HPLC chromatograms of the addition of linker **b** to peptide **46** in the presence of 1.25 mM aniline, 2 hours following linker addition (black), and 24 hours after the addition of linker **c** in the presence of 1 mM aniline. (C) HPLC chromatograms of the addition of linker **b** to peptide **46** in the presence of 1.25 mM aniline at pH 5, 2 hours following linker addition (black), and 24 hours after the addition of linker **c** in the presence of 1 mM aniline at pH 5.

Parallel experiments were performed where peptide **46** was treated simultaneously with linker **b** and **c** at pH 7 (Figure 57). Following completion of the reaction to yield the previously observed distribution of products for an untemplated reaction, gp41-5 was added and the product distribution monitored by HPLC for up to 24 hours. Under these conditions it was again found that the product distribution does not change. This result was somewhat surprising given the previous observations that oxime stereoisomers can interconvert easily; the observation that even the isomer distribution does not change in this case indicates significant kinetic trapping of the system at non-equilibrium positions.

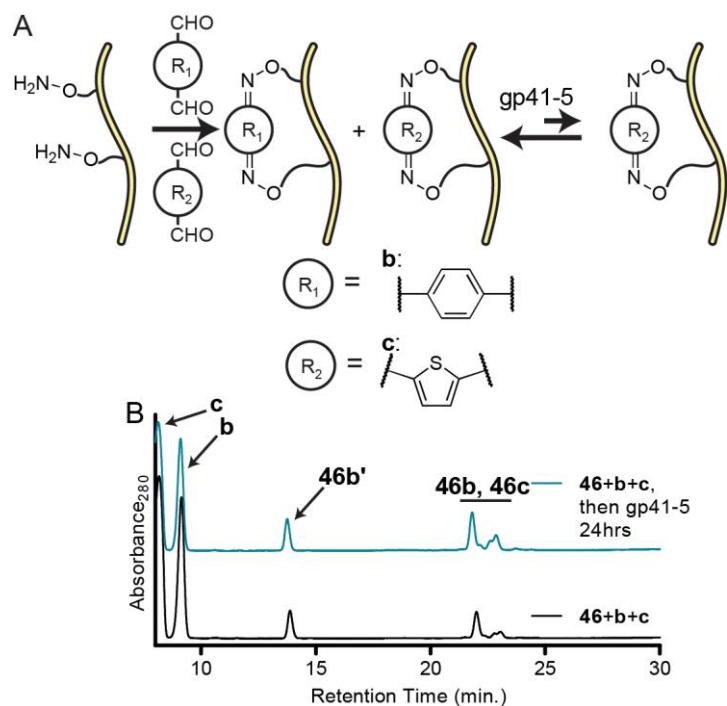


**Figure 57.** Attempted protein-templated selection of a binary mixture of linkers with peptide **46**. (A) Schematic representation of the reaction performed, where the selection of one cross-linked product is possible upon addition of protein template. (B) HPLC chromatograms of the reaction of peptide **46** with simultaneous addition of linkers **b** and **c** before (black) and 24 hours after (blue) addition of gp41-5 as a protein template.

#### 4.4 CONCLUSIONS AND PROSPECTIVE

Oxime formation to generate side-chain to side-chain cross-links between aminoxy-bifunctionalized peptides and dialdehyde based linkers is uniquely capable of being utilized under conditions compatible with peptide ligand-protein interactions. A series of peptides based on the gp41-5 C-terminal heptad repeat sequence bearing two aminoxy-functionalized residues were designed to have low inherent helical folding in the absence of receptor. Of this peptide series, peptides **46** and **47** are principally unstructured in the absence of receptor, and the addition of organic linkers does not lead to significant helical folding as determined by circular dichroism spectroscopy. Peptide **48** displays CD spectra characteristic of  $\beta$ -sheet folding both prior to and following the formation of side chain cross-links. These peptides cross-linked in the absence of receptor exhibit differing affinities for gp41-5 as determined by competition fluorescence polarization assays, with the general order of affinity being dependent upon the linker utilized ( $c > a > b$ ). In one case (product **48c**) the affinity by competition fluorescence polarization of the cross-linked product was higher than that of the starting linear peptide.

With the ultimate goal of utilizing this method as a way to generate complex mixtures of cross-linked peptides which would then be subjected to a protein receptor mediated selection process, we undertook a series of experiments to determine if the protein receptor, gp41-5, was capable of influencing the outcome of cross-linking reactions. In the case of the addition of a single linker to peptide **46** either bound or unbound to the protein receptor, differences are observed in the outcome of cross-linking reactions in some cases, principally in the distribution of products in cross-linking reactions involving linker **b**. However, the use of binary mixtures (e.g. simultaneous addition of linkers **b** and **c**) in analogous experiments demonstrate little to no selectivity for a given collection of cross-linked isomers due to the presence of the protein receptor. Stereoisomers of **46c** are not selectively formed over stereoisomers of **46b** in these reactions. This is contrary to the expectation that the cross-linked products more compatible with receptor binding should be selectively formed under the reaction conditions. Instead, the collective

outcome of the experiments suggests that the reaction outcome is determined kinetically and leads to a roughly statistical mixture of cross-linked products of **46b** and **46c**.

A series of experiments performed to gauge (1) whether or not the system is capable of dynamic covalent exchange and (2) whether or not addition of the protein receptor gp41-5 changes the distribution of products were unsuccessful. In the prior case, it was found that even under conditions which should be optimal for oxime exchange (mildly acidic pH, nucleophilic catalyst present) the product distribution remains unchanged following addition of a second linker even after 24 hours. The most likely explanation for this outcome is kinetic trapping of the system in a non-equilibrium position, given that the outcome of the reaction of sequential addition of linkers is markedly different than the outcome of the same linkers added simultaneously. In the case of attempted template-mediated amplification of products from a pre-equilibrated mixture, the lack of any observed selectivity (even to yield previously observed changes in product distribution based on the presence of the receptor) again suggests significant kinetic trapping, even amongst oxime stereoisomers. This kinetic trapping effect is unique to this system amongst the oxime cross-linking systems described in earlier chapters; in prior cases, even in the absence of significant dynamic covalent exchange of oximes, the distribution of oxime isomers formed were found to interconvert readily, which does not occur in this case.

Addressing the limitations of this system presents a challenge; it is possible that the use of additional dialdehyde based linkers and/or peptide sequences with different aminoxy-functionalized residue spacing may yield oligomers with improved affinity for gp41-5. However, given the lack of receptor-templated selectivity beyond a change in the distribution of cross-linked products for single linker additions to bound versus unbound peptide, and the proposed significant kinetic trapping of the system, it is unlikely that the use of additional linkers and/or peptides will yield the desired selectivity. It is important to note that under the conditions of the experiments performed and described above, the receptor is present in equal concentration as the peptide ligand; thus, under the experimental conditions, all of the linear peptide is presumed to be bound to the protein receptor. This experimental design is commonly used in protein-templated selection experiments involving small molecule DCLs,<sup>14, 15</sup> but may

not be ideal in this case. An experimental design wherein the ligand and protein concentration are significantly lower (e.g. nanomolar concentrations) such that one cross-linked product may more efficiently bind to the protein receptor at the expense of another cross-linked product is more likely to yield the desired selectivity. However, this design poses significant analytical challenges, as the sensitivity of the analytical methods used here is insufficient. Further development of this method may require either the development of new analytical techniques and/or the generation of peptide ligands which have decreased affinity for the protein receptor and thus can be analyzed at concentrations relevant to protein-mediated amplification.

## 4.5 EXPERIMENTAL

### 4.5.1 Peptide Synthesis And Purification

Protected Fmoc- $\alpha$ -amino acids and NovaPEG Rink Amide Resin were purchased from NovaBioChem. Fmoc-protected versions of aminoxy residues **X<sub>5</sub>** and **X<sub>4</sub>** were prepared by previously used protocols (Chapter 2.4.2). Peptides **41-48** were prepared by manual Fmoc-solid phase peptide synthesis with microwave heating (CEM Mars microwave reactor). Coupling reactions were performed in *N*-methyl-2-pyrrolidinone (NMP) using 5 equiv of amino acid, 5 equiv of activating agent (HCTU for natural  $\alpha$ -amino acids, PyBOP for unnatural **X** residues) and 7.5 equiv of DIEA. The microwave coupling program consisted of a 2 minute ramp to 70 °C followed by a 4 minute hold at 70 °C. Removal of the N-terminal Fmoc-protecting group was achieved by treatment with 20% 4-methylpiperidine in DMF. The microwave deprotection program consisted of a 2 minute ramp to 80 °C followed by a 2 minute hold at 80 °C. The resin was washed three times with DMF after each coupling and deprotection reaction. Following completion of the peptide sequence on resin and removal of the N-terminal Fmoc group, the N-terminus was acetylated by treatment with 8:2:1 v:v:v DMF:DIEA:Ac<sub>2</sub>O at room temperature for 15 minutes. The

resin was then washed with DMF, DCM, and methanol and dried under vacuum. Cleavage of the peptide from resin and concomitant side chain deprotection were performed by treatment with 92.5:3:3:1.5 TFA:H<sub>2</sub>O:EDT:TIS for 2.5-3 hours. The cleaved peptide was then precipitated into chilled diethyl ether, centrifuged, and the ether decanted. The pelleted crude peptide was dissolved in 30% by volume 0.1% TFA in acetonitrile and 70% by volume 0.1% TFA in water for purification by preparative HPLC. Preparative HPLC was performed using a Phenomenex Luna-C<sub>18</sub> column and gradients between 0.1% TFA in water and 0.1% TFA in acetonitrile. Fractions containing the desired peptide were frozen immediately for lyophilization due to previous observations of unknown byproducts resulting from prolonged exposure of aminoxy-functionalized peptides to acetonitrile containing solution. All peptide samples used for biophysical characterization and cross-linking reactions were  $\geq 95\%$  pure as determined by analytical HPLC.

**Table 9.** MALDI-TOF Data for peptides **42-48**, their cyclic products, protein gp41-5 and Flu-C38.

Peptide	[M+H] <sup>+</sup> (m/z)		Peptide	M+H] <sup>+</sup> (m/z)	
	Calculated	Observed		Calculated	Observed
<b>42</b>	2812.5	2812.3	<b>47</b>	2788.4	2788.3
<b>43</b>	2706.3	2706.3	<b>47a</b>	2886.4	2886.3
<b>44</b>	2600.5	2600.4	<b>47b</b>	2886.4	2886.6
<b>45</b>	2515.3	2515.4	<b>47b'</b>	2904.5	2904.7*
<b>46</b>	2816.5	2816.5	<b>47c</b>	2892.4	2982.4
<b>46a</b>	2914.5	2914.6	<b>48</b>	2816.5	2816.3
<b>46b</b>	2914.5	2914.7	<b>48a</b>	2914.5	2914.8
<b>46b'</b>	2932.5	2932.7*	<b>48b</b>	2914.5	2914.2
<b>46c</b>	2920.4	2920.2	<b>48b'</b>	2932.5	2932.8*
			<b>48c</b>	2920.4	2920.5
gp41-5	22228.7 <sup>†</sup>	22232.1 <sup>†</sup>			
Flu-C38	5089.3	5089.5			

\*Mass also observed corresponding to the acyclic hydrate, 2949.5 (**46b'**, **48b'**) or 2921.5 (**47b'**)

<sup>†</sup>Calculated and observed average [M+H]<sup>+</sup> masses

#### 4.5.2 Expression And Purification Of gp41-5

The DNA fragment encoding for gp41-5 subcloned into the expression vector pRSET (Invitrogen) and previously utilized for expression of gp41-5<sup>112</sup> was transformed into *Eschericia coli* BL21 DE3 cells. The transformed *E. coli* cells were grown in an overnight culture at 37 °C in 2xYT with ampicillin (100 mg/mL) and chloramphenicol (5 mg/mL). Following overnight culture, 2xYT growth medium was inoculated with media containing *E. coli* cells and allowed to grow at 37 °C to OD<sub>600</sub> = 0.5-0.6. IPTG (500 µM final concentration) was then added and the culture incubated 4.5-5 hours at 37 °C. Following this time, the cells were pelleted by centrifugation for 10 minutes at 2000 rpm at 4 °C. The cell pellet was then dissolved in cold glacial acetic acid and incubated on ice for 30 minutes. Cell debris was then removed by ultracentrifugation (20,000 rpm, 30 min), and the supernatant diluted to 10% acetic acid with deionized water, frozen, and lyophilized. Following lyophilization, the crude protein was dissolved in 0.1% TFA in acetonitrile (35% by volume) and 0.1% TFA in water (65% by volume) and purified by preparative HPLC on a Phenomenex Jupiter-C<sub>18</sub> column using gradients between 0.1% TFA in water and 0.1% TFA in acetonitrile. Fractions containing the desired protein were frozen and lyophilized. Purity of the protein was assessed by analytical HPLC using a Phenomenex Jupiter-C<sub>18</sub> column.

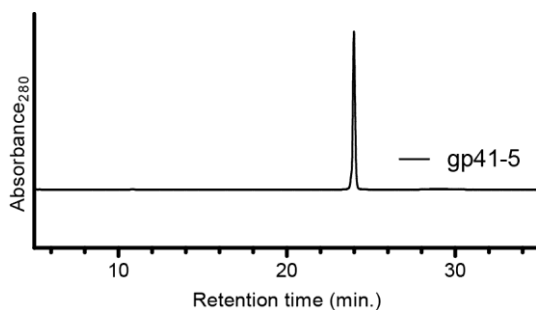


**Figure 58.** Analytical HPLC chromatogram of purified gp41-5.

### 4.5.3 Refolding Of gp41-5

Purified and lyophilized gp41-5 was dissolved in 6M guanidinium hydrochloride (0.1-0.3 mg/mL protein) and dialyzed against 100 mM glycine at pH 3.5 overnight, then dialyzed against phosphate buffered saline (pH 7.2) over the course of 3 days with the dialysis buffer changed daily. Following refolding, the protein solution was concentrated by centrifugation through a 3 kDa cutoff filter (Amicon Ultra). Purity of the refolded material was determined by gel permeation chromatography (GPC) on an AKTA purifier FPLC system equipped with Superdex 75 column (GE Healthcare). GPC was performed using an isocratic elution gradient consisting of 140 mM NaCl, 3 mM KCl and 10 mM phosphate buffer pH 7.4. A molecular weight calibration curve for the column was obtained by analyzing a solution of 0.2 mg/mL each of bovine serum albumin, myoglobin, cytochrome C, and insulin.

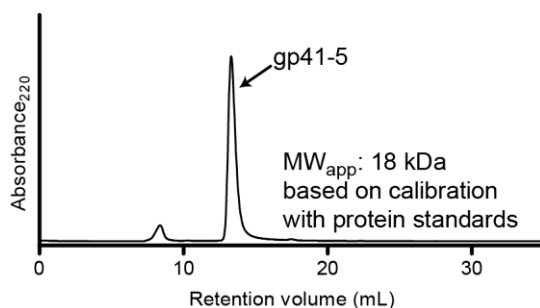


**Figure 59.** Analytical GPC chromatogram of refolded gp41-5.

### 4.5.4 Cross-Linking Reactions

Stock solutions of peptides **46-48** were prepared in water and their concentration determined by UV-Vis spectroscopy based on Trp and Tyr absorbance at 280 nm ( $\epsilon_{280} = 12660 \text{ M}^{-1} \text{ cm}^{-1}$ )<sup>102</sup> following 5x dilution of the peptide stock into 8M guanidinium hydrochloride. The concentration of refolded gp41-5 in phosphate buffered saline ( $\epsilon_{280} = 42390 \text{ M}^{-1} \text{ cm}^{-1}$ )<sup>102</sup> was determined identically. Stock solutions of linkers **a-c** were prepared in water. The concentration of linkers **a** and **b** were determined by UV-Vis (**a**,  $\epsilon_{292} =$

$1120 \text{ M}^{-1} \text{ cm}^{-1}$ ; **b**,  $\epsilon_{296} = 1950 \text{ M}^{-1} \text{ cm}^{-1}$ ).<sup>110</sup> The concentration of linker **c** was determined by mass to volume. Linkers **a-c** were well soluble in water and were delivered to the reactions from stock solutions containing 400-700  $\mu\text{M}$  linker in water. All cross-linking reactions were performed in 0.1 M phosphate buffer pH 7 with 10  $\mu\text{M}$  peptide and 4 equiv (40  $\mu\text{M}$ ) of the appropriate linker(s) with or without 10  $\mu\text{M}$  gp41-5. For samples containing gp41-5, the sample was prepared containing peptide and gp41-5 in pH 7 phosphate buffer and equilibrated for 40 minutes at room temperature prior to dilution by addition of linker(s) to furnish the reaction solutions described above. Reactions were analyzed by analytical HPLC on a Phenomenex Luna- $\text{C}_{18}$  column and by MALDI-TOF MS following collection of the eluent.

For attempted linker exchange reactions, a sample of cyclic peptide **46b** or was prepared in 0.1 M phosphate buffer at pH 7 or 0.1 M phosphate buffer at pH 5 from peptide **46** (12.5  $\mu\text{M}$ ) and linker **b** (50  $\mu\text{M}$ ) in the presence of 1.25 mM aniline. After complete conversion to **46b** as determined by analytical HPLC and MALDI-TOF MS (after 2 hours) linker **c** (4 equiv) was added from an aqueous stock solution to yield a final composition of 10  $\mu\text{M}$  peptide, 40  $\mu\text{M}$  each of linkers **b** and **c** in 0.1 M phosphate buffer at pH 7 or pH 5 and 1 mM aniline. The resulting reaction mixtures were monitored by HPLC for any changes in the distribution of products for up to 24 hours.

For attempted receptor-mediated selection of cross-linked products, peptide **46** at 15  $\mu\text{M}$  concentration in 0.1 M phosphate buffer at pH 7 was reacted with linkers **b** and **c** added simultaneously. Following completion of the reaction as determined by analytical HPLC (4 hours), gp41-5 was added from an aqueous stock solution to yield a final reaction composition of 10  $\mu\text{M}$  peptide **46**, 10  $\mu\text{M}$  gp41-5, and 40  $\mu\text{M}$  each of linkers **b** and **c** and the reaction mixture was monitored by analytical HPLC for a change in reaction composition over the course of 24 hours.

#### 4.5.5 Circular Dichroism Spectroscopy

Samples of linear peptides **42**, **44**, and **45** as well as **46-48** were prepared in 0.1 M phosphate buffer pH 7 at a concentration of 50  $\mu\text{M}$ . Samples of cyclized peptides **46a-46c**, **47a-47c**, and **48a-48c**

were prepared in 0.1 M phosphate buffer at pH 7 containing 50  $\mu$ M peptide and 4 equiv (200  $\mu$ M) linker and allowed to react 4 hours at room temperature. Following completion of the cross-linking reaction as determined by HPLC and MALDI-TOF MS, CD scans were performed on an Olis DSM17 circular dichroism spectrophotometer. Scans were performed from 200 to 260 nm with 1-nm step size, 2-nm bandwidth and 5 second integration time at 20 °C in 1 mm cuvettes. Raw CD data were smoothed by the Savitsky-Golay method as implemented in GraphPad Prism.

#### 4.5.6 Fluorescence Polarization Assays

Fluorescence polarization assays were conducted at room temperature in non-treated 96-well black polystyrene plates (Costar) on an Envision 2100 plate reader. All measurements were performed in triplicate wells containing 100  $\mu$ L total volume. The assay buffer was composed of 20 mM phosphate buffer pH 7.4, 50 mM NaCl, 1 mM EDTA, 0.2 mM NaN<sub>3</sub> and 0.5 mg/mL Pluronic-F68. All assay plates contained four wells of each of the following: (1) assay buffer (90  $\mu$ L + 10  $\mu$ L H<sub>2</sub>O), (2) Flu-C38 (90  $\mu$ L at 1.1 nM concentration diluted with 10  $\mu$ L H<sub>2</sub>O to a final concentration of 1.0 nM) and (3) Flu-C38 and gp41-5 (1.1 nM and 2.2 nM, respectively), in 90  $\mu$ L of assay buffer diluted with 10  $\mu$ L water to a final concentration of 1.0 nM Flu-C38 and 2.0 nM gp41-5. Direct binding experiments to determine the affinity of Flu-C38 for gp41-5 were performed by serial dilutions of gp41-5 against a solution containing 2 nM Flu-C38, and the K<sub>d</sub> determined to be  $\leq$  1 nM, in agreement with literature values.<sup>112</sup> Competition fluorescence polarization assays for linear peptides **42**, **44**, **45** and **46-48** were conducted by addition of 10  $\mu$ L of serial dilutions from peptide stocks in water to the assay buffer described above, 90  $\mu$ L containing 1.1 nM Flu-C38 and 2.2 nM gp41-5 to assay wells containing final concentrations of 1.0 nM Flu-C38 and 2.0 nM gp41-5.

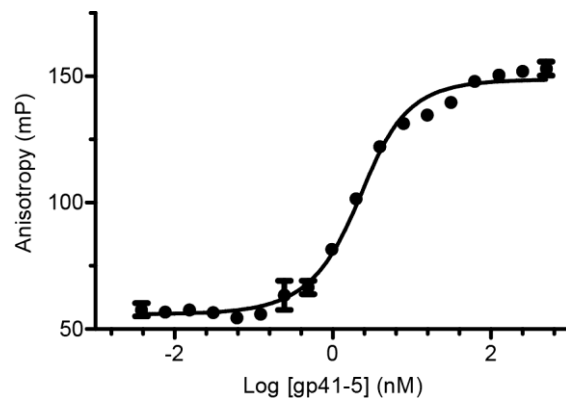


**Figure 60.** Direct binding fluorescence polarization assay of gp41-5 and Flu-C38.

Competition fluorescence polarization assays for cyclized peptides **46a-46c**, **47a-47c**, and **48a-48c** were prepared similarly. Cross-linking reactions of each peptide were prepared as described above and allowed to rest for 4-5 hours, until completion of the reaction was determined by MALDI-TOF MS. The cyclized peptide was then serially diluted into appropriate linker stocks containing 40  $\mu$ M linker in assay buffer. The serial dilutions were then added (10  $\mu$ L) into 90  $\mu$ L assay buffer to a final composition of cross-linked product with 1.0 nM Flu-C38 and 2.0 nM gp41-5.

All assay plates were allowed to equilibrate for 30 minutes to 1 hour at room temperature prior to analysis. Fluorescence polarization direct binding data were analyzed in GraphPad prism using published methods.<sup>114</sup> The concentration of ligand was constrained to 2.0 nM in the fit and the molar emissivity ratio of the bound ligand to that of the unbound ligand was taken as the ratio of the total fluorescence of the control wells lacking receptor and control wells of fluorescent tracer bound to the protein in the assay plate. Competition fluorescence polarization data were analyzed in GraphPad Prism using published methods<sup>115</sup> where  $K_d$  of the tracer was set to 0.4 nM based on literature precedent.<sup>112</sup> In the fit of competition fluorescence polarization data, the parameters describing the top,  $K_i$ , and slope of each curve were allowed to float. Not all compounds exhibited complete inhibition at the highest peptide concentration; the parameter for the bottom of each curve was set as a shared value (the mP of the unbound tracer from the control wells described above) for each assay plate.

## APPENDIX A. INVESTIGATION OF THE THERMODYNAMICS OF CROSS-LINKING

### A.1. INTRODUCTION

The use of side-chain to side-chain cyclization (referred to as “cross-linking,” or “stapling,”) of peptides has developed considerably over the course of the last decade with an eye towards generating peptide scaffolds with improved biophysical and therapeutic characteristics.<sup>40</sup> Several successful strategies have been implemented in developing peptide-based inhibitors of protein-protein interactions. The leading hypothesis for the success of side-chain to side-chain cyclization in nucleating and stabilizing helical structures is that the side chain cross-links lead to preorganization of the peptide backbone into a helical conformation.<sup>39</sup> This implies an entropic stabilization of the helical fold through constraint of backbone conformations. Prior study has shown how cross-linked oligomers change the folding free energy associated with protein-protein interactions.<sup>116, 117</sup> Additional work has examined the relative ability of different cross-linking strategies to nucleate helical folding patterns.<sup>118</sup> However, there has yet to be a direct test of the hypothesis that side chain cross-linking influences helical folding through entropic stabilization. In order to directly test the hypothesis that side chain cross-links are entropically stabilizing to helical folds, we utilized a folded monomeric protein containing an  $\alpha$ -helical region into which were inserted three different types of cross-links. Subsequent global analysis of the folding free energy landscape of the resulting oligomers in their linear and cyclic forms through circular dichroism thermal-chemical denaturation<sup>119, 120, 121</sup> allows for direct comparison of different cross-linking strategies in their ability to stabilize a monomeric helical fold. This strategy also allows for determination if any resulting gain in stability of the folded peptide is due to changes in the enthalpy or entropy of folding.

## A.2. MODEL SYSTEM SELECTION AND DESIGN

As noted above, previous studies have investigated thermodynamic changes associated with peptide cross-linking in the context of protein-protein interactions.<sup>116, 117</sup> However, in these analyses the process of quaternary structure formation and monomeric folding are inextricably entwined, which complicates analysis. In order to answer the open questions regarding the thermodynamic consequences of cross-link formation, a peptide model system is needed with particular characteristics: (1) a well-folded, monomeric and stable tertiary structure in aqueous solution, (2) one or more  $\alpha$ -helical regions in which to insert cross-linking residues, and (3) a length and sequence amenable to solid-phase peptide synthesis and post-synthetic manipulations associated with cross-link formation.

We chose to utilize the villin headpiece domain (VHP) as a model system for our studies (Figure A1).<sup>122</sup> This domain has previously been utilized to investigate the kinetics and thermodynamics of folding for short, fast-folding polypeptide sequences, and is comprised of 36-residues found in three short helical regions.<sup>123, 124, 125</sup> The folding of the VHP domain results from the formation of hydrophobic packing interactions between residues found on one face of each helix.<sup>126</sup> The wild-type VHP domain was altered by replacement of methionine residues with norleucine, in order to avoid potential oxidation of methionine during synthesis or analysis of cross-linked oligomers requiring oxidative conditions.

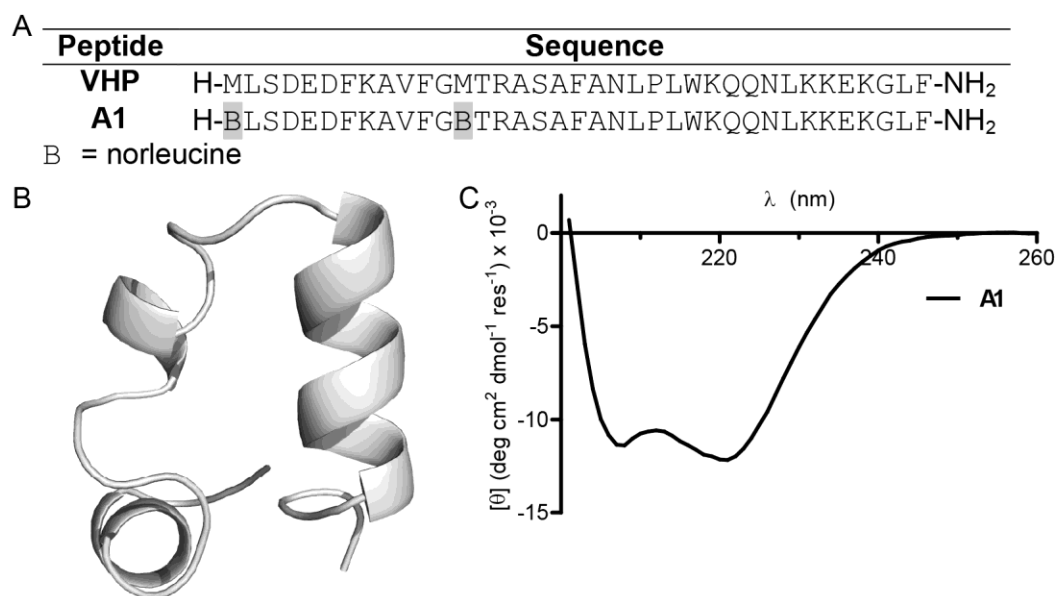


**Figure A1.** Sequence of VHP and peptide **A1**, wild-type structure, and CD spectrum of **A1**. (A) Sequence of VHP and analogue **A1** where methionine has been replaced with norleucine. (B) Structure of the wild-type VHP domain from PDB: 1VII. (C) CD scan of peptide **A1**.

Having generated a suitable analogue of the VHP domain, peptide **A1**, we investigated its folding by circular dichroism spectroscopy. Peptide **A1** was found to have a CD spectrum consistent with that of the wild-type VHP domain.<sup>126</sup> Temperature-dependent CD spectroscopy was used to ascertain the thermal stability of peptide **A1**. The mutation of methionine to norleucine was found to have a small impact on the thermal stability of the fold ( $T_m = 64$  °C) as compared to the wild-type VHP domain ( $T_m = 70$  °C).<sup>126</sup> We used thermal-chemical denaturation circular dichroism experiments to investigate the thermodynamics of unfolding in VHP analogue **A1**. Thermal-chemical denaturation circular dichroism spectroscopy has previously been used to evaluate the folding free energy of the *Arabidopsis* N-terminal ribosomal transcription factor, NTL9,<sup>119</sup> the thermodynamic changes associated with side-chain fluorination in well-folded peptides,<sup>120</sup> and the consequences of insertion of  $\beta$ -residues into  $\alpha$ -peptide backbones in a well-folded tertiary structure.<sup>121</sup> Thermal denaturation experiments were performed in 50  $\mu$ M solutions of peptide in the presence of guanidinium hydrochloride in 0.5 M increments between 0 and 5.5 M (Figure

A2). Analysis of the thermal-chemical denaturation data provides the thermodynamic parameters associated with unfolding of the peptide backbone (Table A1).

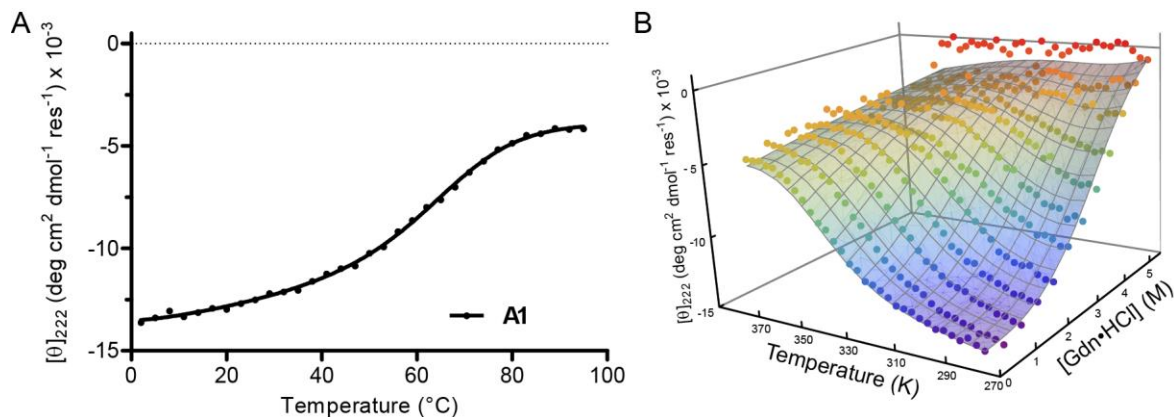


**Figure A2.** CD thermal and thermal-chemical denaturation experiments of **A1**.

(A) CD melt of peptide **A1** where molar ellipticity at 222 nm is monitored as a function of temperature. (B) Thermal-chemical CD denaturation of peptide **A1**. Molar ellipticity at 222 nm is monitored as a function of temperature and chemical denaturant. Raw data (points) are fit (surface) to extract thermodynamic parameters of the unfolding equilibrium.

Having validated the use of the VHP domain **A1** as a suitable model system, we designed oligomers (**A2-4**) containing residues appropriate for the introduction of side chain to side chain cross-links (Figure A3). In each peptide **A2-A4** lysine or a close analogue of lysine (azidolysine in **A3**, **X** in **A4**) is substituted at position 31. These substitutions are conservative or nearly so for the lysine at that position in the natural sequence. A complementary amino acid for the cross-linking type employed is placed at position 27 in the sequence, for an  $i \rightarrow i+4$  spacing of the residues. Peptide **A2** contains orthogonally protected lysine and aspartic acid residues which can be deprotected by treatment with mild acidic conditions on resin and cyclized to form a lactam cross-link. Peptide **A3** contains D-propargylglycine at position 27 and azidolysine at position 31 to be used in the formation of a triazole cross-link. Peptide **A4** contains an aminooxy-functionalized residue at position 31 and a serine-acylated residue at position 27 in order to generate an oxime cross-link.

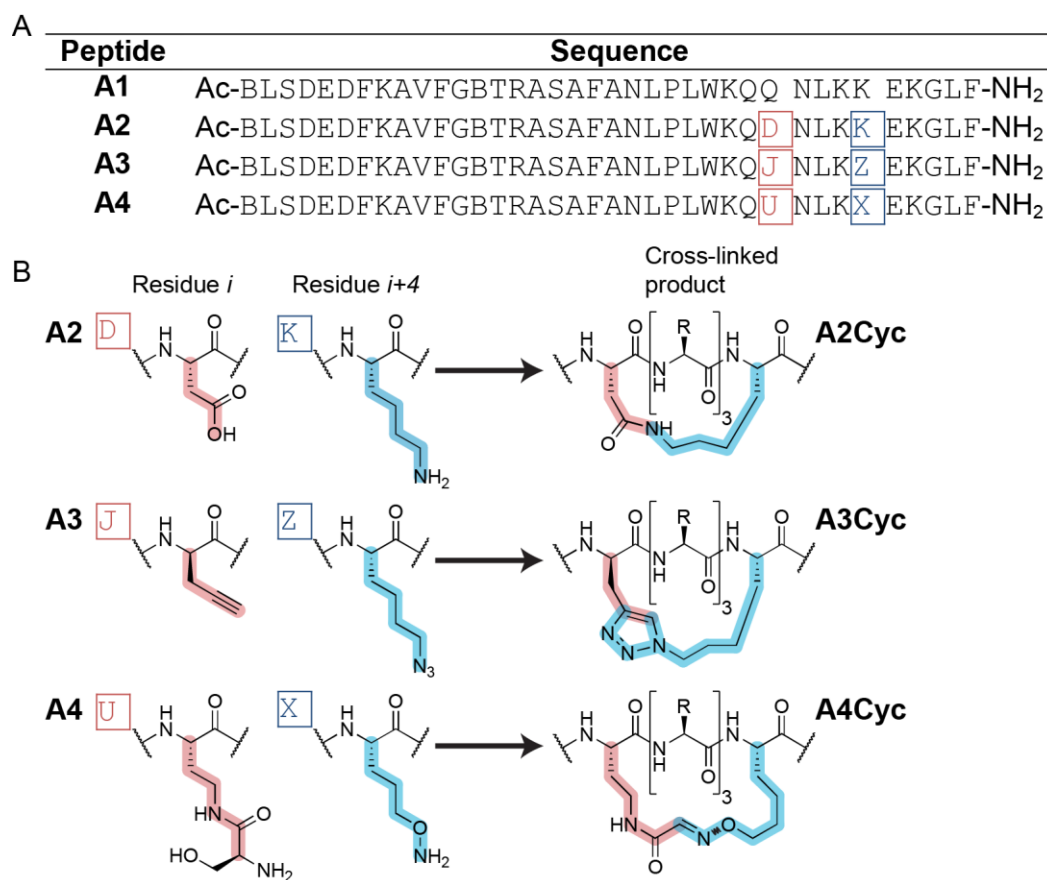
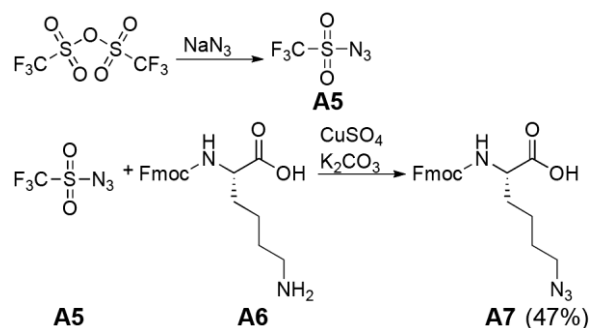


**Figure A3.** Sequences of peptides **A1-A4**, residue and cross-link chemical structures.

(A) Sequences of peptides **A1** and variants **A2-A4** in which residues are inserted to form cross-links. (B) Chemical structures of the monomers used in cross-linking and the cyclic products of cross-linking reactions.

Orthogonally protected Fmoc-Lys(Mtt)-OH and Fmoc-Asp(OPip)-OH residues in peptide **A2** and Fmoc-D-propargylglycine used in peptide **A3** were purchased from commercial suppliers. Fmoc-L-azidolysine was synthesized according to literature procedures (Scheme A1). Triflic azide was prepared by reaction of triflic anhydride with sodium azide. The crude triflic azide was directly reacted with Fmoc-Lys-OH to form Fmoc-azidolysine. Fmoc-protected aminoxy monomer **X** and serine-acylated monomer **U** were prepared as described in section 2.4.2.



**Scheme A.1.** Synthesis of Fmoc-L-azidolysine

Peptides **A2-A4** were synthesized by standard Fmoc-based SPPS. Peptide **A2** was then subjected to mild acid treatment to deprotect orthogonally protected lysine and aspartic acid residues. The peptide was then subjected to on-resin cyclization by reaction with PyBOP and DIEA under microwave irradiation to form peptide **A2Cyc**. Peptides **A3** and **A4** were synthesized, cleaved, and purified by HPLC. Peptide **A3Cyc** was prepared by copper(I)-mediated azide-alkyne cycloaddition. Peptide **A4Cyc** was generated by treatment of **A4** with aqueous sodium periodate and subsequent formation of oxime-cyclized product **A4Cyc**. Cyclic products **A3Cyc** and **A4Cyc** were purified by HPLC prior to biophysical analysis.

### A.3. CROSS-LINK EFFECT ON FOLDING AND STABILITY

With peptides **A2-A4** and in hand, we examined their folding behavior by CD spectroscopy. In each case, the CD spectrum is indicative of  $\alpha$ -helical folding (Figure A4). Products **A2Cyc**, **A3Cyc**, and **A4Cyc** were found to have similar CD spectra as compared to their linear counterparts. Cumulatively, CD scans show that side chain cross-linking in these peptides has a minimal impact on the helical fold.

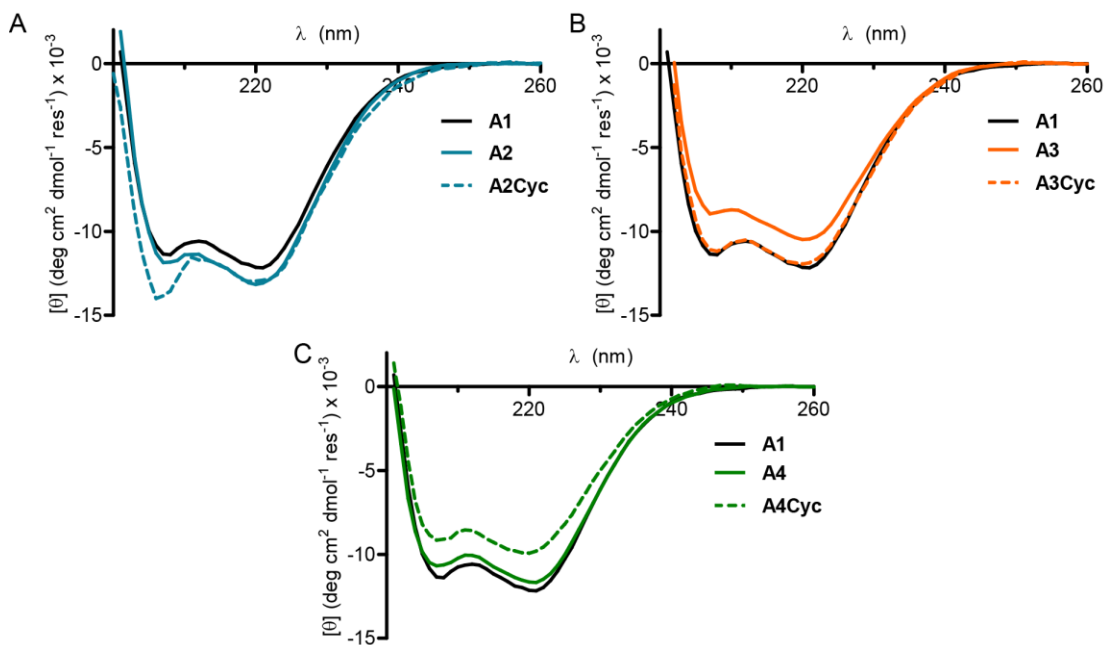


**Figure A4.** CD scans of peptides **A1-A4** and cyclic products **A2Cyc**, **A3Cyc** and **A4Cyc**.

(A) CD scans of peptide **A1**, **A2**, and **A2Cyc** at 50  $\mu\text{M}$  concentration in 50 mM phosphate buffer, pH 7. (B) CD scans of peptide **A1**, **A3**, and **A3Cyc** at 50  $\mu\text{M}$  concentration in 50 mM phosphate buffer, pH 7. (C) CD scans of peptide **A1**, **A4**, and **A4Cyc** at 50  $\mu\text{M}$  concentration in 50 mM phosphate buffer, pH 7.

CD thermal denaturation experiments were used to compare the thermal stability of **A2-A4** and their cyclized products (Figure A5). Peptides **A2** and **A4** showed two-state thermal transitions and had thermal melting temperatures similar to control peptide **A1**. Peptide **A3** showed a two-state thermal transition but was significantly destabilized as compared to **A1**. We attribute this destabilization to the insertion of D-propargylglycine into the sequence. While D-propargylglycine was found to be most effective in stabilization of helical folding in a short helical peptide,<sup>76</sup> the insertion of D-amino acids can be destabilizing to helical folds. CD thermal denaturation experiments with peptide **A3Cyc** showed a nearly identical thermal transition as compared to its linear counterpart **A3**. In contrast, the thermal denaturation of peptides **A2Cyc** and **A4Cyc** led to shallower thermal transitions over the temperature range of the experiment. Fitting to a two-state thermal denaturation model failed for **A2Cyc** and **A4Cyc** due to the nearly linear nature of the thermal transition.

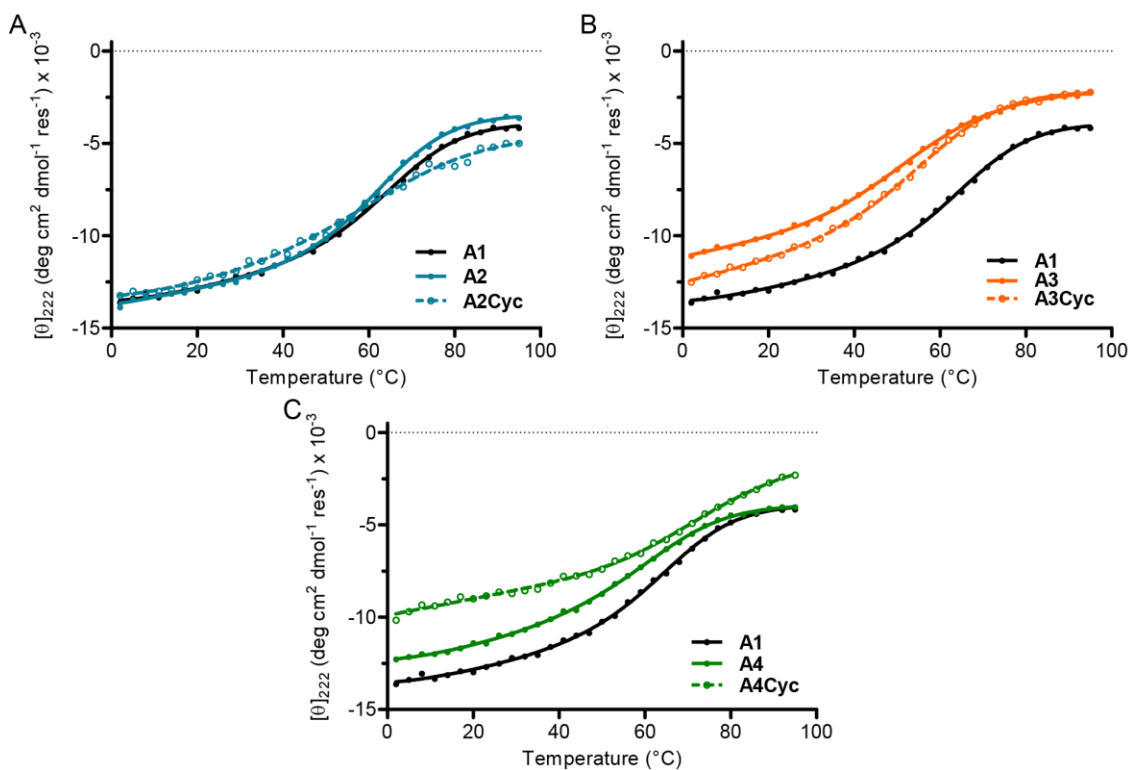


**Figure A5.** CD melts of peptides **A1-A4** and cyclized products **A2Cyc**, **A3Cyc**, and **A4Cyc**. (A) CD melts of peptides **A1**, **A2**, and **A2Cyc**. (B) CD melts of peptides **A1**, **A3** and **A3Cyc**. (C) CD melts of peptides **A1**, **A4**, and **A4Cyc**.

#### A.4. THERMODYNAMICS OF UNFOLDING BY THERMAL-CHEMICAL DENATURATION

Thermal-chemical denaturation CD experiments were performed to analyze the thermodynamic equilibrium of unfolding for peptides **A2-A4** and their cyclized products. Despite ambiguous fitting of peptides **A2Cyc** and **A4Cyc** in simple thermal denaturation experiments, all peptides were successfully fit to two-state folding model (Figure A6). Peptide **A3Cyc** was found to have almost identical thermodynamic parameters to its linear counterpart **A3** (Table A1). In contrast, peptides **A2Cyc** and **A4Cyc** were found to have significantly different thermodynamic parameters of unfolding (Table A1).

**Table A1.** Thermodynamic parameters of unfolding for **A1-A4**, **A2Cyc**, **A3Cyc**, and **A4Cyc**.

<b>Peptide</b>	$\Delta H_{\text{unfold}}$ (kcal mol <sup>-1</sup> )	$\Delta S_{\text{unfold}}$ (cal mol <sup>-1</sup> )	$\Delta C_{p,\text{unfold}}$ (kcal mol <sup>-1</sup> K <sup>-1</sup> )	$m$ (kcal mol <sup>-1</sup> M <sup>-1</sup> )
<b>A1</b>	7.4 ± 0.5	19.3 ± 1.3	0.30 ± 0.04	0.55 ± 0.04
<b>A2</b>	10.8 ± 0.1	28.3 ± 1.5	0.44 ± 0.04	0.81 ± 0.04
<b>A2Cyc</b>	3.6 ± 0.5	10.7 ± 2.6	0.16 ± 0.05	0.32 ± 0.06
<b>A3</b>	9.0 ± 0.4	24.8 ± 1.1	0.35 ± 0.03	0.73 ± 0.03
<b>A3Cyc</b>	8.9 ± 0.5	24.3 ± 1.6	0.37 ± 0.04	0.68 ± 0.04
<b>A4</b>	9.2 ± 0.5	24.0 ± 1.2	0.34 ± 0.03	0.70 ± 0.04
<b>A4Cyc</b>	5.6 ± 0.3	13.2 ± 1.1	0.26 ± 0.04	0.48 ± 0.04

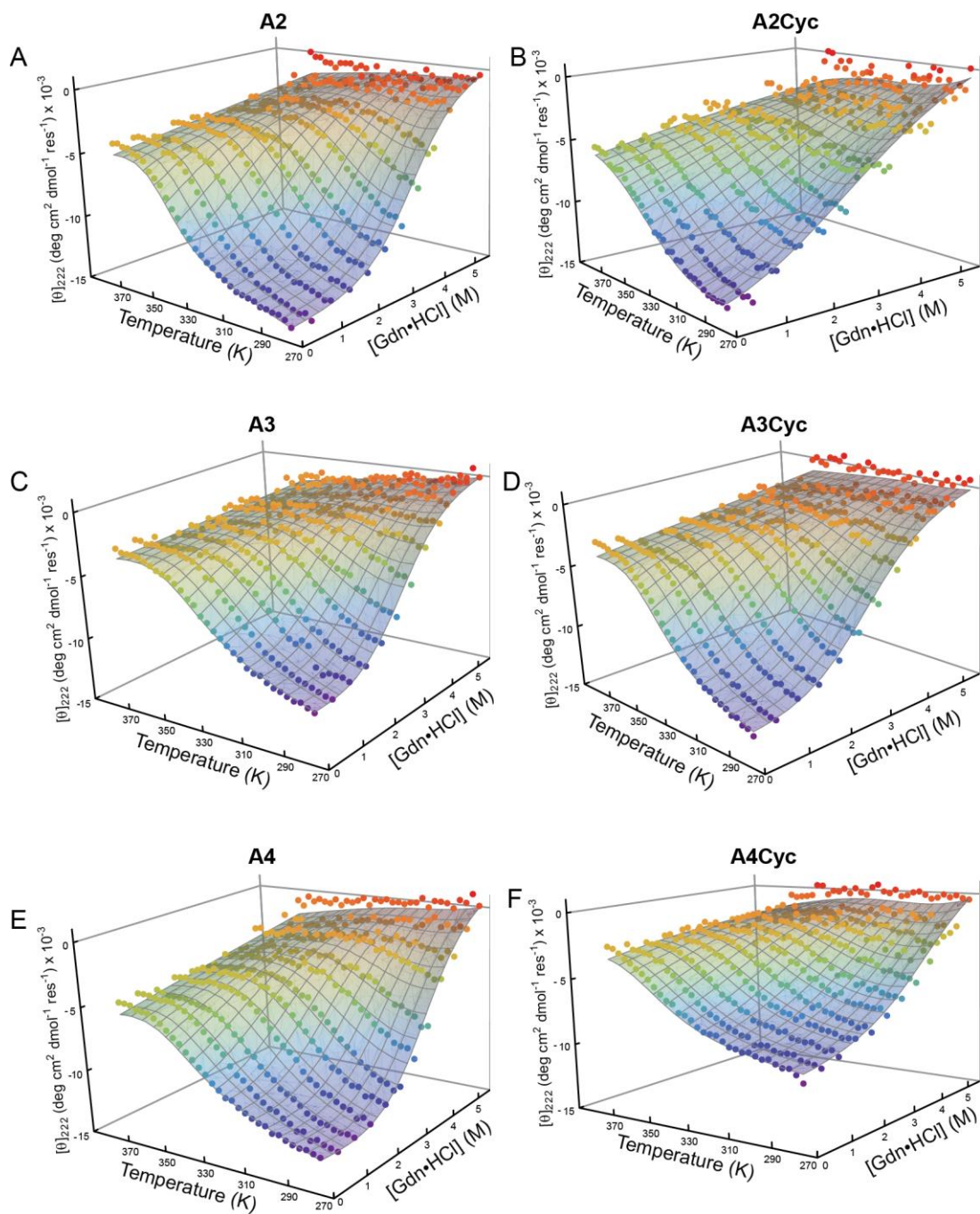


**Figure A6.** 3D melts of peptides **A2-A4** and cyclic products **A2Cyc**, **A3Cyc**, and **A4Cyc**. CD signature at 222 nm is monitored as a function of temperature and chemical denaturant. Raw data (points) are fit (surface) to extract thermodynamic parameters of the folding equilibrium. (A) 3D CD melt of peptide **A2**. (B) 3D CD melt of peptide **A2Cyc**. (C) 3D CD melt of peptide **A3**. (D) 3D CD melt of peptide **A3Cyc**. (E) 3D CD melt of peptide **A4**. (F) 3D CD melt of peptide **A4Cyc**.

The enthalpy change associated with unfolding is considerably smaller in **A2Cyc** versus **A2**; this is also true of **A4Cyc** versus **A4** (Figure A7). One possible origin of the unfavorable change of  $\Delta H_{\text{unfold}}$  accompanying side-chain cyclization is a change in backbone interactions with solvent. Cross-linking may limit solvent accessibility for hydrogen bonding interactions with backbone amides. This would cause significant changes to the enthalpy associated with hydrogen bonding interactions between the folded and unfolded states of the peptide. An alternative explanation is the removal of stabilizing intramolecular polar interactions in the cyclized peptides. Sequestration of the residues utilized in cross-link formation (Asp, Lys in **A2**, U and X in **A4**) may remove enthalpically favorable interactions. Of note is that the enthalpy of unfolding for peptides **A3** and **A3Cyc** are the same within the error associated with the fitting analysis (Figure A7). This suggests that there are few changes to enthalpic solvent-peptide interactions and/or intrapeptide interactions involved in the cyclization reaction between D-propargylglycine and azidolysine.

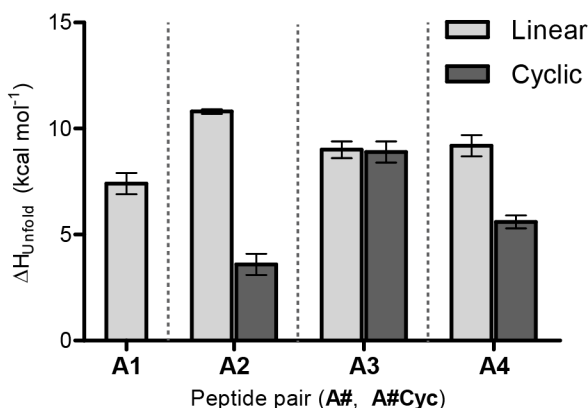


**Figure A7.** Enthalpy change of unfolding for peptides **A2-A4** and cyclic products. Each bar represents the  $\Delta H_{\text{unfold}}$  from fitting of raw 3D melt data. Error bars represent the uncertainty of the fit.

The entropy change associated with unfolding is significantly smaller in peptide **A2Cyc** versus **A2**; a similar difference is observed for **A4Cyc** versus **A4**. Taken in concert with the above observations

about the change in enthalpy associated with unfolding for peptide pairs **A2**, **A2Cyc** and **A4**, **A4Cyc**, this suggests significant entropy-enthalpy compensation is occurring. This effect has been noted for the thermal denaturation of other proteins.<sup>127</sup> As is the case for the enthalpy change of unfolding for peptide pair **A3** and **A3Cyc**, the entropy change of unfolding is unchanged upon cyclization. The observation that the entropy of unfolding does not change in all cases is somewhat surprising. It is expected that side chain cross-linking should introduce conformational constraints on the unfolding process. This should lead to a decrease in the entropy change associated with the unfolding of the peptide backbone. However, in the case of **A3Cyc** versus **A3**, this is not the case. One possible explanation is that the macrocycle present in **A3Cyc** is too flexible to effectively constrain the backbone. However, the macrocycle of **A3Cyc** is nearly isosteric with that in **A2Cyc**, where a change in the entropy of unfolding is associated with cyclization.

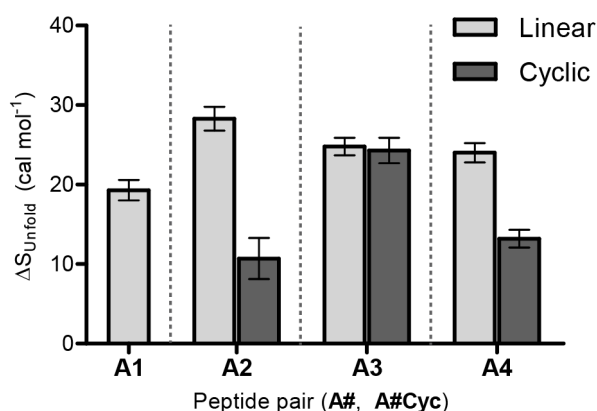


**Figure A8.** Entropy change of unfolding for peptides **A2-A4** and cyclic products. Each bar represents the  $\Delta S_{\text{unfold}}$  from fitting of raw 3D melt data. Error bars represent the uncertainty of the fit.

Protein folding is often accompanied by positive changes in heat capacity, which result from differences in the interaction of water with the folded versus unfolded state.<sup>128</sup> The magnitude of the change in heat capacity depends on a number of factors, which include residual structure in the denatured ensemble. The constraint of backbone atoms introduced by side chain to side chain cross-links would thus be expected to have an impact on the change in heat capacity associated with unfolding. As observed

previously, this is not the case for peptide **A3Cyc** versus **A3**. However, this hypothesis is supported by the heat capacity changes associated with peptide **A2Cyc** versus **A2** and **A4Cyc** versus **A4**. The observations from **A2** and **A4** and their cyclized counterparts are consistent with changes to the denatured conformational ensemble to favor more compact structures. This is further supported by observations in the change in  $m$  between the cyclized and linear sets of **A2** and **A4**. The parameter  $m$  is a measure of the dependence of the folding free energy on denaturant concentration.<sup>129</sup> This dependence of free energy of unfolding on denaturant concentration, combined with changes to heat capacity, are correlated to the change in solvent accessible surface area that accompanies unfolding. That the dependence of free energy on denaturant concentration,  $m$ , decreases for **A2Cyc** versus **A2** and for **A4Cyc** versus **A4**, but not for **A3Cyc** versus **A3** correlates well to prior observations.

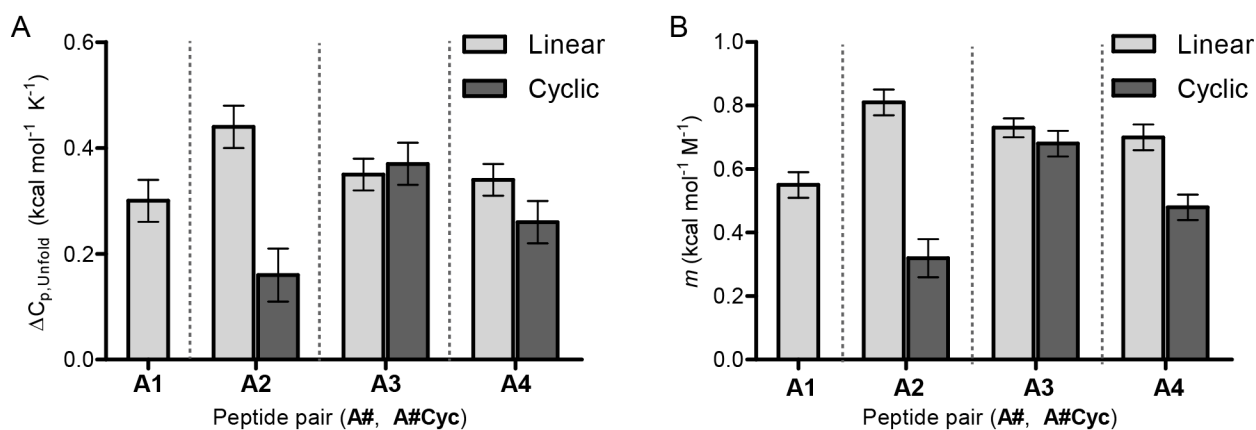


**Figure A9.** Heat capacity and  $m$  for peptides **A1-A4** and cyclic products.

(A) Change in heat capacity ( $\Delta C_p$ ) of unfolding for peptides **A1-A4** and cyclic products. Each bar represents the  $\Delta C_p$  from fitting of raw 3D melt data. Error bars represent the uncertainty of the fit. (B) Dependence of folding free energy on denaturant concentration ( $m$ ) for peptides **A1-A4** and cyclic products. Each bar represents the  $m$  value from fitting of raw 3D melt data. Error bars represent the uncertainty of the fit.

Overall, the thermodynamic parameters of unfolding associated with unfolding of cyclized peptides versus their linear counterparts supports the hypothesis that cross-linking constrains the backbone and decreases the entropy associated with unfolding. This decrease in the entropy of unfolding

is further supported by changes to heat capacity and  $m$ , which follow the same general trend. Of note is that one cyclic and linear pair (**A3Cyc** and **A3**) do not vary considerably in any of the thermodynamic parameters associated with unfolding. This is likely due to inappropriate design of the substitution pattern for cross-linking residues. Prior study of triazole cross-linked helical peptides noted that the monomer pairing of D-propargylglycine and azidolysine led to significant stabilization of a helical fold.<sup>76</sup> However, in that study the alkyne-functionalized side chain utilized in cross-link formation was C-terminal to the corresponding azide-functionalized side chain. It is likely that reversal of the residue positions, as implemented in **A3** and **A3Cyc** is destabilizing to the helical fold due to insertion of D-propargylglycine. However, it is still surprising that cyclization of peptide **A3** does not change the thermodynamic parameters associated with unfolding. Even if the helical fold is destabilized, it is expected that cross-link formation would change the thermodynamics of unfolding; this outcome is not observed.

## A.5. CONCLUSIONS

The use of VHP as a model sequence has provided valuable data which largely supports the hypothesis that cross-linking conformationally restricts the peptide backbone thus stabilizing helical folds. However, the inability to fit the thermal denaturation experiments of **A2Cyc** and **A4Cyc** to a simple two-state unfolding model argues that this model system is not ideal. It was previously observed (see section 2.2) that oxime cross-links can significantly decrease the sigmoidal nature of the two-state thermal denaturation of a peptide quaternary structure. In extreme cases, this change results in a nearly linear dependence of helical folding on temperature. It is likely that in the VHP system similar changes to the sigmoidal nature of the thermal denaturation curve are responsible for the ambiguity in two-state thermal denaturation model fitting. It is unclear if this results from significant changes to the overall folding pathway of the peptide, or if it is due to changes in the thermodynamic parameters of unfolding along the same unfolding pathway. A potential avenue to explore this phenomenon further is to utilize a system

which has a greater change in the magnitude of the CD minima monitored during thermal-chemical denaturation experiments. The *Streptococcal* protein GB1 has proven to be a valuable model system in our lab for this type of analysis.<sup>121</sup> While its 56-residue length makes its synthesis non-trivial, a series of variants of GB1 bearing cross-linking residues may be synthesized by semisynthetic procedures adapted from larger proteins. GB1 has a much sharper thermal denaturation transition than is observed for VHP. Utilizing a different model system would allow for confidence in the global analysis of thermodynamic parameters even if the sigmoidal transition is broadened due to the presence of cross-links.

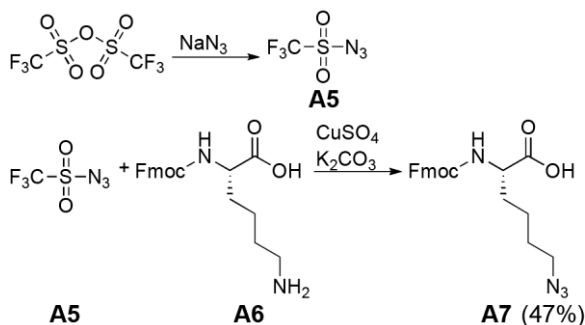
## A.6. EXPERIMENTAL

### A.6.1. General Information

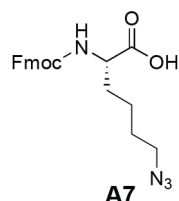
Solvents and other reagents were purchased from Sigma Aldrich, Baker, EMD, Fisher, or Acros Organics and used as received unless otherwise specified. Cbz-Asp-OBn, Cbz-Glu-OBn, and Fmoc-Lys-OH were purchased from Chem-Impex. 2-(6-chloro-1H-benzotriazole-1-yl)-1,1,3,3-tetramethylaminium hexafluorophosphate (HCTU), (benzotriazol-1-yloxy)tripyrrolidinophosphonium hexafluorophosphate (PyBOP), Nova-Peg Rink Amide Resin, 9-fluorenylmethoxycarbonyl-N-hydroxysuccinamide and Fmoc-protected  $\alpha$ -amino acids were purchased from NovaBiochem. Flash column chromatography was performed using SorbTech (60 Å, 40-63  $\mu$ m) silica gel. NMR spectra were recorded on a Bruker Avance-400 spectrometer. MALDI-TOF mass spectrometry was performed on a Voyager DE Pro instrument. Circular dichroism spectra were recorded on an Olis DSM17 Circular Dichroism Spectrometer using quartz cuvettes of 0.1 cm path length. Preparative and analytical HPLC were performed with Phenomenex Luna C<sub>18</sub> columns.

### A.6.2. Monomer Synthesis

Fmoc-protected aminoxy-functionalized residue **12a** and serine-acylated residue **16b** were synthesized as described in section 2.4.2. Fmoc-L-azidolysine was synthesized by a previously reported procedure.<sup>130</sup>



**Scheme A.2.** Synthesis of Fmoc-L-azidolysine (**A7**).



**N-(9-Fluorenylmethoxycarbonyl)-2-(S)-amino-6-azidohexanoic acid (Fmoc-Lys(N<sub>3</sub>)-OH; A7):**<sup>130</sup> Sodium azide (5.75 g, 88.6 mmol, 5.0 equiv) was dissolved in 15 mL water

and cooled to 0 °C under nitrogen. Trifluoromethanesulfonic anhydride (5.0 g, 17.7 mmol, 1.0 equiv) was dissolved in 12 mL dichloromethane and added to the reaction vessel dropwise.

The resulting mixture was stirred for 2 hours under nitrogen at 0 °C. Following this time the reaction mixture was poured into a separatory funnel and the organic layer separated. The aqueous layer was extracted twice with 8 mL dichloromethane, the organic layers combined, and washed once with 10 mL saturated aqueous Na<sub>2</sub>CO<sub>3</sub>. The organic layer containing trifluoromethanesulfonyl azide (**A5**) was used directly in the next step without concentration or further purification. Trifluoromethanesulfonyl azide is explosive and should not be isolated. Following preparation of compound **A5**, Fmoc-Lys-OH (3.26 g, 8.86 mmol, 1.0 equiv), CuSO<sub>4</sub>•5H<sub>2</sub>O (22.1 mg, 0.089 mmol, 0.01 equiv) and K<sub>2</sub>CO<sub>3</sub> (2.57 g, 18.61 mmol, 2.1 equiv) were suspended in 80 mL anhydrous methanol under nitrogen. Water (10 mL) was added to aid dissolution. The dichloromethane containing trifluoromethanesulfonyl azide from the previous step

(assumed to be 17.72 mmol, 2.0 equiv) was added slowly to the reaction vessel. The reaction was stirred overnight at room temperature, then concentrated by rotary evaporation. The resulting aqueous solution was diluted with 30 mL 5% w/v NaHCO<sub>3</sub> and extracted twice with 50 mL ethyl acetate. The aqueous layer was then acidified to pH 1 with 1 M HCl and extracted four times with 40 mL ethyl acetate. The organic layers were combined and washed with 40 mL brine, then dried over anhydrous magnesium sulfate and concentrated. The resulting oil was purified by flash column chromatography (50%→100% ethyl acetate in hexanes) to afford product **A7** as a viscous yellow oil (4.16 mmol, 46%). Spectra agreed with previously reported data.<sup>130</sup>

### **A.6.3. Peptide Synthesis And Cyclization**

Peptides **A1-A4** and cyclized products **A2Cyc**, **A3Cyc**, and **A4Cyc** were synthesized on NovaPEG Rink Amide Resin with microwave heating (MARS microwave reactor, CEM). Amino acid couplings were performed with 5.0 equiv of amino acid to resin. Natural  $\alpha$ -amino acids were preactivated with HCTU (5.0 equiv to resin) and DIEA (7.5 equiv to resin) for in NMP for 2-3 minutes. Unnatural residues Fmoc-D-propargylglycine, Fmoc-L-azidolysine, serine-acylated monomer **16a** and aminoxy-functionalized monomer **12b** were preactivated with PyBOP (5.0 equiv to resin) and DIEA (7.5 equiv to resin). The preactivated amino acid was then added to the resin in a reaction vessel equipped with a stir bar, and a microwave program consisting of a 2 minute ramp to 70 °C followed by a 4 minute hold at 70 °C was run. Following the coupling program, the resin was washed three times with DMF. After washing, the resin was treated with 20% 4-methylpiperidine in DMF with a microwave deprotection program consisting of a 2 minute ramp to 80 °C followed by a 2 minute hold at 80 °C. Following Fmoc deprotection, the resin was washed with DMF, and the couple-wash-deprotect cycle repeated until the desired peptide chain was obtained on resin. Subsequent N-terminal deprotection and cleavage using 92.5% trifluoroacetic acid, 3% water, 3% ethanedithiol, and 1.5% triisopropylsilane afforded crude peptides **A1-A4**.

Peptide **A2Cyc** was prepared by on-resin cyclization procedures.<sup>44</sup> Following assembly of the desired peptide chain on resin, but prior to N-terminal Fmoc deprotection, the resin was washed five times with dichloromethane. Following this washing procedure, the resin was subjected to treatment with 3% trifluoroacetic acid and 5% triisopropylsilane in dichloromethane for five minutes. This treatment with dilute trifluoroacetic acid is preceded for the removal of the 4-methyltrityl (Mtt) protecting group on lysine and the phenylisopropyl ester (OPip) protecting group on aspartic acid.<sup>44</sup> The deprotection and washing procedure was repeated three times total to achieve deprotection of the desired residues. Following side chain deprotection, the resin was washed three times with DMF, then subjected to treatment with PyBOP (1 equiv to resin) and DIEA (1.5 equiv to resin) under the microwave coupling program described above. This procedure was repeated twice to form the desired lactam cross-link between Asp<sub>27</sub> and Lys<sub>31</sub>. Following on-resin cyclization, the N-terminus was deprotected under the standard microwave deprotection procedure and the peptide cleaved and purified under identical conditions to those used for the linear peptides **A1-A4**.

Following cleavage of peptides **A1-A4** and **A3Cyc** from resin, the crude peptide was precipitated in cold diethyl ether and centrifuged. The ether was decanted and the resulting crude material was dissolved in 0.1% TFA in water and 0.1% TFA in acetonitrile and sonicated for 30-40 minutes prior to purification. Purification by HPLC was performed in a Luna C18 preparative column using gradients between 0.1% TFA in water and 0.1% TFA in acetonitrile. Identities of the purified peptides were confirmed by MALDI-TOF MS. All peptides used in subsequent biophysical characterization or cyclization were judged to be  $\geq 95\%$  pure by analytical HPLC.

Cyclized product **A3Cyc** was prepared from peptide **A3** by copper(I)-mediated azide-alkyne cycloaddition in solution. Pure, lyophilized **A3** and CuSO<sub>4</sub>•5H<sub>2</sub>O (4.4 equiv) were dissolved in 2:1 v:v water:*tert*-butanol to give a final peptide concentration of 1 mg/mL. Sodium L-ascorbate (4.4 equiv) dissolved in water was added in 4 portions over the course of 1 hour. The reaction was placed on a shaker

at room temperature for 2 hours following completion of sodium ascorbate addition. The reaction was then purified by preparative HPLC.

Cyclized product **A4Cyc** was prepared from peptide **A4** by treatment with aqueous sodium periodate. Pure lyophilized **A4** was dissolved in water and its concentration determined by UV-Vis spectroscopy ( $\epsilon_{280} = 5690 \text{ M}^{-1} \text{ cm}^{-1}$  based on Trp absorbance).<sup>102</sup> A stock of sodium periodate prepared in water and the concentration of periodate determined by UV-Vis spectroscopy ( $\epsilon_{280} = 317 \text{ M}^{-1} \text{ cm}^{-1}$ ).<sup>103</sup> Oxidation and cross-linking was performed by dilution of the peptide stock with water, buffer, and periodate to a final concentration of 100  $\mu\text{M}$  peptide in 100 mM phosphate buffer with 1 equiv (100  $\mu\text{M}$ ) sodium periodate in a total volume of 2 mL. The reaction was allowed to rest for 15 minutes, then product **A4Cyc** was purified by preparative HPLC. The above procedure was repeated to obtain sufficient purified **A4Cyc** for subsequent biophysical characterization.

**Table A2.** MALDI-TOF data for peptides **A2-A4**, **A2Cyc**, **A3Cyc**, and **A4Cyc**.

Peptide	$[\text{M}+\text{H}]^+$ ( $m/z$ )	
	Calculated	Observed
<b>A1</b>	4151.3	4151.1
<b>A2</b>	4138.2	4138.0
<b>A2Cyc</b>	4120.2	4120.3
<b>A3</b>	4144.2	4144.1
<b>A3Cyc</b>	4144.2	4144.3
<b>A4</b>	4212.3	4212.3
<b>A4Cyc</b>	4163.2	4163.0

#### **A.6.4. Circular Dichroism Spectroscopy And Data Analysis**

Stock solutions of peptides **A1-A4**, **A2Cyc**, **A3Cyc**, and **A4Cyc** were prepared in water and the concentration of peptide determined by UV-Vis spectroscopy based on Trp absorbance ( $\epsilon_{280} = 5690 \text{ M}^{-1} \text{ cm}^{-1}$ ).<sup>102</sup> Samples for CD spectroscopy were prepared by dilution of the peptide stock with water and

buffer to yield samples consisting of 50  $\mu\text{M}$  peptide in 50 mM phosphate buffer, pH 7. Additional samples containing varying concentrations of guanidinium hydrochloride were prepared identically excepting addition of guanidinium hydrochloride from an 8 M aqueous stock solution. CD scans were performed from 200-260 nm with 1 nm step size, 2 nm bandwidth, and 5 second integration times. CD melts were performed by monitoring molar ellipticity at 222 nm over the range of 2  $^{\circ}\text{C}$  to 95  $^{\circ}\text{C}$  in 3  $^{\circ}\text{C}$  increments, a dead band of 0.5  $^{\circ}\text{C}$  and a 2 minute equilibration time at each temperature. All measurements were baseline corrected for buffer. Circular dichroism scans were smoothed by the Savitsky-Golay method as implemented in GraphPad Prism. Thermal melts of samples lacking guanidinium hydrochloride were processed using GraphPad prism and fit to a two-state thermal denaturation model.<sup>104</sup>

Raw data from thermal-chemical denaturation experiments were fit using Mathematica 8 (Wolfram) and equations reported previously<sup>119</sup> and summarized below. The protein folding free energy ( $\Delta G$ ) at a given temperature ( $T$ ) and concentration of guanidinium ( $[Gdm]$ ) is given by the modified Gibbs-Helmholtz equation (8):

**Equation 8**

$$\Delta G = \Delta H^{\circ} - T\Delta S^{\circ} + \Delta C_p \times (T - T^{\circ} + T \times \ln(\frac{T}{T^{\circ}})) - m \times [Gdm]$$

In the above equation,  $\Delta H^{\circ}$  and  $\Delta S^{\circ}$  are the folding enthalpy and entropy at a reference temperature,  $T^{\circ}$  (293 K).  $\Delta C_p$  is the change in heat capacity and  $m$  is the dependence of folding free energy on denaturant concentration,  $[Gdm]$ . The observed ellipticity at 222 nm ( $\theta_{obs}$ ) at a particular temperature,  $T$ , and  $[Gdm]$  is given by equation 9:

**Equation 9**

$$\theta_{obs} = \frac{(\theta_n + \theta_u \times \exp(\frac{-\Delta G^{\circ}}{RT}))}{(1 + \exp(\frac{-\Delta G^{\circ}}{RT}))}$$

In the above equation,  $\theta_n$  and  $\theta_u$  are the ellipticity of the folded and unfolded states, respectively. Based on literature precedent<sup>119</sup> and inspection of the thermal-chemical denaturation data,  $\theta_n$  was assumed to vary linearly with  $T$ . The ellipticity of the folded protein as a function of  $T$  and  $[Gdm]$  is given by equation 10:

**Equation 10**

$$\theta_n(T, [Gdm]) = a + b \times T + c \times [Gdm]$$

The ellipticity of the unfolded state,  $\theta_u$ , showed curvature in ellipticity as a function of temperature and therefore the quadratic term  $f \times T^2$  was added to equation 11.

**Equation 11**

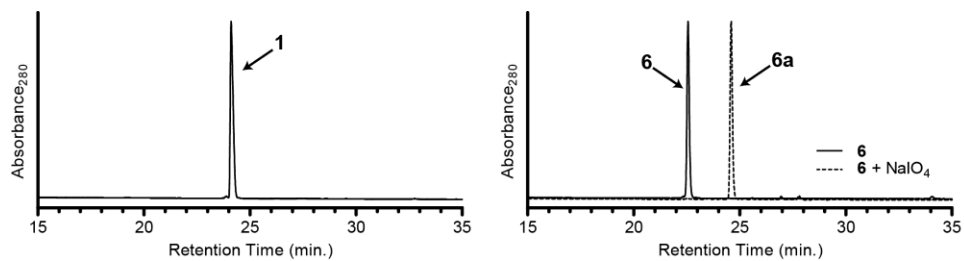
$$\theta_u(T, [Gdm]) = d + e \times T + f \times T^2 + g \times [Gdm]$$

Combining equations 1-4 provides the equation 12 used to fit the two-dimensional surface (Figures A2, A6):

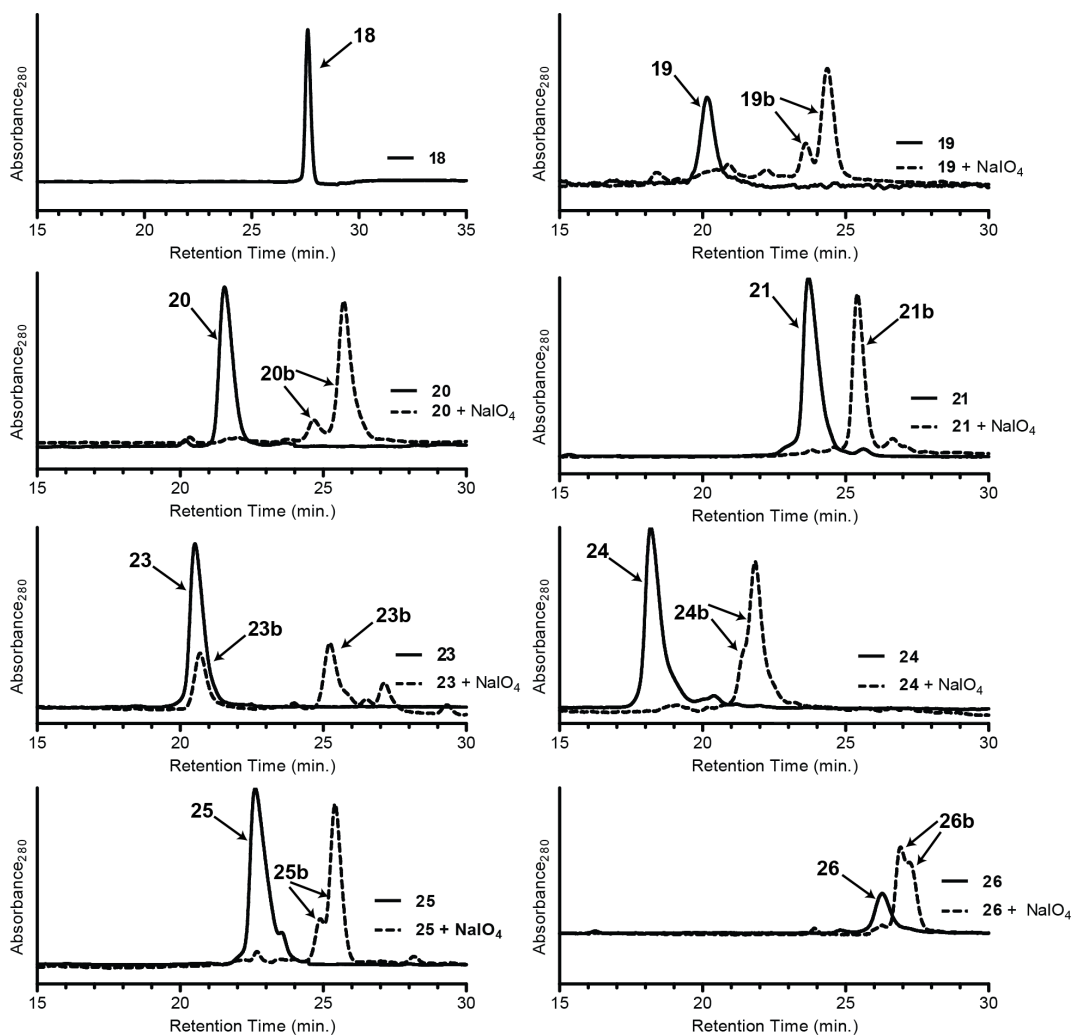
**Equation 12**

$$\theta_{222} = \frac{(\theta_n + \theta_u \times \exp(\frac{-\Delta G^\circ(T, [Gdm])}{RT}))}{(1 + \exp(\frac{-\Delta G^\circ(T, [Gdm])}{RT}))}$$

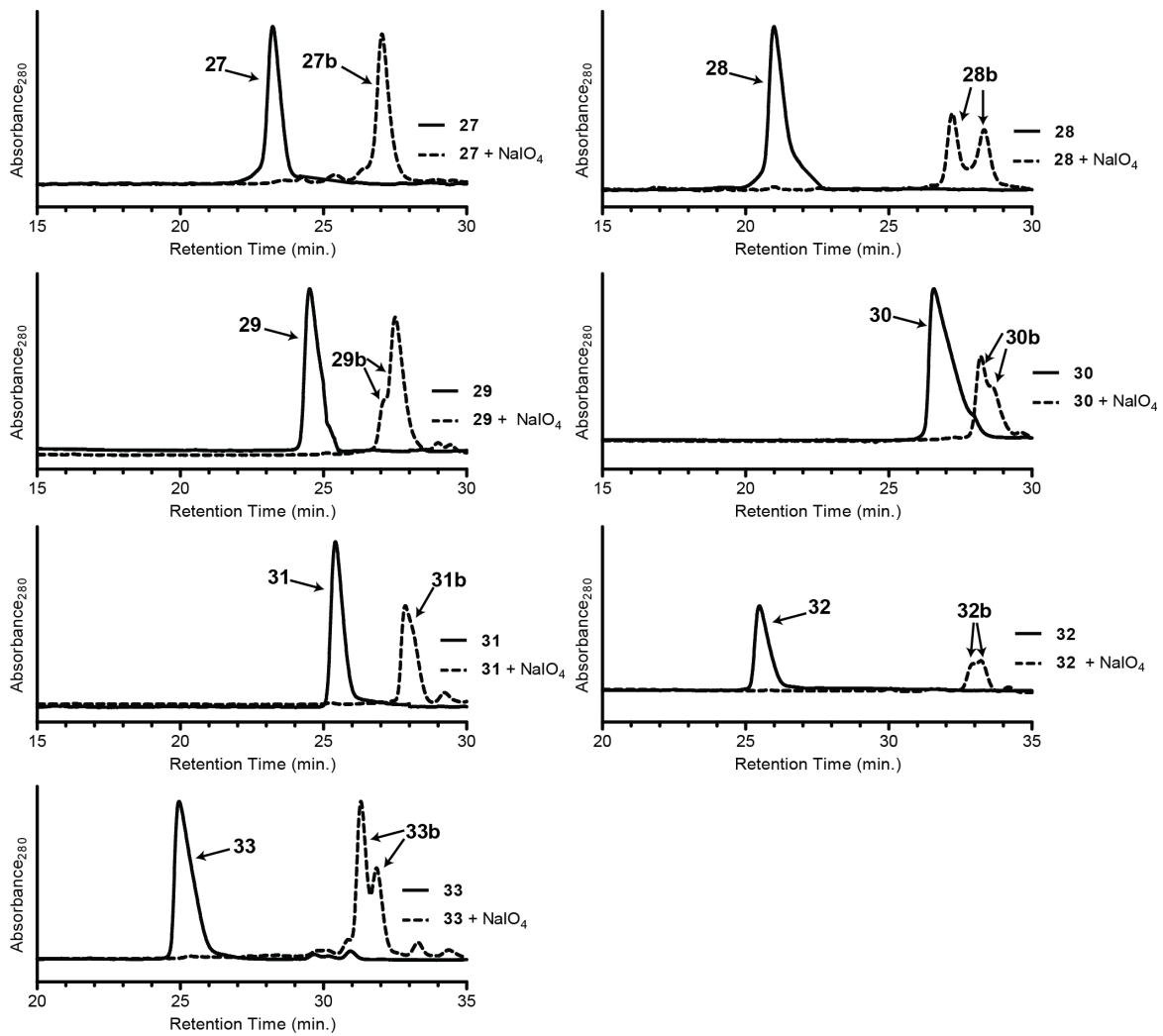
## APPENDIX B. HPLC CHROMATOGRAMS



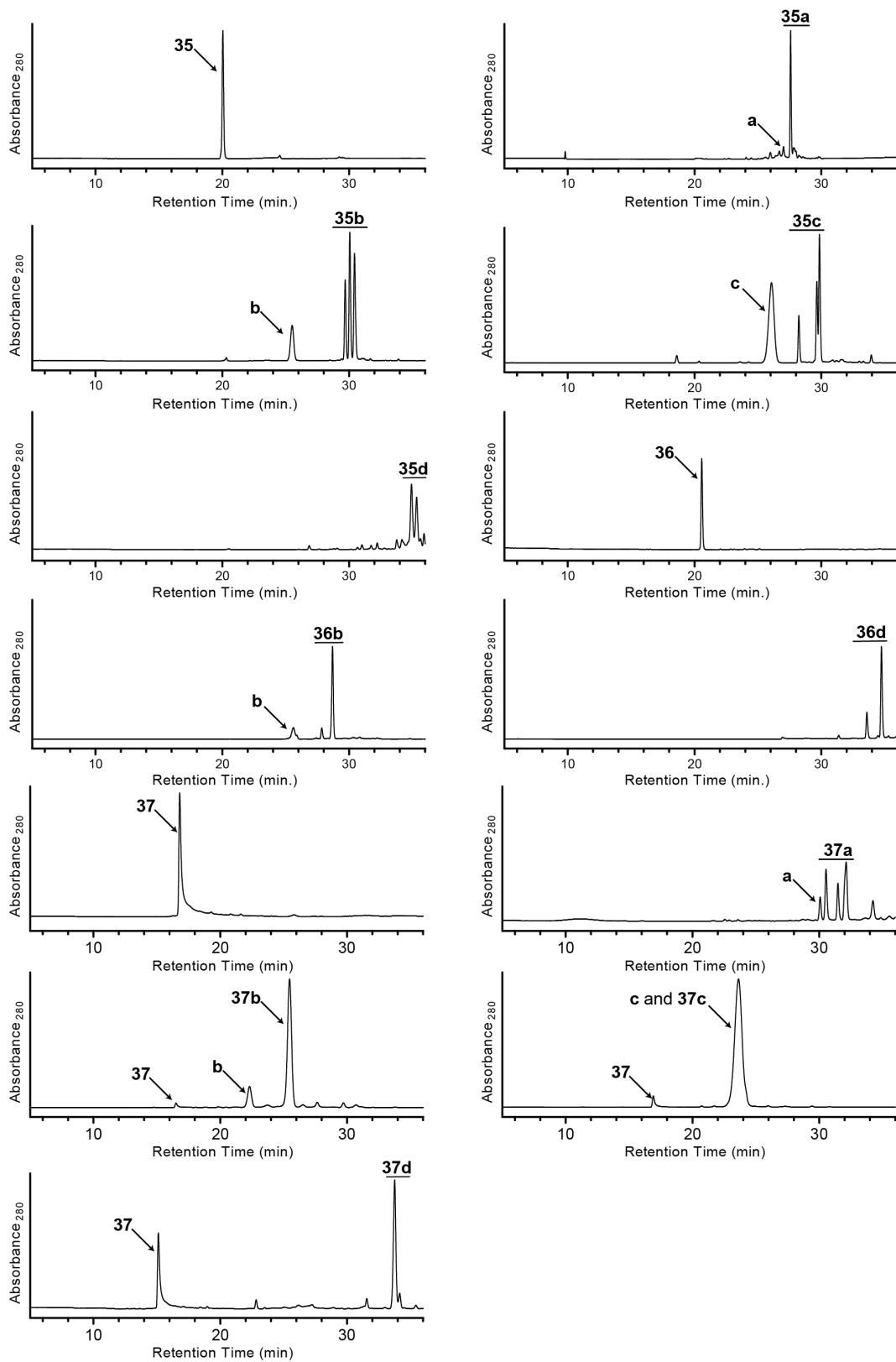
**Figure B1.** Chromatograms of peptides **1**, **6**, and **6a**.



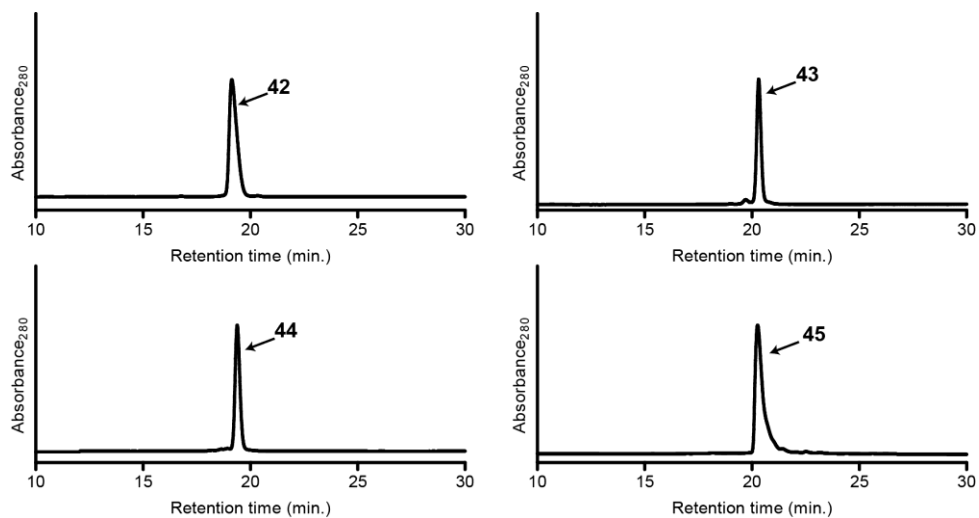
**Figure B2.** Chromatograms of peptides **18-26** before (solid) and after (dashed) addition of  $\text{NaIO}_4$ .



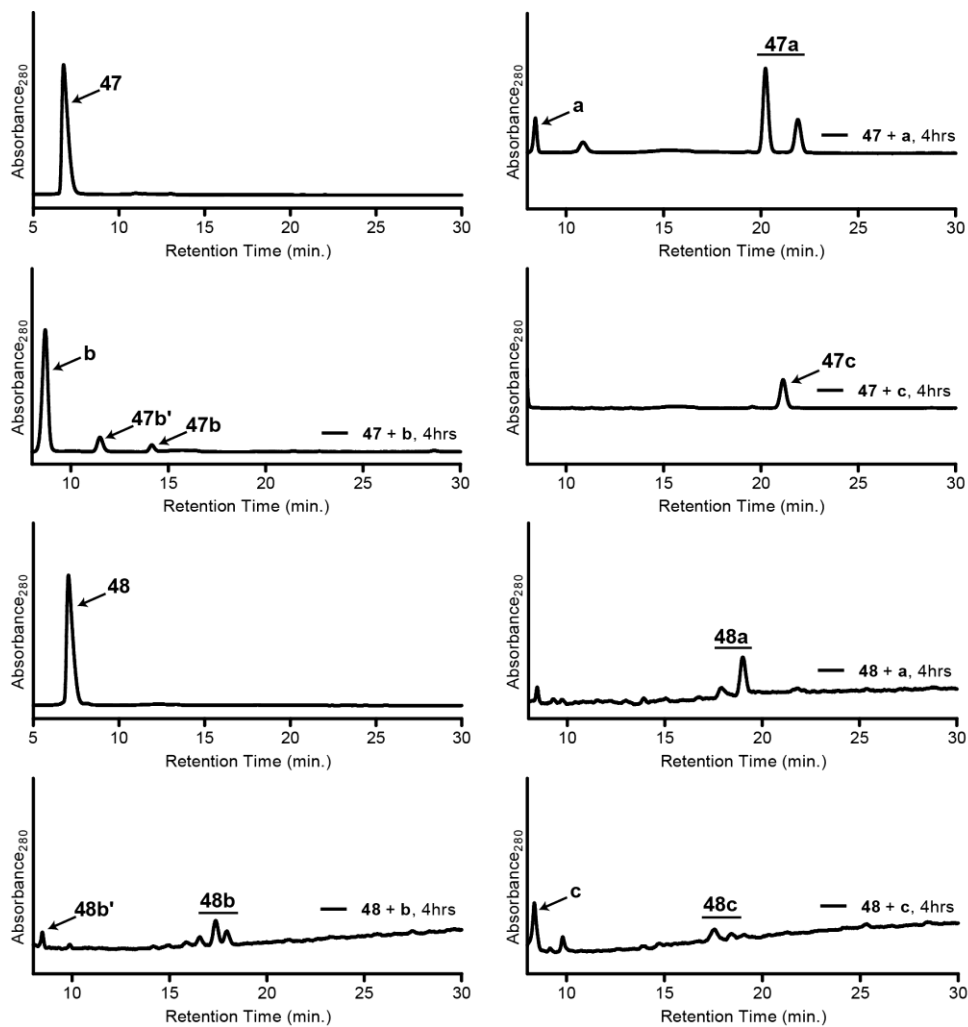
**Figure B3.** Chromatograms of peptides **27-33** before (solid) and after (dashed) addition of  $\text{NaIO}_4$ .



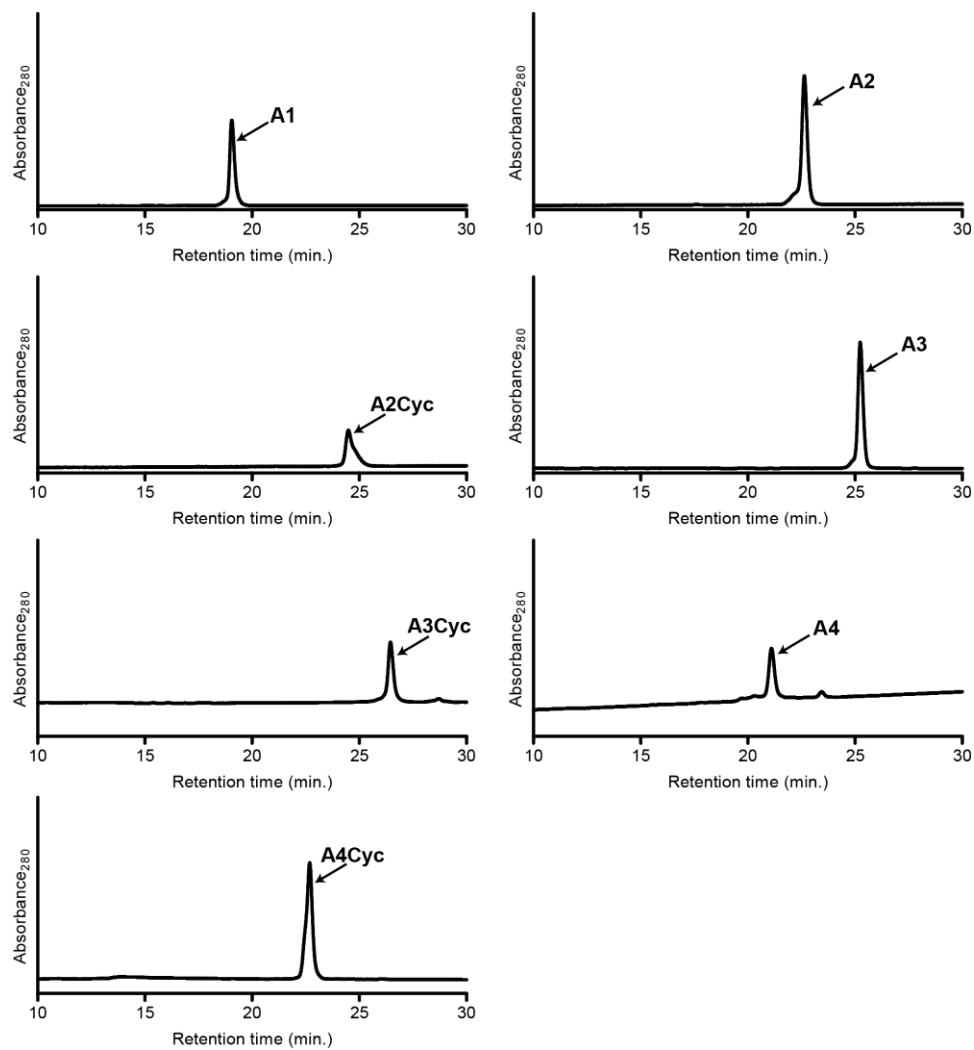
**Figure B4.** Chromatograms of peptides 35-37 and cyclized products.



**Figure B5.** Chromatograms of peptides 42-45.

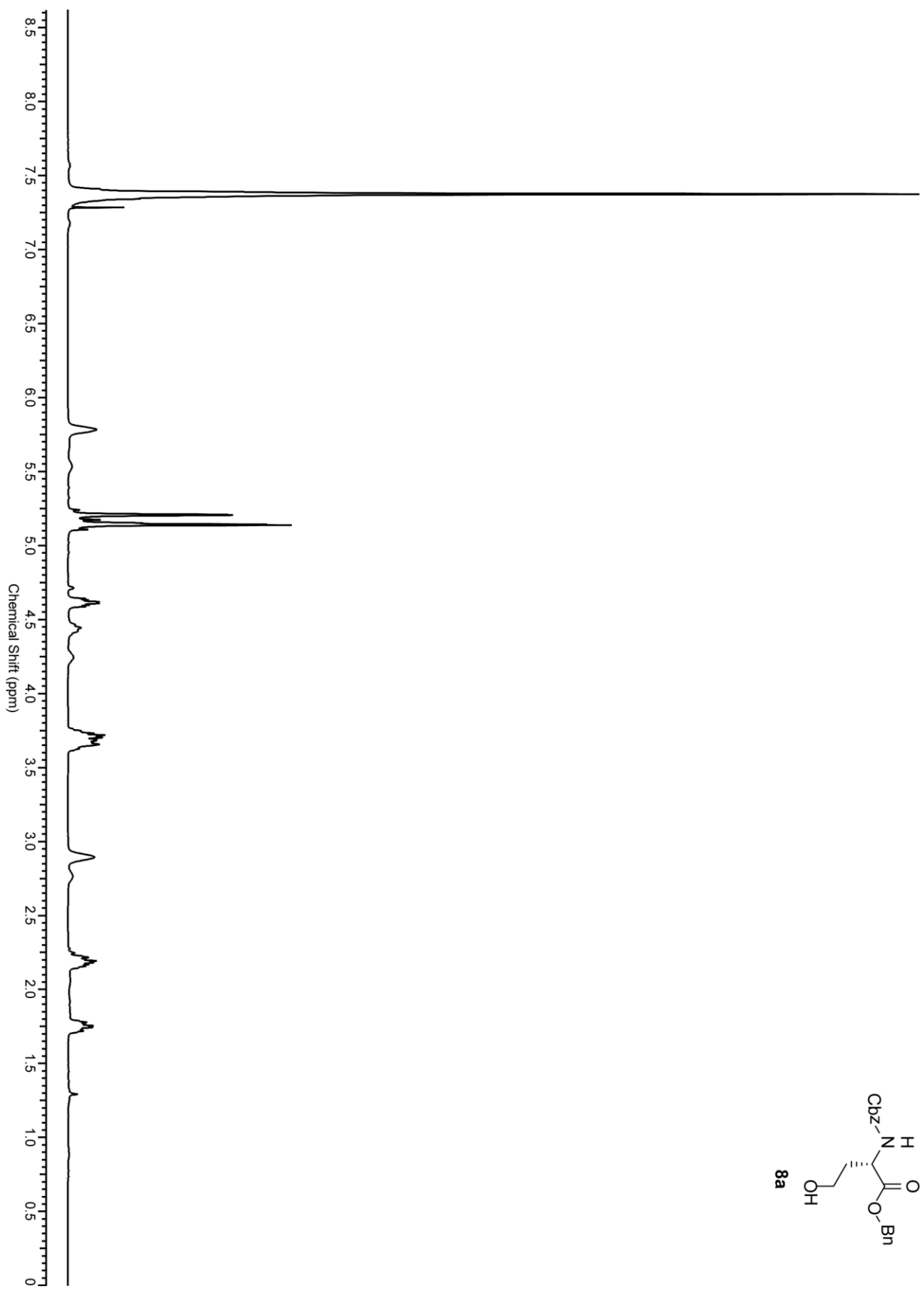
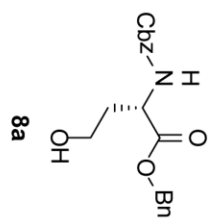


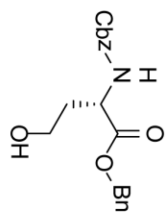
**Figure B6.** Chromatograms of peptides 47-48 and cyclized products.



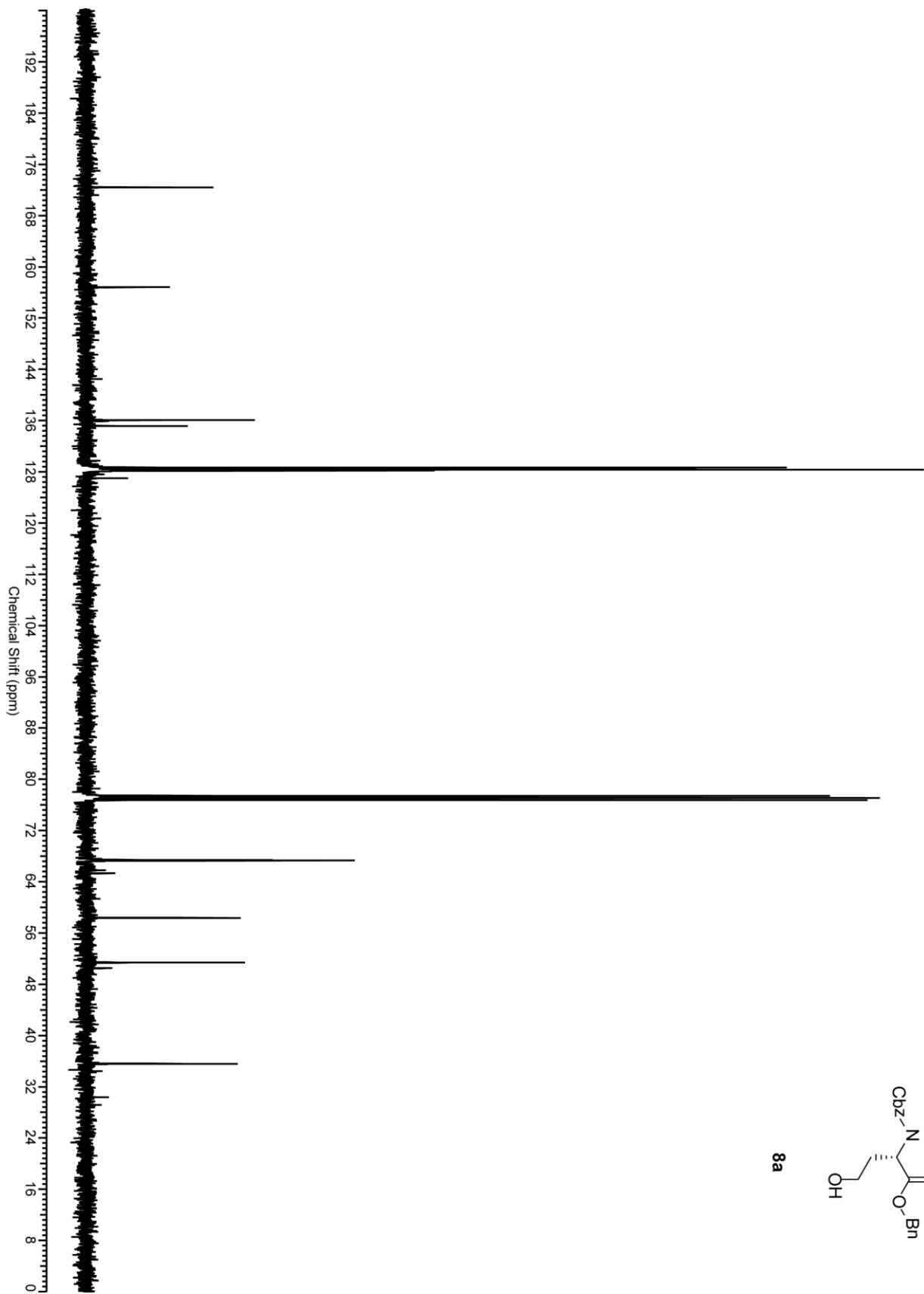
**Figure B7.** Chromatograms of peptides **A1-A4** and cyclic products **A2Cyc**, **A3Cyc**, and **A4Cyc**.

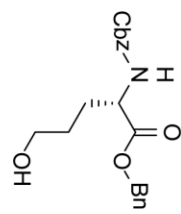
## APPENDIX C. NMR SPECTRA



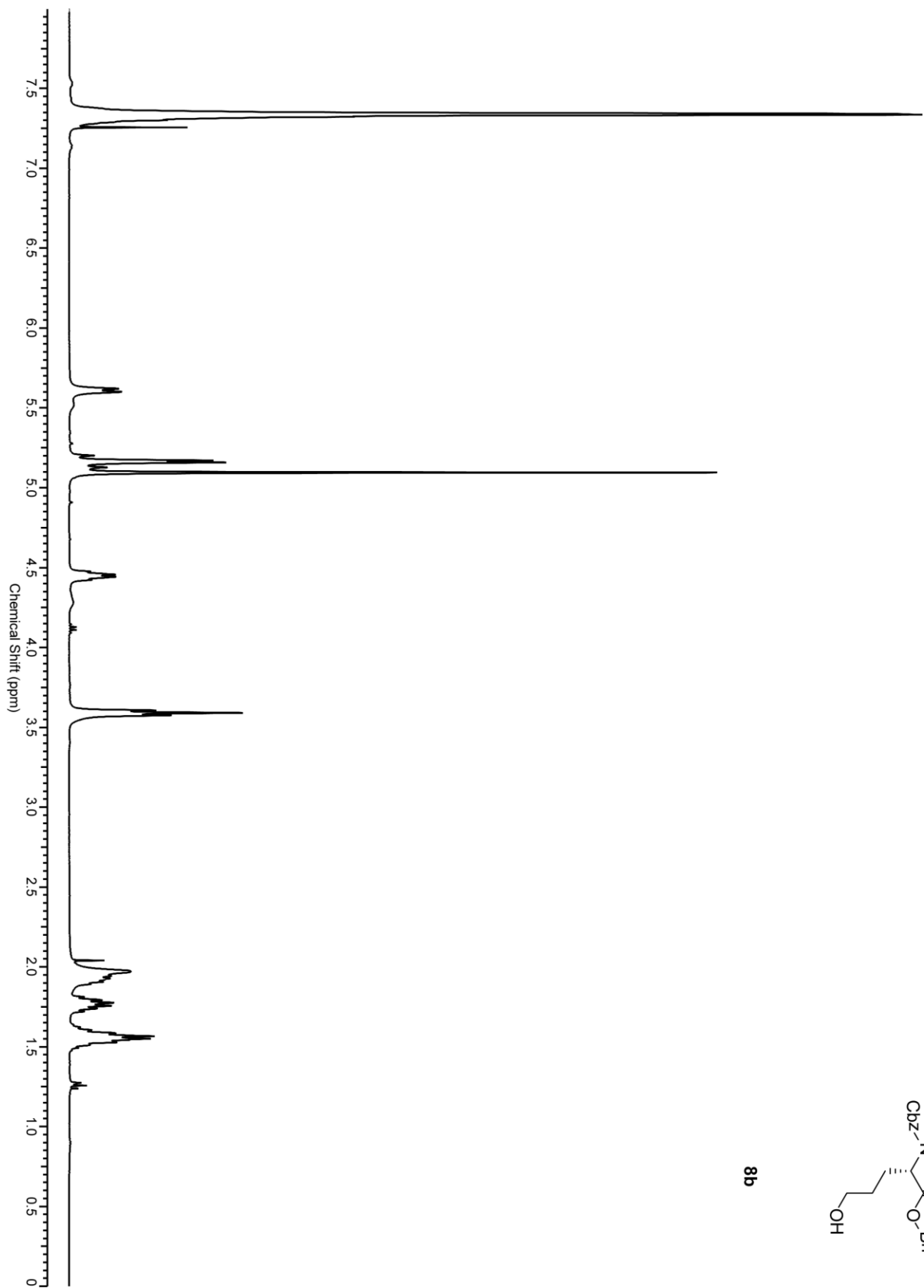


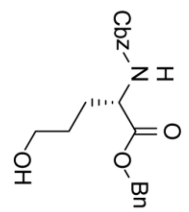
8a



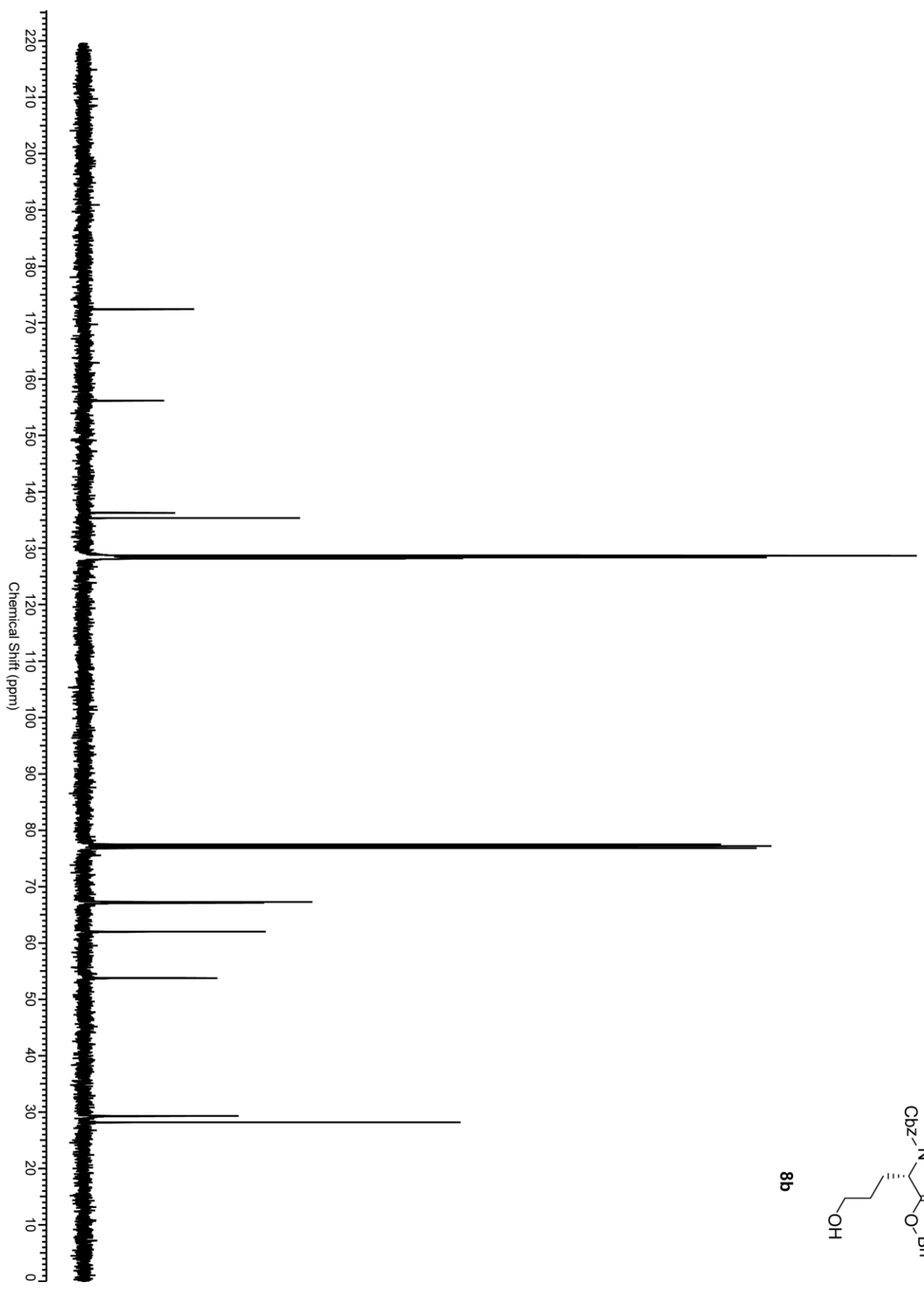


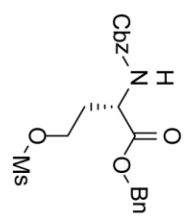
8b



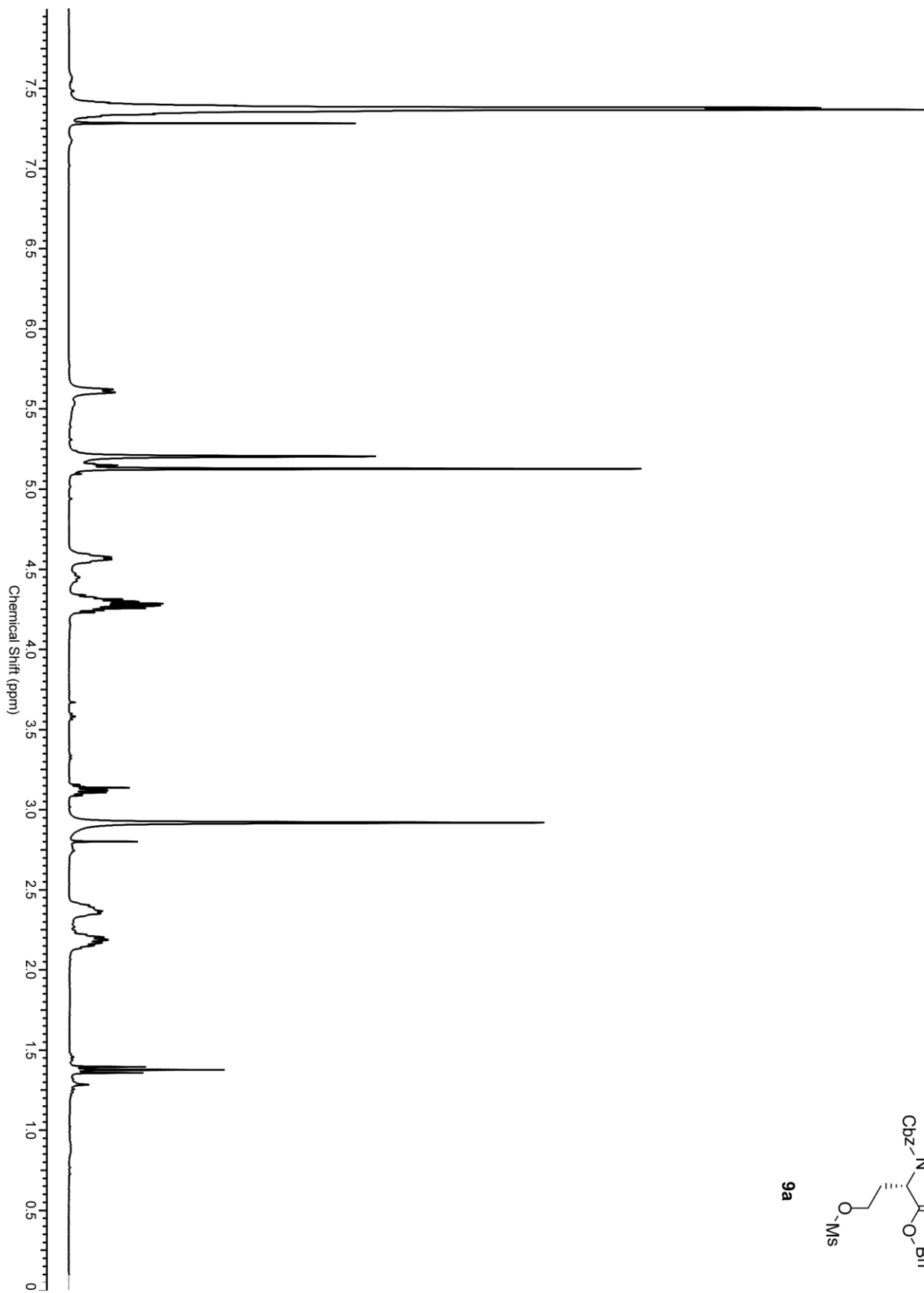


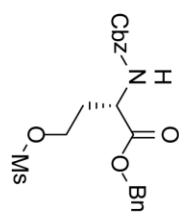
8b



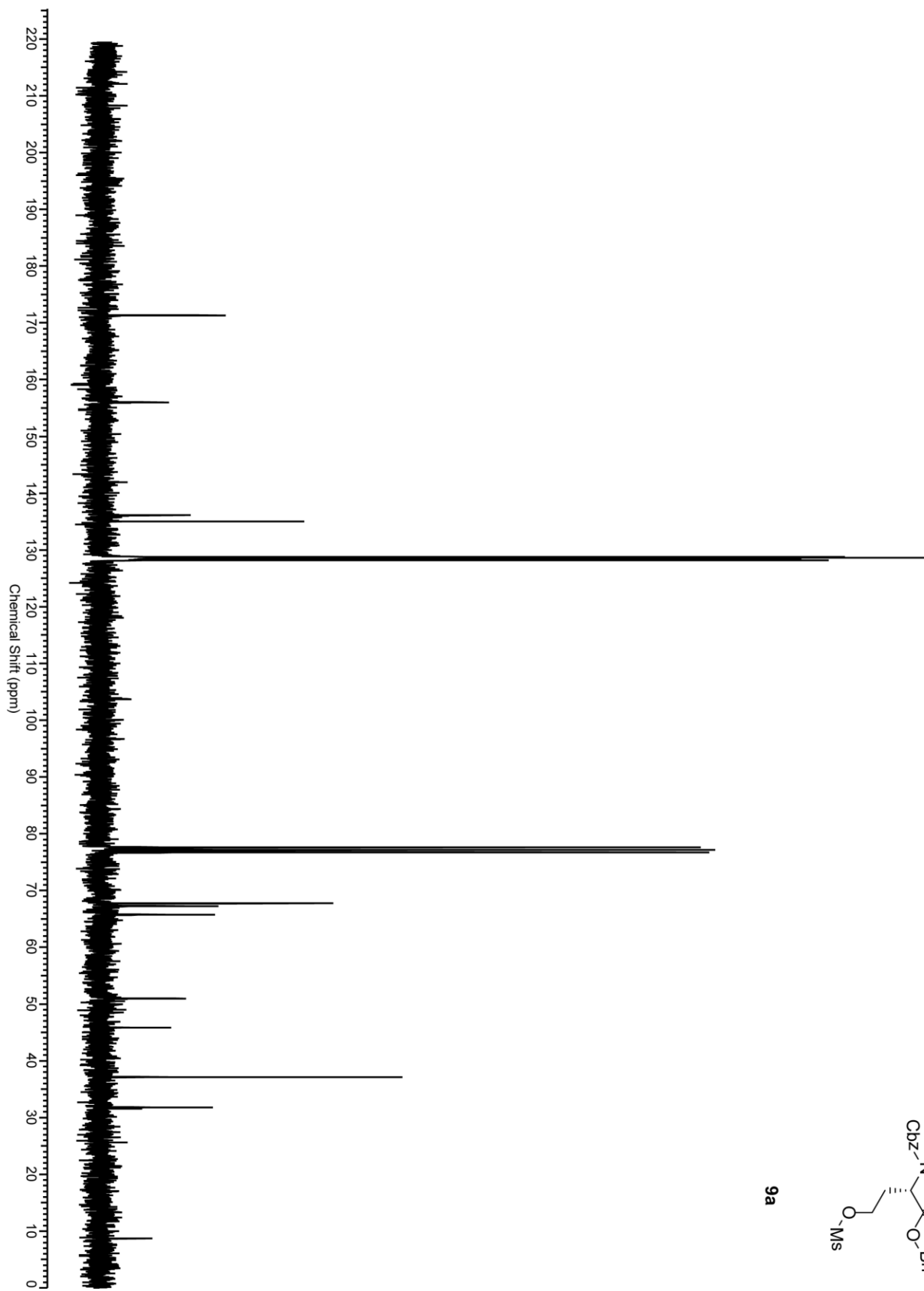


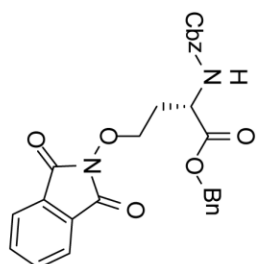
9a



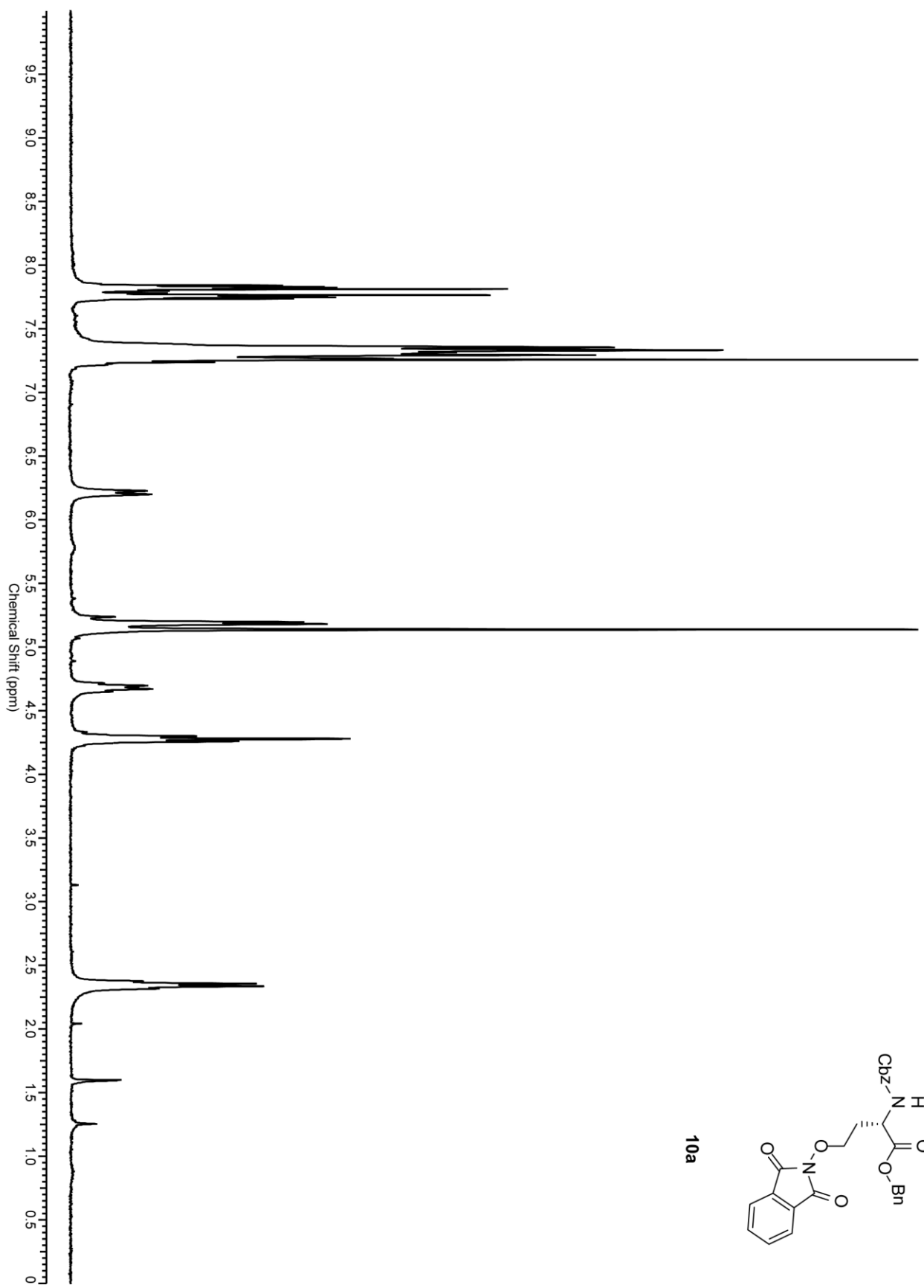


9a

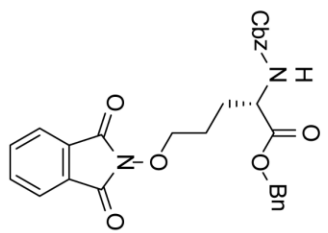




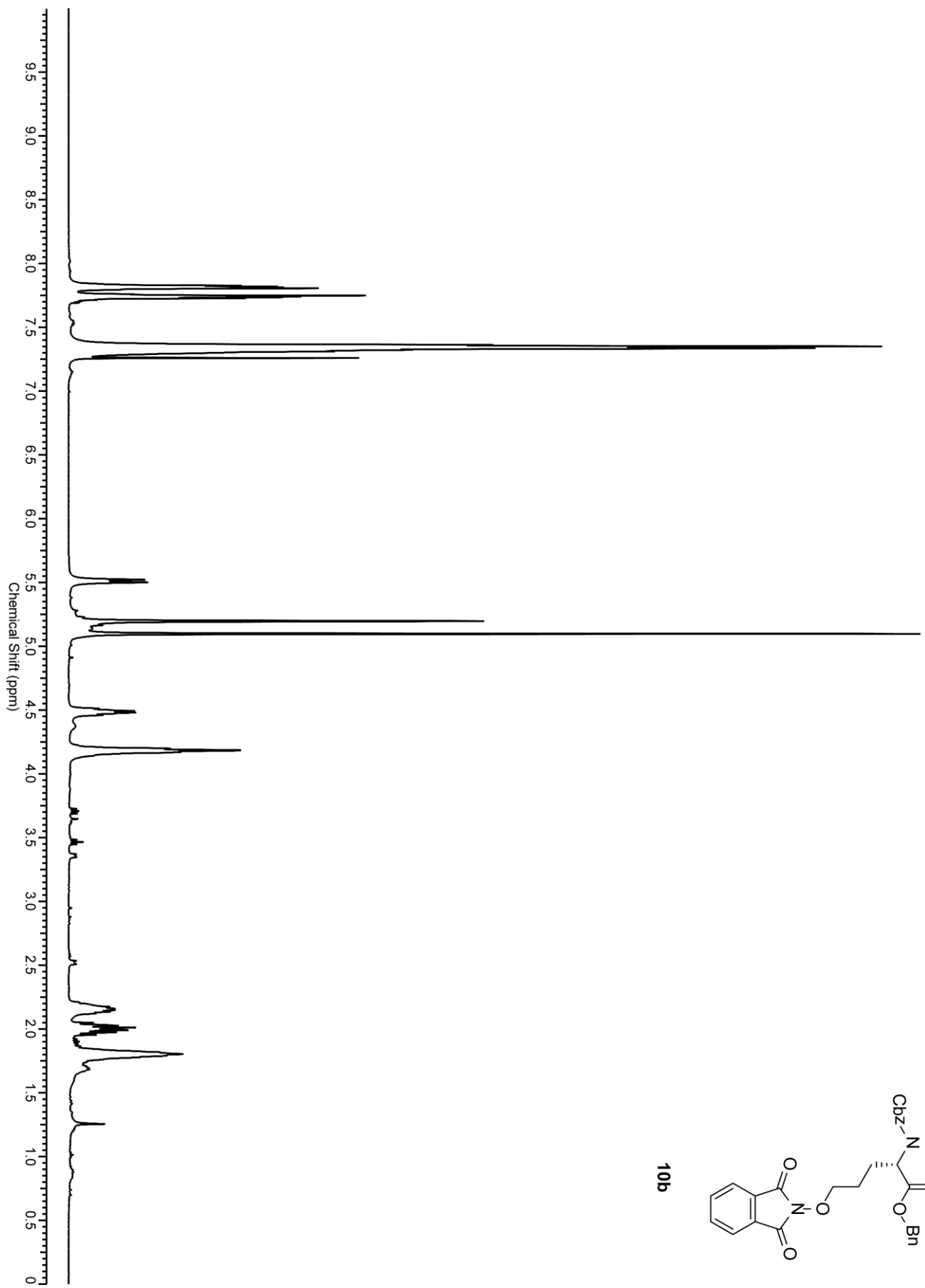
10a

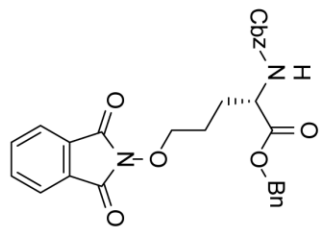




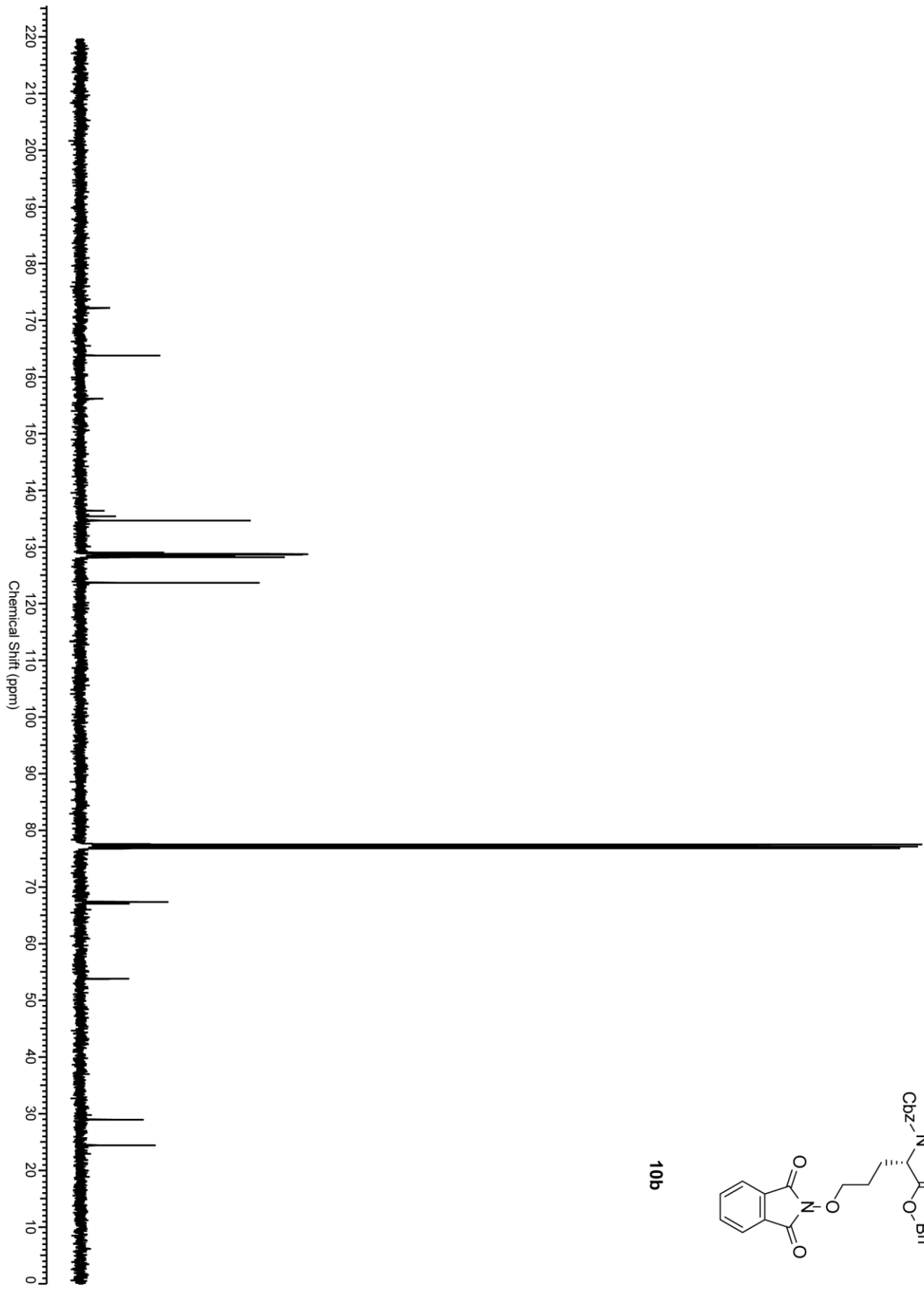


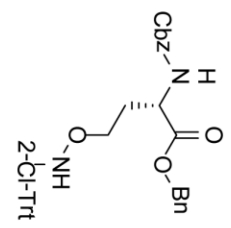
10b



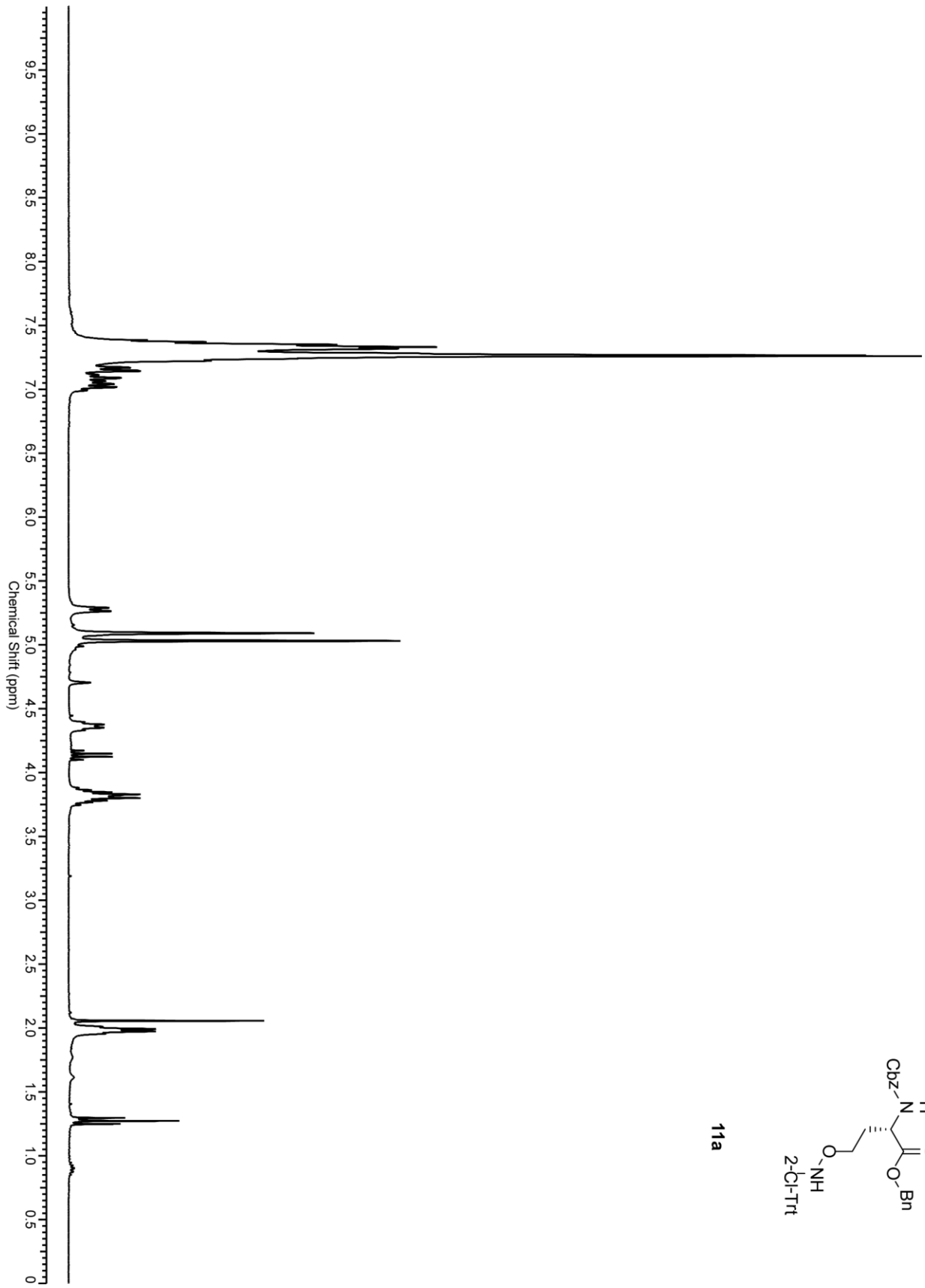


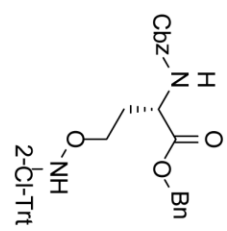
10b



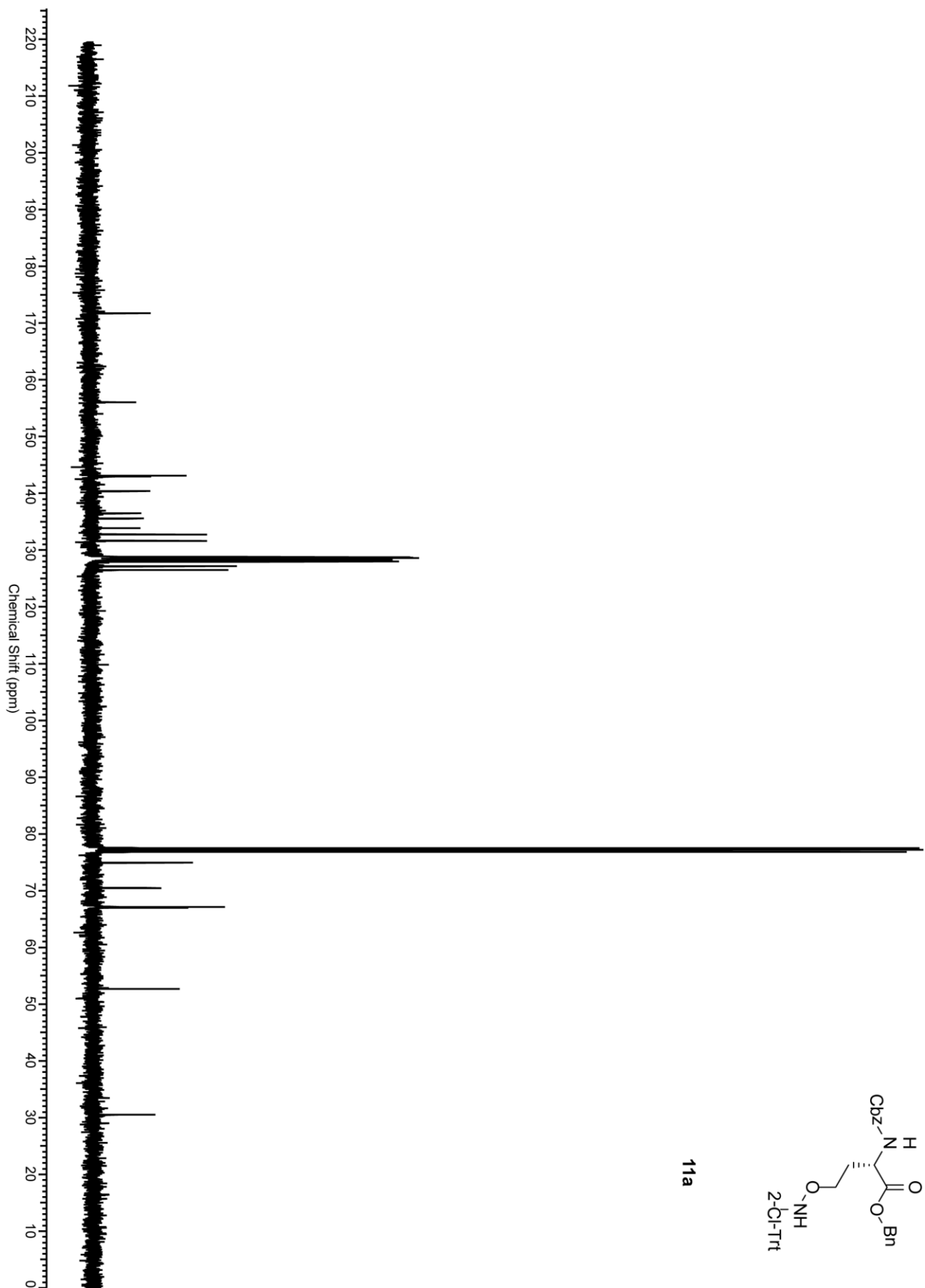


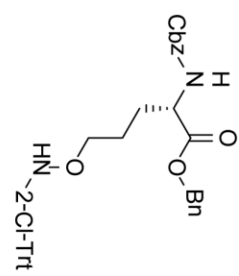
11a



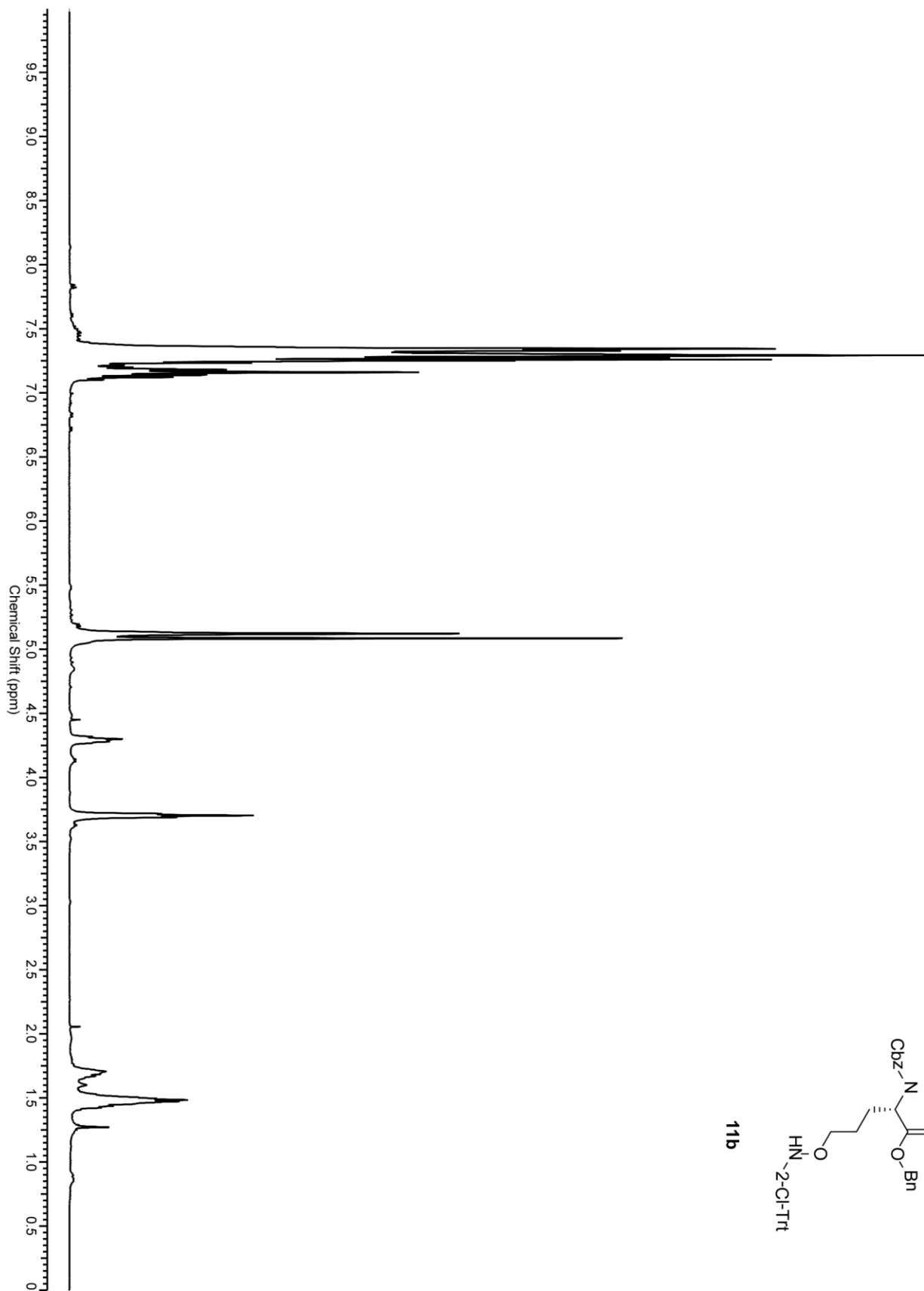


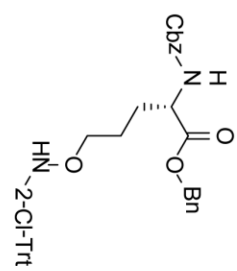
11a



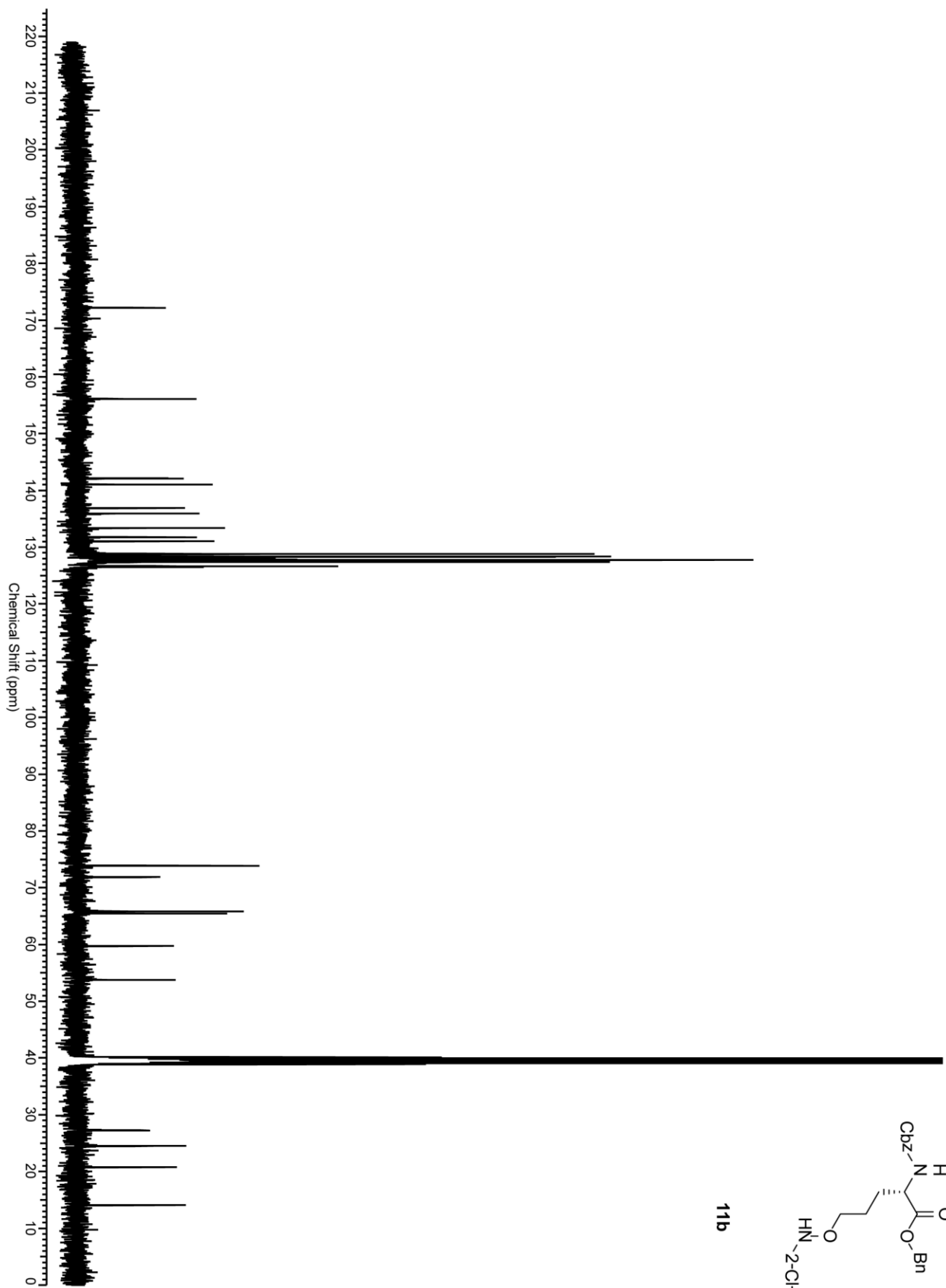


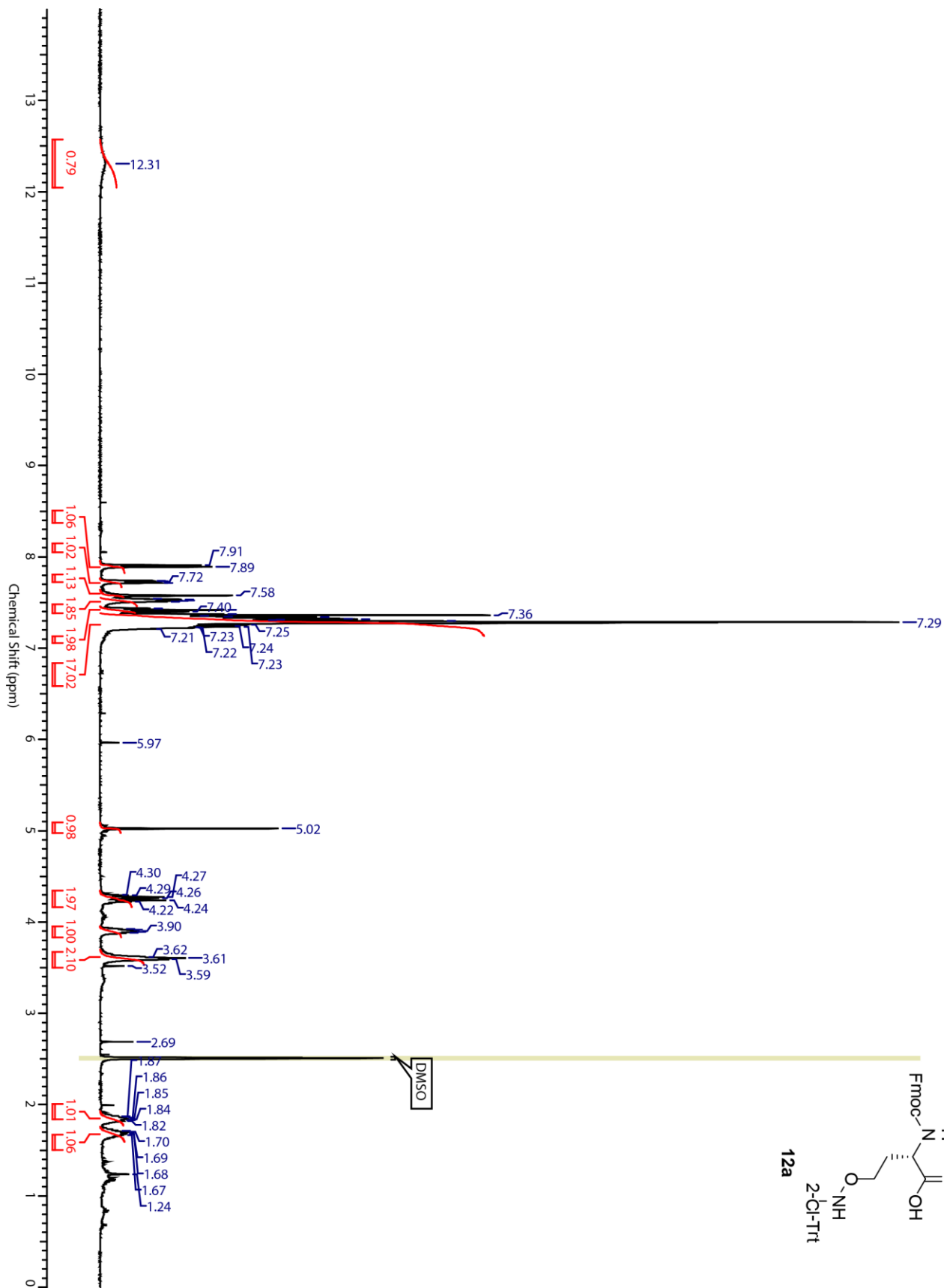
11b

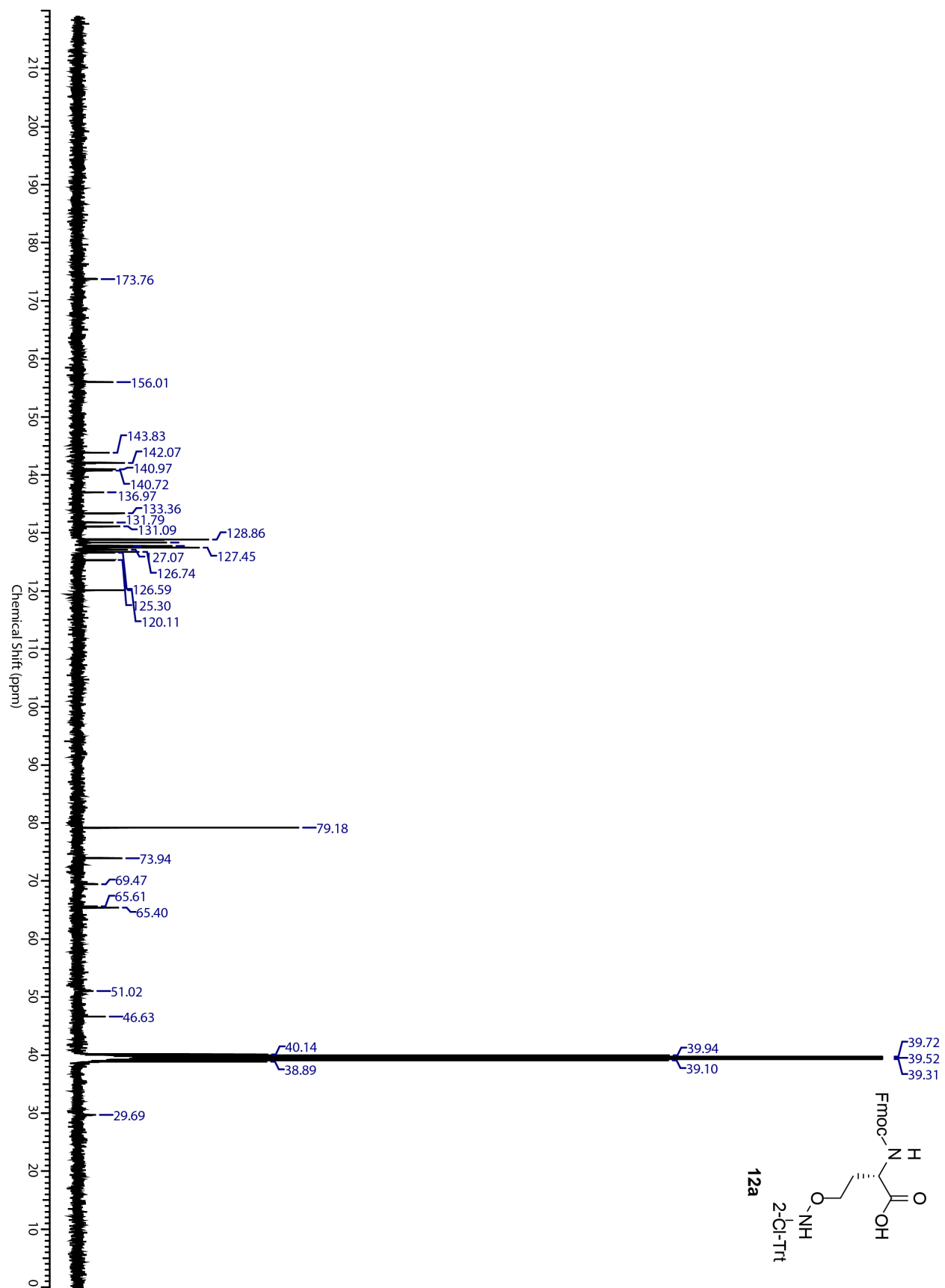


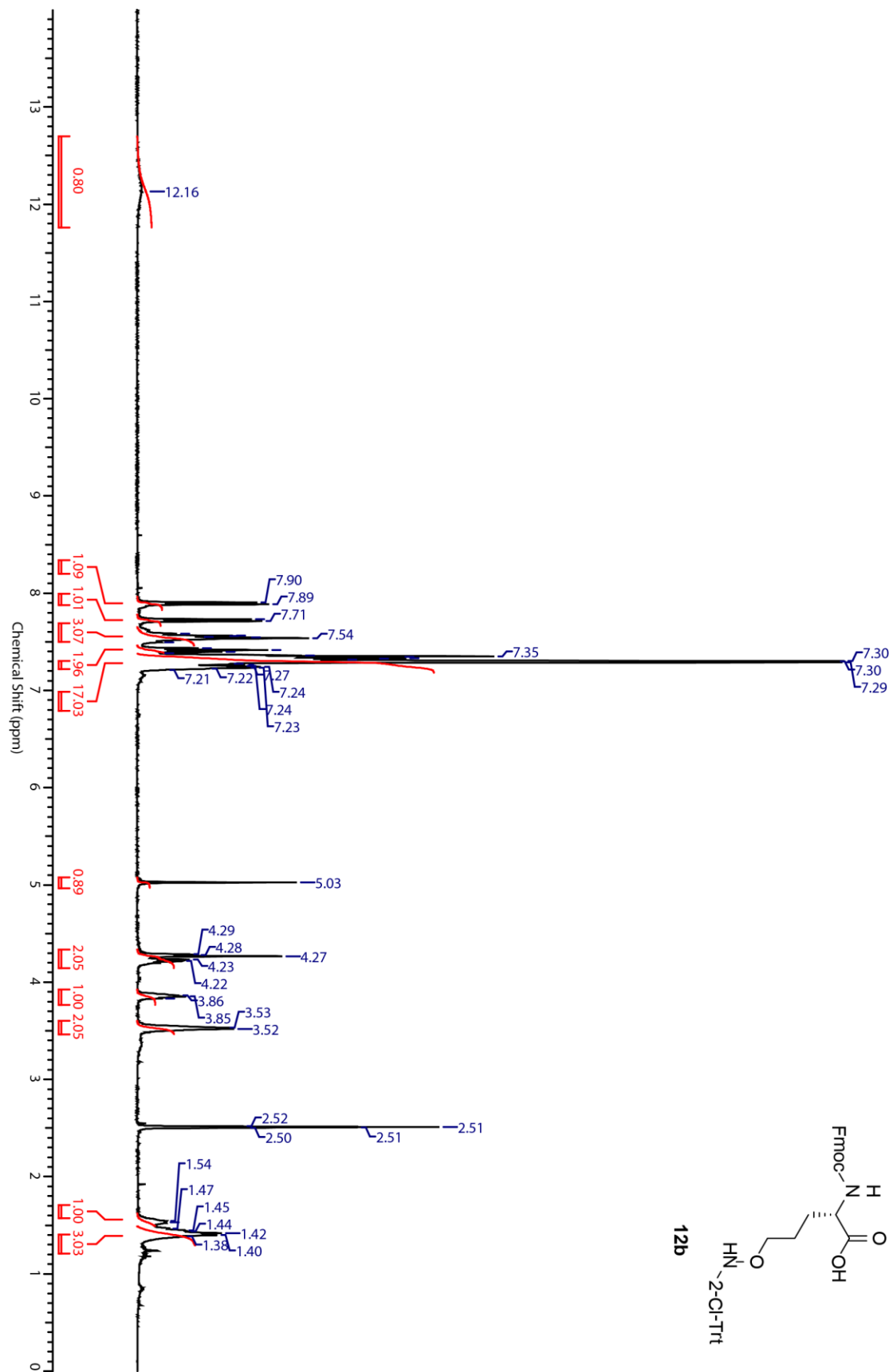


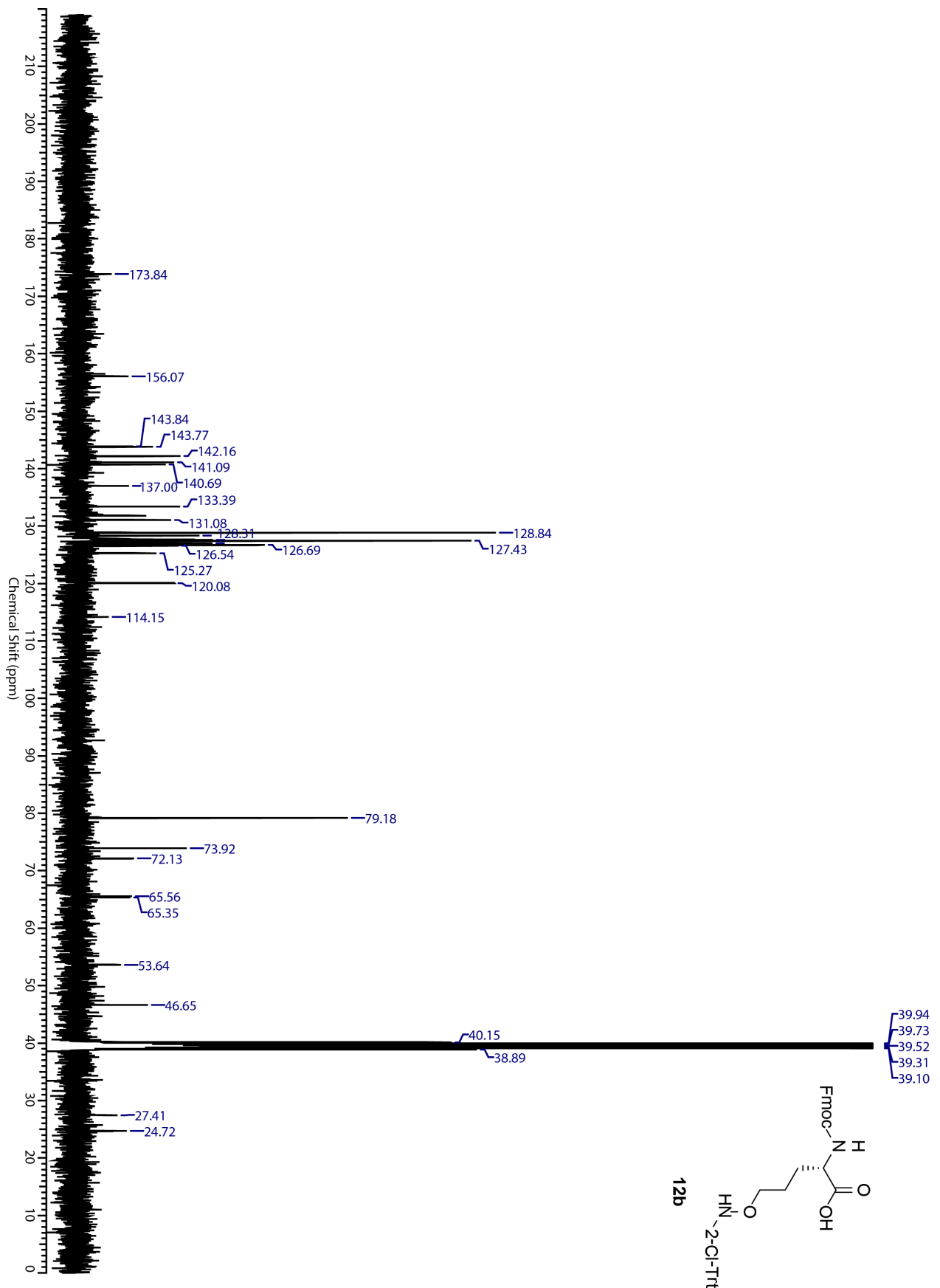
11b

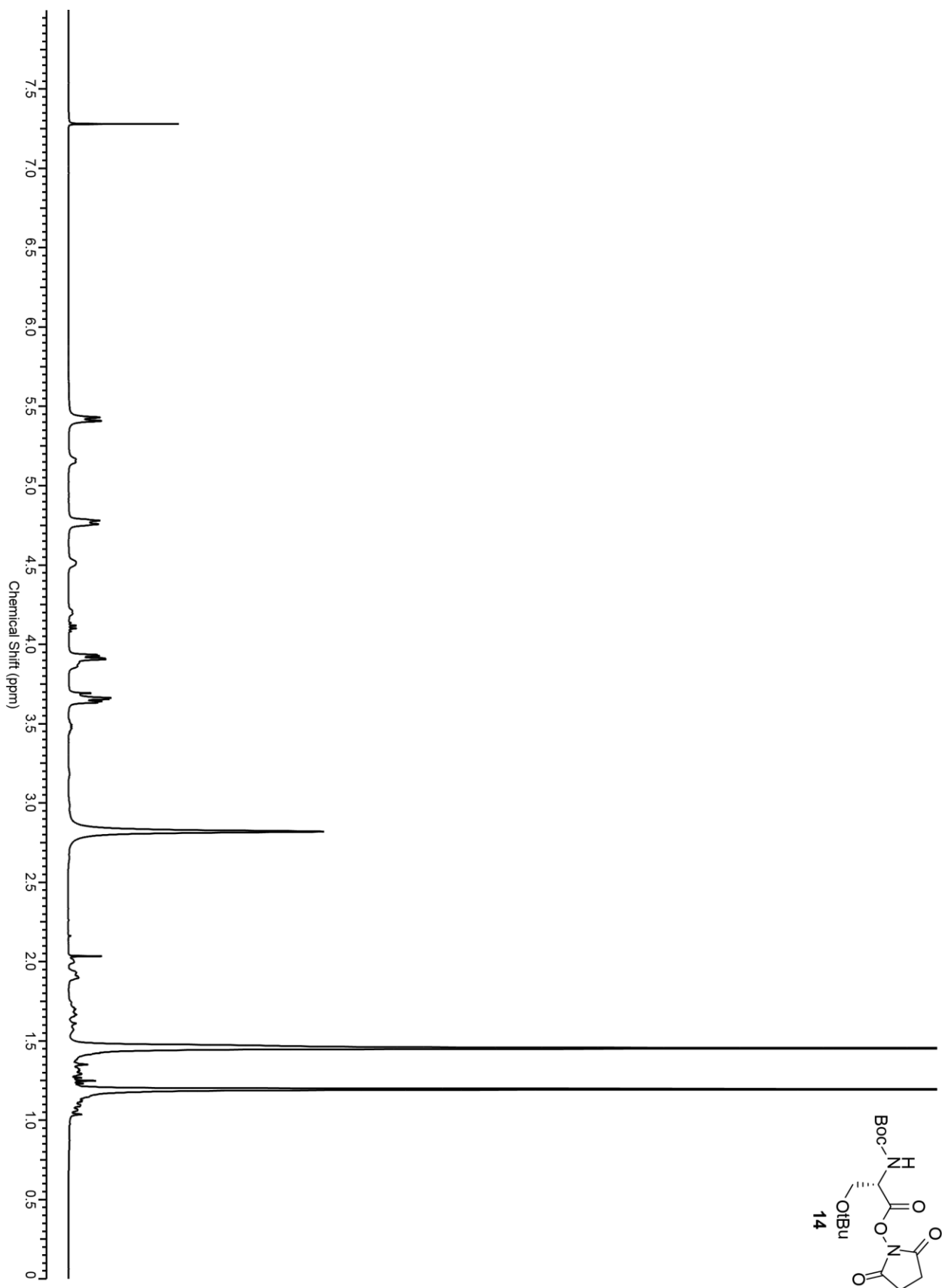
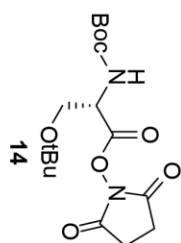


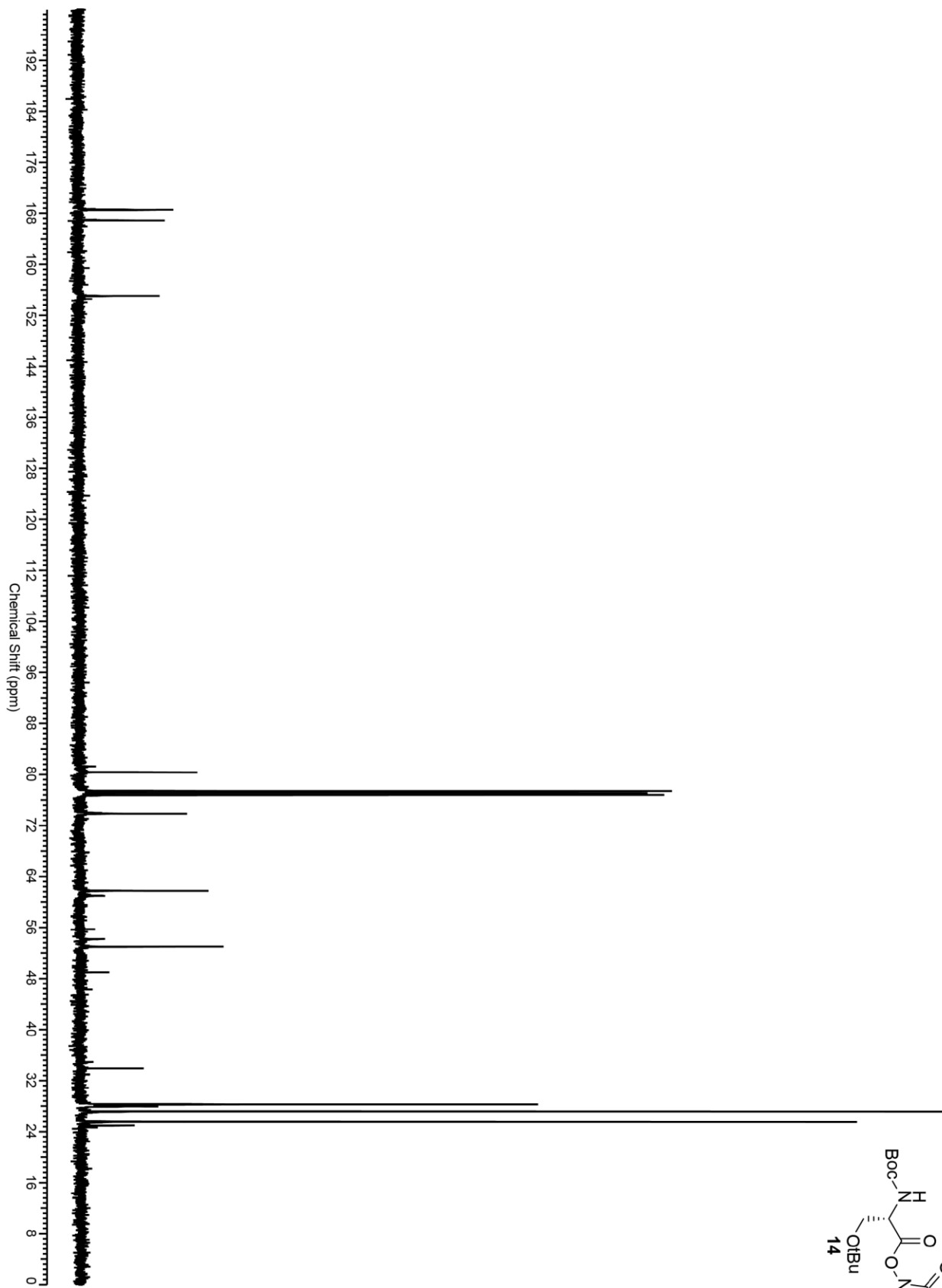
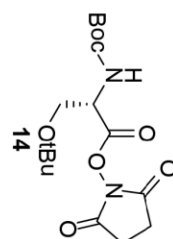


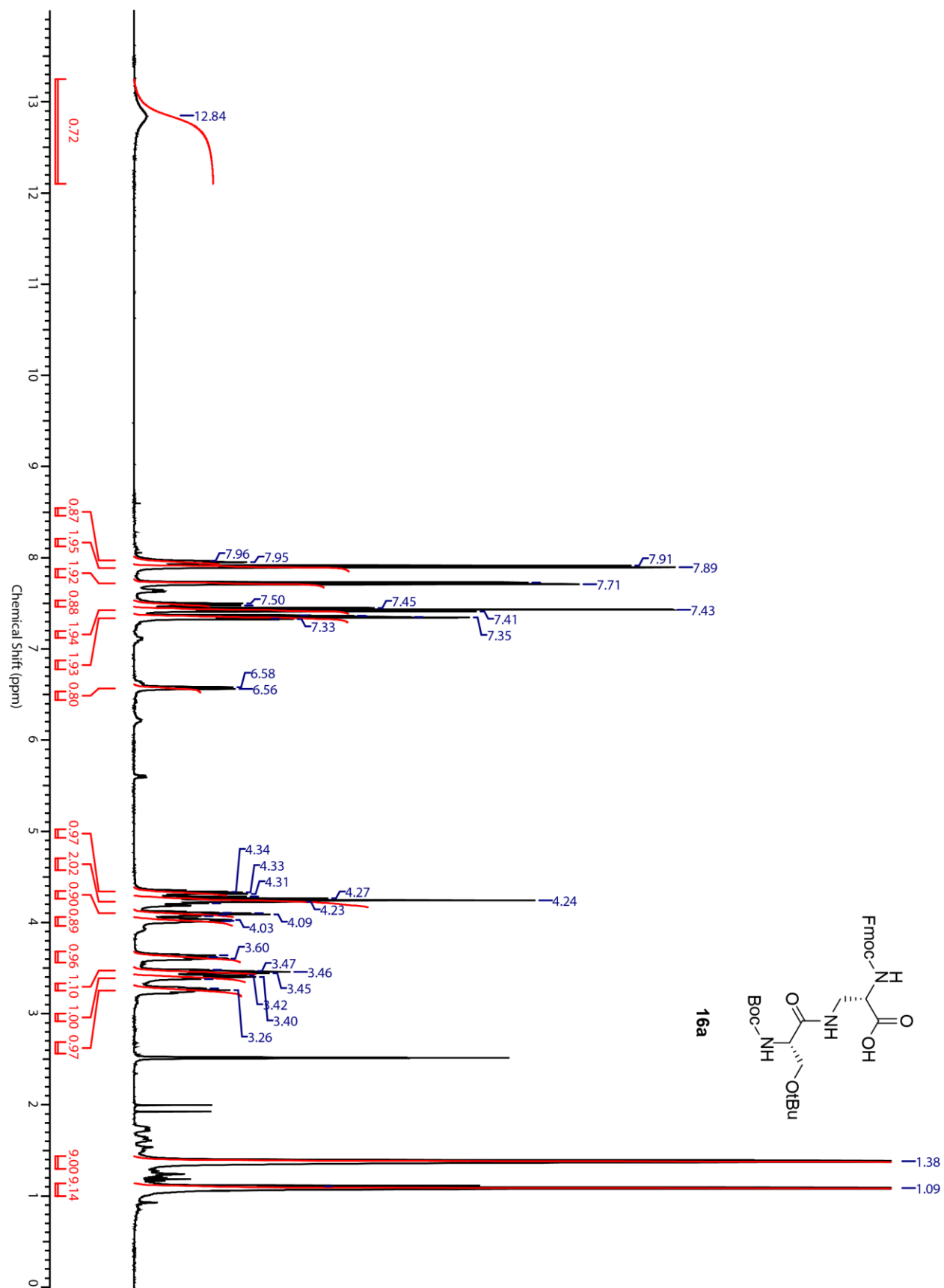


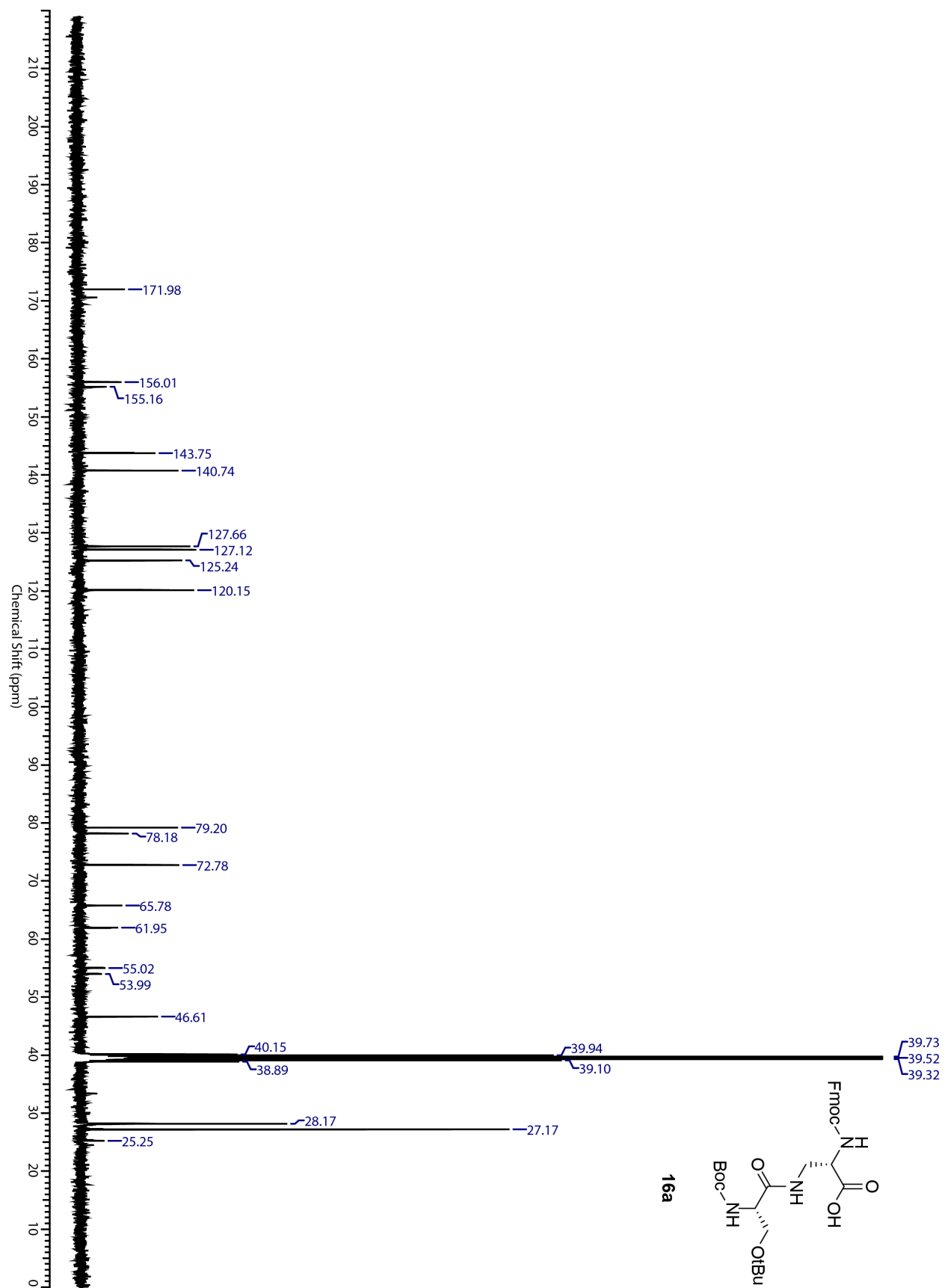


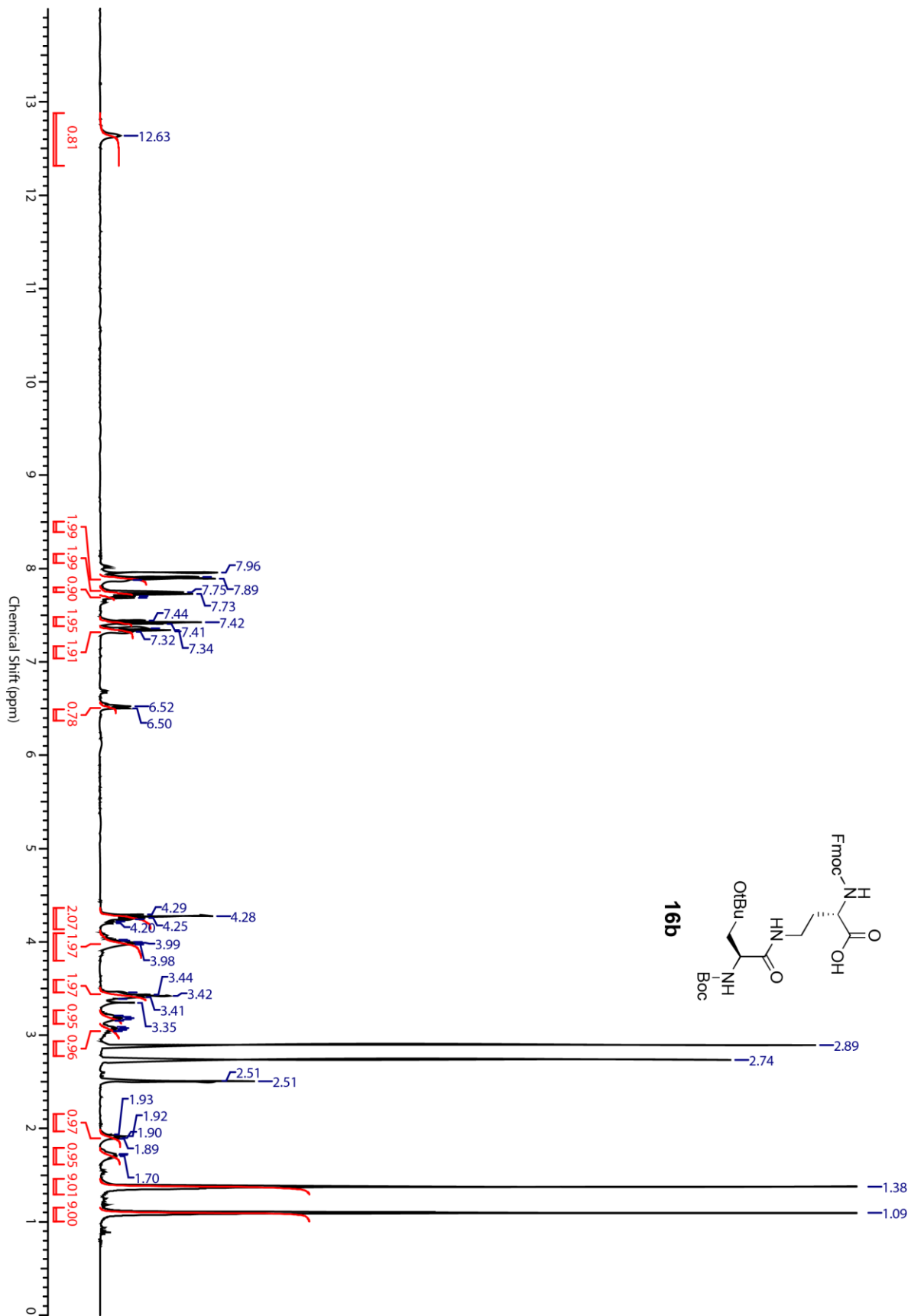


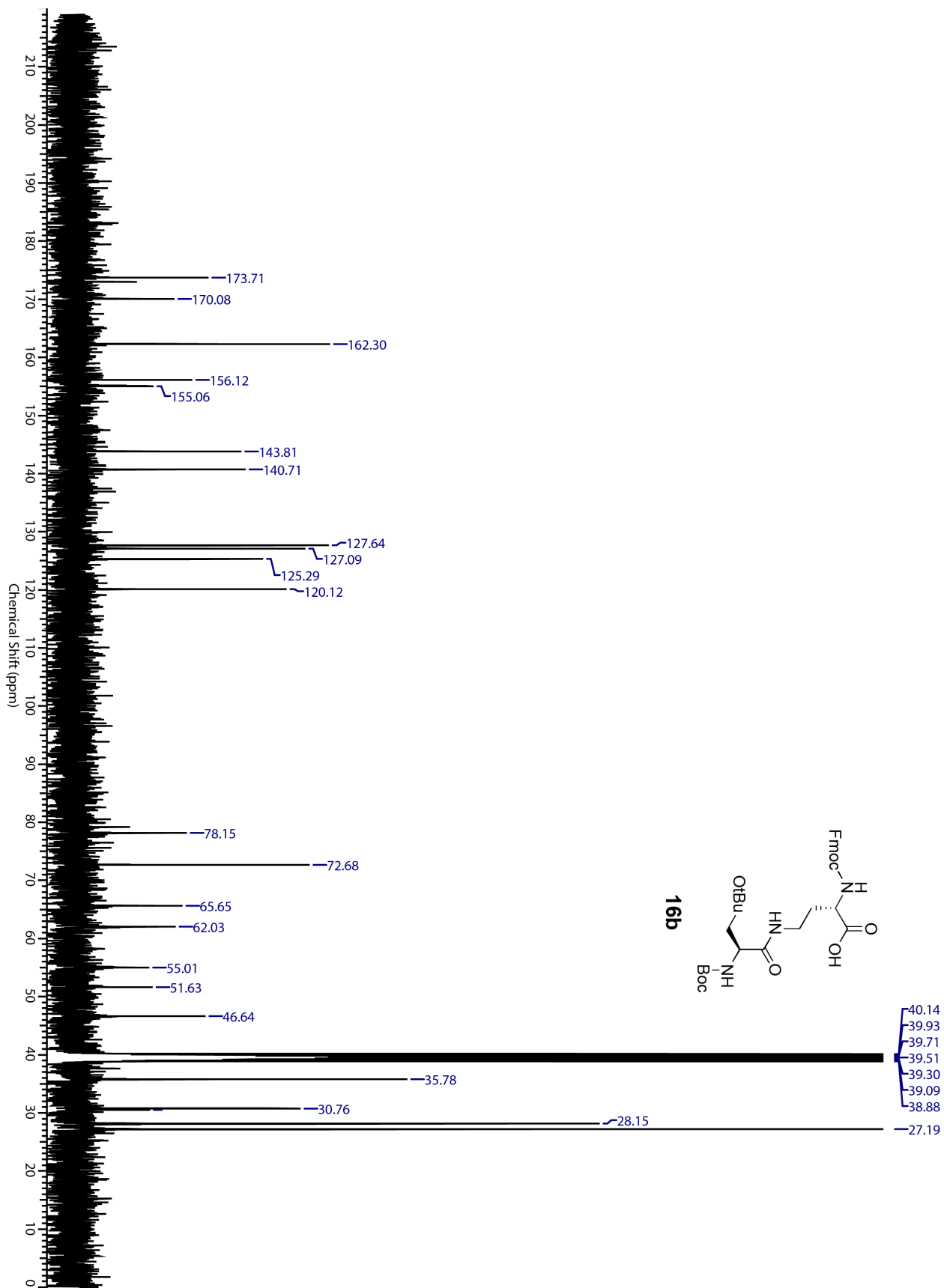


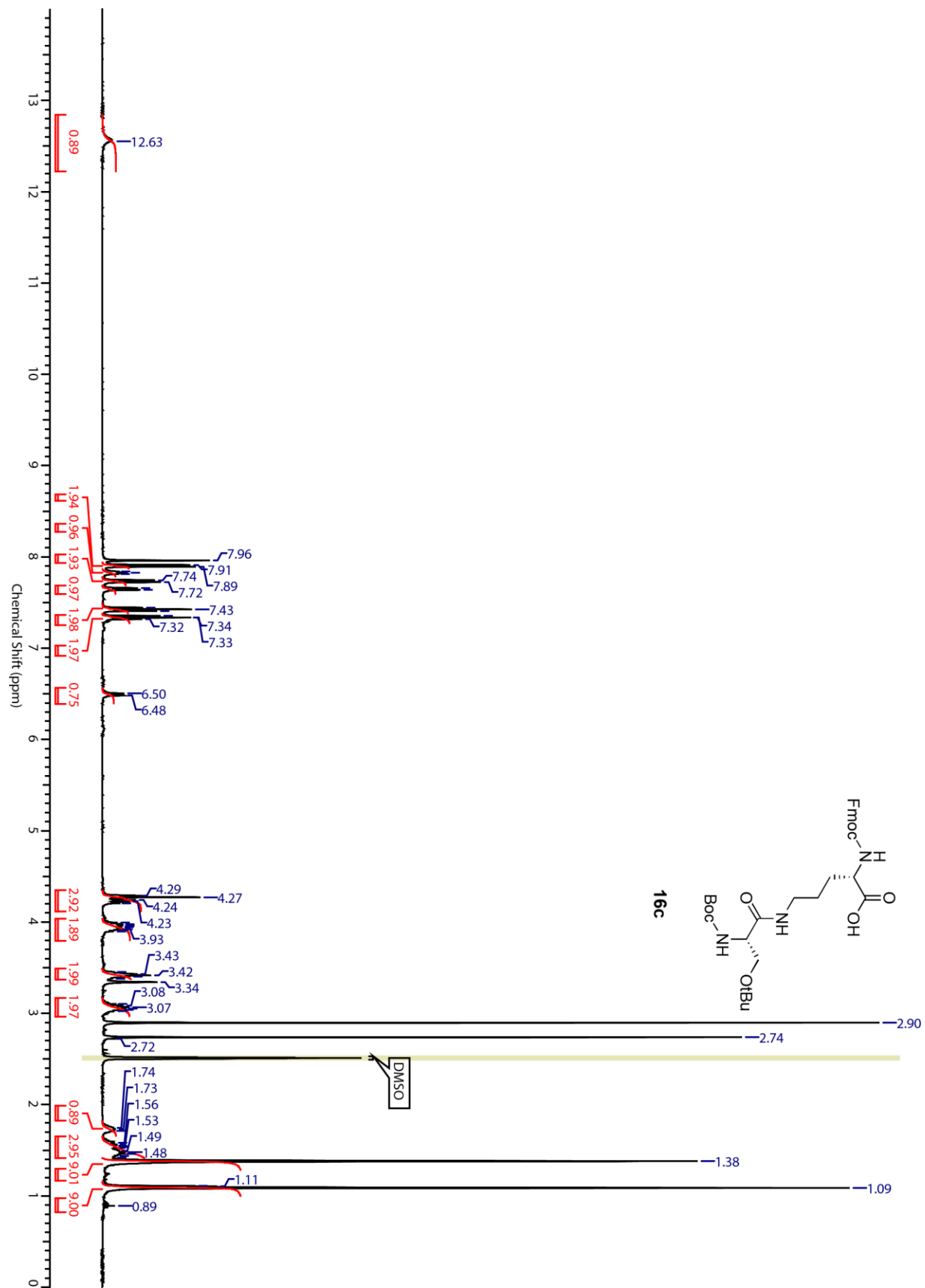


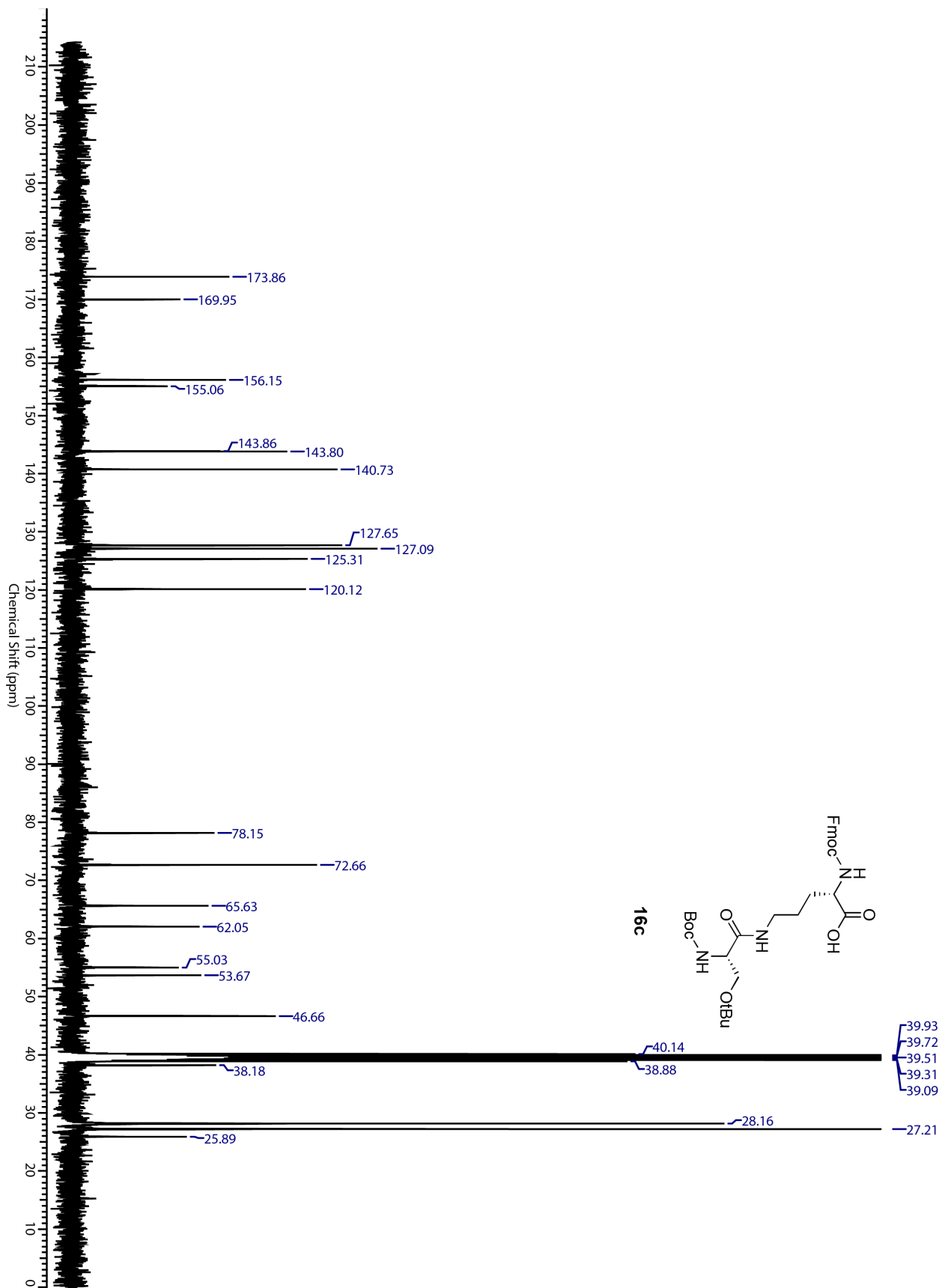


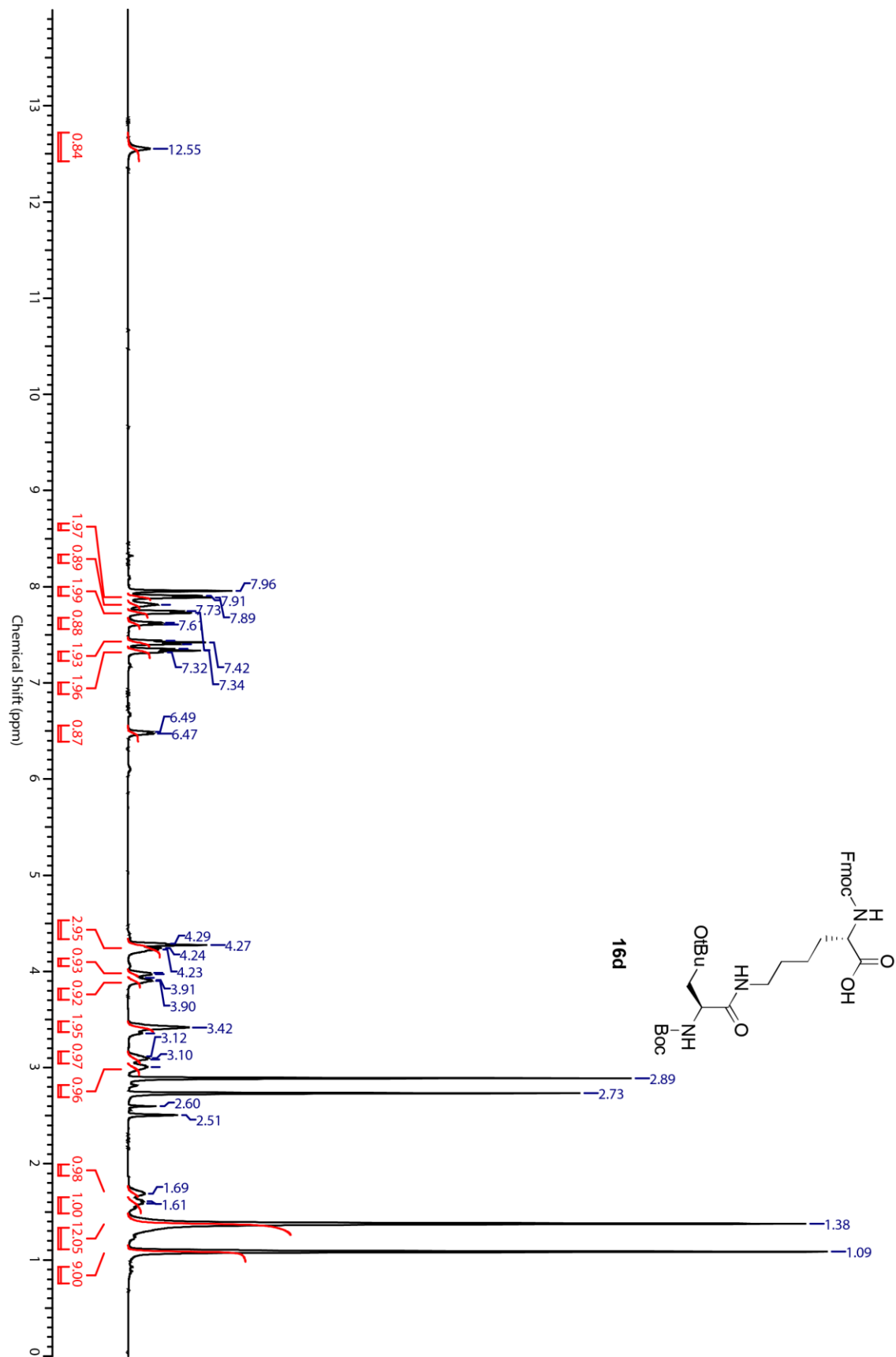


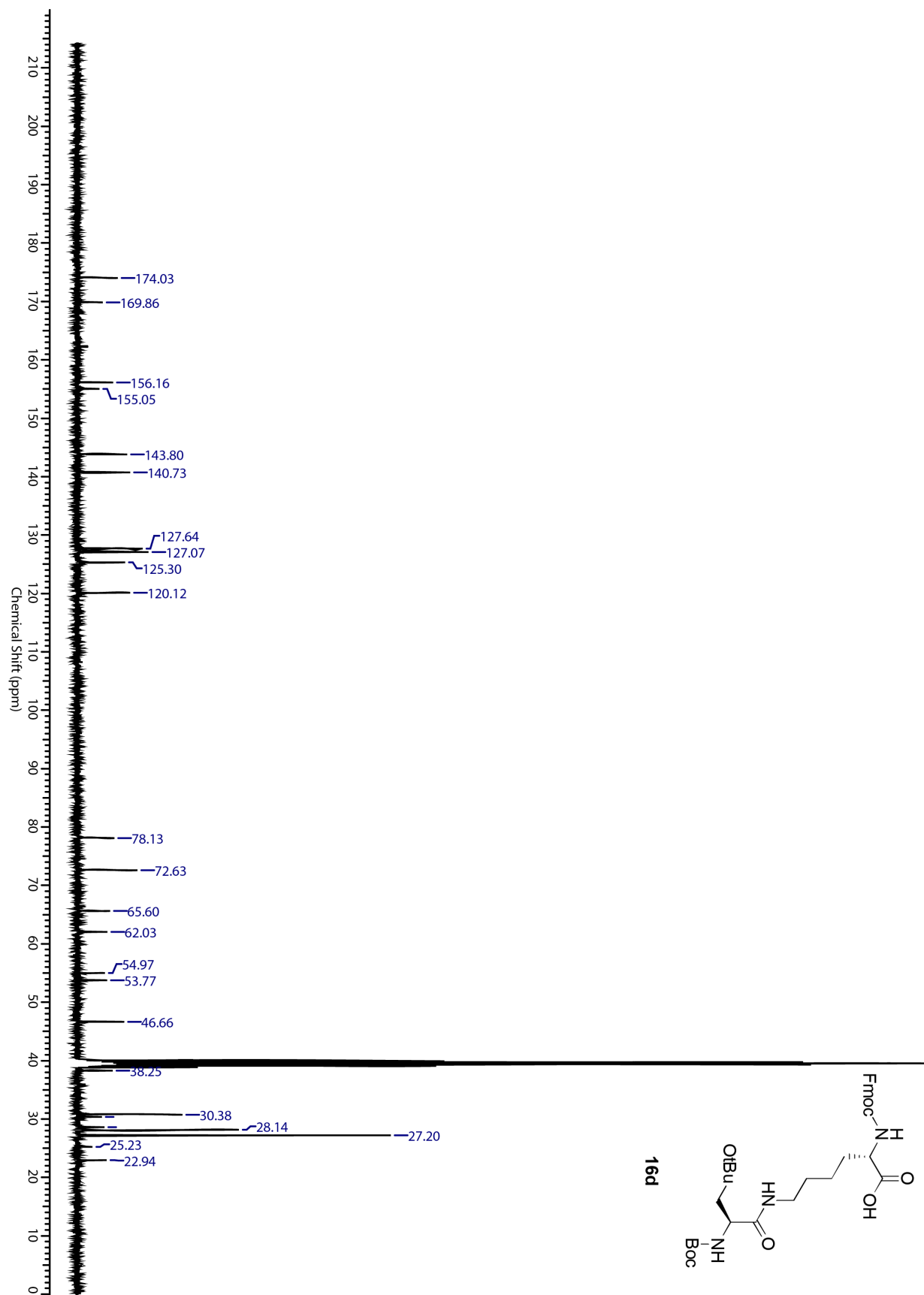


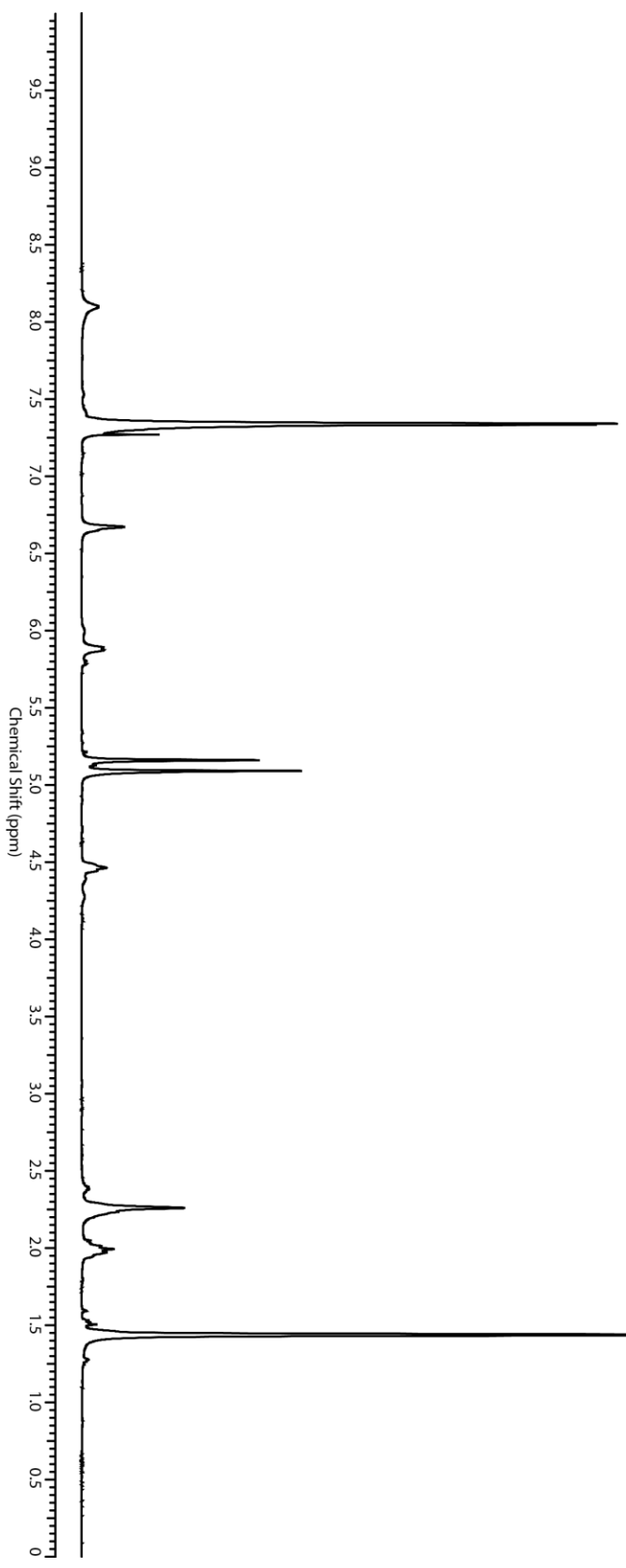
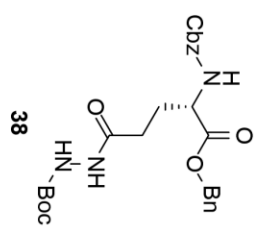


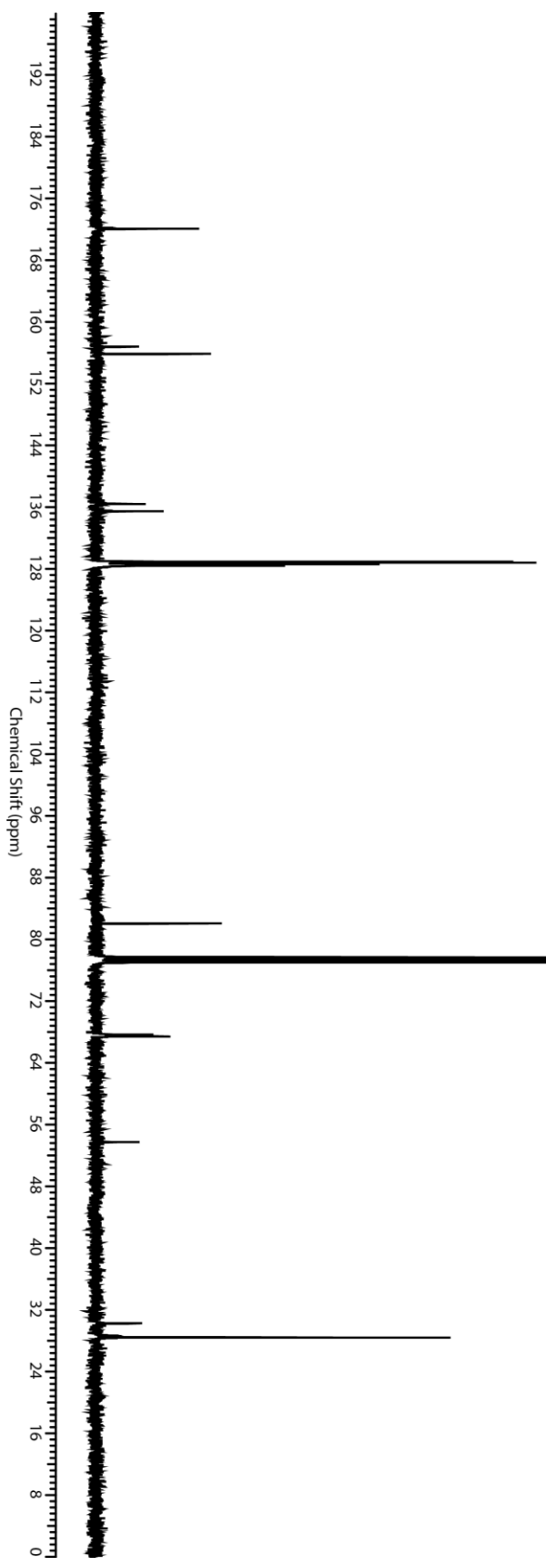
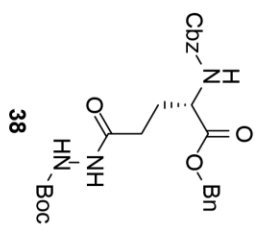


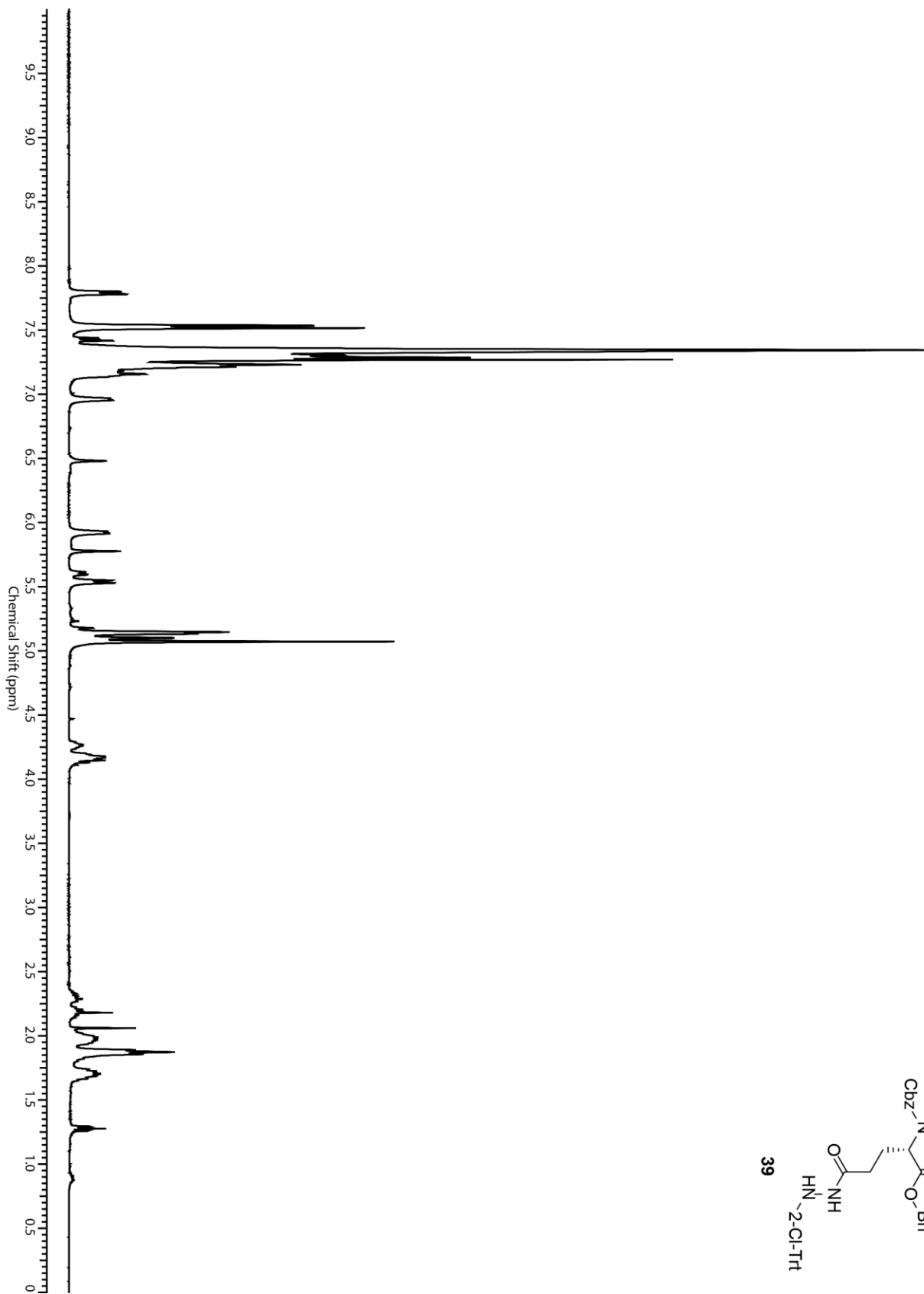
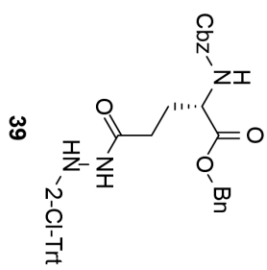


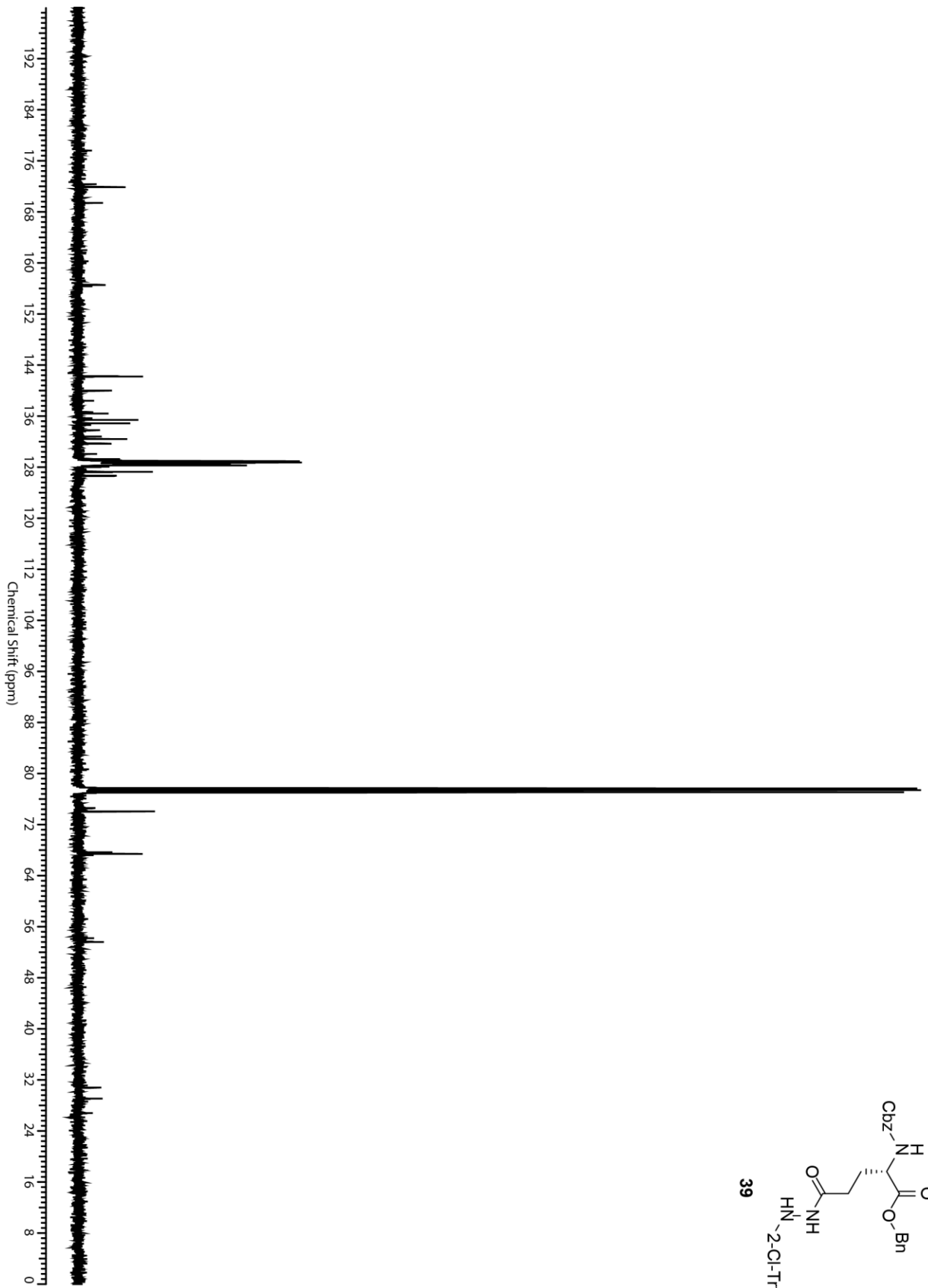
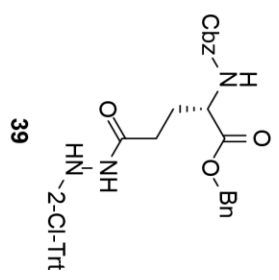


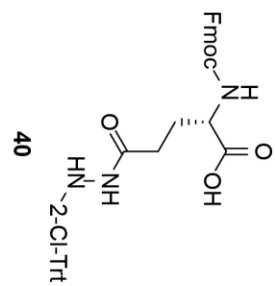
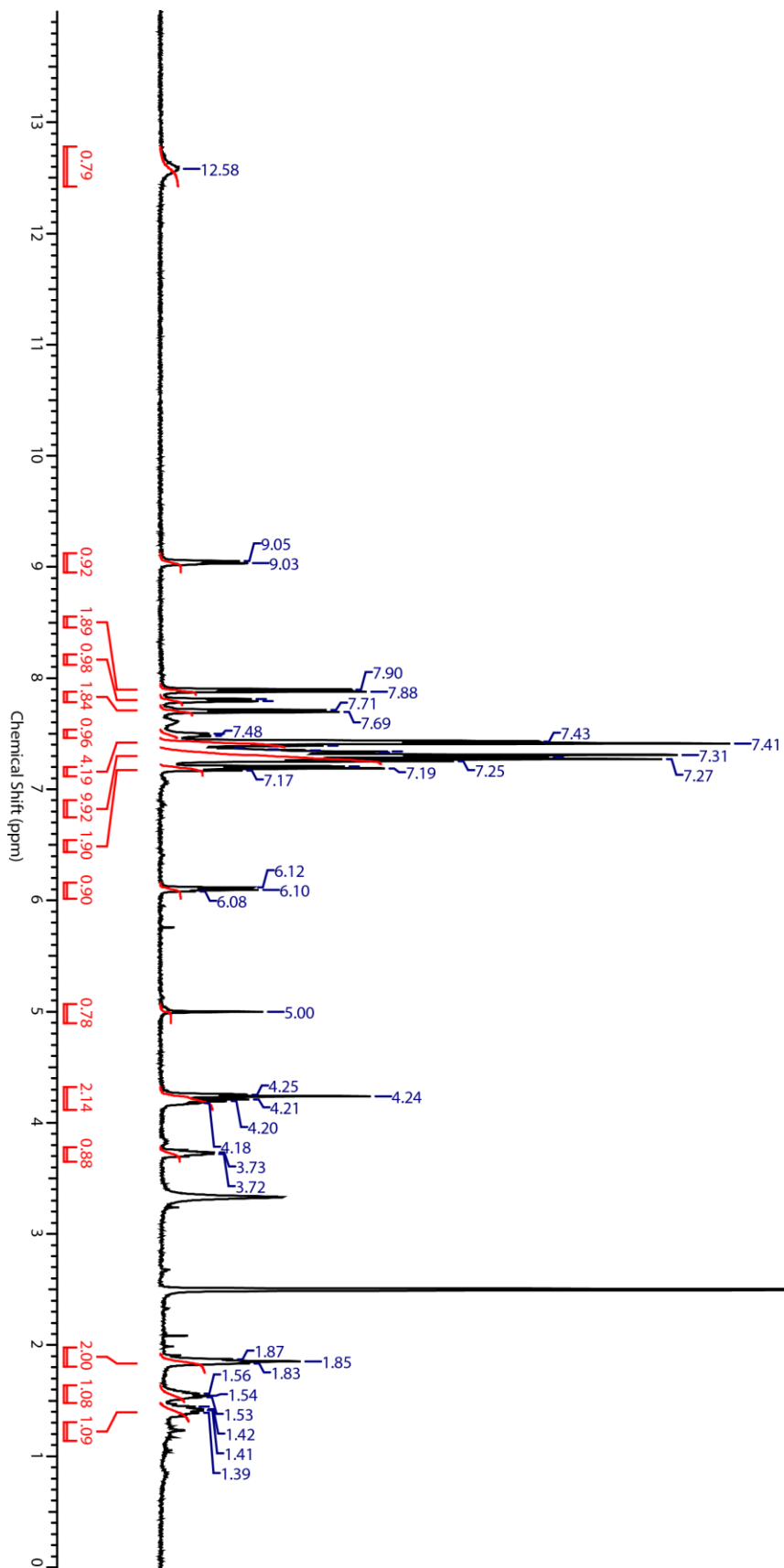


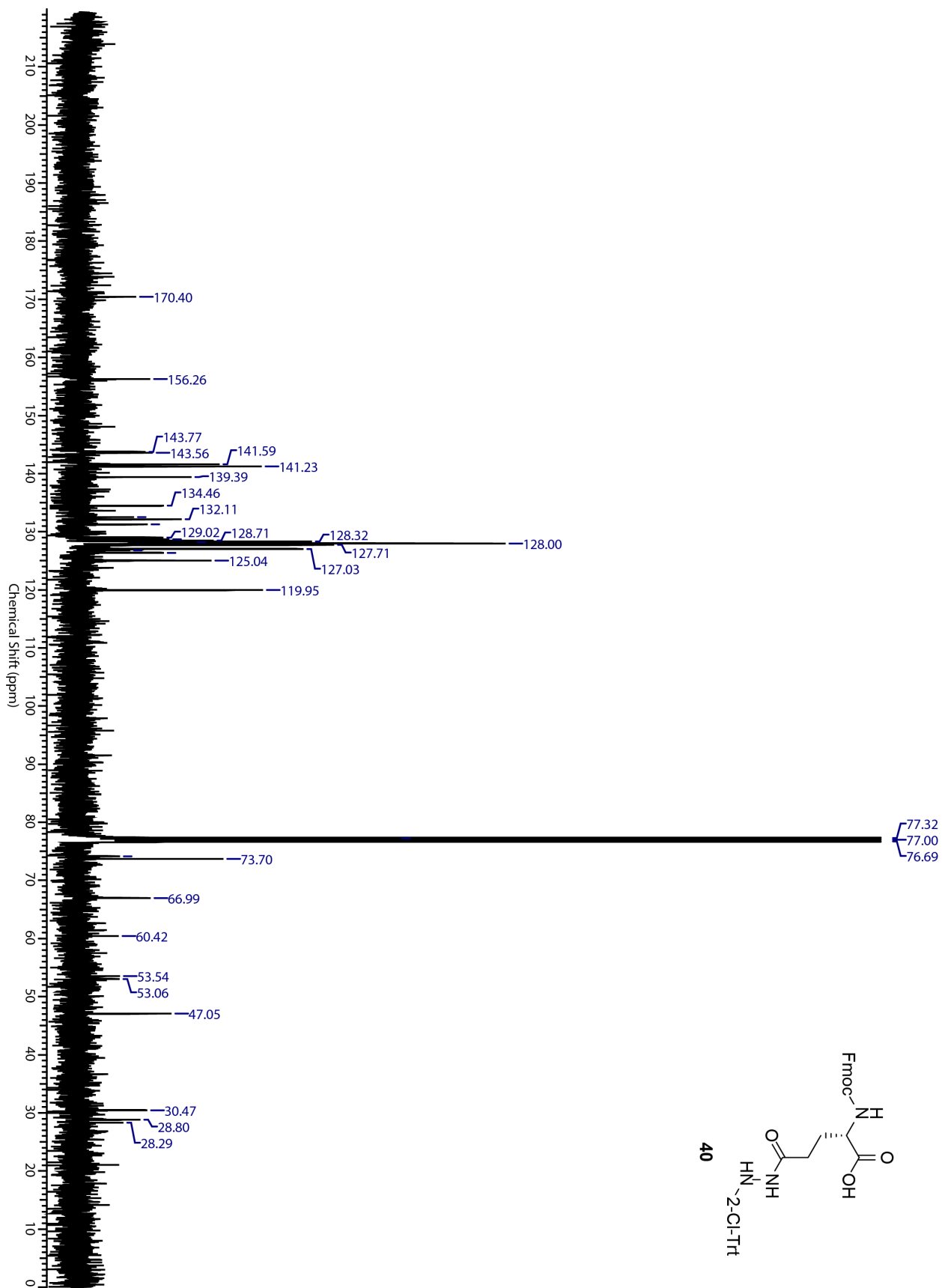


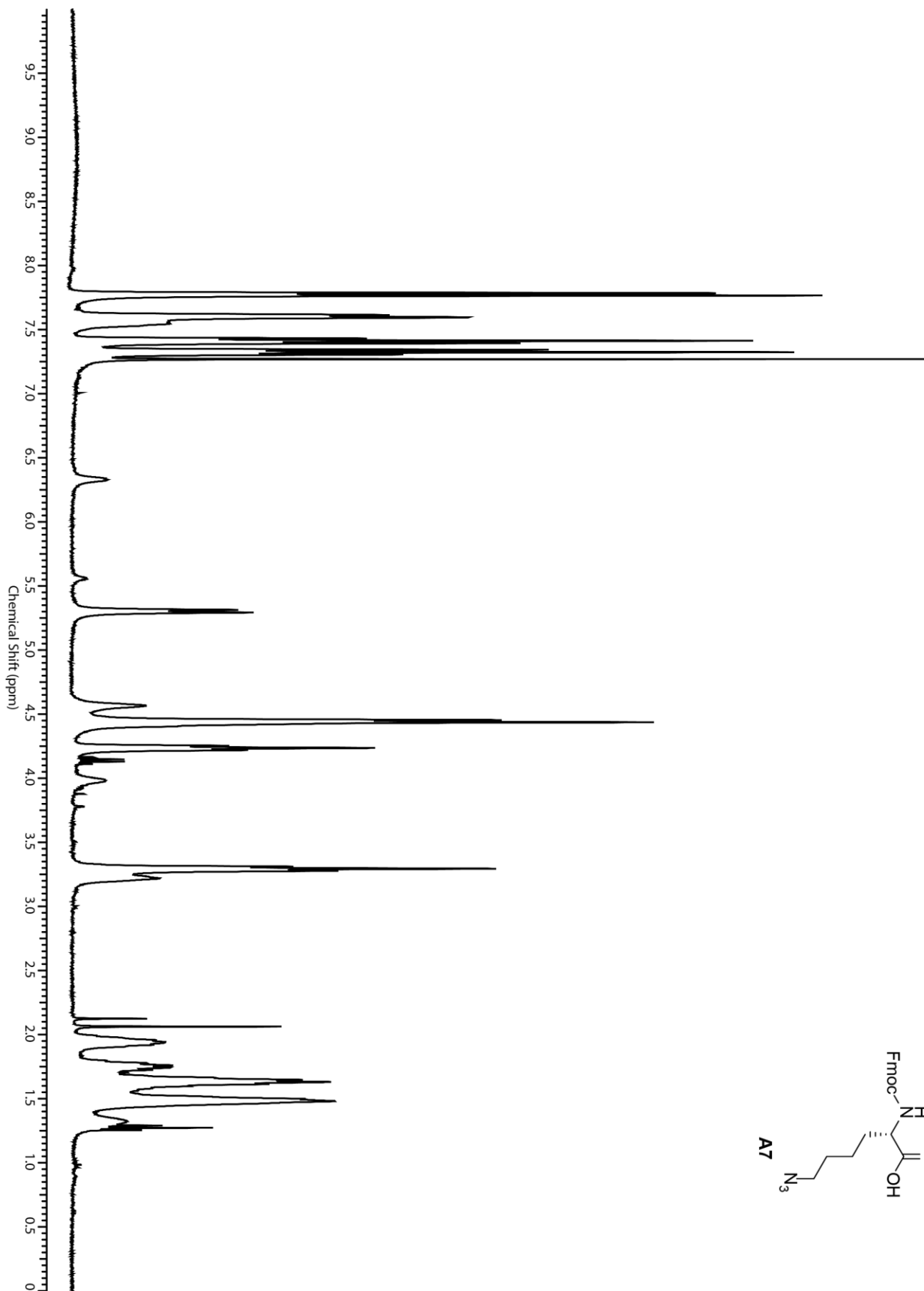
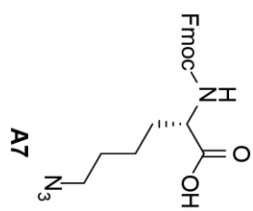












## BIBLIOGRAPHY

1. Rowan, S. J.; Cantrill, S. J.; Cousins, G. R. L.; Sanders, J. K. M.; Stoddart, J. F. "Dynamic Covalent Chemistry," *Angew. Chem. Int. Ed.* **2002**, *41*, 898.
2. Corbett, P. T.; Leclaire, J.; Vial, L.; West, K. R.; Wietor, J. L.; Sanders, J. K. M.; Otto, S. "Dynamic Combinatorial Chemistry," *Chem. Rev.* **2006**, *106*, 3652.
3. Otto, S. "Dynamic Molecular Networks: From Synthetic Receptors to Self-Replicators," *Acc. Chem. Res.* **2012**, *45*, 2200.
4. Hermann, A. "Dynamic combinatorial/covalent chemistry: a tool to read, generate, and modulate the bioactivity of compounds and compound mixtures," *Chem. Soc. Rev.* **2014**, *43*, 1899.
5. Stefankiewicz, A. K.; Sambrook, M. R.; Sanders, J. K. M. "Template-directed synthesis of multi-component organic cages in water," *Chem. Sci.* **2012**, *3*, 2326.
6. Ingerman, L. A.; Cuellar, M. E.; Waters, M. L. "A small molecule receptor that selectively recognizes trimethyl lysine in a histone peptide with native protein-like affinity," *Chem. Commun.* **2010**, *46*, 1839.
7. James, L. I.; Beaver, J. E.; Rice, N. W.; Waters, M. L. "A synthetic receptor for asymmetric dimethyl arginine," *J. Am. Chem. Soc.* **2013**, *135*, 6450.
8. Pons, M.; Albericio, F.; Royo, M.; Giralt, E. "Disulfide bonded cyclic peptide dimers and trimers: an easy entry to high symmetry peptide frameworks," *Synlett.* **2000**, 172.
9. Krishnan-Ghosh, Y.; Balasubramanian, S. "Dynamic Covalent Chemistry on Self-Templating Peptides: Formation of a Disulfide-linked  $\beta$ -Hairpin Mimic," *Angew. Chem. Int. Ed.* **2003**, *42*, 2171.
10. Case, M. A.; McLendon, G. L. "Metal-Assembled Modular Proteins: Toward Functional Protein Design," *Acc. Chem. Res.* **2004**, *37*, 754.

11. Woll, M. G.; Gellman, S. H. "Backbone Thioester Exchange: A New Approach to Evaluating Higher Order Structural Stability in Polypeptides," *J. Am. Chem. Soc.* **2004**, *126*, 11172.
12. Ulrich, S.; Dumy, P. "Probing secondary interactions in biomolecular recognition by dynamic combinatorial chemistry," *Chem. Commun.* **2014**, *50*, 5810.
13. Poulsen, S.-A. "Direct screening of a dynamic combinatorial library using mass spectrometry," *J. Am. Soc. Mass. Spectrom.* **2006**, *17*, 1074.
14. Bhat, V. T.; Caniard, A. M.; Luksch, T.; Brenk, R.; Campopiano, D. J.; Greaney, M. F. "Nucleophilic catalysis of acylhydrazone equilibration for protein-directed dynamic covalent chemistry," *Nat. Chem.* **2010**, *2*, 490.
15. Clipson, A. J.; Bhat, V. T.; McNae, I.; Caniard, A. M.; Campopiano, D. J.; Greaney, M. F. "Bivalent enzyme inhibitors discovered using dynamic covalent chemistry," *Chem. Eur. J.* **2012**, *18*, 10562.
16. Milanesi, L.; Hunter, C. A.; Sedelnikova, S. E.; Waltho, J. P. "Amplification of bifunctional ligands for calmodulin from a dynamic combinatorial library," *Chem. Eur. J.* **2006**, *12*, 1081.
17. Sindelar, M.; Lutz, T. A.; Petrera, M.; Wanner, K. T. "Focused pseudostatic hydrazone libraries screened by mass spectrometry binding assay: optimizing affinities towards  $\gamma$ -aminobutyric acid transporter 1," *J. Med. Chem.* **2013**, *56*, 1323.
18. Liu, F.; Stephen, A. G.; Adamson, C. S.; Gousset, K.; Aman, M. J.; Freed, E. O.; Fisher, R. J.; Terrence R. Burke, J. "Hydrazone- and Hydrazide-containing N-substituted glycines as peptoid surrogates for expedited library synthesis: application to the preparation of Tsg101-directed HIV-1 budding antagonists," *Org. Lett.* **2008**, *8*, 5165.
19. Arkin, M. R.; Wells, J. A. "Small-molecule inhibitors of protein-protein interactions: progressing towards the dream," *Nat. Rev. Drug Disc.* **2004**, *3*, 301.
20. Garner, J.; Harding, M. M. "Design and synthesis of  $\alpha$ -helical peptides and mimetics," *Org. Biomol. Chem.* **2007**, *5*, 3577.
21. Leader, B.; Baca, Q. J.; Golan, D. E. "Protein therapeutics: a summary and pharmacological classification," *Nat. Rev. Drug Disc.* **2008**, *7*, 21.
22. Matthews, T.; Salgo, M.; Greenberg, M.; Chung, J.; DeMasi, R.; Bolognesi, D. "Enfuvirtide: the first therapy to inhibit the entry of HIV-1 into host CD4 lymphocytes," *Nat. Rev. Drug Disc.* **2004**, *3*, 215.

23. Gladwell, T. D. "Bivalirudin: a direct thrombin inhibitor," *Clin. Ther.* **2002**, *24*, 38.
24. Parry, M. A. A.; Maraganore, J. M.; Stone, S. R. "Kinetic Mechanism for the Interaction of Hirulog with Thrombin," *Biochem.* **1994**, *33*, 14807.
25. Tyndall, J. D.; Nall, T.; Fairlie, D. P. "Proteases universally recognize beta strands in their active sites," *Chem. Rev.* **2005**, *105*, 973.
26. McGregor, D. P. "Discovering and Improving Novel Peptide Therapeutics," *Curr. Opin. Pharmacol.* **2008**, *8*, 616.
27. Venkatraman, J.; Shankaramma, S. C.; Balaram, P. "Design of Folded Peptides," *Chem. Rev.* **2001**, *101*, 3131.
28. Kabsch, W.; Sander, C. "Dictionary of protein secondary structure: Pattern recognition of hydrogen-bonded and geometrical features," *Biopolymers* **1983**, *22*, 2577.
29. Jones, S.; Thornton, J. M. "Principles of Protein-Protein Interactions," *Proc. Nat. Acad. Sci. USA* **1996**, *93*, 13.
30. Jochim, A. L.; Arora, P. S. "Systematic Analysis of Helical Protein Interfaces Reveals Targets for Synthetic Inhibitors," *ACS Chem. Biol.* **2010**, *5*, 919.
31. Padmanabhan, S.; Marqusee, S.; Ridgeway, T.; Laue, T. M.; Baldwin, R. L. "Relative helix-forming tendencies of nonpolar amino acids," *Nature* **1990**, *344*, 268.
32. O'Neil, K. T.; DeGrado, W. F. "A thermodynamic scale for the helix-forming tendencies of the commonly occurring amino acids," *Science* **1990**, *250*, 646.
33. Marqusee, S.; Baldwin, R. L. "Helix stabilization by Glu-...Lys+ salt bridges in short peptides of de novo design " *Proc. Nat. Acad. Sci. USA* **1987**, *84*, 8898.
34. Fairman, R.; Shoemaker, K. R.; York, E. J.; Stewart, J. M.; Baldwin, R. L. "Further studies of the helix dipole model: effects of a free  $\alpha$ -NH<sub>3</sub><sup>+</sup> or  $\alpha$ -COO<sup>-</sup> group on helix stability," *Proteins* **1989**, *5*, 1.
35. Doig, A. J.; Baldwin, R. L. "N- and C-capping preferences for all 20 amino acids in  $\alpha$ -helical peptides," *Protein Sci.* **1995**, *4*, 1325.

36. Cascales, L.; Craik, D. J. "Naturally occurring circular proteins: distribution, biosynthesis and evolution," *Org. Biomol. Chem.* **2010**, *8*, 5035.
37. Daly, N. L.; Craik, D. J. "Bioactive cysteine knot proteins," *Curr. Opin. Chem. Biol.* **2011**, *15*, 362.
38. Ganz, T. "Defensins: antimicrobial peptides of innate immunity," *Nat. Rev. Immun.* **2003**, *3*, 710.
39. Henchey, L. K.; Jochim, A. L.; Arora, P. S. "Contemporary strategies for the stabilization of peptides in the  $\alpha$ -helical conformation," *Curr. Opin. Chem. Biol.* **2008**, *12*, 692.
40. White, C. J.; Yudin, A. K. "Contemporary strategies for peptide macrocyclization," *Nat. Chem.* **2011**, *3*, 509.
41. Holland-Nell, K.; Meldal, M. "Maintaining biological activity by using triazoles as disulfide bond mimetics," *Angew. Chem. Int. Ed.* **2011**, *50*, 5204.
42. Park, J. H.; Waters, M. L. "Positional effects of click cyclization on  $\beta$ -hairpin structure, stability, and function," *Org. Biomol. Chem.* **2013**, *11*, 69.
43. Felix, A. M.; Wang, C. T.; Heimer, E. P.; Fournier, A. "Applications of BOP reagent in solid phase synthesis," *Int. J. Pept. Protein Res.* **1988**, *31*, 231.
44. Taylor, J. W. "The synthesis and study of side-chain lactam-bridged peptides," *Peptide Science* **2002**, *66*, 49.
45. Shepherd, N. E.; Hoang, H. N.; Desai, V. S.; Letouze, E.; Young, P. R.; Fairlie, D. P. *J. Am. Chem. Soc.* **2006**, *128*, 13284.
46. R. S. Harrison, N. E. S., H. N. Hoang, G. Ruiz-Gomez, T. A. Hill, R. W. Driver, V. S. Desai, P. R. Young, G. Abbenante, D. P. Fairlie. "Downsizing human, bacterial, and viral proteins to short water-stable alpha helices that maintain biological potency " *Proc. Nat. Acad. Sci. USA* **2010**, *107*, 11686.
47. Blackwell, H. E.; Grubbs, R. H. "Highly Efficient Synthesis of Covalently Cross-Linked Peptide Helices by Ring-Closing Metathesis," *Angew. Chem. Int. Ed.* **1998**, *37*, 3281.
48. Schafmeister, C. E.; Po, J.; Verdine, G. L. "An All-Hydrocarbon Cross-Linking System for Enhancing the Helicity and Metabolic Stability of Peptides," *J. Am. Chem. Soc.* **2000**, *122*, 5891.

49. Kim, Y.-W.; Kutchukian, P. S.; Verdine, G. L. "Introduction of All-Hydrocarbon  $i,i+3$  Staples into  $\alpha$ -Helices via Ring-Closing Olefin Metathesis," *Org. Lett.* **2010**, *12*, 3046.
50. Walensky, L. D.; Kung, A. L.; Escher, I.; Malia, T. J.; Barbuto, S.; Wright, R. D.; Wagner, G.; Verdine, G. L.; Korsmeyer, S. J. "Activation of Apoptosis in Vivo by a Hydrocarbon-Stapled BH3 Helix," *Science* **2004**, *305*, 1466.
51. Bernal, F.; Tyler, A. F.; Korsmeyer, S. J.; Walensky, L. D.; Verdine, G. L. "Reactivation of the p53 Tumor Suppressor Pathway by a Stapled p53 Peptide," *J. Am. Chem. Soc.* **2007**, *129*, 2456.
52. Moellering, R. E.; Cornejo, M.; Davis, T. N.; Bianco, C. D.; Aster, J. C.; Blacklow, S. C.; Kung, A. L.; Gilliland, D. G.; Verdine, G. L.; Bradner, J. E. "Direct inhibition of the NOTCH transcription factor complex," *Nature* **2009**, *462*, 182.
53. Verdine, G. L.; Hilinski, G. J. "Stapled peptides for intracellular drug targets," *Methods Enzymol.* **2012**, *503*, 3.
54. Okamoto, T.; Zobel, K.; Fedorova, A.; Quan, C.; Yang, H.; Fairbrother, W. J.; Huang, D. C. S.; Smith, B. J.; Deshayes, K.; Czabotar, P. E. "Stabilizing the pro-apoptotic BimBH3 helix (BimSAHB) does not necessarily enhance affinity or biological activity," *ACS Chem. Biol.* **2013**, *8*, 297.
55. Brunel, F. M.; Dawson, P. E. "Synthesis of constrained helical peptides by thioether ligation: application to analogs of gp41," *Chem. Commun.* **2005**, 2552.
56. Cabezas, E.; Satterthwait, A. C. "The Hydrogen Bond Mimic Approach: Solid-Phase Synthesis of a Peptide Stabilized as an  $\alpha$ -Helix with a Hydrazone Link," *J. Am. Chem. Soc.* **1999**, *121*, 3862.
57. Chapman, R. N.; Dimartino, G.; Arora, P. S. "A Highly Stable Short  $\alpha$ -Helix Constrained by a Main-Chain Hydrogen-Bond Surrogate," *J. Am. Chem. Soc.* **2004**, *126*, 12252.
58. Wang, D.; Liao, W.; Arora, P. S. "Enhanced Metabolic Stability and Protein-Protein Binding Properties of Artificial  $\alpha$ -Helices Derived from a Hydrogen-Bond Surrogate: Application to Bcl-XL," *Angew. Chem. Int. Ed.* **2005**, *44*, 6525.
59. Wang, D.; Chen, K.; III, J. L. K.; Arora, P. S. "Evaluation of Biologically Relevant Short  $\alpha$ -Helices Stabilized by a Main-Chain Hydrogen-Bond Surrogate," *J. Am. Chem. Soc.* **2006**, *128*, 9248.

60. Henchey, L. K.; Kushal, S.; Dubey, R.; Chapman, R. N.; Olenyuk, B. Z.; Arora, P. S. "Inhibition of Hypoxia Inducible Factor 1—Transcription Coactivator Interaction by a Hydrogen Bond Surrogate  $\alpha$ -Helix," *J. Am. Chem. Soc.* **2010**, *132*, 941.
61. Mahon, A. B.; Arora, P. S. "Design, synthesis and protein-targeting properties of thioether-linked hydrogen bond surrogate helices," *Chem. Commun.* **2012**, *48*, 1416.
62. Muppidi, A.; Wang, Z.; Li, X.; Chen, J.; Lin, Q. "Achieving cell penetration with distance-matching cysteine cross-linkers: a facile route to cell-permeable peptide dual inhibitors of Mdm2/Mdmx," *Chem. Commun.* **2011**, *47*, 9396.
63. Muppidi, A.; Doi, K.; Edwardraja, S.; Drake, E. J.; Gulick, A. M.; Wang, H.-G.; Lin, Q. "Rational Design of Proteolytically Stable, Cell-Permeable Peptide-Based Selective Mcl-1 Inhibitors," *J. Am. Chem. Soc.* **2012**, *134*, 14734.
64. Fujimoto, K.; Kajino, M.; Inouye, M. "Development of a Series of Cross-Linking Agents that Effectively Stabilize  $\alpha$ -Helical Structures in Various Short Peptides," *Chem. Eur. J.* **2008**, *14*, 857.
65. Kajino, M.; Fujimoto, K.; Inouye, M. "Side-Chain Cross-Linked Short  $\alpha$ -Helices That Behave like Original Proteins in Biomacromolecular Interactions," *J. Am. Chem. Soc.* **2011**, *133*, 656.
66. Jackson, D. Y.; King, D. S.; Chmielewski, J.; Singh, S.; Schultz, P. G. "General Approach to the Synthesis of Short  $\alpha$ -Helical Peptides," *J. Am. Chem. Soc.* **1991**, *113*, 9391.
67. Jo, H.; Meinhardt, N.; Wu, Y.; Kulkarni, S.; Hu, X.; Low, K. E.; Davies, P. L.; DeGrado, W. F.; Greenbaum, D. C. "Development of  $\alpha$ -Helical Calpain Probes by Mimicking a Natural Protein-Protein Interaction," *J. Am. Chem. Soc.* **2012**, *134*, 17704.
68. Spokoyny, A. M.; Zou, Y.; Ling, J. J.; Yu, H.; Lin, Y.-S.; Pentelute, B. L. "A Perfluoroaryl-Cysteine  $S_NAr$  Chemistry Approach to Unprotected Peptide Stapling," *J. Am. Chem. Soc.* **2013**, *135*, 5946.
69. Zou, Y.; Spokoyny, A. M.; Zhang, C.; Simon, M. D.; Yu, H.; Lin, Y.-S.; Pentelute, B. L. "Convergent diversity-oriented side-chain macrocyclization scan for unprotected polypeptides," *Org. Biomol. Chem.* **2014**, *12*, 566.
70. Hong, V.; Presolski, S. I.; Ma, C.; Finn, M. G. "Analysis and optimization of copper-catalyzed azide-alkyne cocladdition for bioconjugation," *Angew. Chem. Int. Ed.* **2009**, *48*, 9879.
71. Horne, W. S.; Stout, C. D.; Ghadiri, M. R. "A heterocyclic peptide nanotube," *J. Am. Chem. Soc.* **2003**, *125*, 9372.

72. Horne, W. S.; Yadav, M. K.; Stout, C. D.; Ghadiri, M. R. "Heterocyclic peptide backbone modifications in an  $\alpha$ -helical coiled coil," *J. Am. Chem. Soc.* **2004**, *126*, 15366.
73. Larregola, M.; Lequin, O.; Karoyan, P.; Guianvarc'h, D.; Lavielle, S. " $\beta$ -Amino acids containing peptides and click-cyclized peptides as  $\beta$ -turn mimics: a comparative study with 'conventional' lactam- and disulfide-bridged hexapeptides," *J. Pept. Sci.* **2011**, *17*, 632.
74. Chouhan, G.; James, K. "Efficient construction of proline-containing  $\beta$ -turn mimetic cyclic tetrapeptides via CuAAC macrocyclization," *Org. Lett.* **2013**, *15*, 1206.
75. Ingale, S.; Dawson, P. E. "On Resin Side-Chain Cyclization of Complex Peptides using CuAAC," *Org. Lett.* **2011**, *13*, 2822.
76. Kawamoto, S. A.; Coleska, A.; Ran, X.; Yi, H.; Yang, C.-Y.; Wang, S. "Design of Triazole-Stapled BCL9  $\alpha$ -Helical Peptides to Target the  $\beta$ -Catenin/B-Cell CLL/lymphoma 9 (BCL9) Protein-Protein Interaction," *J. Med. Chem.* **2012**, *55*, 1137.
77. Pallin, T. D.; Tam, J. P. "Cyclisation of totally unprotected peptides in aqueous solution by oxime formation," *J. Chem. Soc. Chem. Commun.* **1995**, 2021.
78. Wahl, F.; Mutter, M. "Analogues of oxytocin with an oxime bridge using chemoselectively addressable building blocks" *Tetrahedron Lett.* **1996**, *37*, 6861.
79. Klopman, G.; Tsuda, K.; Louis, J. B.; Davis, R. E. "Supernucleophiles - I. The Alpha Effect," *Tetrahedron* **1970**, *26*, 4549.
80. Kalia, J.; Raines, R. T. "Hydrolytic Stability of Hydrazones and Oximes," *Angew. Chem. Int. Ed.* **2008**, *47*, 7523.
81. Dirksen, A.; Dawson, P. E. "Rapid Oxime and Hydrazone Ligations with Aromatic Aldehydes for Biomolecular Labeling," *Bioconj. Chem.* **2008**, *19*, 2543.
82. Ulrich, S.; Boturyn, D.; Marra, A.; Renaudet, O.; Dumy, P. "Oxime Ligation: A Chemoselective Click-Type Reaction for Accessing Multifunctional Biomolecular Constructs," *Chem. Eur. J.* **2013**, *20*, 34.
83. Melnyk, O.; Fehrentz, J. A.; Martinez, J.; Gras-Masse, H. "Functionalization of peptides and proteins by aldehyde or keto groups," *Biopolymers* **2000**, *55*, 165.

84. Liu, F.; Thomas, J.; Burke, T. R. "Synthesis of a Homologous Series of Side-Chain-Extended Orthogonally Protected Aminoxy-Containing Amino Acids " *Synthesis* **2008**, *15*, 2432.
85. Rodriguez, M.; Llinares, M.; Doulut, S.; Heitz, A.; Martinez, J. "A facile synthesis of chiral N-protected  $\beta$ -amino alcohols," *Tetrahedron Lett.* **1991**, *32*, 923.
86. Guy, C. A.; Fields, G. B. "Trifluoroacetic acid cleavage and deprotection of resin-bound peptides following synthesis by Fmoc chemistry," *Methods Enzymol.* **1997**, *289*, 67.
87. Pejkovic-Tadic, I.; Hranisavljevic-Jakovljevic, M.; Nestic, S.; Pascual, C.; Simon, W. "Protonenresonanzspektren von Oximen aromatischer Aldehyde," *Helv. Chim. Acta* **1965**, *48*, 1157.
88. O'Ferrall, R. A. M.; O'Brien, D. "Rate and equilibrium constants for hydrolysis and isomerization of (*E*)- and (*Z*)-*p*-methoxybenzaldehyde oximes," *J. Phys. Org. Chem.* **2004**, *17*, 631.
89. Jencks, W. P., Mechanism and Catalysis of Simple Carbonyl Group Reactions. In *Progress in Physical Organic Chemistry*, Cohen, S. G., Ed. John Wiley & Sons: New York, 1964; Vol. 2, pp 63.
90. Dirksen, A.; Dirksen, S.; Hackeng, T. M.; Dawson, P. E. "Nucleophilic Catalysis of Hydrazone Formation and Transimination: Implications for Dynamic Covalent Chemistry," *J. Am. Chem. Soc.* **2006**, *128*, 15602.
91. Chin, D. H.; Woody, R. W.; Rohl, C. A.; Baldwin, R. L. "Circular dichroism spectra of short, fixed-nucleus alanine helices," *Proc. Nat. Acad. Sci. USA* **2002**, *99*, 15416.
92. O'Shea, E. K.; Klemm, J. D.; Kim, P. S.; Alber, T. "X-ray structure of the GCN4 leucine zipper, a two-stranded, parallel coiled coil.," *Science* **1991**, *254*, 539.
93. Zitzewitz, J. A.; Ibarra-Molero, B.; Fishel, D. R.; Terry, K. L.; Matthews, R. C. "Preformed Secondary Structure Drives the Association Reaction of GCN4-p1, a Model Coiled-coil System," *J. Mol. Biol.* **2000**, *296*, 1105.
94. Kretsinger, J. K.; Schneider, J. P. "Design and Application of Basic Amino Acids Displaying Enhanced Hydrophobicity," *J. Am. Chem. Soc.* **2003**, *125*, 7907.
95. Moran, L. B.; Schneider, J. P.; Kentsis, A.; Reddy, G. A.; Sosnick, T. R. "Transitions state heterogeneity in GCN4 coiled coil folding studied by using multisite mutations and crosslinking," *Proc. Nat. Acad. Sci. USA* **1999**, *96*, 10699.

96. Ibarra-Molero, B.; Zitzewitz, J. A.; Matthews, C. R. "Salt-bridges can Stabilize but do not Accelerate the Folding of the Homodimeric Coiled-coil Peptide GCN4-p1," *J. Mol. Biol.* **2004**, 336, 989.
97. Lumb, K. J.; Kim, P. S. "Measurements of Interhelical Electrostatic Interactions in the GCN4 Leucine Zipper," *Science* **1995**, 268, 436.
98. Meijer, E. W.; Lempens, E. H. M.; Helms, B. A.; Merckx, M. "Efficient and Chemoselective Surface Immobilization of Proteins by Using Aniline-Catalyzed Oxime Chemistry," *ChemBioChem* **2009**, 10, 658.
99. Haney, C. M.; Horne, W. S. "Oxime Side-Chain Cross-Links in an  $\alpha$ -Helical Coiled-Coil Protein: Structure, Thermodynamics, and Folding-Templated Synthesis of Bicyclic Species," *Chem. Eur. J.* **2013**, 19, 11342.
100. Lumb, K. J.; Carr, C. M.; Kim, P. S. "Subdomain Folding of the Coiled Coil Leucine Zipper from the bZIP Transcriptional Activator GCN4," *Biochem.* **1994**, 33, 7361.
101. Vila-Perelló, M.; Gallego, R. G.; Andreu, D. "A Simple Approach to Well-Defined Sugar-Coated Surfaces for Interaction Studies," *ChemBioChem* **2005**, 6, 1831.
102. Gill, S. C.; Hippel, P. H. v. "Calculation of protein extinction coefficients from amino acid sequence data," *Analytical Biochem.* **1989**, 182, 319.
103. Rauscher, E.; Csekő, G.; Horváth, A. K. "On the Complexity of Kinetics and the Mechanism of the Thiosulfate-Periodate Reaction," *Inorg. Chem.* **2011**, 50, 5793.
104. Shortle, D.; Meeker, A. K.; Friere, D. "Stability mutants of staphylococcal nuclease: large compensating enthalpy-entropy changes for the reversible denaturation reaction," *Biochem.* **1988**, 27, 4761.
105. Fersht, A., Protein Stability. In *Structure and Mechanism in Protein Science*, M. R. Julet, G. L. Hadler, Ed. W. H. Freeman and Company: New York, 1999; pp 508.
106. Zhang, F. Z.; Sadvoski, O.; Xin, S. J.; Woolley, G. A. "Stabilization of Folded Peptide and Protein Structures via Distance Matching with a Long, Rigid Cross-Linker," *J. Am. Chem. Soc.* **2007**, 129, 14154.
107. Lau, Y. H.; Andrade, P. d.; Quah, S.-T.; Rossmann, M.; Laraia, L.; Skold, N.; Sum, T. J.; Rowling, P. J. E.; Joseph, T. L.; Verma, C.; Hyvonen, M.; Itzhaki, L. S.; Venkitaraman, A. R.; Brown, C. J.; Lane, D. P.; Spring, D. R. "Functionalized staple linkages for modulating the cellular activity of stapled peptides," *Chem. Sci.* **2014**, 5, 1804.

108. Dirksen, A.; Hackeng, T. M.; Dawson, P. E. "Nucleophilic Catalysis of Oxime Ligation," *Angew. Chem. Int. Ed.* **2006**, *45*, 7581.
109. Dufau, L.; Ressureicao, A. S. M.; Fanelli, R.; Kihal, N.; Vidu, A.; Milcent, T.; Soulier, J.-L.; Rodrigo, J.; Desvergne, A.; Leblanc, K.; Bernadat, G.; Crousse, B.; Reboud-Ravaux, M.; Onger, S. "Carbonylhydrazide-Based Molecular Tongs Inhibit Wild-Type and Mutated HIV-1 Protease Dimerization," *J. Med. Chem.* **2012**, *55*, 6762.
110. McDonald, R. S.; Martin, E. V. "The kinetics and equilibrium of the hydration of phthalaldehyde," *Can. J. Chem.* **1979**, *57*, 506.
111. Frey, G.; Rits-Volloch, S.; Zhang, X.-Q.; Schooley, R. T.; Chen, B.; Harrison, S. C. "Small molecules that bind the inner core of gp41 and inhibit HIV envelope-mediated fusion," *Proc. Nat. Acad. Sci. USA* **2006**, *103*, 13938.
112. Horne, W. S.; Johnson, L. M.; Ketas, T. J.; Klasse, P. J.; Lu, M.; Moore, J. P.; Gellman, S. H. "Structural and biological mimicry of protein surface recognition by  $\alpha/\beta$ -peptide foldamers," *Proc. Nat. Acad. Sci. USA* **2009**, *106*, 14751.
113. Dwyer, J. J.; Wilson, K. L.; Davidson, D. K.; Freel, S. A.; Seedorff, J. E.; Wring, S. A.; Tvermoes, N. A.; Matthews, T. L.; Greenberg, M. L.; Delmedico, M. K. "Design of helical, oligomeric HIV-1 fusion inhibitor peptides with potent activity against enfuvirtide-resistant virus," *Proc. Nat. Acad. Sci. USA* **2007**, *104*, 12772.
114. Zhang, R.; Mayhood, T.; Lipari, P.; Wang, Y.; Durkin, J.; Syto, R.; Gesell, J.; McNemar, C.; Windsor, W. "Fluorescence polarization assay and inhibitor design for MDM2/p53 interaction," *Analytical Biochem.* **2004**, *331*, 138.
115. Roehrl, M. H. A.; Wang, J. Y.; Wagner, G. "A general framework for development and data analysis of competitive high-throughput screens for small molecule inhibitors of protein-protein interactions by fluorescence polarization," *Biochem.* **2004**, *43*, 16056.
116. Luo, P.; Braddock, D. T.; Subramanian, R. M.; Meredith, S. C.; Lynn, D. G. "Structural and thermodynamic characteristics of a bioactive peptide model of apolipoprotein E: side-chain lactam bridges to constrain the conformation," *Biochem.* **1994**, *33*, 12367.
117. Glas, A.; Bier, D.; Hahne, G.; Rademacher, C.; Ottmann, C.; Grossmann, T. N. "Constrained peptides with target-adapted cross-links as inhibitors of a pathogenic protein-protein interaction," *Angew. Chem. Int. Ed.* **2014**, *53*, 2489.

118. Araujo, A. D. d.; Hoang, H. N.; Kok, W. M.; Diness, F.; Gupta, P.; Hill, T. A.; Driver, R. W.; Price, D. A.; Liras, S.; Fairlie, D. P. "Comparative  $\alpha$ -helicity of cyclic pentapeptides in water," *Angew. Chem. Int. Ed.* **2014**, *126*, 7085.
119. Kuhlman, B.; Raleigh, D. P. "Global analysis of the thermal and chemical denaturation of the N-terminal domain of the ribosomal protein L9 in H<sub>2</sub>O and D<sub>2</sub>O. Determination of the thermodynamic parameters  $\Delta H$ ,  $\Delta S$ , and  $\Delta C_p$ , and evaluation of solvent isotope effects," *Protein Sci.* **1998**, *7*, 2405.
120. Buer, B. C.; Levin, B. J.; Marsh, E. N. G. "Influence of fluorination on the thermodynamics of protein folding," *J. Am. Chem. Soc.* **2012**, *134*, 13027.
121. Reinert, Z. E.; Horne, W. S. "Folding thermodynamics of protein-like oligomers with heterogeneous backbones," *Chem. Sci.* **2014**, *5*, 3325.
122. Chiu, T. K.; Kubelka, J.; Herbst-Irmer, R.; Eaton, W. A.; Hofrichter, J.; Davies, D. R. "High-resolution X-ray crystal structures of the villin headpiece subdomain, an ultrafast folding protein," *Proc. Nat. Acad. Sci. USA* **2005**, *102*, 7517.
123. Brewer, S. H.; Vu, D. M.; Tang, Y.; Li, Y.; Franzen, S.; Raleigh, D. P.; Dyer, R. B. "Effect of modulating unfolded state structure on the folding kinetics of the villin headpiece subdomain," *Proc. Nat. Acad. Sci. USA* **2005**, *102*, 16662.
124. Kubelka, J.; Eaton, W. A.; Hofrichter, J. "Experimental tests of villin subdomain folding simulations," *J. Mol. Biol.* **2003**, *329*, 625.
125. Godoy-Ruiz, R.; Henry, E. R.; Kubelka, J.; Hofrichter, J.; Munoz, V.; Sanchez-Ruiz, J. M.; Eaton, W. A. "Estimating free-energy barrier heights for an ultrafast folding protein from calorimetric and kinetic data," *J. Phys. Chem. B* **2008**, *112*, 5938.
126. Frank, B. S.; Vardar, D.; Buckley, D. A.; McKnight, C. J. "The role of aromatic residues in the hydrophobic core of the villin headpiece subdomain," *Protein Sci.* **2002**, *11*, 680.
127. Liu, L.; Yang, C.; Guo, Q.-X. "A study on the enthalpy-entropy compensation in protein unfolding," *Biophys. Chem.* **2000**, *84*, 239.
128. Prabhu, N. V.; Sharp, K. A. "Heat capacity in proteins," *Annu. Rev. Phys. Chem.* **2005**, *56*, 521.
129. Myers, J. K.; Pace, C. N.; Scholtz, J. M. "Denaturant  $m$  values and heat capacity changes: relation to changes in accessible surface areas of protein unfolding," *Protein Sci.* **1995**, *4*, 2138.

130. Katayama, H.; Hoja, H.; Ohira, T.; Nakahara, Y. "An efficient peptide ligation used azido-protected peptides via the thioester method," *Tetrahedron Lett.* **2008**, *49*, 5492.